MAR 29 1949

THE PHYSICAL REVIEW

VOLUME 75 Second Series NUMBER 6

MARCH 15, 1949

Published for the

AMERICAN PHYSICAL SOCIETY

by the

AMERICAN INSTITUTE OF PHYSICS

LANCASTER, PA., AND NEW YORK, N. Y.

THE PHYSICAL REVIEW

A journal of experimental and theoretical physics established by E. L. Nichols in 1893

Published by the American Institute of Physics
for the

AMERICAN PHYSICAL SOCIETY

Officers

President

F. W. Loomis
University of Illinois
Urbana, Illinois

Vice-President

I. I. Rabi
Columbia University
New York, New York

Secretary

K. K. Darrow
Bell Telephone Laboratories
Office:
Columbia University
New York 27, New York

Treasurer

G. B. Pegram
Columbia University
New York 27, New York

Local Secretary
for the Pacific Coast

J. Kaplan
University of California at Los Angeles
Los Angeles, California

Managing Editor

John T. Tate
University of Minnesota
Minneapolis, Minnesota

BOARD OF EDITORS

Editor — *Assistant Editor*

John T. Tate — J. W. Beams

Associate Editors

L. A. Beutler	S. A. Goudsmit	W. E. Lamb, Jr.
A. Hemmendinger	E. M. Purcell	R. G. Sachs
J. H. Zachariasen	V. F. Weisskopf	J. Barcroft

Manuscripts for publication should be submitted to John T. Tate, University of Minnesota, Minneapolis, Minnesota. The authors' institutions are requested to pay a publication charge of $4 per page which, if honored, entitles them to 100 free reprints. Instructions will be sent with galley proofs.

Proofs and all correspondence concerning papers in the process of publication should be addressed to the Publication Manager, American Institute of Physics, 57 East 55 Street, New York 22, New York.

Subscription Price

United States and Canada $15.00
Members $10.00

Back Numbers

Complete set: Series 2,[1] Vol. 1, 1913–Vol. 74, 1948—$648.00
Yearly rate: $20.00
Single copies: $2.00 each, prior to July, 1929;
$1.00 each, July, 1929–December, 1941;
$2.00 each, January, 1942–December, 1946.
Current issues: $2.00 each.

Subscriptions and orders for back numbers should be addressed to the Business Office of the Physical Review, Prince and Lemon Streets, Lancaster, Pennsylvania, or to the American Institute of Physics, 57 East 55 Street, New York 22, New York.

Changes of address in the case of members of the American Physical Society should be addressed to the Treasurer; in the case of other subscribers to the Publication Manager, American Institute of Physics.

[1] Succeeds Physical Review, Cornell University, Ithaca, New York.

The Physical Review is published monthly at Prince and Lemon Streets, Lancaster, Pennsylvania.

Entered as second-class matter [illegible] at the Post Office at Lancaster, Pennsylvania, under the Act of March 3, [illegible]

Acceptance for mailing at special rate of [illegible] provided for in paragraph 4, section 538, P. L. & R., authorized January 23, [illegible]

THE
PHYSICAL REVIEW

A journal of experimental and theoretical physics established by E. L. Nichols in 1893

SECOND SERIES, VOL. 75, NO. 6 MARCH 15, 1949

The Scattering of Fast Argon Atoms in Argon Gas

H. W. BERRY
Department of Physics, Syracuse University, Syracuse, New York
(Received November 29, 1948)

Apparatus is described for the production of argon atom beams of energies of 500 ev to 3500 ev and for the measurement of the elastic scattering of these beams in argon gas at rest. Differential scattering cross sections are found and from them an interaction potential over a range of 0.6 to 1.2A is determined. This is compared to the exponential repulsive term of the potential suggested by Buckingham for argon. The agreement is within the experimental error.

INTRODUCTION

ONE of the most direct ways of investigating the force of interaction between atoms is to study the elastic scattering of a beam of such atoms when it traverses a like gas. Hoyt[1] has developed for classical scattering a method by which numerical values of the potential as a function of distance may be obtained without any assumption as to the analytical form of the potential function. To observe primarily the repulsive force and to investigate the potential for close distances of approach an energetic atom beam of several hundred to several thousand electron volts is required. In this energy range much work[2] has been done on the scattering and absorption of positive ions but here charge exchange between the ion and the gas atom may introduce complicating effects. The scattering of thermal energy molecular beams which, however, lack homogeneity in energy has also been extensively investigated.[3] But very little work has been done with fast homogeneous neutral atom beams[4] with energy variable over a large range. Such beams may be produced by first forming an ion beam of the desired energy and then by means of charge exchange with gas atoms present neutralize the ions thus having a neutral atom beam with the same energy as the original ion beam. Generally here because of the higher energies usually used techniques different than those developed in molecular beam work are employed. In the work reported here homogeneous argon atom beams of energies of 500 ev to 3500 ev have been produced, allowed to traverse a region containing argon gas, and the resulting scattering measured.

EXPERIMENTAL PROCEDURE

The sectional schematic diagram of Fig. 1 illustrates the essential parts of the apparatus. The ion gun is a modification of an ion source developed by Finklestein.[5] There, ions are produced in a field free region P by bombardment of electrons from the filament F. The accelerating voltage for the electrons is generally $60V$ so as to produce a preponderance of singly ionized argon ions.[6] These ions are then accelerated to the desired energy by the potential difference V. The ion beam next enters a region where argon gas is present at a pressure of several microns and where a charge exchange between the ions in the beam and the gas atoms may occur. If the charge exchange collision occurs with only slight deflection the now fast atom may continue through the $\frac{3}{32}$-inch holes in the succeeding diaphragms to the scattering chamber. The diaphragm D is at a potential of 45 volts more

[1] F. C. Hoyt, Phys. Rev. **55**, 664 (1939).
[2] Some of these are: W. J. Hamm, Phys. Rev. **63**, 433 (1943); A. J. Dempster, Phil. Mag. **3**, 115 (1927); J. S. Tompson, Phys. Rev. **35**, 1196 (1930); A. G. Rouse, Phys. Rev. **52**, 1238 (1937); J. H. Simons, *et al.* J. Chem. Phys. **11**, 307 (1943).
[3] Some of these are: S. Rosin and I. I. Rabi, Phys. Rev. **48**, 373 (1935); F. Knauer, Zeits. f. Physik **90**, 559 (1934); R. M. Zabel, Phys. Rev. **46**, 411 (1934).
[4] I. Amdur and H. Pearlman, J. Chem. Phys. **9**, 503 (1941); I. Amdur, J. Chem. Phys. **11**, 157 (1943).
[5] A. T. Finklestein, Rev. Sci. Inst. **11**, 94 (1940).
[6] W. Bleakney, Phys. Rev. **36**, 1303 (1930).

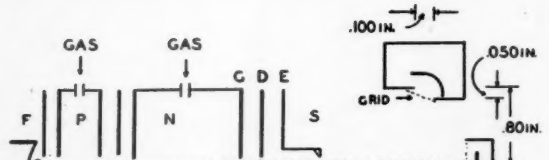

FIG. 1. Schematic diagram of apparatus.

positive than the ion accelerating electrode to remove any unneutralized particles in the beam. To assure that the entire area of the opening is at the potential of the plate a fine wire mesh was placed in the diaphragm hole.

The neutral argon beam of energy equal to that of the original ion beam now enters the scattering chamber S where argon gas is present at a pressure of 1.6 microns. To facilitate the measurement of the scattered atoms the collector was made to receive the full azimuthal angle. As shown in Fig. 1 scattered atoms from the axis of the system can enter the collector if scattered at the proper angle from different positions along the axis. Behind the receiver slit is a tantalum sheet so shaped that atoms entering through the center of the slit will strike it normally. If the electrode is slightly negative secondary electrons will be removed and thus be a measure of the number of scattered atoms entering the collector. A slightly positive grid at the entrance slit prevented the field for removing secondaries from extending out into the space about the slit and pulling stray positive ions to the collector. The collector is movable along the axis of the system by means of a mounting in a Wilson seal. A smaller concentric cylinder contained another tantalum strip which could be bombarded by the unscattered beam. When this cylinder is placed just beyond the entrance hole in E, the secondary electron current from K is a measure of the unscattered beam size. Also since this inner cylinder when pushed in would block the cone of scattered atoms to the collector, it could be used to check for spurious or background currents that might be collected by the electrodes and leads. This secondary electron current produced by bombardment of collector surface by the scattered atoms was of the order of 10^{-11} to 10^{-12} ampere and was measured by an FP-54 circuit in conjunction with a galvanometer. The secondary electron current produced by the unscattered beam on electrode K was well within galvanometer range.

TABLE I. Values of the cross section for attenuation of the beam for various beam energies in electron volts.

Energy (ev)	500	1000	1500	2000	2500	3000	3500
$\sigma_A \times 10^{16}$ cm^2	4.0	2.2	1.7	1.5	1.3	1.2	1.1

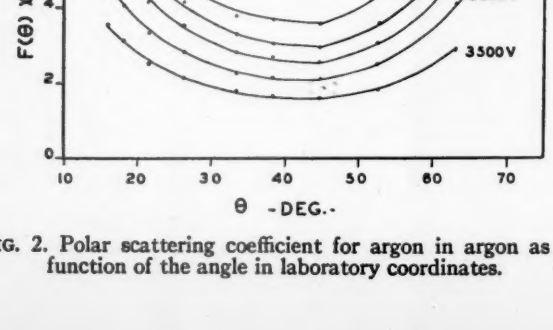

FIG. 2. Polar scattering coefficient for argon in argon as a function of the angle in laboratory coordinates.

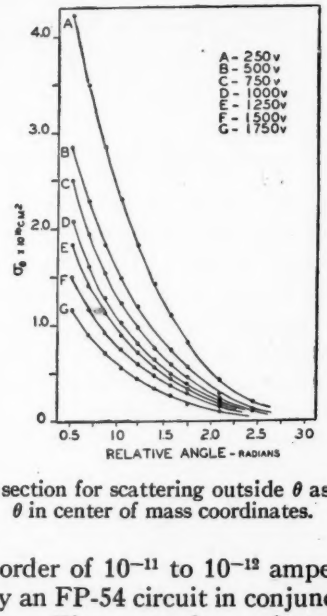

FIG. 3. Cross section for scattering outside θ as a function of θ in center of mass coordinates.

As the collector R is moved away from the entrance hole the angular range of scattered atoms directed to the collector is increased with the smallest angle of scattering collected occuring for the element of path just inside the scattering chamber. This increase in the secondary electron current caused by moving the collector a distance dx from the entrance aperture can be written in terms of the polar scattering coefficient $f(\theta)$ as,

$$dS = \kappa_\theta I N \{f(\theta_m) + f(90° - \theta_m)\} d\theta_m dx - N\sigma_A S dx,$$

where the first term represents the increase in the collector current S caused by the additional scattering path dx. And the second term represents the

decrease in S that results from the further attenuation of the unscattered beam by the introduction of this additional path dx. In the equation, S = secondary electron current in the collector, κ_θ = number of secondary electrons removed per neutral particle[7,8] with energy characteristic of θ_m, I = unscattered beam intensity, N = number of scattering atoms per cm^3, $f(\theta)$ = polar scattering coefficient for beam atoms, $f(90°-\theta)$ = polar scattering coefficient for knocked on atoms since the particles are of equal mass, $d\theta_m$ = angle subtended by collector slit at the center of the element of path dx at entrance aperture, and σ_A = cross section for attenuation of unscattered beam. This equation may be solved for $F(\theta_m)=f(\theta_m)+f(90°-\theta_m)$,

$$F(\theta_m)=[ds/dx+N\sigma_A S]/\kappa_\theta I N d\theta_m.$$

Since the atoms scattered from the element dx at the entrance hole into the collector may undergo additional scattering, the $F(\theta)$ obtained above is divided by $e^{-N\sigma_A d}$, where d is the distance from dx to the collector slit. Actually the cross section for this process will depend upon the angle subtended by the collector slit at the scattering point. For, the particle is lost to the scattering cone only if it is again scattered outside of this angle. Since the average angle subtended by the slit is small, the same cross section is used as for the beam attenuation.

To determine S as a function of x the collector is moved back in 5-mm steps starting at the entrance hole. Each reading was corrected for background currents by intercepting the scattered atom cone with the inner cylinder. From a curve of S *vs.* x the slope dS/dx for various angles θ_m is obtained and $F(\theta)$ calculated.

Since the corrections involving σ_A are small (a few percent except for the 500-ev scattering where a maximum correction of 15 percent was applied) only a rough value of σ_A was determined. A diaphragm with a small hole is placed in the front of the collector assembly such that the collector can receive atoms scattered only from about 35° to 90° no matter what its position. Consequently if the scattered current is measured for two positions l cm apart, the ratio of the currents $=e^{-N\sigma_A l}$ from which σ_A may be determined for the different beam energies. These are given in Table I.

RESULTS

The curves of $F(\theta)$ obtained as a result of the treatment outlined above are shown in Fig. 2. As would be expected the curves have a minimum at 45°, but are not symmetrical about this minimum. Since the larger angles correspond to small x and small S, there exists for these a greater error in measurement. A small error in x or alignment of the apparatus will produce sizable errors in the calculation of the angle θ_m for large values of θ, producing little error for angles less than 45°. Also, the values of κ_θ used for the large angles (low energies) were found by extrapolation of the curves given in reference 7, following the trend indicated in reference 8. This too may be a source of large error. Consequently, only the part of the curve from 15° to 45° was used in determining the polar scattering coefficient $f(\theta)$. To find this, the following approximate graphical method is used. A curve is drawn such that

$$f(\theta)=\tfrac{1}{2}F(\theta) \text{ at } \theta=45°$$
$$f(\theta)=0 \text{ at } \theta=90°$$
$$f(\theta)\to F(\theta) \text{ as } \theta\to 0°$$

and such that the sum of $f(\theta)$ and $f(90°-\theta)$ equals $F(\theta)$ for intervening points. For the method of analysis used here the cross section for scattering outside of the angle θ is needed. So the $f(\theta)$ curves were integrated graphically to give the curves shown in Fig. 3, where

$$\sigma_{\theta'}=\int_\pi^{\theta'} f(\theta')d\theta',$$

θ' = relative angle of scattering and $\theta'=2\theta$ (laboratory coordinates). The energies shown for the curves are also those in the center of mass system.

As described by Hoyt,[1] the method for deducing the interaction potential from the scattering cross section is as follows. The equation for the angle of deflection θ can be rewritten in terms of a deflection parameter, $\rho=\pi/2-\theta/2$, and with angular momentum L = constant. The equation for ρ will contain the energy E of the particle as a parameter and can be rewritten so as to have the form of an Abelian integral equation. This can be solved for a known function of r, the distance between atom

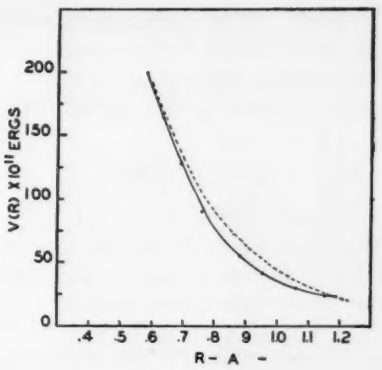

FIG. 4. Interaction potential for argon from experimental results (solid line). Repulsive term of Buckingham's potential function for argon (dashed line).

[7] H. W. Berry, Phys. Rev. **74**, 848 (1948).
[8] A. Rostagni, Zeits. f. Physik **88**, 55 (1934).

centers, in terms of an integral over the energy. Choosing a value of angular momentum within the experimental range, values of σ_θ are obtained for the values of E used in the experiment from the equation

$$\sigma_\theta = \pi L^2/2mE,$$

where m = reduced mass.

From the experimental curves of σ_θ *vs.* θ, θ may be found for a given L and E, and consequently $\rho(E)$. From these values the integral

$$\frac{1}{r} = \frac{(2m)^{\frac{1}{2}}}{\pi L}\int_0^U \frac{\rho(E)dE}{(U-E)^{\frac{1}{2}}}$$

can be found graphically where

$$U = V(r) + L^2/2mr^2$$

and $V(r)$ the interaction potential deduced.

The potential curve so determined with $L = 15 \times 10^{-25}$ g-cm^2/sec. is shown in Fig. 4. If a different L is chosen, say $L = 20 \times 10^{-25}$ g-cm^2/sec., which is about the upper value that may be used with this data a slightly different $V(r)$ is obtained, fitting closely the curve shown from 0.8 to 1.2A and about 10 percent lower for smaller values of r. If $L = 10 \times 10^{-25}$ g-cm^2/sec., again the values for $V(r)$ fit the curve in Fig. 4 from 0.8 to 1.2A but are about 10 percent higher for smaller r.

Also plotted in Fig. 4 as the dashed line is the repulsive term from Buckingham's[9] potential function for argon atoms. This is $V(r) = 1690e^{-(r/0.273)} \times 10^{-11}$ ergs with r in A. The fit is surprisingly good in view of the much higher interaction energies used here in comparison with the thermal energies for which range the potential function was determined. An exponential term of this type has also been suggested by calculations of Bleich and Mayer[10] for neon and Slater and Kirkwood[11] for helium.

[9] R. A. Buckingham, Proc. Roy. Soc. **A168**, 264 (1938).

PRESENCE OF POSITIVE IONS

When the collector electrode is made positive with respect to the grid, secondary electrons will be held and the current measured would be that of the charged particles striking the surface. For the higher energy beams there occurred under these circumstances a small positive current indicating positive ions directed to the collector. This positive ion current increased as the angular range of acceptance increased from 90° to 65° or 70°. Beyond this it remained about constant and was about 5 percent of the secondary current produced by incoming neutrals at 15°. This might indicate a preponderance of positive ions produced by inelastic scattering at the larger angles, but because of the large cross section for neutralization[7,12] of an ion in its own gas, this is very uncertain.

This work was supported in part by the Office of Naval Research under project NR-019-610.

[10] W. E. Bleich and J. E. Mayer, J. Chem. Phys. **2**, 252 (1934).

[11] J. C. Slater and J. G. Kirkwood, Phys. Rev. **37**, 682 (1931).

[12] B. Rosen and H. Kallmann, Zeits. f. Physik **61**, 61 (1930).

The Energy Spectrum of the Delayed Neutrons from O^{17}

EVANS HAYWARD
Radiation Laboratory, University of California, Berkeley, California
(Received December 10, 1948)

Following the β-decay of N^{17} an excited state of O^{17} is formed that is unstable against neutron emission. The energy distribution of these neutrons has been measured with a hydrogen-filled cloud chamber. The results indicate that the β-decay of N^{17} leaves the O^{17} nucleus in one or more excited states and that, if there is only one excited state, it is at least 0.6 Mev wide.

WHEN bombarded with high energy deuterons, the elements just above oxygen in the periodic table have been found to yield delayed neutrons[1] analogous to those found in fission products.[2] The neutrons are emitted with a period that corresponds to a 4.14-second half-life.[1] The nucleus responsible for this period has been identified by Alvarez[3] to be N^{17}, which β-decays to give an excited state of O^{17}, which in turn emits a neutron and becomes O^{16}.

Alvarez[3] has some preliminary data which indicate that there is a spread in the energy of the neutrons from O^{17} and hence that the energy level from which they come is broad. The object of this investigation was to determine the neutron energy spectrum from the ranges of the knock-on protons in a hydrogen-filled cloud chamber. The cloud-chamber equipment was essentially the same as that used in a previous experiment[4] except that the chamber was removed from the magnet. The target was a LiF crystal ($\frac{1}{2}''\times\frac{1}{2}''\times\frac{1}{4}''$) which was clamped to a spool and blown back and forth between the cyclotron and the cloud chamber through a pneumatic tube. The spool was stopped at a position in the tube such that the target was three feet outside of the concrete shielding and six feet from the cloud chamber (see Fig. 1). The target was bombarded by the circulating 195-Mev deuteron beam of the cyclotron for thirty seconds and then blown out to the cloud chamber which was expanded manually a few seconds after the target came to rest. The cloud-chamber clearing field was not turned off until the time of the expansion so that those ions that were formed before the target stopped moving were swept out before the vapor could condense on them. The cyclotron was turned off after the bombardment, and since the target spent about ten seconds moving out to the cloud chamber, we may be certain that those events that occurred in the chamber were due to the target.

The neutron energy is related to the energy of its knock-on proton by the equation $En=Ep/\cos^2\theta$, where θ is the scatter angle. The proton range and the angle that the proton makes with the direction of the incident neutron have been measured by reprojection.[4] The range-energy curve (Fig. 2) for the chamber pressure, which was 129.4 cm of H_2 saturated with a 2:1 alcohol-water mixture, has been calculated by A. A. Garren.

A region in the cloud chamber was chosen for selecting the tracks such that all those that started within this region would also end in the illuminated

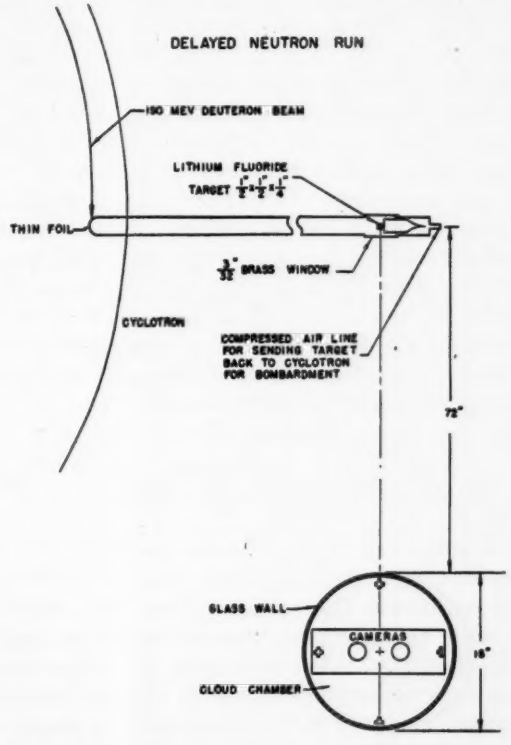

FIG. 1. The experimental arrangement showing the position of the cloud chamber relative to the pneumatic tube, target, and cyclotron.

[1] Knable, Lawrence, Leith, Moyer, and Thornton, Bull. Am. Phys. Soc. F9 (April 29, 1948); W. W. Chupp and E. M. McMillan, Bull. Am. Phys. Soc. F10 (April 29, 1948).

[2] Snell, Nedzel, Ibsen, Levinger, Wilkinson, and Sampson, Phys. Rev. **72**, 541 (1947); Snell, Levinger, Meiners, Sampson, and Wilkinson, Phys. Rev. **72**, 545 (1947); R. B. Roberts, R. C. Meyer, and P. Wang, Phys. Rev. **55**, 510 (1939); Roberts, Meyer, Hafstad, and Wang, Phys. Rev. **55**, 664 (1939); E. T. Booth, J. R. Dunning, and F. G. Slack, Phys. Rev. **55**, 876 (1939); Hughes, Dabbs, Cahn, and Hall, Phys. Rev. **73**, 111 (1948).

[3] L. W. Alvarez, Bull. Am. Phys. Soc. F11 (April 1948).

[4] Brueckner, Hartsough, Hayward, and Powell, Phys. Rev. (in press).

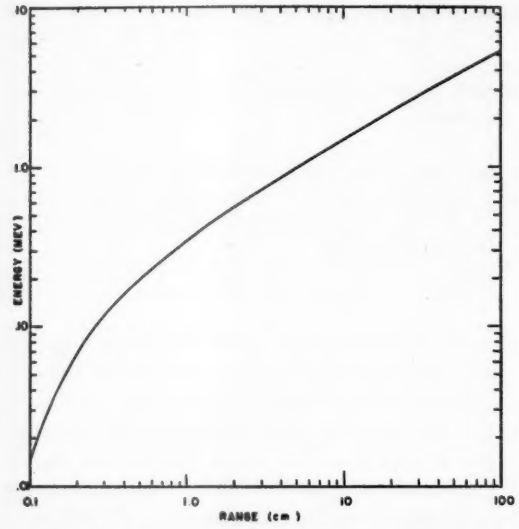

FIG. 2. Range of protons in hydrogen gas, alcohol, and water vapor at a 2:1 ratio by volume (of the liquid), at 129.4 cm Hg, and 20°C.

area. All tracks having scatter angles larger than 30° were excluded in order to minimize the error which is introduced by including recoils from neutrons that have scattered first from the walls of the chamber before producing a knock-on proton in the gas. If all scatter angles are included, the neutron energy distribution contains a few neutrons with energies as high as 10 Mev, but these all arise from protons with large scatter angles and hence are due to neutrons that did not come directly from the target. In the early stages of the experiment a small number of tracks, large scatter angles included, were measured. Out of twenty protons with scatter angles greater than 30°, only two gave exorbitant neutron energies. From this we estimate that about 10 percent of the neutrons included had undergone scattering previous to producing the recoil in the gas. Of course, those protons that have small scatter angles give the most accurate determination of the energy of the neutron producing them. There are not many protons with scatter angles smaller than 10°, but when the neutron energy distribution that they yield is plotted, it is found to agree very well with that obtained when all scatter angles up to 30° are included.

The ranges of all the protons produced by neutrons having energies greater than 0.5 Mev have been measured. The proton ranges were measured to 1 mm. This gives an error in the neutron energy small compared to that caused by the errors in measuring the angles. Tracks of all ages have been included. The width of a track gives a rough estimate of its age. It has been assumed that all "new" tracks, those less than 0.1 cm wide, were produced by protons that traversed the cloud chamber after the expansion and that all those wider than 0.1 cm passed through before the expansion. In obtaining the energy from the proton range, the expanded pressure was used for all "new" tracks and the compressed pressure for all the rest. This seems justifiable since, when the data were divided into four different groups corresponding to four different ages, all gave essentially the same energy distribution. In Fig. 3 the solid histogram represents all the data and the dotted one only those obtained from sharp tracks. More weight should be attached to the new tracks than to the old, since their scatter angles can be measured to $\pm 1°$ whereas the old tracks were measured to only $\pm 3°$. The errors in the neutron energies due to measurement have been estimated to be ± 6 percent for diffuse tracks and ± 2 percent for sharp ones.

One factor that made the determination of the scatter angles difficult was the multiple scattering of the protons by the gas. This is unimportant in the case of the sharp tracks because they are so easy to measure, and since the neutron distributions obtained from either kinds of tracks are essentially the same (Fig. 3), we conclude that there are no large errors in the energy distribution because of multiple scattering.

One of the checks made in the experiment was to calculate the number of neutrons scattered per unit solid angle in the center of mass system for three

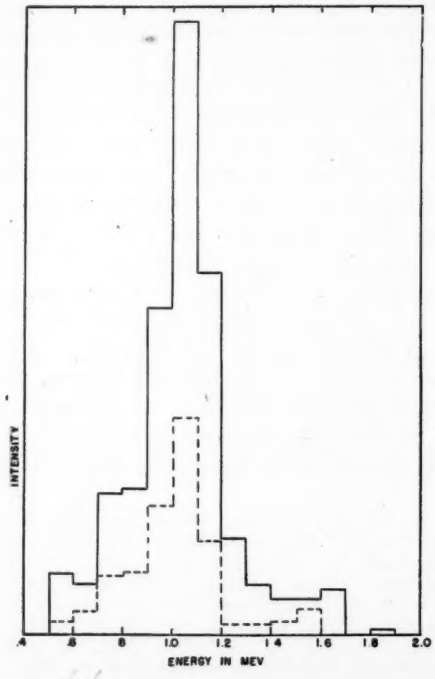

FIG. 3. The solid histograms shows the neutron energy distribution based on all 391 tracks. The dotted histogram is that obtained when only new tracks (those less than 0.1 cm wide) are included; their energies have been corrected for the fact that these particles traversed the cloud chamber after the pressure had fallen by 13 percent.

groups of tracks. This number should be a constant independent of the angle. The results, which agree well within the standard deviations, are 305 ± 42, 276 ± 23, and 270 ± 19. The standard deviations are based on the number of tracks.

The solid histogram in Fig. 3, based on 391 proton recoils, shows the energy distribution of the neutrons; it has been corrected for the variation of the scattering cross section with energy using the experimental data cited by Bohm and Richman.[5] The spread in the curve is about commensurate with that to be expected from experimental error in the measurement of a single energy. However, it should be pointed out that the high energy tail is real since it comes from proton recoils that have energies as high as 1.6 Mev (see Fig. 4). The lower energy end of the curve is not so clear-cut since the recoils responsible for it may be produced by neutrons that have already been scattered before producing knock-ons in the gas of the chamber. This neutron distribution permits one of two conclusions. The first is that the energy level from which the neutron comes is at least 0.6 Mev wide. The other alternative is that there is more than one neutron energy—for example, one at 1 Mev and a second near 1.8 Mev. The higher energy neutron would then be emitted very infrequently compared to the 1-Mev neutron. Alvarez has tried to correlate two such neutron energies with their corresponding β-rays. His result is not conclusive and certainly not inconsistent with either alternative.

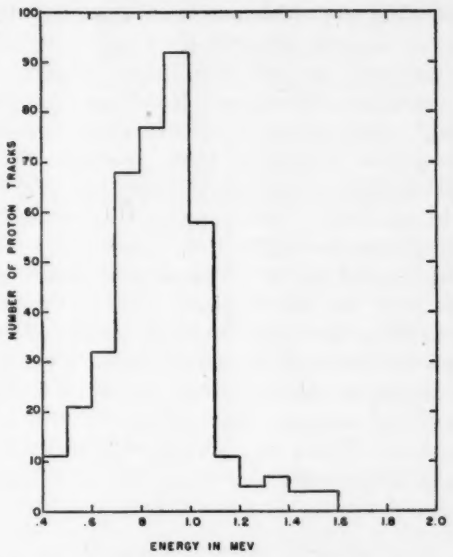

FIG. 4. This histogram shows the energy spectrum of the knock-on protons as they were actually observed. The small, though significant, number of protons having energies above 1.2 Mev indicates that the high energy end of the neutron energy spectrum is real and not due to neutrons that have scattered before producing knock-ons in the gas.

The author wishes to express appreciation to Professor Ernest O. Lawrence for his interest and encouragement and to acknowledge the very helpful discussions with Drs. R. L. Thornton, L. W. Alvarez, W. M. Powell, and E. Segrè. I wish to thank Marguerite Hayward, Walter Hartsough, Raymond Butler, and Wallace Kilpatrick for their help.

This paper is based on work performed under the auspices of the Atomic Energy Commission.

[5] D. Bohm and C. Richman, Phys. Rev. **71**, 567 (1947).

PHYSICAL REVIEW VOLUME 75, NUMBER 6 MARCH 15, 1949

Upper Limits of the Fission Cross Sections of Bismuth, Lead, Mercury, Gold, Iridium, and Tungsten for 14-Mev Neutrons*

ANNE N. PHILLIPS, LOUIS ROSEN, AND R. F. TASCHEK
Los Alamos Scientific Laboratory, Los Alamos, New Mexico

(Received November 12, 1948)

A photographic technique was used to set upper limits on the fission cross section of some of the naturally occurring heavy elements below radium when these are bombarded by 14-Mev neutrons; the Los Alamos Van de Graaff, utilizing the $T(d, n)He^4$ reaction, comprised the neutron source. It is established that the fission cross sections of the elements investigated are less than approximately 10^{-5} of the cross section of U^{238}.

I. INTRODUCTION

MANY of the investigations of the fissionabilities of various elements, from number 83 down,[1] date back to the early experiments on fission. In all of this work rather weak neutron sources were used, and it is therefore not too surprising that negative results were obtained in nearly all studies. An exception to this was the

* This document is based on work performed at Los Alamos Scientific Laboratory of the University of California under Government Contract W-7405-eng-36.

[1] F. Joliot, Comptes Rendus **208**, 341 (1939); J. de phys. et rad. (7) **10**, 159 (1939); J. Thibaud and A. Moussa, Comptes Rendus **208**, 134 (1939); A. Jdanoff and L. Myssowsky, Nature **143**, 794 (1939); L. W. Alvarez and C. K. Green, Phys. Rev. **55**, 417 (1939).

work of Magnan[2] who used an ionization chamber to observe what he thought were fission pulses from gold, tungsten, and even titanium bombarded by Li-D neutrons. However, Roberts, Meyer, and Hafstad,[3] also using Li-D neutrons, could not find fission in bismuth, lead, thorium, mercury, gold, platinum, or tungsten greater than 0.001 of the effect in uranium. Unfortunately this cross-section ratio appears to refer to a mixture of neutron energies, including neutrons slowed down in paraffin as well as the primary distribution of fast neutrons from the Li-D reaction. Some of the best work on the fissionability of the naturally occurring heavy elements below radium, although the results are described as very approximate by the authors, was done by Broda and Wright,[4] again using Li-D neutrons. Their results indicate the following upper limits for the cross sections of lead and bismuth:

$$[\sigma(Pb^{206})/\sigma(U^{238})] \leqslant 9\times10^{-5},$$
$$[\sigma(Pb^{207})/\sigma(U^{238})] \leqslant 9\times10^{-4},$$
$$[\sigma(Pb^{208})/\sigma(U^{238})] \leqslant 4\times10^{-5},$$
$$[\sigma(Bi)/\sigma(U^{238})] \leqslant 7\times10^{-5}.$$

However, as is pointed out by the authors, this work, too, is far from conclusive, even within the limits set by the result. In the first place, the method used to detect fission consisted of bombarding considerable quantities of lead and bismuth with neutrons, extracting and measuring the amount of radioactive iodine and calculating from this the number of fissions produced. This method not only assumes that one of the fission products of the element under investigation will be iodine, but also that the probability of formation of this fission product is of the same order as it is in uranium. It should also be noted that the above deduced cross sections refer to the whole Li-D neutron spectrum. Although it is true that the maximum neutron energy from Li-D reaction is approximately 14 Mev for this deuteron energy, only about ten percent of the neutrons are in this energy range.[5] This, together with the fact that relatively large masses of material were used (10 kg in the case of lead and 4.5 kg in the case of bismuth, allowing possible energy loss from scattering in the material) introduces another large uncertainty into the measurements, since the fission cross section is probably very energy-sensitive near threshold. Broda,[6] utilizing the same neutron source as above, also attempted to determine the upper limits of the fission cross sections of lead and bismuth by the use of Ilford alpha-sensitive emulsions. His conclusions are as follows:

$$[\sigma(Pb^{206})/\sigma(U^{238})] \leqslant 1.47\times10^{-4},$$
$$[\sigma(Pb^{208})/\sigma(U^{238})] \leqslant 8\times10^{-4},$$
$$[\sigma(Bi)/\sigma(U^{238})] \leqslant 5.5\times10^{-4}.$$

Although in this work the difficulties inherent in the chemical method previously used were overcome, the uncertainty due to the non-monoenergetic neutron beam still remained.

Borst and Floyd[7] have made a precise study of the fissionabilities of lead, bismuth, and polonium for thermal neutrons. Since not even U^{238} or Th^{230} fissions for thermal neutrons, it was not surprising that a negative result was again obtained.

The above summary includes most of the negative evidence, along with some indication of positive evidence, for the neutron fission of naturally occurring heavy elements below number 83.

It has recently been shown by Perlman, Goeckermann, Templeton, and Howland[8] that fission can be induced in elements occurring in the range of atomic number 83 to 73 with at least one of the following particles produced by the 184-inch Berkeley cyclotron: 400-Mev alphas, 200-Mev deuterons, 100-Mev neutrons. This result was established by chemically identifying many of the fission products. It has also been found by Kelley and Wiegand,[9] using counter techniques, that the elements from lead to bismuth all show fission for neutron energies below 90 Mev and down to 28 Mev in the case of bismuth, no data being obtained below 28 Mev, presumably due to difficulties in obtaining enough intensity at such low energies with the 184-inch Berkeley cyclotron.

It has been shown by Mattauch[10] that theoretical considerations, based on the liquid drop model of the nucleus, do not exclude fission of the elements of atomic number 83 and less. If one considers the compound nucleus formed by neutron capture in lead and bismuth, the threshold energies expected would be as follows:

Bi^{210}— 9.3 Mev,
Pb^{207}—10.0 Mev,
Pb^{208}—10.4 Mev,
Pb^{209}—10.7 Mev.

If one assumes the neutron binding energies to be 5.4 Mev and 6.4 Mev for initial nuclei with even and odd number of neutrons, respectively, only 3.9 Mev would have to be supplied to Bi^{209}, and 4.6, 4.0, and 5.3 Mev to Pb^{206}, Pb^{207}, and Pb^{208}, respectively as kinetic neutron energy to reach the fission threshold.

[2] C. Magnan, Comptes Rendus **208**, 742 (1939).
[3] R. B. Roberts, R. C. Meyer, and L. R. Hofstad, Phys. Rev. **55**, 416 (1939).
[4] E. Broda and P. K. Wright, Nature **158**, 871 (1946).
[5] H. T. Richards, Phys. Rev. **59**, 796 (1941).
[6] E. Broda, Nature **158**, 872 (1946).
[7] L. B. Borst and J. J. Floyd, Phys. Rev. **70**, 107 (1946).
[8] Perlman, Goeckermann, Templeton, and Howland, Phys. Rev. **72**, 351 (1947).
[9] E. L. Kelley and C. Wiegand, Phys. Rev. **73**, 1135 (1948).
[10] J. Mattauch, *Kernphysikalische tabellen* (Berlin, 1942), p. 6.

Frankel and Metropolis[11] have very recently made much more elaborate calculations with the aid of an electronic calculator, the Eniac, from which they deduce that the fission threshold for bismuth, for example, is approximately 18 Mev. However even this value is somewhat lower than the total energy that was available to us in the form of kinetic neutron energy and neutron binding energy.

Since we had available a monoenergetic source of 14-Mev neutrons, it was felt desirable to ascertain whether the fission threshold, in terms of kinetic nentron energy necessary to produce fission, for some of the elements under consideration might be below 14 Mev and, if so, to determine the fission cross section at this energy.

II. EXPERIMENTAL PROCEDURE

The method chosen for doing this experiment was very similar to that employed by Borst and Floyd in their studies with thermal neutrons. It essentially consisted of determining the ratio of the number of fission tracks recorded in a photographic emulsion which had been in contact with a thin foil of the element under investigation to the number of fission tracks recorded in a similar photographic emulsion which had been in contact with a thin foil of U^{238}, after each had been simultaneously exposed to approximately the same neutron flux.

It has been shown by Borst and Floyd[7] and verified by the present authors for the emulsions which we used, that Eastman "special fission particle plates," although extremely insensitive to gammas, protons, and alpha-particles, respond with 100 percent efficiency to fission fragments, whether one records the track due to both or to one of the fragments, as was the case in the present experiment. Since, from mass considerations, the kinetic energy liberated in the fission of elements from bismuth to tungsten would be approximately the same as is liberated in the case of uranium, one would certainly expect to record fission tracks from these elements with the same efficiency as from uranium.

Figure 1 shows a typical track produced by one fission fragment originating in one of our U^{238} monitoring foils. This photomicrograph, taken at 900 diameters, has not been retouched at any stage of its development. From this it can be seen that fission tracks are quite easily resolved from background.

The foils used in this experiment were approximately 1.0 mg per cm² thick. These foils were made as follows:*

U—"Zapon technique"—$UO_2(NO_3)_2 \cdot 6H_2O$ was added to a one percent solution of Zapon in Zapon thinner; the resulting solution was painted on platinum and reduced to oxide by heating.

Bi, Pb, and Au—Electroplating on platinum.

Ir—"Burn-on method"[12]—$IrCl_3$ was dissolved in hexyl-alcohol and a small amount of oil of rosemary. The solution was painted on glass and reduced by heating.

Hg—Slurry technique—water dispersion of HgO.

W—A solution of ammonium tungstate, glycerine, and water was painted on platinum and heated to 600°C.

The amount of material in each foil was determined by weighing to an accuracy of about 0.5 percent. The U^{238} concentrations in the monitor foils were checked by making an alpha-particle count. The neutron source was the Los Alamos Van de Graaff, utilizing the $T(d, n)He^4$ reaction. The source strength was about 5×10^8 neutrons per second and the total energy spread about 500 kev at 14-Mev neutron energy. It is not possible in the present experimental set-up to exclude neutrons of, say, less than half the above energy, but all indications at lower bombarding energies (up to 200-kev deuterons) in this reaction and in comparable Q value reactions such as $Li^6(d, \alpha)He^4$, $Q=22$ Mev; $Li^7(p, \alpha)He^4$, $Q=17$ Mev, and $Li^7(p, \gamma)Be^8$, $Q=17$ Mev, are that no excited states for He^4 exist to an excitation energy of about 20 Mev and therefore the neutrons used here should be monoenergetic. The exact procedure for the experiment was as follows: Foils of the elements to be investigated were placed in contact with Eastman "special fission plates." Also placed in contact with fission plates were two foils of U^{238} which acted as neutron monitors. The foils of the elements under investigation, each now in contact with a fission plate, were sandwiched between the monitoring assemblies and exposed to the neutron beam in such an orientation that one of the monitors was closest to the target from which the neutrons were emitted, while the second monitor was farthest

FIG. 1. Typical tracks each produced by one fission fragment in one of the U^{238} monitoring foils.

[11] S. Frankel and N. Metropolis, Phys. Rev. 72, 914 (1947).

* All foils were made by James Gilmore and Robert Potter of the Los Alamos Scientific Laboratory.

[12] J. Strong, *Procedures in Experimental Physics* (Prentice-Hall, Inc., New York, 1946), p. 150.

from the target. After a time such that the monitor plates would have recorded approximately 8 tracks per field of view at 900 diameters, the plates were developed and their analysis begun. All plates were investigated at 900 diameters, using dark field illumination, an apochromatic 1.5 millimeter objective with iris diaphragm and compensating eyepieces.

The plates which had been in contact with the U^{238} monitoring foils were first examined and the number of tracks for 1000 fields of view determined. The plates which had been in contact with the elements under study were then investigated, approximately 10,000 fields of view being searched for fission tracks in each plate, and the number of fission tracks per thousand fields of view again determined. The solid angle correction for the neutron intensity at each of the foils under study was determined from the variation of neutron intensity at the two monitors. This correction could be accurately applied since the intensity at the two monitors varied by only 20 percent.

III. RESULTS

Two fission tracks were found in the emulsion which had been in contact with lead and one in each of the emulsions which had been in contact with bismuth, mercury, and gold. No tracks were found in the emulsions which had been in contact with tungsten and iridium. It was of course realized that very small amounts of uranium or thorium contamination could account for the observed tracks. Each of the elements was therefore spectrographically analysed for uranium. This analysis was done under supervision of John B. Marling. The analysis indicated less than 0.01 percent uranium impurities. However, since much less uranium impurity would have accounted for the observed number of fission tracks, the results of the analysis are quite inconclusive. It is therefore only possible to give an upper limit for the fission cross section of the elements investigated. The cross section of each element is given in terms of the cross section of U^{238} by

$$\frac{\sigma}{\sigma(U^{238})} \leqslant \frac{Ct_{U^{238}}A}{C_{U^{238}}tA_{U^{238}}},$$

where C = number of tracks per 1000 fields of view, t = foil thickness, A = atomic weight. In the case of U^{238}, C has been corrected so that it gives the number of tracks per 1000 fields of view if the monitoring foil were at the same place as the foil whose cross section is being computed. The results are given below, the effect in lead being proportionately ascribed to each of the normally occurring isotopes.

$$\begin{aligned}
\sigma(_{Bi}) &\leqslant 1.4\times10^{-29}\\
\sigma(_{Pb^{204}}) &\leqslant 1.3\times10^{-27}\\
\sigma(_{Pb^{206}}) &\leqslant 8.2\times10^{-29}\\
\sigma(_{Pb^{207}}) &\leqslant 8.6\times10^{-29}\\
\sigma(_{Pb^{208}}) &\leqslant 3.7\times10^{-29}\\
\sigma(_{Hg}) &\leqslant 6.7\times10^{-30}\\
\sigma(_{Au}) &\leqslant 1.2\times10^{-29}\\
\sigma(_{Ir}) &\leqslant 1.5\times10^{-29}\\
\sigma(_{W}) &\leqslant 1.2\times10^{-29}
\end{aligned}$$

IV. CONCLUSIONS

Although it is quite possible to get better statistics on the results of these cross section measurements (the statistical standard error now of course being about 100 percent), it is felt not worth while to do this in view of the uncertainty concerning uranium contamination. What would be more to the point, in view of the results of Kelley and Wiegand[9] and the calculations of Frankel and Metropolis,[11] is a repetition of the above experiment on bismuth and lead for monoergic neutrons in the energy range from 14 to 30 Mev, in order to determine whether there is a more or less sharp threshold, and if such does not exist, to determine at what energies the cross sections become measurable (approximately equal to 10^{-4} that of uranium).

ACKNOWLEDGMENTS

The authors wish to thank the crew of the Los Alamos Van de Graaff for their cooperation.

The Intensity of Heavily Ionizing Penetrating Particles at 4300-Meter Altitude*

FRANK L. HEREFORD
Bartol Research Foundation of the Franklin Institute, Swarthmore, Pennsylvania
(Received December 3, 1948)

The counting efficiency of a low pressure Geiger-Mueller counter for the ionizing cosmic radiation penetrating various thicknesses of lead has been measured at 4300-meter altitude. From existing data it is possible to determine the counting efficiency expected for mesotrons alone at that altitude. For thicknesses greater than 100 g/cm² electrons are excluded, and the observed excess in counting efficiency over that expected for mesotrons can be interpreted as due to heavily ionizing particles. On the assumption that these are protons the data indicate, for example, that 17±5 percent of the radiation penetrating 167 g/cm² Pb consists of protons.

THE ionizing component of cosmic radiation in the atmosphere is thought to be comprised of electrons, mesotrons (of various kinds), protons, and heavier nuclear particles. The intensity variations of the different sub-components with atmospheric depth furnish the most useful information from which conclusions may be drawn regarding the collision processes involved in their genesis and absorption.

The principal means[1] which have been employed heretofore to distinguish these various particles are the cloud chamber and the proportional counter. Geiger counter experiments have also been performed in which some particular property of the radiation concerned (e.g., radioactive decay, absorption properties, shower production) is utilized to distinguish the component. In addition it was suggested some years ago[2] that the use of low pressure Geiger counters might afford a means of discriminating between components without sacrificing the simplicity and ruggedness of ordinary coincidence circuits.

We have recently given further attention to this suggestion with the aim of using such methods to resolve the components at various altitudes. The basis of the method lies in the dependence of the efficiency of a low pressure counter upon the primary ionization of a particle which traverses its sensitive volume. The dependence which is well known is as follows:

$$\epsilon = 1 - e^{-l_a J P}. \qquad (1)$$

Here l_a is the average path length through the sensitive volume, J the primary ionization (N.T.P.), P the counter pressure in atmospheres. Such a counter could count 10^8-ev mesotrons (J=min.) with 20 percent efficiency but 10^8-ev protons (J=4×min.) with about 60 percent efficiency. The relation given above depends only upon the assumptions that the initiation of a single ion pair within the counter will cause a discharge and that a negligible number of secondaries emerge from the counter wall upon the passage of a particle. Both points have received indirect experimental confirmation;[2,3] the latter is investigated more thoroughly in the appendix.

The low pressure counter method has been successfully applied to the determination of the primary ionization in various gases by sea-level cosmic radiation[2,3] and to the variation of primary ionization with the energy of fast electrons.[4] This paper reports the results of an experiment carried out at 4300-meters altitude (summit of Mt. Evans, Colorado) in which was observed the variation of the counting efficiency of a low pressure counter with the penetrating power of the ionizing radiation at that altitude. The results indicate the presence of heavily ionizing penetrating particles. If it is assumed that they are protons, a rough determination of their intensity relative to the total ionizing component penetrating various thicknesses of lead

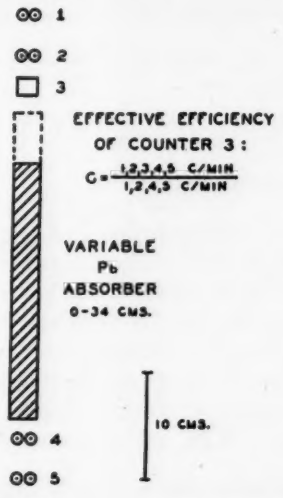

FIG. 1. Counter telescope.

* This investigation was assisted by the joint program of the ONR and the AEC. Also supported in part by the National Geographic Society.

[1] See, for example, W. F. G. Swann, Reports on Progress in Physics 10, 1 (1946).

[2] W. E. Danforth and W. E. Ramsey, Phys. Rev. 49, 854 (1936).

[3] M. G. E. Cosyns, Bull. Acad. Belg. 5, 498 (1937).

[4] F. L. Hereford, Phys. Rev. 74, 579 (1948).

is possible. With the exception of the part played by σ-mesons,[5] this component is probably responsible for the observed nuclear reactions in cosmic-ray phenomena.

EXPERIMENTAL METHOD

The counter telescope employed in the present experiment (Fig. 1) consisted of four trays of argon-butane counters (1, 2, 4, 5) and a single low pressure hydrogen counter (3) constructed of square cross-section brass tubing. The total counter wall thickness in the telescope was 6.1 gm/cm². Counter 3 was filled with pure hydrogen to a pressure of 4.0 cm Hg, the hydrogen being admitted through a palladium leak after the usual cleaning and baking procedures were completed. In the coincidence

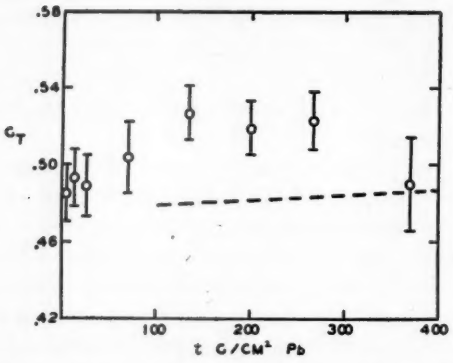

FIG. 2. The observed ratio of fivefold to fourfold coincidence rates for the radiation penetrating various thicknesses of lead. The dotted line shows the expected ratio for mesotrons alone at 4300-meters altitude.

circuits this counter was quenched externally by a circuit of the Neher-Harper type. The square cross-section cathode was used in order that existing calculations[6] could be applied directly to the determination of the average path length through the counter.

The actual experiment consisted only of determining the ratio $G_T(t)$,

$$G_T(t)=\frac{(1,2,3,4,5)c/\text{min.}}{(1,2,4,5)c/\text{min.}}. \qquad (2)$$

This clearly gives the effective efficiency of counter 3 for all particles of sufficient energy to penetrate the thickness t g/cm² Pb or *of sufficient energy to create secondaries in the lead which penetrate trays 4 and 5*. The data which were obtained are shown in Fig. 2 with the statistical errors indicated by the vertical lines through the experimental points.

The following factors are of interest concerning the possibility of instrumental errors. Fivefold and fourfold coincidences were recorded simultaneously. With proper normalization the fourfold rates yield an absorption curve in lead which is in agreement with that obtained by Hall[7] at the same altitude. Data were taken with the thicknesses of lead chosen in random order (e.g., 34 cm, 2 cm, 18 cm, etc.). Hence a progressive instrumental change could not account for the shape of the experimental curve in Fig. 2. The data, however, are in error due to various incidental but real effects, and these have been considered and dealt with as follows:

Accidental coincidences.—The resolving time of the circuits employed was approximately 8×10^{-6} sec. rendering both the fourfold and fivefold accidental rates completely negligible with respect to the genuine coincidence rates.

Side showers.—The contribution to the counting rates as a result of side showers was determined by placing tray 1 out of line, and inserting enough lead to prevent real (2, 4, 5) coincidences due to electrons belonging to cascade showers which might also discharge tray 1. Fivefold and fourfold rates were taken and found to be less than 1.5 percent of the genuine coincidence rates. Their ratio showed that counter 3 had an *over-all efficiency* of 25 ± 5 percent for side showers. On the other hand, the observed values of the counting efficiency for real events (Fig. 2) were in the neighborhood of 50 percent. It is then clear that side shower effects tend to lower the experimental points of Fig. 2; hence the choice to neglect them is a conservative one.

Secondaries from walls accompanying mesotrons.—A more important process is the production in the counter walls above counter 3 of secondary electrons which penetrate into the sensitive volume and discharge the counter coincidentally with the passage of a mesotron. Though the number of such events is small their effect must be considered in interpretation of the results. The probability that a secondary electron will be produced by a mesotron traversing a small thickness of material ($t\ll$radiation length) is easily computed from the differential collision probability for spin 0 mesotrons given by Bhabba[8] (see Appendix). It is further possible to estimate for a given mesotron energy the probability that such an electron will penetrate the remaining thickness of the material and emerge in this case into the sensitive volume of the counter. The results of this calculation are given in Fig. 3 where the solid line shows ν, the probability in percent that a mesotron of momentum p in traversing the counter walls will produce a secondary which penetrates into the sensitive volume of the counter.

Also shown is the mesotron momentum spectrum

[5] Lattes, Muirhead, Occhialini, Powell, Nature 160, 486 (1947).
[6] E. E. Witmer and M. A. Pomerantz, J. Frank. Inst. 246, 293 (1948).
[7] D. B. Hall, Phys. Rev. 66, 321 (1944).
[8] H. J. Bhabba, Proc. Roy. Soc. 164, 257 (1938).

deduced from Hall's absorption curve in lead taken at 4300-meters altitude.[7] From these two distributions can be obtained the average probability of a secondary emerging from the wall per mesotron passage for all mesotrons with momenta greater than p, viz.,

$$\text{av. } \nu(p)=\int_p^\infty \nu(p)I(p)dp/\int_p^\infty I(p)dp. \qquad (3)$$

If we now convert from momentum to range in lead (g/cm²), we can plot $f(t)$, the fraction of mesotrons capable of penetrating t gm/cm² Pb which are accompanied by a secondary electron emerging from the counter wall. It is this curve (Fig. 4) which will be of use below in correcting the data.

DISCUSSION OF RESULTS

In analysis of the results it was felt that for thicknesses of lead less than 100 g/cm², the presence of electrons in addition to mesotrons and heavier particles complicated matters to the extent that unambiguous interpretation was impossible. As a consequence it was decided to consider only those experimental points taken for greater thicknesses which amounts to an analysis of the hard component only. We shall assume then that the total vertical intensity $T(t)$ penetrating t g/cm² ($t>100$) consists of a mesotron component $M(t)$ plus an N-component, $N(t)$, consisting of protons and heavier particles. We shall adopt *coincidences per minute* as our unit of vertical intensity and denote by $G_T(t)$, $G_M(t)$, and $G_N(t)$ the ratio of fivefold to fourfold coincidence rates for that part of the indicated components penetrating t g/cm² Pb. The fraction of mesotrons penetrating t g/cm² which are accompanied by secondary electrons from the counter wall has been denoted by $f(t)$. The counter 3 will have a 100 percent counting efficiency for this fraction. We may then write for a given thickness t g/cm²,

$$T=M+N=(1, 2, 4, 5)c/\text{min.}$$
$$G_TT=G_MM(1-f)+fM+G_NN=(1,2,3,4,5)c/\text{min.}$$

The ratio, N/T, of the N-component to the total intensity, T, penetrating t g/cm² is then,

$$N/T=\frac{G_T-G_M(1-f)-f}{G_N-G_M(1-f)-f}. \qquad (4)$$

Our experimental data furnish values of $G_T(t)$, and the fraction $f(t)$ which is small has been estimated above. It remains then to determine G_M and G_N, the expected efficiency of counter 3 for the mesotron and N-components alone.

The value of G_M for various lead thicknesses is easily determined. The operation of the telescope at sea level with 66 g/cm² Pb yields the efficiency of counter 3 for mesotrons with the sea-level momentum distribution which is well known. The observed value, corrected in this case for side showers, was

$$G_T'(66)=G_M'=.485\pm.012 \quad \text{(Swarthmore)}.$$

It is assumed that there are a negligible number of protons at sea level and relatively few mesotrons of momentum less than 10^8 ev/c both of which facts are born out by experiment. With the knowledge of the mesotron momentum distributions at sea level[9] and at 4300 meters[7] and the ratio $J_M/J_{\min}$[4] (ratio of the primary ionization by sea-level mesotrons to the minimum ionization, viz., 1.2) one can determine with the help of expression (1) values of $G_M(t)$ at 4300-meters. The above value of G_M at sea-level yields $J_M=5.8$; hence, $J_{\min}=4.85$. The variation of J with momentum

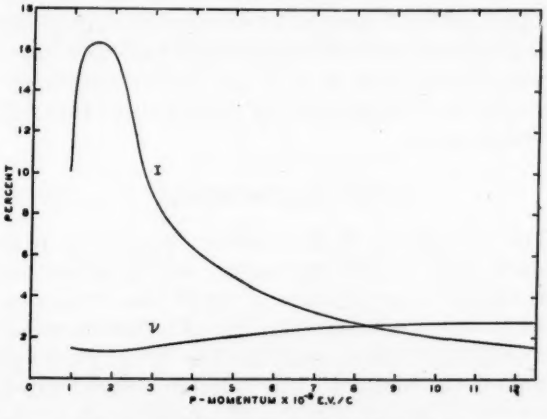

FIG. 3. The curve I represents the differential momentum spectrum for mesotrons at 4300-meters as given by Hall. ν represents the probability that a mesotron of momentum p will produce at least one secondary electron in the counter walls above counter 3 which will penetrate into the sensitive volume of this counter (see Appendix).

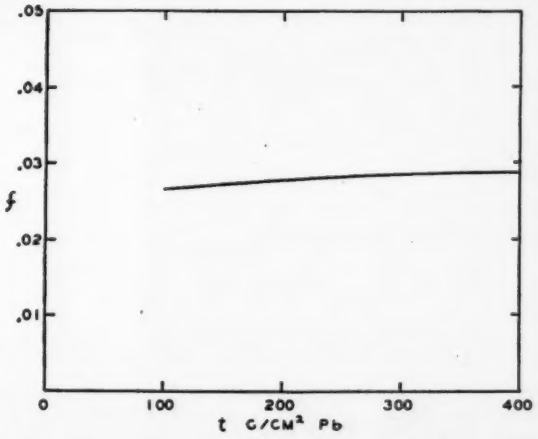

FIG. 4. The fraction of mesotrons f, penetrating t gm/cm² accompanied by secondary electrons reaching the sensitive volume of counter 3.

[9] H. Jones, Rev. Mod. Phys. 11, 235 (1939).

has been given by Bethe[10] and has been experimentally confirmed.[4] Using Bethe's curve we may then compute the effective efficiency $G_M(p)$ of counter 3 for all mesotrons of momenta greater than p on the basis of the momentum distribution $I(p)$ at 4300 meters given by Hall.

$$G_M(p)=\int_p^\infty \epsilon(p)I(p)dp/\int_p^\infty I(p)dp, \qquad (5)$$

where

$$\epsilon(p)=1-e^{-I_a J(p)P}.$$

It should be realized that this seemingly complicated process is, in principal, very simple, and is not dependent upon arbitrary assumptions. The value of the minimum primary ionization used in the graphical integrations of expression (5) was determined from the sea-level data taken with the same apparatus with which the data of Fig. 2 were obtained. If in the expression (5) we now convert from momentum to range in g/cm² Pb we have $G_M(t)$ as shown in Fig. 5. The fact that the expected values of $G_M(t)$ at 4300-meters are generally less than the observed value $G_M'(66)$ at sea level is in accordance with the greater intensity of mesotrons with the minimum ionization ($p\sim10^8$ ev/c) at 4300 meters.

The values of N/T are relatively insensitive to the choice of $G_N(t)$. Undoubtedly, some particles heavier than protons exist at 4300 meters but they are presumably few in number. Consequently, for a first approximation we shall assume that the N-component consists of protons alone and use the values of $J_P(p)$ given by Bethe[10] and an assumed p^{-2} differential intensity distribution to determine $G_N(t)$. This curve is also shown in Fig. 5.

Now with all quantities on the right side of Eq. (4) determined for various values of lead thickness we can compute N/T, the fraction of the total ionizing component penetrating t g/cm² which consists of protons (Fig. 6). The relative probable errors of the points defining the N/T curve are about 30 percent.† It is seen, for example, that the fraction of protons in the hard component ($t>167$ gm/cm²) is approximately 17 ± 5 percent. Though this value is somewhat higher than the estimates of proton intensity from previous cloud chamber work at 4300 meters,[11] it seems to be in fair agreement with the results of Anderson *et al.*[12] who deduced that approximately 33 percent of the particles observed by them in a cloud chamber at 30,000 ft. (9100 meters) with momenta greater than 4×10^8 ev/c were protons. The unpublished Pike's Peak data of Anderson and Neddermeyer is also quoted in reference 12 as indicating that the change in the characteristics of the penetrating component is much smaller between 4300 meters and 9100 meters than between sea level and 4300 meters. This fact is, of course, supported by the above data. The absolute intensity of protons, N, based on the experimental data is also shown in Fig. 6.

In arriving at this absorption curve, $N(t)$, we have assumed a p^{-2} differential distribution of protons to exist in order to determine $G_N(t)$. Actually these two distributions very nearly coincide in the region of momenta considered. However, the finally deduced curve depends most heavily upon the experimental data (i.e., the difference between $G_T(t)$ and $G_M(t)$). The choice of a $p^{-2.5}$ distribution, for example, does not appreciably alter the values of N/T or the shape of the absorption curve $N(t)$.

The point should be made that if the computation were made from the experimental points of Fig. 2 rather than the smooth curve through these points, the values of N/T and hence of N might depart from the curves of Fig. 6. Indeed for the point at 370 gm/cm² N/T is negative with a sufficiently large probable error to render this particular value meaningless. The values of N/T at smaller thicknesses, however, differ from zero by two to three times the probable error.

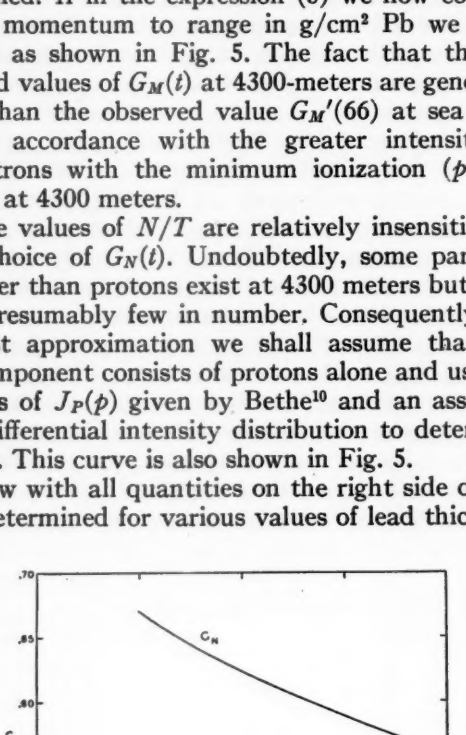

FIG. 5. The curve G_N represents the expected counting efficiency for protons penetrating various thicknesses of lead assuming a p^{-2} differential momentum distribution. G_T is a smooth curve through the experimental points of Fig. 2. G_M represents the expected counting efficiency for mesotrons penetrating various thicknesses of lead at 4300-meters altitude.

ACKNOWLEDGMENTS

The assistance of Mr. Alden Stevenson in the construction of the apparatus was a substantial contribution toward the success of the experiment. Thanks are also due Mr. M. A. Pomerantz for frequent suggestions, and to Drs. W. F. G. Swann and L. Eisenbud for their part in helpful discus-

[10] H. A. Bethe, *Handbuch der Physik* (1933), **24**, p. 522.

† For thicknesses greater than 300 g/cm² the error is considerably larger (see Fig. 2).

[11] W. M. Powell, Phys. Rev. **69**, 385 (1946).

[12] Adams, Anderson, Lloyd, Rau, and Saxena, Rev. Mod. Phys. **20**, 334 (1948).

sions. The work at Mt. Evans was made possible through the financial support of the National Geographic Society and the facilities of the Inter-University High Altitude Laboratory. All counters used were constructed by Mr. Austin Nester.

APPENDIX

We wish to determine the probability that a mesotron of energy E will produce a secondary electron in the counter walls above counter 3 which will penetrate into the sensitive volume of this counter.

The probability $\chi(E, Q)dQ$ for a mesotron of mass μ, charge ± 1, spin 0, and energy E, traversing a thickness dx (g/cm²), to transfer an amount of energy between Q and $Q+dQ$ to a free electron as given by Bhabba[8] is,

$$\chi(E, Q)dQ=\frac{2Cm}{\beta^2}\frac{dQ}{Q^2}\left(1-\beta^2\frac{Q}{Q_M}\right). \quad (1)$$

Here m is the electronic mass, Q_M the maximum transferable energy, and C a constant which in the notation and units of Rossi and Greisen[13] is

$$C=0.15(Z/A).$$

Denoting by p the momentum of the incident mesotron, if $p\ll\mu^2/m\sim 2\times 10^{10}$(e.v./$c$), it can be shown that,

$$Q_M=2m(p/\mu c)=2m(\beta^2/(1-\beta^2)). \quad (2)$$

If further Q is small compared with both E and Q_M, it can be shown that the collision probability is independent of spin justifying the use of the spin 0 collision probability of Eq. (1). These inequalities are satisfied in the problem to be considered.

The probability of a collision occurring in the interval x to $x+dx$ in which a mesotron of energy E produces a secondary electron of energy between Q and $Q+dQ$ *which penetrates the remaining wall thickness* is

$$\chi(E, Q)P(Q, x)dQdx, \quad (3)$$

where $P(Q, x)$ is the probability that an electron of energy Q will penetrate x g/cm², viz.,

$$P(Q, x)=\begin{cases}1, \text{ for } x\leqq R(Q)\cos\theta(E, Q)\\ 0, \text{ for } x>R(Q)\cos\theta(E, Q).\end{cases} \quad (4)$$

In this expression $R(Q)$ and $\theta(E, Q)$ are, respectively, the range and angle of emission of an electron of energy Q produced by a mesotron of energy E (Fig. 7). Hence the probability of a collision occurring in a thickness x g/cm² in which a mesotron of energy E produces a secondary electron

[13] B. Rossi and K. Greisen, Rev. Mod. Phys. **13**, 240 (1941).

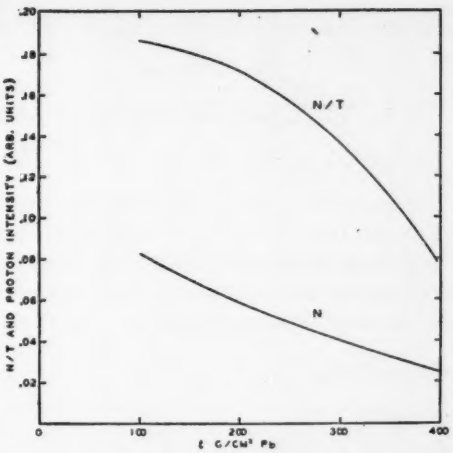

FIG. 6. The curve N/T shows the fraction of the total ionizing component penetrating various thicknesses of lead which consists of protons as derived from the data. The curve N shows the corresponding proton absorption curve in arbitrary intensity units.

of energy greater than η which penetrates the remaining wall thickness is

$$\nu_\eta(E)=\int_\eta^{Q_M}dQ\int_0^x\chi(E, Q)P(Q, x)dx.$$

In view of Eq. (4) this may be written,

$$\nu_\eta(E)=\int_\eta^{Q_M}\chi(E, Q)R(Q)\cos\theta(E, Q)dQ.$$

The computation of this integral can be greatly simplified if one removes the function $\cos\theta(E, Q)$ from under the integral sign and gives it a mean value $\langle\cos\theta(E)\rangle_{Av}$. The exact computation of a few cases justifies this step; the error incurred is negligible for our purposes. One can then approximate $\langle\cos\theta(E)\rangle_{Av}$ as follows. From the theory of elastic collisions,

$$\langle\cos\theta(E)\rangle_{Av}=\left[\frac{(p/\mu c)^2+1}{(p/\mu c)^2+Q_M/\bar{Q}}\right]^{\frac{1}{2}}, \quad (5)$$

where

$$\bar{Q}=\frac{\int_\eta^{Q_M}Q\chi(E, Q)dQ}{\int_\eta^{Q_M}\chi(E, Q)dQ}=\eta\log\frac{Q_M}{\eta}.$$

Hence the expression for $\nu_\eta(E)$ can be written,

$$\nu_\eta(E)=\langle\cos\theta(E)\rangle_{Av}\int_\eta^{Q_M}\chi(E, Q)R(Q)dQ. \quad (6)$$

In our case, however, for counter-wall thickness x_0 (2 g/cm² in our case) there is a maximum value

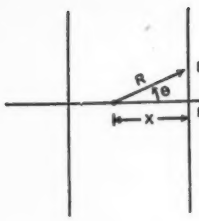

FIG. 7.

which $R(Q)$ can have, viz., $R(Q_0)\sim x_0$. Beyond this point $R(Q)$ is constant and equal to x_0. Thus Eq. (6) becomes the sum of two integrals,

$$\nu_\eta(E)=\langle\cos\theta(E)\rangle_{Av}\times\left\{\int_\eta^{Q_0}\chi(E,Q)R(Q)dQ+x_0\int_{Q_0}^{Q_M}\chi(E,Q)dQ\right\}. \quad (7)$$

Now for energies less than Q_0 (3 Mev in our case) the range energy curve for electrons can be closely approximated by,[14]

$$R(Q)=0.4Q^{1.5} \qquad (Q \text{ in Mev}).$$

In view of this relation and that of Eq. (1) one obtains by performing the integrations in Eq. (7) and setting $x_0=2$ g/cm² for our particular case,

$$\nu_\eta(E)=\frac{2Cm}{\beta^2}\langle\cos\theta(E)\rangle_{Av}\left[k\left(\sqrt{Q_0}-\sqrt{\eta}-\frac{\beta^2Q_0^{\frac{1}{2}}}{3Q_M}\right)+\frac{1}{Q_0}-\frac{1}{Q_M}-\frac{\beta^2}{Q_M}\log\frac{Q_M}{Q_0}\right], \quad (8)$$

where $\langle\cos\theta(E)\rangle_{Av}$ is given by Eq. (5), Q_M by Eq. (2), and $k=8\times10^{-10}$ g/cm². Secondary electrons of energy less than 10^4 ev will not contribute appreciably to the values of $\nu_\eta(E)$. Hence, if one sets $\eta=10^4$ ev, takes the value of the constant C appropriate for brass, and converts from energy to momentum of the incident mesotron, $\nu(p)$ can be plotted from Eq. (8). This curve is shown in Fig. 3 of the text for mesotron momenta between 10^8 and 1.2×10^9 ev/c. It should be noted that through the choice of the constant C appropriate to brass the number of secondaries produced in the glass counter envelopes is overestimated. Furthermore, scattering losses reduce the number reaching the sensitive volume of the counter. The computed values of $\nu(p)$ are consequently high which makes the estimated proton intensity (Fig. 6) conservatively low.

[14] L. E. Glendenin, Nucleonics 2, 12 (1948).

PHYSICAL REVIEW VOLUME 75, NUMBER 6 MARCH 15, 1949

Reflection and Refraction of Plane Shear Waves in Viscoelastic Media

H. T. O'NEIL
Bell Telephone Laboratories, Inc., Murray Hill, New Jersey
(Received December 1, 1948)

The shear elasticity and viscosity of liquids have been measured at ultrasonic frequencies by utilizing plane shear waves in an elastic solid and measuring the reflection loss and phase shift caused by reflection at a plane interface of the solid and a liquid. The first measurements of this type involved normal incidence. In a recent modification of the method, oblique incidence results in an enhanced effect. This paper derives the theoretical relations between the constants of the two media, the complex reflection coefficient and the angle of incidence. The theory describes some of the general properties of reflected and refracted shear waves in isotropic viscoelastic media.

INTRODUCTION

THIS paper is concerned with some theoretical relations involved in a method for measuring the shear wave parameters of viscous liquids at ultrasonic frequencies. The experimental details are described in a companion paper by W. P. Mason *et al.*, in this issue. The method is based on the measurement of a reflection coefficient for plane shear waves in an elastic solid, reflected obliquely from a plane interface of the solid and the liquid which is being investigated. A pulsing technique is used to separate the reflections of different orders at the detecting crystal, and the primary shear waves are suitably polarized so that reflection does not produce compressional waves in addition to the reflected shear waves. The complex reflection coefficient is measured by comparing the amplitudes and phases of waves reflected from the solid-liquid interface and from the same surface when the liquid is absent. Compared with normal incidence methods which had been developed previously, the oblique incidence method possesses some experimental advantages, resulting in greater accuracy of measurement, but oblique incidence involves more complicated relationships between the reflection coefficient and the constants of the two media. Solutions for these relations are derived in this paper. The theory describes some of the general properties of plane shear waves in viscoelastic media.

The elements of the system, omitting the elec-

tronic equipment, are shown in Fig. 1. A fused quartz rod with obliquely cut ends has a plane upper surface, which is covered in one part of the test by a thin layer of the liquid under investigation. This surface will be taken as the plane $y=0$ in a system of rectangular x, y, z coordinates, with the z axis perpendicular to the plane of Fig. 1. A suitably oriented Y cut quartz crystal at one end of the rod generates plane shear waves with the displacements in the z direction, and a similar crystal at the other end is used as a detector. The waves are reflected repeatedly at the upper surface and at both ends of the rod, but a pulsing system separates the reflections of different order at the detector. The primary displacement is parallel to the reflecting surfaces and perpendicular to the direction of propagation, and does not vary appreciably across the width of the rod. Hence, the displacements in the reflected and refracted waves also have these properties, and there are practically no compressional components. At ultrasonic frequencies the attenuation in the liquid is so large that a relatively thin layer of the liquid is equivalent to an infinite medium, as regards the effects in the quartz. The measurements indicate that the amplitude and phase of the detector output are practically independent of the thickness of the liquid until the thickness is reduced to a value of the order of 0.001 cm.

SHEAR WAVES IN A VISCOELASTIC MEDIUM

The response of a liquid to shearing stress is an essentially viscous flow if the stress is constant or varies slowly enough, but a liquid may also have a partly elastic character in shear which affects the behavior at high frequencies. The combined viscous and elastic properties can be represented by distributed mechanical admittances or impedances which are complex functions of frequency. T. Alfrey has described the impedance method of representing such properties for a general class of linear viscoelastic media such that the stress-strain relations obey the superposition principle.[1-3] When a medium satisfies this restriction, it is characterized by a set of linear relations between the stresses and the strains and their time derivatives, which may be of various orders. The linear relations are analogous to the voltage-current relations for a passive linear electrical network and they can be expressed in forms similar to the network equations, involving operators which become equivalent to complex impedances or admittances when the disturbance is assumed to be proportional to a complex time factor $e^{i\omega t}$. In particular, for an isotropic linear viscoelastic medium, the typical relation between shearing stress and shearing strain can be expressed in either of the forms

$$T_{zz}=\zeta\dot{S}_{zz} \quad \text{or} \quad YT_{zz}=\dot{S}_{zz}=\partial S_{zz}/\partial t, \tag{1}$$

T_{zz} denotes the shearing stress corresponding to the shearing strain $S_{zz}=\partial\xi_z/\partial z+\partial\xi_z/\partial x$, where ξ_z is the displacement in the z direction, and Y and ζ are operators which are reciprocal functions of the operator $\partial/\partial t$. For a disturbance proportional to $e^{i\omega t}$, Y and ζ are functions of $i\omega$, as $\partial/\partial t$ is then equivalent to $i\omega$. A special case of Eqs. (1) represents purely viscous flow; in this case, Y and ζ are real and $\zeta=\eta=1/Y$, where η is the (shear) viscosity. For a strictly elastic solid of rigidity $\mu=1/s$,

$$T_{zz}=\mu S_{zz}=\zeta\partial S_{zz}/\partial t, \quad \zeta\partial/\partial t=\mu, \quad Y=s\partial/\partial t,$$

and, when $\partial/\partial t=i\omega$, $\zeta=\mu/i\omega$, $Y=i\omega s=1/\zeta$.

In general, when $\partial/\partial t$ is equivalent to $i\omega$, ζ and Y are complex and can be represented by

$$\begin{aligned}\zeta(i\omega)&=\eta+\mu/i\omega=\eta-i\mu/\omega=1/Y(i\omega),\\ Y(i\omega)&=\nu+i\omega s=1/\eta'+i\omega/\mu'=1/\zeta(i\omega),\end{aligned} \tag{2}$$

where $\eta, \mu, \nu, s, \eta', \mu'$ are real and may all be functions of frequency. If stress is considered to be analogous to voltage and rate of change of strain as analogous to current, ζ corresponds to an impedance operator or complex impedance and Y is the corresponding admittance operator or complex admittance. At a given frequency, η and η' are two different types of effective viscosities and μ and μ' are different types of effective rigidities, such that η and $1/\mu$ correspond, respectively, to resistance and capacitance in series, and η' and $1/\mu'$ correspond to resistance and capacitance in parallel. The values of η, μ, η', μ' may vary with frequency, but they are always ≥ 0. If the phase angles of the complex ζ and Y are denoted by $\arg\zeta$ and $\arg Y$,

$$\begin{aligned}&\zeta(i\omega)=|\zeta|e^{i\arg\zeta}, \quad Y(i\omega)=|Y|e^{i\arg Y}\\ &-\arg\zeta=\arg Y=\tan^{-1}Q,\\ &Q=\mu/\omega\eta=\omega s/\nu=\eta'\omega/\mu'\geq 0\\ &-\pi/2\leq\arg\zeta\leq 0\leq\arg Y\leq\pi/2.\end{aligned} \tag{3}$$

For different materials, or for a given material at varying frequency, the properties become relatively more elastic and less viscous as Q increases. As shown above, Q increases with μ/ω and with η' but

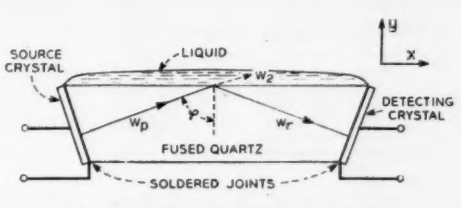

FIG. 1. Experimental arrangement.

[1] T. Alfrey, Jr., *Mechanical Behavior of High Polymers* (Interscience Publishers, Inc., New York, 1948).
[2] T. Alfrey, Jr., "Non-homogeneous stresses in viscoelastic media," Quart. App. Math. **2**, 113 (1944).
[3] T. Alfrey, Jr., "Methods of representing the properties of viscoelastic materials," Quart. App. Math. **3**, 143 (1945).

decreases as μ'/ω and η increase. If η' and μ' are independent of frequency, Q is proportional to frequency and is equal to unity at the relaxation frequency $f_r=\mu'/2\pi\eta'$; the viscous effect tends to predominate at frequencies below f_r and the elastic effect at frequencies above f_r.

The stress subscripts can be assigned so that positive T_{zz} represents a stress directed toward increasing z, acting on a part of the medium which has an outward normal directed toward increasing x. The stresses T_{zz} and T_{xx} are equal at any point, and positive T_{zz} denotes a tension. If ρ is the density and $D_x=\partial/\partial x$, the equation of motion in the z direction is

$$D_xT_{xz}+D_yT_{yz}+D_zT_{zz}=\rho D_t^2\xi_z=\rho D_tw=\rho\partial w/\partial t,$$

where w is the particle velocity in the z direction.

For a disturbance in an isotropic viscoeleastic medium such that the displacement is in the z direction and independent of z, the strains which do not vanish are $S_{xz}=D_x\xi_z$ and $S_{yz}=D_y\xi_z$, the tension T_{zz} is equal to zero, and the above equations result in the relations

$$\begin{aligned}&\dot{S}_{xz}=D_xw=YT_{xz},\quad \dot{S}_{yz}=D_yw=YT_{yz},\\ &D_xT_{xz}+D_yT_{yz}=\rho D_tw,\quad (D_x^2+D_y^2)w=\rho D_tYw.\end{aligned}\tag{4}$$

If w is independent of both y and z in Eqs. (4), the stress T_{yz} vanishes and

$$D_xw=YT_{xz},\quad D_xT_{xz}=\rho D_tw.$$

These equations are analogous to the voltage-current relations for an electrical transmission line. If current is now regarded as analogous to particle velocity instead of to strain rate, with voltage corresponding to stress as before, the density ρ corresponds to series inductance per unit length of the equivalent line and Y corresponds to the shunt admittance operator or complex shunt admittance per unit length. In Eqs. (2), the reciprocal viscosity $\nu=1/\eta'$ corresponds to shunt conductance per unit length and the compliance $s=1/\mu'$ to shunt capacitance per unit length. If η' and μ' are independent of frequency, the elements of the equivalent line are as indicated in Fig. 2. If η and μ are constant, the equivalent line is as shown in Fig. 3.

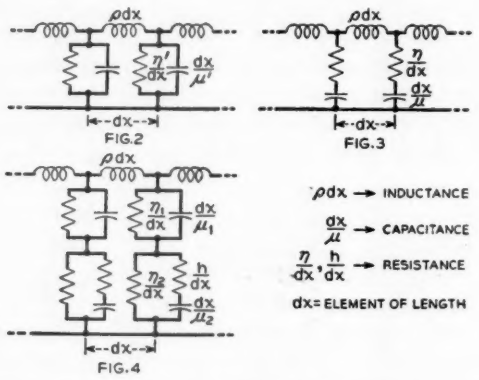

FIGS. 2, 3, and 4. Equivalent circuits.

Measurements described in a recent paper[4] indicate that certain long chain polymer liqiuds have shear properties at frequencies below 10^5 c.p.s. which correspond approximately to equivalent lines of the type shown in Fig. 2, with constant η' and μ'. Later measurements have been extended to 60 megacycles and show more complicated effects, which are described in the companion paper in this issue. In the larger frequency range, the shear properties of the long chain polymer liquids correspond more nearly to the equivalent line shown in Fig. 4, instead of the one in Fig. 2. The numerical values involved are such that the two circuits are nearly equivalent in the lower part of the frequency range. In Fig. 4, h denotes a resistance element which is inversely proportional to frequency; it represents approximately some effects due to a hysteresis type of nonlinearity in the stress-strain relations.[5]

When the motion is assumed to be proportional to $e^{i\omega t}$, the last Eq. (4) becomes

$$(D_x^2+D_y^2)w=\Gamma^2w,$$

where $\Gamma^2=i\omega\rho Y$. For motion independent of both y and z, this equation reduces to $D_x^2w=\Gamma^2w$, which has the general solution $w=(Ke^{-\Gamma x}+K'e^{\Gamma x})e^{i\omega t}$. From the first Eq. (4), the corresponding stress is

$$T_{xz}=Z(-Ke^{-\Gamma x}+K'e^{\Gamma x})e^{i\omega t},\text{ where } Z=\Gamma/Y.$$

Γ is the characteristic propagation constant of the medium and Z is the characteristic impedance for plane shear waves. They satisfy the relations

$$\begin{aligned}&\Gamma=YZ=i\omega\rho/Z=(i\omega\rho Y)^{\frac{1}{2}}=\alpha+i\beta,\\ &\qquad\qquad\beta=\omega/c=2\pi/\lambda,\\ &Z=\Gamma/Y=i\omega\rho/\Gamma=(i\omega\rho/Y)^{\frac{1}{2}}=R+iX,\end{aligned}\tag{5}$$

where α, β, R, and X are real; α is an attenuation constant, β is a phase constant, c is a phase velocity, and λ is a wave-length. The velocity c is always different from zero, and the sign of Γ is chosen so that β and c are positive. The phase angle of Γ is therefore in the range 0 to π and, as a result of (3),

$$\begin{aligned}&0\leq\arg Z\leq\pi/4\leq\arg\Gamma\leq\pi/2,\\ &0\leq X\leq R,\quad 0\leq\alpha\leq\beta.\end{aligned}\tag{6}$$

One limiting case corresponds to a strictly elastic medium, for which

$$\begin{aligned}&Y=i\omega/\mu,\quad \alpha=0,\quad \beta=\omega/c,\quad c=(\mu/\rho)^{\frac{1}{2}},\\ &Z=R=\rho c,\quad X=0.\end{aligned}$$

[4] W. P. Mason, W. O. Baker, H. J. McSkimin, and J. H. Heiss, "Mechanical properties of long chain molecule liquids at ultrasonic frequencies," Phys. Rev. **73**, 1074 (1948).

[5] W. P. Mason, *Piezoelectric Crystals and Applications to Ultrasonics*, Chap. 12, Appendices A.8, A.9; in process of publication.

In the other extreme, for strictly viscous flow,

$$Y=1/\eta, \quad \alpha=\beta=(\omega\rho/2\eta)^{\frac{1}{2}}, \quad c=(2\eta\omega/\rho)^{\frac{1}{2}},$$
$$R=X=(\omega\rho\eta/2)^{\frac{1}{2}}.$$

For a progressive plane shear wave advancing toward increasing x, the particle velocity and stress are (the real parts of)

$$w=w_0e^{-\Gamma x}=Ke^{-\alpha x+i(\omega t-\beta x)}, \quad T_{xz}=-Zw. \quad (7)$$

The negative sign in the last equation is a consequence of the stress sign conventions described previously. T_{xz} is a stress across a plane $x=$ constant, parallel to the wave fronts, and the part of the medium on the forward or increasing x side of this plane is acted upon by a stress which has the same direction as positive w when T_{xz} is negative; this corresponds to a positive value of (the real part of) $-T_{xz}=Zw$.

For shear waves such that the motion in the z direction may vary with both x and y, the particle velocity and stresses satisfy Eqs. (4). When this motion is assumed to be proportional to $e^{i\omega t}$, $\rho D_t Y$ is equivalent to Γ^2 and $Y=\Gamma/Z$. Hence, Eqs. (4) are then equivalent to

$$(D_x^2+D_y^2)w=\Gamma^2w, \quad (8)$$

$$T_{xz}=Z\Gamma^{-1}D_xw, \quad T_{yz}=Z\Gamma^{-1}D_yw. \quad (9)$$

A typical solution of Eq. (8) is

$$w_p=w_0e^{-Gx-Hy}=w_0e^{-\Gamma(mx+ny)}, \quad (10)$$

where

$$G^2+H^2=\Gamma^2, \quad m^2+n^2=1.$$

G and H are auxiliary propagation constants for the x and y directions and can have arbitrary complex values, subject to the boundary conditions and the restriction $G^2+H^2=\Gamma^2$. The corresponding restriction on m and n is $m^2+n^2=1$, and because of this equation, m and n can be represented by $m=\sin\varphi$ and $n=\cos\varphi$. However, φ is not necessarily a real angle, as m and n can, in general, be complex. If φ is real, $mx+ny$ is a real distance which increases in the direction of propagation and Eqs. (7) and (10) then represent waves of the same type traveling in different directions. The characteristics of waves such that φ is complex will be considered later.

REFLECTION AND REFRACTION OF PLANE SHEAR WAVES

Assume that the plane $y=0$ is a common boundary of two isotropic viscoelastic media. One of these may be an essentially elastic solid and the other a liquid, as in the system described in the introduction. Let subscripts 1 and 2 refer to the negative y and positive y regions, respectively, and with Γ replaced by Γ_1, let Eqs. (10) represent a primary wave generated by suitable motion of a boundary in a plane $mx+ny=$ constant, where $m=\sin\varphi$, $n=\cos\varphi$, and $0\leq\varphi\leq\pi/2$. The real angle φ is then equal to the angle of incidence relative to the normal to the $y=0$ interface. The primary wave is partially reflected at the interface, and a refracted wave is transmitted into the second medium. Since the displacement of the interface caused by the primary wave is in the plane of the interface and is independent of distance in the direction of the displacement, the reflected and refracted disturbances are non-dilatational and the displacements in these waves are also parallel to the z axis and independent of z. Hence, in the absence of reflections from other surfaces, the resultant particle velocities and stresses satisfy Eqs. (8) and (9), when the appropriate values are assigned to Γ and Z for each medium. The sum of the primary and reflected particle velocities must be equal to the refracted particle velocity at the $y=0$ interface if there is no slip at this surface, and the stress across planes parallel to the interface must also be continuous at the interface.

The boundary conditions at $y=0$ can be satisfied if the particle velocities in the two media are proportional to the same function of x, and the wave equation for the first medium will be satisfied if the primary and reflected particle velocities are proportional to the same function of x and to functions of y in which the coefficients of y differ only in sign. The resultant particle velocity in the first medium will then have the form

$$w_1=w_0e^{-Gx}(e^{-Hy}+re^{Hy}), \quad G=\Gamma_1m, \quad H=\Gamma_1n. \quad (11)$$

At $y=0$,

$$w_1=(1+r)w_0e^{-Gx}.$$

The refracted particle velocity w_2 will satisfy the wave equation for the second medium and the boundary condition $w_1=w_2$ at $y=0$ if

$$w_2=\tau w_0e^{-Gx-H_2y}, \quad \tau=1+r, \quad (12)$$

$$H_2=(\Gamma_2^2-G^2)^{\frac{1}{2}}=(\Gamma_2^2-\Gamma_1^2m^2)^{\frac{1}{2}}=\alpha_y+i\beta_y, \quad (13)$$

where α_y and β_y are real, representing an attenuation constant and a phase constant of the refracted wave for the y direction.

To represent attenuation and propagation of phase in the direction away from the interface, toward increasing y, α_y and β_y must both be positive, and therefore the imaginary part of H_2^2 must also be positive. In terms of the "characteristic" attenuation and phase constants of the two media,

$$H_2^2=(\alpha_2+i\beta_2)^2-(\alpha_1+i\beta_1)^2m^2$$
$$=(\beta_1^2-\alpha_1^2)m^2-(\beta_2^2-\alpha_2^2)+i2(\alpha_2\beta_2-\alpha_1\beta_1m^2)$$
$$=\alpha_y^2-\beta_y^2+i2\alpha_y\beta_y,$$
$$\alpha_y\beta_y=\alpha_2\beta_2-\alpha_1\beta_1m^2=2\pi(\alpha_2/\lambda_2-m^2\alpha_1/\lambda_1). \quad (14)$$

To make $\alpha_y\beta_y$ positive for all angles of incidence, it will be assumed that the refracting medium has the

larger attenuation per wave-length, $\alpha_2/\lambda_2 > \alpha_1/\lambda_1$. This restriction is satisfied by the experimental system indicated in Fig. 1, as the attenuation per wave-length in fused quartz is negligible in comparison with the attenuation per wave-length in a liquid. (Other cases are discussed in an appendix of this paper.)

The solution for the refracted particle velocity can be expressed in another form by letting $G=\Gamma_2 M$ and $H_2=\Gamma_2 N$. Then $M^2+N^2=1$. Hence, M and N are equivalent to the sine and cosine of an angle, not necessarily real. Separating the primary and reflected components of w_1, Eqs. (11) and (12) are equivalent to the following set of equations:

$$\begin{aligned} w_p &= w_0 e^{-\Gamma_1(mx+ny)}, & w_r &= rw_0 e^{-\Gamma_1(mx-ny)}, \\ w_1 &= w_p + w_r, & w_2 &= \tau w_0 e^{-\Gamma_2(Mx+Ny)}, \end{aligned} \tag{15}$$

$$\begin{aligned} m &= \sin\varphi, & n &= \cos\varphi, \\ M &= \sin\psi = m\Gamma_1/\Gamma_2, & N &= \cos\psi = H_2/\Gamma_2. \end{aligned} \tag{16}$$

The angle of reflection is equal to the angle of incidence, φ, and in special cases such that ψ is real, ψ is the angle of refraction. However, ψ is generally complex.

Equations (9) and (15) result in the following formulas for the stresses in the two media, and the values of T_{yz} lead to a second relation between the reflection coefficient r and the transmission coefficient $\tau=1+r$.

$$\begin{aligned} &\text{When } y\leq 0, \\ &\quad T_{zz} = -mZ_1 w_1, \quad T_{yz} = -nZ_1(w_p - w_r). \\ &\text{When } y\geq 0, \\ &\quad T_{zz} = -MZ_2 w_2, \quad T_{yz} = -NZ_2 w_2. \end{aligned} \tag{17}$$

As T_{yz} is a stress across a plane $y=$ constant, parallel to the interface, this stress must be continuous at $y=0$, and as a result of Eqs. (11), (12), and (17), the stress across the interface itself is given by either of the formulas

$$T_{yz}(x, 0) = -nZ_1(1-r)w_0 e^{-Gx} = -NZ_2 \tau w_0 e^{-Gx}. \tag{18}$$

Hence,

$$nZ_1(1-r) = NZ_2\tau = NZ_2(1+r). \tag{19}$$

The reflection and transmission coefficients therefore have the following values:

$$\begin{aligned} r &= (nZ_1 - NZ_2)/(nZ_1 + NZ_2) \\ &= (Z_1\cos\varphi - Z_2\cos\psi)/(Z_1\cos\varphi + Z_2\cos\psi), \\ \tau &= 1+r = 2nZ_1/(nZ_1+NZ_2). \end{aligned} \tag{20}$$

The stress T_{zz} is not necessarily continuous at the interface. Since $w_1=w_2$ at $y=0$, Eqs. (17) indicate that as the interface is approached from opposite sides, the values of T_{zz} approach two limits the ratio of which is mZ_1/MZ_2. Because of Eqs. (16) and (5), this ratio is also equal to $\Gamma_2 Z_1/\Gamma_1 Z_2 = Y_2/Y_1$, which is generally different from unity. The value of this ratio does not depend on the direction of propagation.

The product NZ_2 which appears in the solution for the reflection coefficient is the impedance of the second medium for the refracted wave per unit area of the interface $y=0$ or of any plane $y=$ constant. This is shown by the last Eq. (17). Similarly, if there were no reflection at $y=0$, nZ_1 would be the impedance of the first medium for the primary wave per unit area of a plane $y=$ constant. The negative signs in Eqs. (17) are due to reasons similar to those discussed in connection with the sign of the stress in the last Eq. (7).

When ψ is complex, the refracted wave is a disturbance of a different type from an ordinary plane wave such as the one represented by Eqs. (7). Some of the properties of the refracted wave can be investigated by resolving the quantity $Gx+H_2y$ into its real and imaginary parts. Some of the sign relations involved will be utilized later in the application of the theory to the experimental measurements. With α_y and β_y both positive in Eqs. (13), the phase angle of H_2 is between zero and $\pi/2$, and from (3) and (16) it then follows that

$$-\pi/4 \leq \arg M \leq \pi/4, \quad -\pi/2 \leq \arg N \leq \pi/4.$$

Hence, the real parts of M and N are ≥ 0. Let $\psi = A+iB$ where A and B are real. Then, from (16),

$$\begin{aligned} N &= \cos\psi = \cos A\,\cosh B - i\sin A\,\sinh B; \\ M &= \sin\psi = \sin A\,\cosh B + i\cos A\,\sinh B \\ &= m\Gamma_1/\Gamma_2 = m[(\alpha_1+i\beta_1)/(\alpha_2+i\beta_2)] \\ &= m\{[(\alpha_1\alpha_2+\beta_1\beta_2)+i\beta_1\beta_2(\alpha_2/\beta_2-\alpha_1/\beta_1)]/ \\ &\qquad [\alpha_2^2+\beta_2^2]\}. \end{aligned} \tag{21}$$

Since $\cosh B \geq 1$ and the real parts of M and N are ≥ 0, $\sin A$ and $\cos A$ are also ≥ 0 and $0 \leq A \leq \pi/2$. B has the same sign as $m(\alpha_2/\beta_2 - \alpha_1/\beta_1)$. For the case corresponding to the experimental measurements, $\alpha_1/\beta_1 \ll \alpha_2/\beta_2 < 1$, hence B and the imaginary part of M are positive and the imaginary part of N is negative, providing $m \neq 0$. For normal incidence, $m=0=M$. An additional restriction on A results from the relations $\sin A \leq |M| < |\Gamma_1|/\beta_2$, and when α_1 is small, $|\Gamma_1|/\beta_2 \approx \beta_1/\beta_2 = c_2/c_1$. In the experimental system, the velocity ratio c_2/c_1 is small, certainly less than 0.7, hence $0 \leq A < \pi/4$. This result will be useful later.

Multiplying the above values of M and N by $\Gamma_2 = \alpha_2 + i\beta_2$, it can be shown that

$$\begin{aligned} G &= \Gamma_2 M = \alpha' \sin(A-a) + i\beta' \sin(A+b), \\ H_2 &= \Gamma_2 N = \alpha' \cos(A-a) + i\beta' \cos(A+b), \\ \alpha' &= [\alpha_2^2 + (\alpha_2^2+\beta_2^2)\sinh^2 B]^{\frac{1}{2}}, \\ \beta' &= [\beta_2^2 + (\alpha_2^2+\beta_2^2)\sinh^2 B]^{\frac{1}{2}}, \\ a &= \tan^{-1}[(\beta_2/\alpha_2)\tanh B], \\ b &= \tan^{-1}[(\alpha_2/\beta_2)\tanh B]. \end{aligned}$$

Then

$$\begin{aligned} Gx + H_2 y &= \alpha' x' + i\beta' y', \\ x' &= x\sin(A-a) + y\cos(A-a), \\ y' &= x\sin(A+b) + y\cos(A+b). \end{aligned}$$

Substituting these results in (12) and letting $w_0=Ke^{i\omega t}$, the refracted particle velocity has the form

$$w_2=\tau Ke^{-\alpha' x'+i(\omega t-\beta' y')}.$$

These equations indicate that α' is the effective attenuation constant, β' the effective phase constant, and ω/β' the effective phase velocity of the refracted wave; x' and y' are real distances measured in certain directions such that $x'=$constant represents a plane of uniform amplitude and $y'=$constant represents a plane of uniform phase. In general, these two sets of planes are not parallel. Hence, the amplitudes are generally non-uniform over any wave front; x' increases in the direction of the greatest rate of attenuation and y' increases in the direction of propagation of phase. The angles between these directions and the direction of increasing y are $A-a$ and $A+b$, respectively. Thus when ψ is complex there are two angles of refraction, one for the direction of propagation, $A+b$, and one for the direction of greatest attenuation, $A-a$. The angles a and b are of like sign, with the same sign as B and therefore the same sign as $\alpha_2/\beta_2-\alpha_1/\beta_1$. The effective attenuation α' per unit distance is greater than the "characteristic" attenuation α_2 and the velocity of propagation is ω/β', which is less than the characteristic velocity of propagation ω/β_2.

EVALUATION OF THE CONSTANTS OF THE REFRACTING MEDIUM

In the system of measurements described in the introduction, the reflection coefficient r is measured experimentally and the preceding theory then leads to solutions for the constants of the refracting medium in terms of the known quantities. With reflections of different orders separated by means of a pulsing method, the reflection coefficient is measured by comparing waves reflected from the interface between the two media with waves reflected from the same surface when the refracting medium is absent. In the latter case, the stress across the reflecting surface is zero and Eq. (18) indicates that the reflection coefficient is then equal to unity. Hence, from Eqs. (15) the particle velocity in the wave reflected from the free boundary is $w_f=w_0e^{-\Gamma_1(mx-ny)}$. With the refracting medium present, r is different from unity and the particle velocity in the reflected wave is $w_r=rw_f$ for equivalent primary waves in the two cases. Hence the complex reflection coefficient r can be evaluated by comparing the amplitudes and phases of w_r and w_f. If $p=mx-ny=$distance in the direction of propagation of the reflected waves,

$$w_f=w_0e^{-\Gamma_1 p}=Ke^{i\omega t-(\alpha_1+i\beta_1)p}=|w_f|e^{i(\omega t-\beta_1 p)},$$
$$w_r=rw_f=|w_r|e^{i(\omega t-\beta_1 p-\theta)},$$
$$r=w_r/w_f=Re^{-i\theta},\ \text{where}\ R=|w_r/w_f|=|r|. \quad (22)$$

R is the relative reduction in amplitude and θ the phase shift of the reflected waves caused by the presence of the refracting medium. If θ is positive, the phase shift is equivalent to an increase of $\beta_1 p$ and therefore corresponds either to an increase of the effective transmission distance p, or to an increase of frequency, as β_1 increases with frequency.

When the reflection coefficient r, angle of incidence φ, and characteristic impedance Z_1 are known, the value of the "refracted wave impedance" NZ_2 can be calculated by means of Eqs. (19) and (22):

$$NZ_2=Z_1n[(1-r)/(1+r)]=Z_1nq, \quad (23)$$

where

$$\begin{aligned}q&=(1-r)/(1+r)\\&=(1-R^2+i2R\sin\theta)/(1+R^2+2R\cos\theta)\\&=[(1+R^2-2R\cos\theta)/(1+R^2+2R\cos\theta)]^{\frac{1}{2}}\\&\quad\times\exp[i\tan^{-1}(2R\sin\theta/(1-R^2))]. \quad (24)\end{aligned}$$

The value of q corresponding to a given complex value of r can also be derived in other ways. Let the amplitude ratio in nepers be denoted by

$$L=\log_e|w_f/w_r|=-\log_e R.$$

Then

$$r=Re^{-i\theta}=e^{-L-i\theta},$$
$$q=\tanh[(L+i\theta)/2]=i\tan[(\theta-iL)/2].$$

Thus q can be evaluated by means of Eqs. (24) or by means of charts of complex hyperbolic or circular tangents, such as Kennelly's charts.[6]

If the densities of the two media are known, besides the values of r, φ, and Z_1, separate solutions for Z_2 and N and the other constants of the system can be derived by the following method, based on preliminary evaluation of $\sin2\psi$ and $\cos2\psi$ from the known data. From Eqs. (5), (16), and (23):

$$m=\sin\varphi,\quad n=\cos\varphi,\quad 2mn=\sin2\varphi;$$
$$M=\sin\psi=m\Gamma_1/\Gamma_2=mkZ_2/Z_1,$$

where $k=\rho_1/\rho_2$;

$$N=\cos\psi=qnZ_1/Z_2=qnk\Gamma_2/\Gamma_1;$$
$$2MN=\sin2\psi=2mnkq=qk\sin2\varphi. \quad (25)$$

Except for an ambiguity of sign, the value of $\cos2\psi$ is then given by $\pm(1-\sin^2 2\psi)^{\frac{1}{2}}$. The sign can be determined with the aid of the formula,

$$\cos2\psi=\cos2A\cosh2B-i\sin2A\sinh2B.$$

It was shown previously that in the experimental system, $0\leq A\leq\pi/4$ and $B\geq0$. Hence the real part of $\cos2\psi$ is ≥0 and the imaginary part is ≤0.

The different steps involved in the solutions can

[6] A. E. Kennelly, *Chart Atlas of Complex Hyperbolic and Circular Functions* (Harvard University Press, Cambridge, 1914).

now be summarized as follows:

$$r=|w_r/w_f|e^{-i\theta},\quad q=(1-r)/(1+r),\quad k=\rho_1/\rho_2;$$
$$\sin 2\psi=qk\sin 2\varphi.$$

If $\varphi>0$:

$$\cos 2\psi=[1-\sin^2 2\psi]^{\frac{1}{2}},$$
real part >0, imaginary part <0; (26)
$$M=\sin\psi=[(1/2)(1-\cos 2\psi)]^{\frac{1}{2}},$$
real part >0, imaginary part >0;
$$N=\cos\psi=[(1/2)(1+\cos 2\psi)]^{\frac{1}{2}},$$
real part >0, imaginary part <0.

If $\varphi=0$, $\psi=0$, $M=0$, and $N=1$. The characteristic impedance and propagation constant of the refracting medium can now be evaluated by means of the alternative formulas:

$$Z_2=Z_1M/mk=Z_1nq/N=i\omega\rho_2/\Gamma_2,$$
$$\Gamma_2=\Gamma_1m/M=\Gamma_1N/nkq=i\omega\rho_2/Z_2. \quad (27)$$

The "characteristic" attenuation constant is the real part of $\Gamma_2=\alpha_2+i\beta_2$, the "characteristic" velocity of propagation is ω/β_2, and the viscoelastic admittance Y_2 and impedance ζ_2 have the values $Y_2=\Gamma_2/Z_2$ and $\zeta_2=Z_2/\Gamma_2$. Separating these into their real and imaginary parts leads to the values of the effective viscosities and effective elastic parameters defined by Eqs. (2). For most viscous liquids, the "parallel" viscosity η' and stiffness μ', and their reciprocals ν and s, will probably be approximately independent of frequency in a fairly wide frequency range; this will not be true of the "series" viscosity η and stiffness μ.

Measurements have been made on a number of viscous liquids covering a large range of viscosities. In each case, $|\sin 2\psi|$ was small relative to unity, and therefore some simple approximations could be used in Eqs. (26) and (27). With the rules given previously to determine the signs, it follows that when $|\sin 2\psi|\ll 1$:

$$\cos 2\psi=[1-\sin^2 2\psi]^{\frac{1}{2}}=1-(1/2)\sin^2 2\psi-\cdots,$$
$$N=\cos\psi=[1/2(1+\cos 2\psi)]^{\frac{1}{2}}$$
$$=1-(1/8)\sin^2 2\psi-\cdots,$$
$$M=\sin\psi=(\sin 2\psi)/(2N)=(1/2)\sin 2\psi+\cdots.$$

For all of the preliminary measurements, the values of $|\sin 2\psi|$ did not exceed 0.2. Hence, N differed from unity by less than two percent. In such cases, Eqs. (27) are very nearly equivalent to the approximations

$$Z_2\approx Z_1nq=[(1-r)/(1+r)]Z\cos\varphi,$$
$$\Gamma_2\approx\Gamma_1/nkq=[\rho_2/\rho_1][\Gamma_1/\cos\varphi][(1+r)/(1-r)]. \quad (28)$$

These approximations will probably be sufficiently accurate for most of the materials likely to be investigated by the oblique incidence method. If the factors $\cos\varphi$ and $1/\cos\varphi$ are omitted in Eqs. (28), these equations have the same forms as the rigorous solutions for normal incidence, but the reflection coefficient r will, of course, have different values for oblique and normal incidence.

APPENDIX

In the theory of refraction derived in this paper, it is assumed that the refracting medium has the larger attenuation per wave-length, in order that the assumed solution for the refracted wave may have appropriate directions of attenuation and propagation of phase. This restriction is satisfied in the experimental system which has been described, as the attenuation in the fused quartz is practically negligible. However, the necessity for the restriction indicates that the equations which have been given do not represent a complete solution for all cases and a question arises concerning the conditions under which the assumed solution is sufficiently accurate. The distinction between the different cases can be explained by the existence of diverging waves which are unimportant in some cases but not in others. In order to derive a complete solution for all cases, it would be necessary to take account of the nature of the source and some associated features of other boundary conditions which were not mentioned previously.

The primary wave represented by the first Eq. (15) can be regarded as generated by motion of a boundary of the first medium occupying part or all of a semi-infinite plane $mx+ny=C=$constant, which meets the boundary $y=0$ at $x=x_0=C/m$. If the entire semi-infinite plane is assumed to have a suitable forced motion, the boundary conditions specified previously apply only to the part of the plane $y=0$ for which $x>x_0$. The second medium must then have an additional boundary where other conditions apply; this may be the rest of the plane $y=0$, or it may be some other boundary—for example, the plane $x=x_0$. In some cases it may be permissible to ignore the additional boundary conditions, but this will not always be true. If the source is assumed to occupy the entire semi-infinite plane $mx+ny=C$, there will be additional complications caused by secondary reflections at the source.

Under certain conditions the problem will be simplified if it is assumed that only part of the plane $mx+ny=C$ is driven, so that the primary disturbance consists of a beam in which the wave fronts are essentially plane, but are of finite width in the direction perpendicular to the z axis. This neglects the effects of divergence at the sides of the beam, which is permissible as regards the primary beam if the width of the driving surface is sufficiently large relative to the wave-length. Then in

some cases, the reflected and refracted disturbances may also consist principally of non-divergent beams, in which the wave fronts are essentially plane. This will tend to be the case if the attenuation is small in the first medium, or in both media, the latter case being analogous to a well-known case of optical reflection and refraction. The solutions for such cases can be represented with sufficient accuracy by Eqs. (15), within the limits of the respective beams. However, a fundamentally different situation may occur if the attenuation in the first medium is relatively large. If the primary wave is represented by the first Eq. (15), within a limited beam, there will be a restricted part of the $y=0$ interface, say the region $x_a<x<x_b$, where the primary particle velocity is

$$w_0 e^{-\Gamma_1 m x} = w_0 e^{-(\alpha_1+i\beta_1)x\sin\varphi}.$$

This is proportional to the real function $e^{-\alpha_1 x \sin\varphi}$ and if $\alpha_1 \sin\varphi$ is large enough, the forced motion of the interface in the vicinity of $x=x_a$ will have the predominant effect, resulting in diverging secondary disturbances in both media, with wave fronts which tend to be cylindrical. Furthermore, if the characteristic attenuation of the second medium is small, then in the vicinity of the plane $y=0$ at sufficient distance from $x=x_a$ the diverging disturbance in the second medium will tend to have a greater intensity than the primary intensity at nearby points on the other side of the interface. Hence, in such a region, the resultant direction of propagation in the second medium will have a component toward the interface instead of away from it. This direction of propagation cannot apply throughout the second medium, of course, especially near $x=x_a$, but in a limited region, the refracted disturbance may correspond approximately to Eqs. (12) and (13), with positive α_y and negative β_y. The region in which this situation exists will become larger as the distance between x_a and x_b increases, but x_a cannot be assumed to approach $-\infty$, as the amplitudes would then be infinite at $x=-\infty$. To derive a general rigorous solution it would be necessary to modify the boundary conditions, taking into account the fact that the primary wave function does not apply to all values of x. The rigorous solution would be very complicated at best.

Equations (14) indicate that the criteria which determine whether the divergent effects are important or not are the angle of incidence and the attenuations per wave-length in the two media. The equation can be expressed in the form

$$\alpha_y\beta_y = \alpha_1\beta_1(m_c^2 - \sin^2\varphi),$$

where

$$m_c^2 = \alpha_2\beta_2/\alpha_1\beta_1 = (\alpha_2/\alpha_1)(c_1/c_2) = (\alpha_2/\lambda_2)/(\alpha_1/\lambda_1).$$

c_1 and c_2 denote the characteristic velocities of propagation in the two media. If the second medium has the larger attenuation per wave-length, $m_c^2>1$ and $\alpha_y\beta_y>0$ for all angles of incidence. For transmission in the reverse direction, the second medium has the smaller attenuation per wave-length, $m_c^2<1$, and $\alpha_y\beta_y$ is positive or negative according as the angle of incidence is less than or greater than the critical angle $\varphi_c=\sin^{-1}m_c$. It seems probable that the solutions derived in this memorandum will be reasonably accurate whenever m_c^2 is large relative to $\sin^2\varphi$, which will be true for all angles of incidence if m_c^2 is large relative to unity. As m_c^2 and $\sin^2\varphi$ approach equality, the formulas become inaccurate as a result of the increasing importance of the divergent effects.

Measurement of Shear Elasticity and Viscosity of Liquids at Ultrasonic Frequencies

W. P. MASON, W. O. BAKER, H. J. MCSKIMIN, AND J. H. HEISS
Bell Telephone Laboratories, Murray Hill, New Jersey

(Received December 1, 1948)

It has long been suspected that if liquids were sheared sufficiently rapidly they would exhibit a shear elastic effect as well as a viscous effect. This supposition was verified recently by one of the writers (see reference 8) by employing a torsionally vibrating crystal and measuring the mechanical loading for the shear wave by observing the increased resistance at resonance and the change in the resonant frequency. By this method it was shown that long chain polymer liquids had shear configurational elasticities in the order of 10^7 dynes/cm^2.

The use of a torsional crystal is limited in frequency to about 2 to 3×10^6 cycles on account of the small sizes needed. In the present paper the range of shear wave measurements in liquids has been extended up to 60 megacycles by observing the effect, on a series of shear waves in a fused quartz rod, of terminating the rod by a thin layer of a liquid. The shear wave in the rod is altered in magnitude and phase by the boundary layer impedance of the liquid. By observing the reflection loss and the change in phase caused by the liquid layer, a measure is obtained of the shear impedance of the liquid. By employing a fused quartz rod for which the shear wave strikes the reflecting surface at an angle from the normal of about 79 degrees, the effect of the shear wave impedance on the boundary is greatly enhanced and a more accurate measurement obtained.

Both the torsional crystal and high frequency shear wave techniques applied to polyisobutylene and poly-α-methylstyrene liquids, show that there are two main relaxation frequencies in these liquids. At frequencies under 100 kc, the shear stiffness is in the order of 3×10^7 dynes/cm^2, while in the high megacycle range it has increased to 5×10^9 dynes/cm^2. The low shear elasticity appears to be associated with a composite motion of molecular rotation and translation that allows a configurational change to occur from the most probable chain shape. When the shear stress is removed, the molecule quickly returns to its most probable shape. This results in a low shear stiffness. At high frequencies this motion cannot take place, and the shear stiffness is determined by motions within single potential wells, and the value approaches that for a crystal. It is shown that the dispersion for longitudinal waves measured recently (see reference 11) is primarily due to the shear mechanisms investigated.

I. INTRODUCTION

IT HAS long been suspected that if liquids were sheared sufficiently rapidly, they would exhibit a shear elastic effect as well as a viscous effect. In fact, Maxwell,[1] on the basis of a gas model, predicted that an instantaneous shear distortion would have a relaxation time τ and a relaxation frequency f_τ given by the formulas

$$\tau=\eta/\mu;\ f_\tau=1/(2\pi\tau)=\mu/(2\pi\eta), \qquad (1)$$

where η is the shear viscosity and μ the shear elasticity. A similar result has recently been obtained by Frenkel[2] by assuming that a liquid has a short range order similar to a solid, and identifying the relaxation time τ as the mean life in a sedentary state. For ordinary light liquids, assuming a shear elasticity similar to a loosely knit crystal—about 10^{10} dynes per square centimeter—and a viscosity of about 0.01 poise, the relaxation frequency is in the order of 10^{11} cycles, which is considerably above any present day ultrasonic equipment.

However, if we use long chain polymer liquids, certain significant new effects appear. Long chain molecules are flexible, and can take up many different shapes. Certain coiled-up shapes are more probable than others and if a molecule is distorted from this shape, the molecule tends to return to it in a very short time when the stress is removed. This type of elasticity is called configurational elasticity, and the rapidity of regain of its most probable shape determines the relaxation time for such configurational elasticities.

When a shearing stress is put on such a molecule, segments of the molecule 20 to 30 chain atoms long are displaced from one configuration to another configuration which coincides with an empty space or hole in the liquid. A single segmental jump will have two effects on the polymer molecule. First, the shape of the molecule will be slightly altered by the motion of the segment, and second, the center of gravity of the molecule will be slightly shifted. The result of a large number of successive segmental jumps will likewise be twofold. First, the molecule will wriggle about from one shape to another, and second, the center of gravity will undergo a slow wandering. When these segment jumps are caused by the application of a shearing stress, the wandering of the center of gravity produces the viscous flow, while the change of shape from the most probable shape produces the shear configurational elasticity.

The flow of segments has to occur over certain energy barriers W, and hence the temperature variations of the viscosity of some polymers such as linear polyesters have been shown to satisfy an equation of the type

$$\eta_1=Ae^{BZ^1}e^{W/RT}, \qquad (2)$$

[1] J. Clark Maxwell, "On the Dynamical Theory of Gases," Phil. Trans. Roy. Soc. 157, 49–88 (1867).
[2] J. Frenkel, *Kinetic Theory of Liquids* (Oxford University Press, London, 1946), Chapter IV, pp. 196–200.

where W is the free energy barrier, R the gas constant, and T the absolute temperature. The probability of the center of gravity of the molecule as a whole moving in a given direction depends on the probability of a number of successive segmental jumps occurring in the same direction, and hence decreases with the increasing molecular weight Z. Equation (2) is an equation proposed by Flory[3] and justified on a theoretical basis by Kauzmann and Eyring.[4] A more general equation which has a similar segmental flow justification[5] is

$$\log\eta = A\log Z + W/RT, \tag{3}$$

and this equation holds for the liquids investigated.

When the stress is removed from the molecule, the molecule returns to its most probable position by a series of segmental jumps. It has been proposed by Alfrey[6] that the activation energy should be the same as for viscous flow, and that there should be no chain length effect or

$$\eta_1 = A' e^{W/RT}. \tag{4}$$

Actual experiments given here and in a previous paper on longitudinal measurements[2] show, however, that the average activation energy is only $\frac{3}{4}$ of that for viscous flow, and there is a chain length effect which is considerably smaller than that for viscous flow.

If we go to still higher frequencies so that single chain segments do not have time to rearrange in the time of a single cycle, the configurational elasticity cannot be excited, but a shear elasticity caused by changing the relative positions of the segments of the molecules in single potential wells can still occur and this is a crystalline type of elasticity which should be of the order of 10^9 to 10^{10} dynes/cm^2. This type of elasticity also occurs at low temperatures for which η_1 and η_2 become so large that the shear stiffness is the dominant impedance. All of these effects can be represented by the equivalent electrical circuit of Fig. 1. The flow viscosity is represented by η_1, the configurational elasticity by μ_2, the configuration viscosity which determines the rate at which the configurational elasticity is relaxed is given by η_2, while μ_3 represents the high frequency crystalline elasticity. Another relation that is equivalent to this is shown by Fig. 1B. The constants of this circuit are related to those of circuit 1A by the equations

$$\begin{aligned}
\eta_1^A &= \eta_1^B + \eta_2^B, \\
\eta_2^A &= \frac{\eta_1^B \eta_2^B (\eta_1^B + \eta_2^B)(\mu_1^B + \mu_2^B)^2}{(\eta_1^B \mu_2^B - \eta_2^B \mu_1^B)^2}, \\
\mu_2^A &= \frac{(\eta_1^B + \eta_2^B)^2 (\mu_1^B + \mu_2^B)\mu_1^B \mu_2^B}{(\eta_1^B \mu_2^B - \eta_2^B \mu_1^B)^2}, \\
\mu_3^A &= \mu_1^B + \mu_2^B.
\end{aligned} \tag{5}$$

Considerable study has been given to the configurational type of elasticity and it has been shown that under equilibrium conditions, the "kinetic" theory of elasticity describes the elastic retractive force, for example as[7]

$$F = -T(\partial S/\partial L) = (kT\nu/L_0)[\alpha - (1/\alpha^2)], \tag{6}$$

where T=absolute temperature, L=length of sample, S=entropy, L_0=length of unstretched sample, ν=number of chains in the volume V, and $\alpha = L/L_0$. Here this theory accounts nicely for the widely observed shear modulus of 10^6 dynes/cm^2 and for its increase with temperature. It is, however, an equilibrium theory and requires time for equilibrium to be established before it is valid. For the torsional crystal measurements reported in the next section, the elasticity is higher than that of Eq. (6), and increases with a decrease in temperature. It appears likely that it is determined by nearest neighbor interaction, rather than an equilibrium between all elements of the chain, and

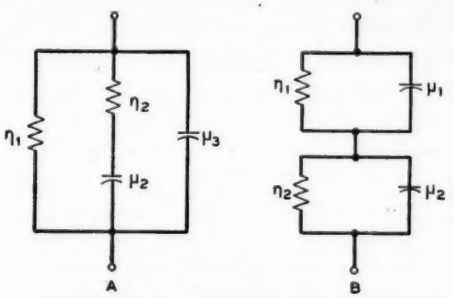

FIG. 1. Equivalent electrical circuits.

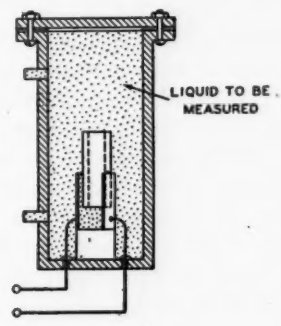

FIG. 2. Experimental arrangement.

[3] P. J. Flory, J. Am. Chem. Soc. 62, 1057 (1940).
[4] Walter Kauzmann and Henry Eyring, J. Am. Chem. Soc. 62, 3113–3125 (1940).
[5] Baker, Fuller, and Heiss, J. Am. Chem. Soc. 63, 2142 (1941).
[6] Turner Alfrey, Jr., *Mechanical Behavior of High Polymers* (Interscience Publishers, Ind., New York, 1948), p. 115.
[7] F. T. Wall, J. Chem. Phys. 10, 132 (1942); 10, 485 (1942); 11, 1527 (1943); P. Flory, Chem. Rev. 35, 51 (1944).

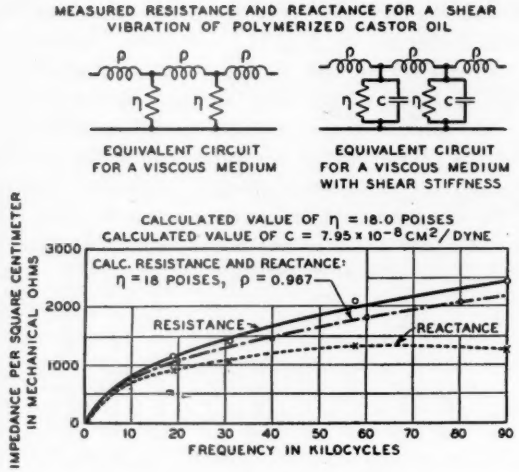
MEASURED RESISTANCE AND REACTANCE FOR A SHEAR VIBRATION OF POLYMERIZED CASTOR OIL
EQUIVALENT CIRCUIT FOR A VISCOUS MEDIUM
EQUIVALENT CIRCUIT FOR A VISCOUS MEDIUM WITH SHEAR STIFFNESS
CALCULATED VALUE OF η = 18.0 POISES
CALCULATED VALUE OF C = 7.95 × 10⁻⁸ CM²/DYNE
CALC. RESISTANCE AND REACTANCE: η = 18 POISES, ρ = 0.967
RESISTANCE
REACTANCE
IMPEDANCE PER SQUARE CENTIMETER IN MECHANICAL OHMS
FREQUENCY IN KILOCYCLES

FIG. 3. Equivalent circuits and measured values for castor oil.

has been designated as a quasi-configurational elasticity.

II. USE OF TORSIONAL CRYSTAL IN MEASURING CONFIGURATIONAL ELASTICITIES AND FLOW VISCOSITIES

Since the configurational elasticity of long chain molecule liquids is in the order of 10^7 dynes/cm^2 while the associated shear viscosities may range from 10 to millions of poises, the relaxation frequencies of such liquids will be in the order of 10^5 to a few cycles, and should be in the range of easily measured frequencies. In fact, by employing a torsionally vibrating crystal whose motion is tangential to the surface, one of the writers[8] showed that the shear viscosity and elasticity of polymer liquids could be measured. In light liquids the method gives directly the viscosity of the liquids. Under temperature-controlled conditions the method is accurate to within a percent.

The method consists of using a torsional quartz crystal, measuring the change in resonant resistance, and change in frequency caused by immersing the crystal in the liquid. Figure 2 shows the experimental arrangement. These measured quantities determine the resistance and reactance components of the liquid for a pure shearing motion. If the liquid is a purely viscous liquid the wave is propagated by having layers of mass ρdx coupled to adjacent layers by the viscosity η/dx of the liquid layer. An equivalent circuit is shown by the left side of Fig. 3. One can readily show[1] that the so-called characteristic impedance Z_0, which is the impedance of an infinitely thick layer, is equal to

$$Z_0=(\pi f\eta\rho)^{\frac{1}{2}}(1+j), \tag{7}$$

and hence the resistance and reactance terms are equal.

It was shown in a reference[8] that when a polymer liquid such as polymerized castor oil was measured, the resistance and reactance terms were no longer equal, but the resistance term was larger than the reactance by increasing amounts as the frequency increased. The curves of Fig. 3 show the measured values for castor oil, while the dot-dash line shows the theoretical value if the liquid were a purely viscous liquid. This divergence can be accounted for if the liquid has a configurational shear elasticity as shown by the equivalent circuit on the right of Fig. 3. The impedance of a liquid with a single relaxation time was calculated[1] and is given by the formula

$$R_M=(\rho\mu)^{\frac{1}{2}}\left[\frac{(f^2/f_1^2)+(f^4/f_1^4+f^2/f_1^2)^{\frac{1}{2}}}{2[1+f^2/f_1^2]}\right]^{\frac{1}{2}};$$
$$X_M=(\rho\mu)^{\frac{1}{2}}\left[\frac{(-f^2/f_1^2)+(f^4/f_1^4+f^2/f_1^2)^{\frac{1}{2}}}{2[1+f^2/f_1^2]}\right]^{\frac{1}{2}} \tag{8}$$

where f_1 is the relaxation frequency $f_1=\mu/(2\pi\eta)$. A plot of this equation is shown in Fig. 4 (by solid lines). At low frequencies, i.e. for frequencies much less than the relaxation frequency, the resistance and reactance terms are equal, and increase proportionally to the square root of the frequency. As the frequency approaches the relaxation frequency, the resistance becomes larger than the reactance, and at very high frequencies the resistance approaches $(\rho\mu)^{\frac{1}{2}}$ while the reactance approaches zero. By fitting the theoretical curves of Fig 4. to the measured curve of Fig. 3 it is found that the viscosity is equal to the value measured by a falling ball method, namely 18 poises, while the configurational stiffness is $\mu=1/C_s=1.26\times10^7$ dynes/cm^2.

Further measurements[2] by this method have been made for a series of polyisobutylene polymer liquids A', B, C, and D, having the viscosity average molecular weights 1060, 3520, 4550, and 5590. The results are shown by Fig. 5. The viscosities agree quite well with those measured by falling ball methods, while the configurational shear elasticities

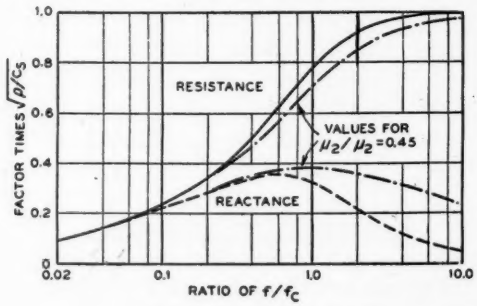

FIG. 4. Plot of Eq. (8).

[8] W. P. Mason, "Measurement of the Viscosity and Shear Elasticity of Liquids by Means of a Torsionally Vibrating Crystal," Proc. A.S.M.E., May 1947.

have values ranging from 6×10^6 dynes/cm^2 to 5×10^7, depending on the temperature and molecular weight. These shear elasticities do not follow the temperature relations established for the "kinetic" theory indicating that equilibrium is not established and that this quasi-configurational elasticity is controlled by the reaction of nearest neighbors. Further measurements by this method have been made and are reported in a previous paper.[9]

III. MEASUREMENTS OF SHEAR ELASTICITIES OF LIQUIDS AT VERY HIGH FREQUENCIES

The measurements made with the torsional crystal can be satisfied by a single relaxation frequency, whereas the discussion in the introduction indicates that polymer liquids should have two main relaxation frequencies, the latter one determined by the high frequency or crystalline elasticity of the liquid. Rough calculations indicated that the second relaxation frequency should come in the upper megacycle range. In order to measure this relaxation frequency it was necessary to devise a different method since the torsional crystal method is limited to about 500 kilocycles on account of the small sizes of the crystal. Consideration was given to the use of a thickness vibrating shear crystal of the AT or BT type, but it was found that the shear motion was too closely coupled to other modes of motion, such as flexure modes, to give reliable results. Hence another method had to be used.

Previous studies[10] had shown that it was possible to set up very pure shear waves in a fused quartz rod by attaching a Y cut or AT shear vibrating crystal to the quartz rod. For permanent connection, silver paste was baked to the quartz rod and the crystal soldered on by a very thin layer of solder. However, for experimental purposes the joint could be made of wax, or preferably, a very thin layer of one of the polyisobutylene liquids. The success of this joint shows that the shear elasticity of this liquid is becoming quite high. By sending a pulse down the rod and picking up the series of pulses by the sending crystal or a receiving crystal on the far end, the purity of the shear motion can be tested. Any longitudinal wave will travel with nearly twice the velocity of the shear wave, and will appear on the cathode-ray oscillograph at a point intermediate between the sent pulse and the first shear pulse. In this way it is found that any longitudinal pulse is at least 50 db down from the received shear pulse, and is entirely negligible.

By using a short length of fused quartz rod which is accurately made parallel and polished on both ends, and using a single crystal for sending and receiving, a series of shear wave pulses was set up in the rod and their relative amplitudes and positions were shown on the cathode-ray oscillograph as shown by Fig. 6. Then a layer of liquid to be studied was put on the polished free end and the difference in the received pulses noted. At 10 megacycles, for example, it was found that the first received pulse was decreased by 1.10 db, the second which had been reflected twice from the fused quartz-liquid joint, by 2.2 db, etc. It was found by experiment that the thickness of the liquid layer did not make any difference until the thickness was extremely small, i.e., less than .001 cm. Hence the liquid layer can be considered an infinite medium, and the effect is only on the reflection coefficient which is given by the formula

$$R_F=(Z_Q-Z_L)/(Z_Q+Z_L), \qquad (9)$$

where Z_Q is the characteristic impedance of the quartz and Z_L, the characteristic impedance of the liquid. The fused quartz having no dispersion and a very small attentuation ($Q>50{,}000$) can be considered a pure resistance within less than 1 part in 50,000. However, the liquid impedance Z_L

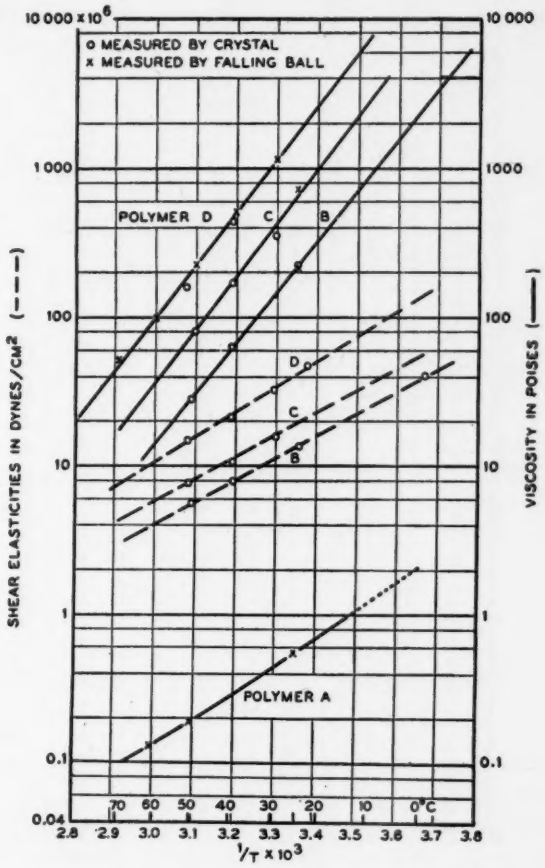

FIG. 5. Shear elasticities and viscosities for polyisobutylene polymer liquids.

[9] W. P. Mason, J. Coll. Sci. III, No. 2 (May 1948).
[10] W. P. Mason and H. J. McSkimin, J. Acous. Soc. Am. 19, 464 (1947).

will certainly have a phase angle. Hence the reflection factor R_F will have a phase angle and can be represented by

$$R_F = Re^{-j\theta}, \tag{10}$$

where R is the absolute value of the reflection coefficient, and θ, the phase angle. Solving for Z_L we find

$$Z_L = R_L + jX_L = 8.3\times10^5\left[\frac{1-R^2+2jR\sin\theta}{1+R^2+2R\cos\theta}\right], \tag{11}$$

where 8.3×10^5 is the shear impedance per square centimeter for a fused quartz rod. Now, since the impedance Z_L for all these liquids is less than $0.1(1+j)$, that for the fused quartz, it can be shown that the phase angle θ will not be greater than 5°, and the reduction in amplitude measures the resistance term R_L quite accurately by using the formula

$$R_L = 8.3\times10^5\left[\frac{1-R}{1+R}\right]. \tag{12}$$

A series of measurements was made for the polyisobutylene liquids shown by Fig. 5 for 25°C, and the resistance components of the shear impedance are shown plotted by Fig. 7. The resistances of the longer chain polymers show a marked rise with frequency which tends to approach an asymptotic value of about 75,000 mechanical ohms per square centimeter. The shorter chain polymers tend to approach a somewhat lower value.

To see if this impedance tends to approach that which should exist for a liquid with two relaxation frequencies, calculations have been made for the case of a liquid with a series element $j\omega\rho dx$ and a shunt element shown by Fig. 1B. The B form is taken since the two relaxation frequencies are easily calculated from it. Introducing the values

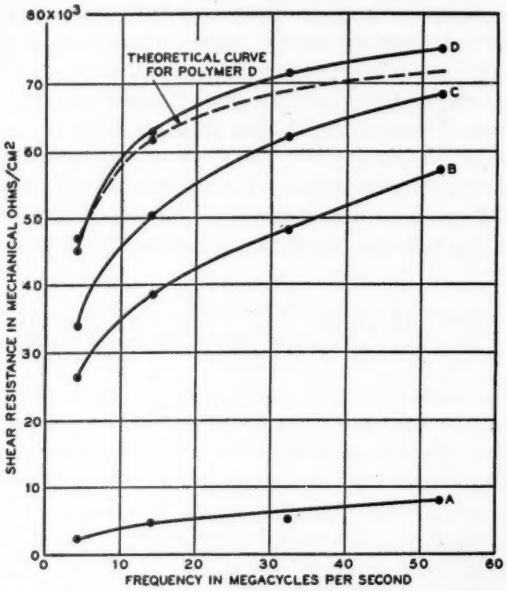

FIG. 7. Resistance components of the shear impedance for the polyisobutylene liquids.

$$Z_1 = j\omega\rho dx;$$

$$Z_2 = \left[\frac{(-j\mu_1\eta_1)/\omega}{\eta_1-(j\mu_1/\omega)} + \frac{(-j\mu_2\eta_2)/\omega}{\eta_2-(j\mu_2/\omega)}\right](1/dx) \tag{13}$$

into the formula

$$Z_0 = (Z_1Z_2)^{\frac{1}{2}},$$

we find

$$Z_0 = \left[\rho(\mu_1+\mu_2)\frac{\left[\frac{f^4}{f_1^2f_2^2}+f^2\left[\frac{\mu_2}{\mu_1+\mu_2}\times\frac{1}{f_2^2}+\frac{\mu_1}{\mu_1+\mu_2}\times\frac{1}{f_1^2}\right]\right] + jf\left[\frac{2\pi(\eta_1+\eta_2)}{\mu_1+\mu_2}+\frac{f^2}{f_1f_2}\left[\left(\frac{\mu_1}{\mu_1+\mu_2}\right)\frac{1}{f_2}+\left(\frac{\mu_2}{\mu_1+\mu_2}\right)\frac{1}{f_1}\right]\right]}{[1+(f^2/f_1^2)][1+(f^2/f_2^2)]}\right]^{\frac{1}{2}}, \tag{14}$$

where f_1 and f_2, the two relaxation frequencies, are given by

$$f_1 = \mu_1/(2\pi\eta_1); \quad f_2 = \mu_2/(2\pi\eta_2). \tag{15}$$

To illustrate the form of the impedance, use is made of the data obtained for the liquid polyisobutylene, polymer D at 26°C. The low frequency viscosity and torsional crystal measurements show that the flow viscosity is 1600 poises, and the configurational shear elasticity is 4×10^7 dynes per square cm. The high frequency longitudinal measurements given in a previous paper[11] show that there is a dispersion in the longitudinal velocity which requires a compressional stiffness of 1.17×10^{10} dynes/cm² higher at an infinite frequency than the stiffness at zero frequency. Compressional stiffnesses are controlled by the Lamé elastic constants $\lambda+2\mu$, and compressional measurements do not

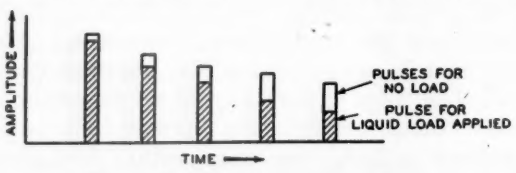

FIG. 6. Series of shear wave pulses.

[11] Mason, Baker, McSkimin, and Heiss, Phys. Rev. 73, 1074–1091 (1948); 74, 1873–1874 (1948).

distinguish whether the dispersion comes in the λ-constant or the μ-constant. By means of the shear measurements presented here, it becomes obvious that the dispersion occurs in the μ-constant.

With the values of the Fig. 1A constants as $\mu_3{}^A=(1.17\times10^{10}/2)=5.85\times10^9$ dynes/cm^2; $\mu_2=4.5\times10^7$ dynes/cm^2

$$\eta_1{}^A=1600 \text{ poise}; \quad \eta_2{}^A=200 \text{ poise}. \tag{16}$$

This results in the elements of the 1B network being

$$\eta_1{}^B=1425 \text{ poises}; \quad \eta_2{}^B=175 \text{ poises};$$
$$\eta_1{}^B=4\times10^7 \text{ dynes/cm}^2;$$
$$\mu_2{}^B=5.81\times10^9 \text{ dynes/cm}^2. \tag{17}$$

Since the 1B constants are separated out in the form of two relaxation frequencies, these constants are more easily evaluated than the constants in the form 1A. For example, at the very high frequencies, $\eta_1{}^B$ is relaxed out by the stiffness $\mu_1{}^B$ and the measurement of the second shear viscosity of Fig. 14, reference 11, divided by two, gives directly $\eta_2{}^B=175$ poise. $\eta_1{}^B+\eta_2{}^B$ is the "steady" flow viscosity, 1600 poises. $\mu_1{}^B$ is the measured shear elasticity of 4×10^7 dynes/cm^2. Substituting these values in Eq. (14), the resulting resistance and reactance terms for the D polymer liquid are shown by Fig. 8. There are two plateaus, one in the region below 100 kc and the other above 100 megacycles. Hence the measurements with the torsional crystal in which the constants were evaluated as though only one relaxation frequency existed, give

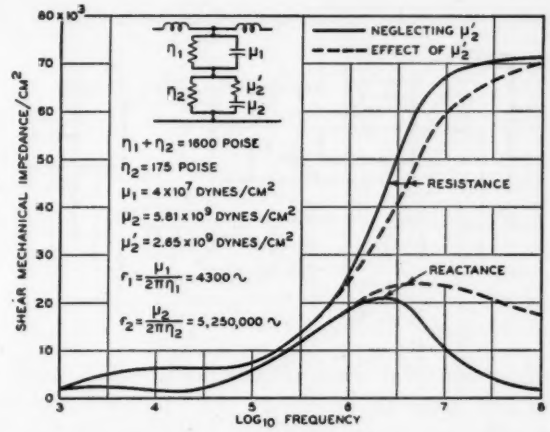
SHEAR MECHANICAL IMPEDANCE/CM²
LOG₁₀ FREQUENCY
NEGLECTING μ₂'
EFFECT OF μ₂'
RESISTANCE
REACTANCE
η₁ + η₂ = 1600 POISE
η₂ = 175 POISE
μ₁ = 4 x 10⁷ DYNES/CM²
μ₂ = 5.81 x 10⁹ DYNES/CM²
μ₂' = 2.85 x 10⁹ DYNES/CM²
r₁ = μ₁/2πη₁ = 4300 ∿
r₂ = μ₂/2πη₂ = 5,250,000 ∿

FIG. 8. Resistance and reactance for the D polymer liquids.

very closely the correct results for the lowest relaxation frequency. For the high frequency range, the theoretical values of Fig. 8 are somewhat too high to agree with the measured curves of Fig. 7. This divergence is mostly due to the fact that the stiffness $\mu_2{}^B$ has a hysteresis component, as shown in the previous paper,[11] and this is not taken account of in the solid lines of Fig. 8. By introducing a series component μ_2' such that the stiffness impedance is

$$(\mu_2'-j\mu_2)/\omega$$

the effect of a hysteresis component is taken care of. This results in an input impedance for a long line of

$$Z_0=\left[\rho(\mu_1+\mu_2)\frac{\left[\left[\frac{\mu_1}{\mu_1+\mu_2}\left(\frac{f^2}{f_1{}^2}\right)\left[1+\left(\frac{\mu_2'}{\mu_2}+\frac{f}{f_2}\right)^2\right]+\frac{\mu_2}{\mu_1+\mu_2}\left(\frac{f^2}{f_2{}^2}\right)\left(1+\frac{f^2}{f_1{}^2}\right)\right]+jf\left[\frac{\mu_1}{\mu_1+\mu_2}\left(\frac{1}{f_1}\right)\left[1+\left(\frac{\mu_2'}{\mu_2}+\frac{f}{f_2}\right)^2\right]+\left(\frac{\mu_2}{\mu_1+\mu_2}\right)\left(\frac{1}{f_2}\right)\left[1+\frac{\mu_2'}{\mu_2}\left[\frac{\mu_2'}{\mu_2}+\frac{f}{f_2}\right]\right]\right]\right]}{\left(1+\frac{f^2}{f_1{}^2}\right)\left(1+\left(\frac{\mu_2'}{\mu_2}+\frac{f}{f_2}\right)^2\right)}\right]^{\frac{1}{2}}. \tag{18}$$

The effect of this is to raise the effective relaxation frequency as shown by the dashed line of Fig. 8. These values were calculated for a ratio of $\mu_2'/\mu_2=0.45$ as found in the previous paper.[11] This tends to make the theoretical and experimental values agree closely as shown by the dashed line of Fig. 7, and hence all the evidence points to a relaxation in the shear elasticity as the cause of the relaxation measured in the longitudinal velocity.

IV. MORE SENSITIVE METHOD FOR MEASURING RESISTANCE AND REACTANCE COMPONENTS OF SHEAR IMPEDANCES OF LIQUIDS

The method discussed previously for measuring the shear impedance of liquids by their effects on the reflection coefficient at normal incidence suffers from the fact that the limiting impedances of the liquids are only about 0.1 that of the fused quartz, and hence the effects on the reflection factor and reflection phase are very small. It has been found[12] that an enhanced effect can be obtained by re-

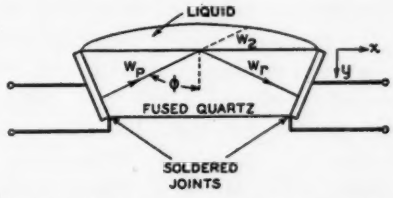

FIG. 9. Arrangement for measuring the shear impedance of liquids by reflection at low angle of incidence.

[12] This idea was suggested and developed by H. J. McSkimin.

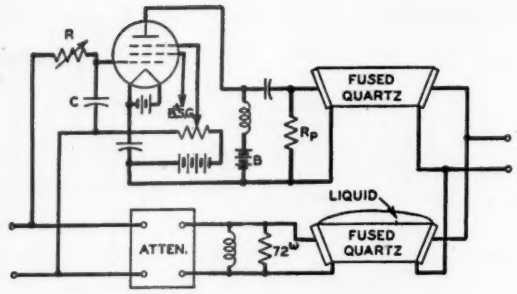

FIG. 10. Circuit connections.

flecting the shear wave off the liquid-solid interface at a low angle of incidence. An exact solution for the reflected wave has been obtained by H. T. O'Neil and will be published in a companion paper. It appears, however, that for all the liquids considered here, the effect of this low angle in determining Z_2 is given by the equation

$$Z_2=R_2+jX_2=\cos\varphi Z_Q\left[\frac{1-R^2+2jR\sin\theta}{1+R^2+2R\cos\theta}\right], \quad (19)$$

where R is the absolute value of the reflection factor, and θ, the phase angle. Hence the effect of the low angle is to transform the shear impedance of the liquid up by an impedance transformation ratio $1/\cos\varphi$, where φ is the angle of incidence from the normal.

In order to make the device a reasonably short length—approximately four inches as shown by Fig. 9—and have it still radiate the whole surface by the directive shear wave, the angle φ was chosen as 79°, giving an impedance transformation ratio of 5.25 to 1. The solution given by Eq. (19) depends on the particle motion of the surface being at right angles to the surface normal. This is secured by putting the x-crystallographic axis of the quartz crystal parallel to the reflecting surface for both sending and receiving crystals.

The method for obtaining the resistance and reactance components is to determine the reflection loss per reflection and the phase change per reflection. The reflection loss is obtained by comparing any one of the reflections with a clear reflecting surface with the same reflection, with the reflecting surface covered by the liquid, and dividing by the number of times this particular component has suffered reflection from the solid liquid interface. To measure phase, two identical fused-quartz rods were constructed with two input and two receiving crystals. These are connected in the circuit shown by Fig. 10. Here the upper reference bar is connected through a pentode vacuum tube with an R-C phase shifting network in the input. Since we are comparing two received pulses occurring at the same time, one has to balance the amplitude and make the phase 180° different. When the variable resistance, R, is equal to zero, the phase shift introduced by the phase shifting network is zero and 180° is introduced by the tube. If we make R_p low so that the gain through the tube is zero, the two received pulses can be balanced out when no liquid is placed on the lower rod. Now, when a liquid is placed on this reflecting surface, the amplitude is reduced and the phase is changed for the pulse received from the lower unit. To balance it out now, the gain of the tube is reduced by introducing a negative bias on the suppressor grid. By comparison methods it is shown that this changes the phase of the upper pulse by less than 1°. Then, to balance out the phase shift introduced in the first reflection by the liquid, the variable resistance R is increased, until the two adjustments annul the received pulse. By calibrating the phase of the adjustable circuit, the reflection phase shift can be measured within a degree. Only a very moderate amount of temperature and frequency stability are required for this system.

A few measurements have been made with this system. Figure 11 shows the resistance and reactance at 10 megacycles and 25°C of a number of polyisobutylene liquids graduated according to molecular weight. The lighest liquid, having a flow viscosity of 0.55 poises, acts nearly like a purely viscous liquid with only a small amount of shear elasticity. As the molecular weight increases, the divergence between resistance and reactance increases, and above a molecular weight of 10,000 the shear elasticity is a very slowly increasing function of the molecular weight.

A number of these liquids have been measured at the three frequencies: 4.5 megacycles, 14 megacycles, and 24 megacycles, over a temperature range. The measurements for three of these liquids

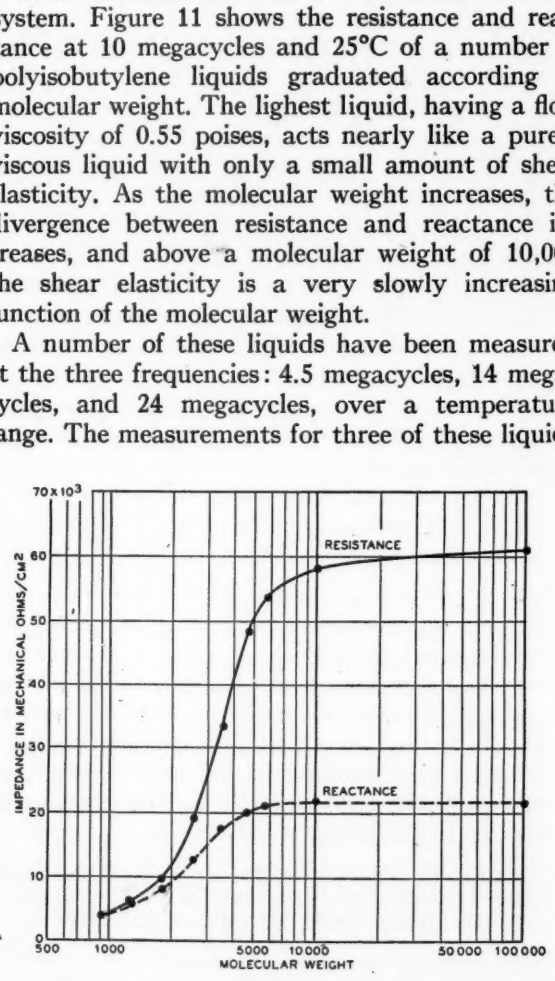

FIG. 11. Resistance and reactance at 10 megacycles and 25°C of polyisobutylene liquids.

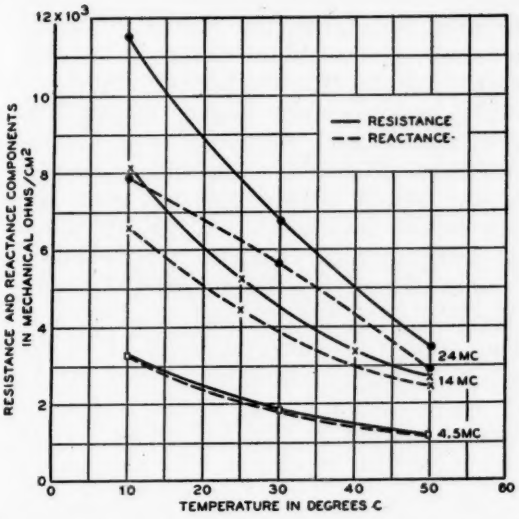

FIG. 12. Resistance and reactance curves at various frequencies for liquids having viscosity average molecular weight of 1060.

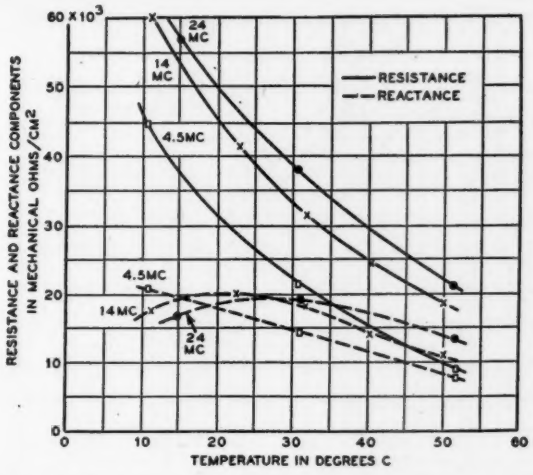

FIG. 13. Resistance and reactance curves at various frequencies for liquids having viscosity average molecular weight of 3520.

having viscosity average molecular weights of 1060, 3520 and 5560 are shown by Figs. 12, 13, and 14. The highest molecular weight material shows a stiffness at all three frequencies that increases with a decrease in temperature. The lowest molecular weight material, on the other hand, appears to be a viscous liquid at 4.5 mc and only shows a stiffness at 24 mc, or at low temperatures.

The measured results can be fitted by an equivalent circuit having the elements shown by Fig. 1B. Here the sum of η_1 and η_2 equals the low frequency viscosity, which for these liquids is shown by Fig. 5. μ_1, the quasi-configurational shear stiffness for a number of liquids, is also shown by Fig. 5. If we plot these as a function of density, it appears that all of the stiffnesses can be plotted on one curve as shown by Fig. 15. If we extrapolate this down to the density of the lowest molecular weight liquid (0.826 at 25°C), the shear stiffness for configurational conditions will have dropped to 2×10^5 dynes/cm² for this liquid. At the same time the viscosity as measured by the reflection coefficient of the shear wave nearly coincides with the static measurements shown by Fig. 5. Hence it appears that the first relaxation mechanism of Fig. 1 can be neglected, and the impedance accounted for by a single mechanism. For the other two liquids, the relaxation frequency of μ_1, η_1 is much less than the measured frequency, and as shown by Fig. 8, the impedance measured can be accounted for by a single relaxation mechanism having the constants μ_2 and η_2.

In order to evaluate these constants, μ_1 is set equal to zero, and f_1 to infinity. Solving for the resistance and reactance terms we find

$$R=(\rho\mu_2)^{\frac{1}{2}}\left[\frac{\dfrac{f^2}{f_2^2}+\left(\dfrac{f^4}{f_2^4}+\dfrac{f^2}{f_2^2}\left[1+\dfrac{\mu_2'}{\mu_2}\left(\dfrac{\mu_2'}{\mu_2}+\dfrac{f}{f_2}\right)\right]^2\right)^{\frac{1}{2}}}{2\left[1+\left(\dfrac{\mu_2'}{\mu_2}+\dfrac{f}{f_2}\right)^2\right]}\right]^{\frac{1}{2}}, \tag{20}$$

$$X=(\rho\mu_2)^{\frac{1}{2}}\left[\frac{\dfrac{-f^2}{f_2^2}+\left(\dfrac{f^4}{f_2^4}+\dfrac{f^2}{f_2^2}\left[1+\dfrac{\mu_2'}{\mu_2}\left(\dfrac{\mu_2'}{\mu_2}+\dfrac{f}{f_2}\right)\right]^2\right)^{\frac{1}{2}}}{2\left[1+\left(\dfrac{\mu_2'}{\mu_2}+\dfrac{f}{f_2}\right)^2\right]}\right]^{\frac{1}{2}}. \tag{21}$$

A plot of these values for a value of $\mu_2'/\mu_2=0.45$ (the value found from longitudinal measurements) is shown by the dot-dash lines of Fig. 4.

Fitting the reactances and resistances measured and shown by Figs. 12, 13, and 14 to these curves, the asymptotic value of $R_\infty=(\rho\mu_2)^{\frac{1}{2}}$ and the relaxation frequencies f_2 can be determined for the different temperatures and different molecular weights.

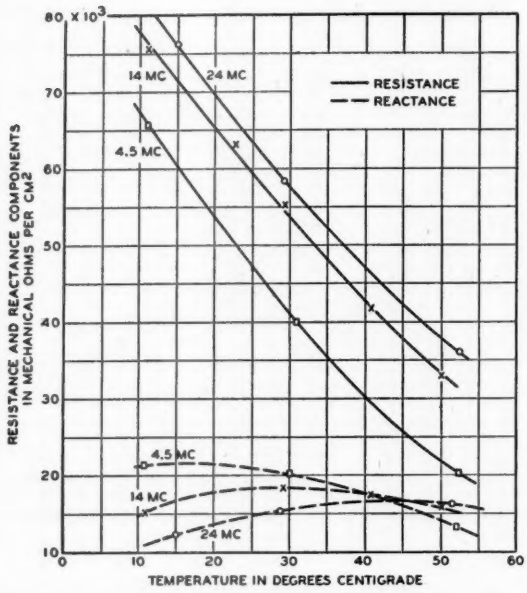

FIG. 14. Resistance and reactance curves at various frequencies for liquids having viscosity average molecular weight of 5560.

Then knowing the density ρ, the value μ_2 can be determined from the equation

$$\mu_2 = R_\infty^2/\rho. \tag{22}$$

The second shear viscosity, η_2, can be determined from the formula

$$\eta_2 = \mu_2/2\pi f_c, \tag{23}$$

where f_c is the relaxation frequency.

The high frequency shear elasticity μ_2 is shown plotted on Fig. 15 as a function of the density.

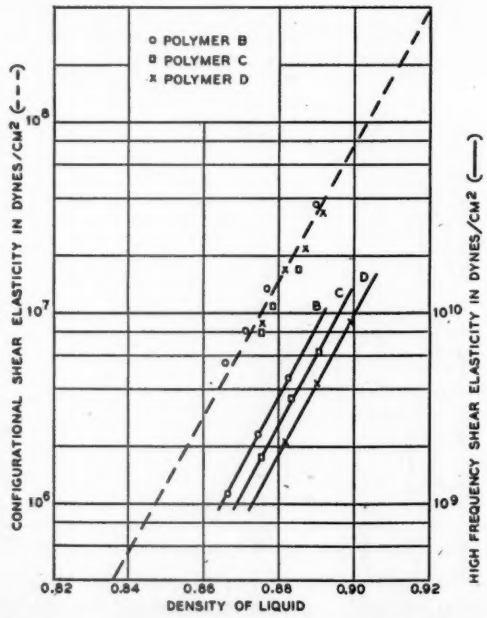

FIG. 15. Shear elasticities plotted as a function of density.

Since over this range the change in density is roughly proportional to the change in temperature, it is seen that the variation in high frequency shear elasticity parallels quite closely the variation in quasi-configurational elasticity as a function of temperature. However, the difference due to molecular weight change does not even approximately follow the variation in density, unlike the quasi-configurational elasticity. The viscosities η_2 are shown plotted as a function of $1/T$ by Fig. 16. All the slopes are approximately parallel, and indicate an activation energy of about 12 kilocalories. The low frequency viscosities, shown by Fig. 5, have an activation energy of 16 kilocalories for molecular weights of 3500 and above, but for the lowest molecular weight of 1060 the slope is less and the indicated activation energy is about 12 kilocalories. Since a molecular weight of 1060 corresponds to a repeating chain of 19 links, i.e., perhaps about the size of an Eyring segment, it may be that an activation energy of 12 kilocalories is the value for the motion of a single segment. The values of η_2 plotted on Fig. 16 then represent the motion of individual segments caused by a chain retraction. There is a chain length effect due to the fact that there is an increased improbability of all the segments moving in the same direction as the chain increases in length.

Since both quasi-configurational (in the sense of relaxation times leading to apparent stiffness for shape changes), and crystalline elasticities in all probability are determined by nearest neighbors, the action of any segment may be represented as

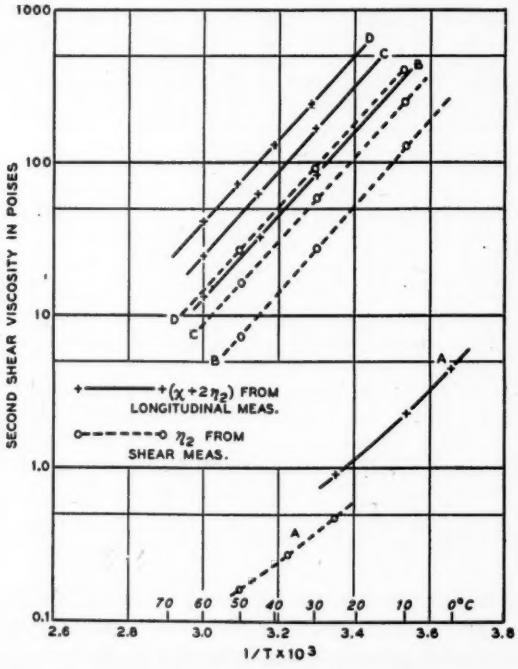

FIG. 16. Second shear viscosity as a function of $1/T$.

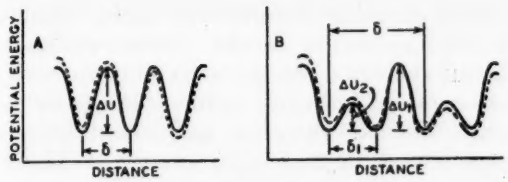

FIG. 17. Potential well distributions.

due to the potential well distribution shown in Fig. 17B. The viscous flow of the molecule requires a translation and rotation and hence occurs over the free energy barrier ΔU_1. On the other hand, an extension or contraction of the chain as a whole, which occurs when configurational elasticity occurs, requires no change in the center of gravity of the chain, and probably results in a lower over-all free energy barrier ΔU_2. When a shearing stress is put on the liquid, one well is lowered compared to the other, as shown by the dotted line. At low frequencies, sufficient time is given so that a viscous flow occurs over the high energy barrier. As the frequency increases there is not time for an actual transfer of the center of gravity in the time of a single cycle, but a local distortion still can occur across the lower energy barrier. This is a reversible process and results in the quasi-configurational elasticity since entropy changes tending always toward most probable chain shapes are concurrently happening. Since the motion that can occur is large, the configurational stiffness is small. At still higher frequencies, even the local distortion cannot occur and the only effect is the displacement of the segment from its equilibrium position. This results in a very high shear stiffness of the crystalline type. According to the measurements, the height of the flow viscosity activation energy barrier is 16 kilocalories per mole, whereas the local distortion energy barrier is 12 kilocalories. The same relative slope of the configurational and crystalline stiffnesses with temperature shown by Fig. 15, indicates that there is a correspondence between the shape of the bottom of the two potential wells and the complete free energy curve. As the chain length decreases, the distinction between a local distortion and a true flow motion disappears, and for liquids having a chain length in the order of one Eyring unit or less, the two potential wells become equal and the potential well distribution is similar to that for a light liquid as shown by Fig. 17A. Under these circumstances the quasi-configurational elasticity disappears.

Another interesting result is obtained by comparing the values of viscosity η_2 measured by the high frequency shear technique with the value measured in longitudinal measurements of Fig. 14, reference 2. The longitudinal measurements, which determine the sum of the compressional viscosity χ plus twice the shear viscosity η_2, are shown plotted by the solid lines of Fig. 16. For the lowest molecular weight (polymer A) the longitudinal viscosity is about 2 times η, indicating a negligible compressional viscosity. The longer chains have a compressional viscosity which is, however, a considerable fraction of the shear viscosity. Evidently com-

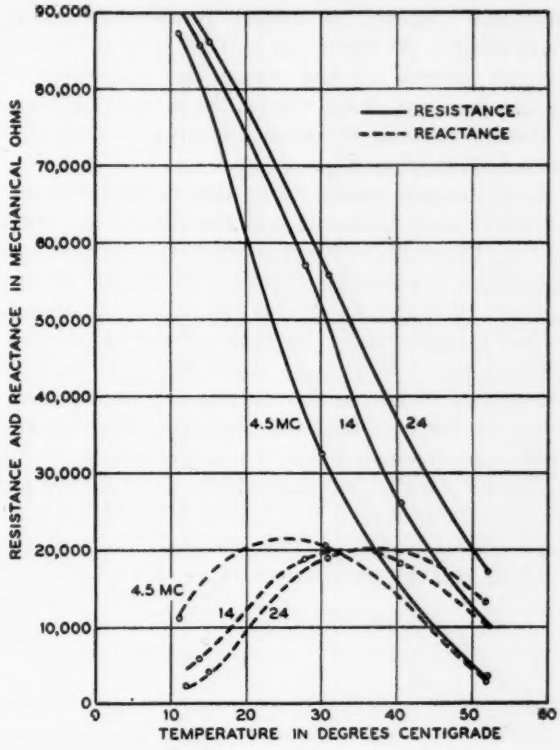

FIG. 18. Resistance and reactance for a poly-α-methyl styrene liquid.

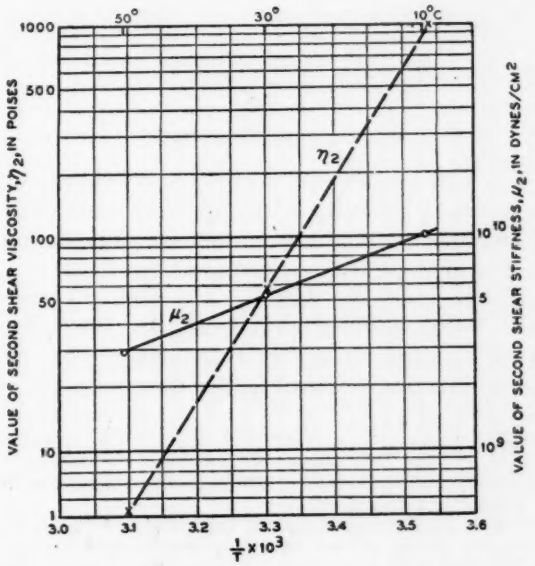

FIG. 19. Second shear viscosity and stiffness for a poly-α-methyl styrene liquid.

pressional viscosity is a steep function of average chain length. As nearly as can be judged from the relative slopes of the viscosities measured by longitudinal and shear waves, the activation energy of the compressional viscosity is equal to that of the second shear viscosity.

Some measurements were also made for a poly-α-methyl styrene liquid and the results are shown by Fig. 18 for three frequencies over a temperature range. One interesting difference is at once obvious, namely, that any hysteresis effects are small, since at low temperatures the ratio of reactance to resistance becomes greater than 50, whereas it did not exceed 8 for polyisobutylene. This correlates also with the fact that the high frequency losses of solid polystyrene are much less than those of high molecular weight polyisobutylene at ordinary temperatures. Analyzing the data of Fig. 18, using the solid curves of Fig. 4, one obtains the shear elasticity μ_2 and the shear viscosity η_2 shown by Fig. 19. The shear elasticity is somewhat higher than that for a 5560 molecular weight polyisobutylene but has about the same change with temperature. The variation of η_2, however, is much larger for poly-α-methyl styrene than for polyisobutylene, and corresponds to an activation energy of 23.6 kilocalories.

Some measurements were also made of very light liquids such as water and cyclohexane. By observing the fifth and seventh reflection for both amplitude and phase changes, measurable results were obtained. For both cases within the experimental error, the values agreed with the steady flow measurements. Hence in agreement with Eq. (1), they are considerably below their relaxation frequencies, and indicate that no configurational type elasticities exist for these liquids. These measurements show that the enhanced losses for longitudinal waves for these liquids must be due to compressional viscosities.

PHYSICAL REVIEW VOLUME 75, NUMBER 6 MARCH 15, 1949

Ultrasonic Measurements on Rochelle Salt Crystals*

W. J. PRICE
*Physics Department, Rensselear Polytechnic Institute, Troy, New York***

(Received November 15, 1948)

A pulse technique at 10 Mc/sec. has been used to study the anomalous elastic properties of rochelle salt single crystals at temperature around the upper Curie temperature. The temperature dependence of foiled crystal constant S_{44}^E and of the attenuation of waves which contain a component of shear strain in the X crystallographic plane is reported. The attenuation measurements are formulated in terms of the interaction theory.

The dependence of the velocity in 45° X cut crystals of rochelle salt on a d.c. field in the X crystallographic direction shows a marked unipolarity. This change in velocity which is caused by the bias field arises from the two following sources: one is the usual saturation on effect which produces a change in velocity that is independent of the polarity; the other is the morphic effect which results from the induced monoclinic constants, and which produces a velocity change, the sign of which is dependent on the polarity.

I. INTRODUCTION

IT is well known that rochelle salt exhibits extraordinary elastic, dielectric, and piezoelectric properties: Several experimental and theoretical studies of these properties have been made.[1]

In the past the data on the elastic properties have been obtained principally by the self-resonance method. Recently Huntington[2] has used a pulsed ultrasonic technique for determining a complete set of elastic moduli for rochelle salt at room temperature. The present paper reports the use of the ultrasonic method to study further certain interesting aspects of rochelle salt.

In the self-resonance experiments the wave-length of the sound waves in the specimen is of the order of the specimen dimensions, while in the pulsed ultrasonic method the frequency is sufficiently high that the specimens are essentially infinite compared to the wave-length of the sound. The boundary conditions for the two cases lead to expression for the velocity in terms of the elastic compliance coefficients S_{ij} and of the elastic moduli C_{ij}, respectively.

The interesting elastic phenomena in Rochelle salt center around the anomalous temperature dependence and the saturation effects (both

---

* This paper is a portion of a dissertation submitted in 1948 to Physics Department of Rensselear Polytechnic Institute in partial fulfillment of the requirements for the degree of Doctor of Philosophy.

** Now at Battelle Memorial Institute, Columbus, Ohio.

[1] For a review of the investigations of rochelle salt, see W. G. Cady, *Piezoelectricity* (McGraw-Hill Book Company, Inc., New York, 1946).

[2] H. B. Huntington, Phys. Rev. **72**, 321 (1947).

mechanical and electrical) of the shear compliance S_{44}^E of the foiled crystal. In the self-resonance experiments S_{44}^E appears in the velocity equations either alone or in a sum with other coefficients S_{ij}. In the pulsed method the quantity C_{44}^*, where[2]

$$C_{44}^* = 1/S_{44}^E = C_{44} - f_{14}^2/\chi_1$$

appears in the velocity equation alone or in a sum with the moduli C_{ij}. However, for the former case S_{44}^E approaches infinity at the Curie points and therefore is the dominant term while for the latter case C_{44}^* approaches zero and other terms become important.

In this work the pulsed method has the following advantages: first, the induced monoclinic elastic constants which are produced by a bias field can be observed since they are not masked by the term C_{44}^*; second, it is possible to make measurement on 45° X cut bars right at the Curie temperature where S_{44}^E approaches infinity.

II. EXPERIMENTAL PROCEDURE

The pulsed method at 10 Mc/sec. has already been described.[2] With it velocities could be measured with an accuracy of about 0.5 percent.

The rochelle salt specimens which were studied in this investigation were obtained from the Brush Development Company. The crystals were rectangular parallelepipeds with dimensions of the order of one inch. The two following cuts were principally used:

1. 45° X cut specimens. X cut quartz transducers were used for transmission in either of the two 45° directions. The X faces of the specimens were foiled.
2. 90° Z cut specimens. The Z dimension, which was the direction of a transmission, was one-quarter inch. The Y cut quartz transducer was oriented so that the transverse mode which was generated was polarized in the Y crystallographic direction. The X faces were foiled.

The temperature of the specimens was controlled to 0.02°C by means of a water bath thermostated by a mercury-tuolene regulator.

When an electrical bias field was required, the field was produced by applying a potential between the foils on the specimen faces. In order to insure a uniform bias field at right angles to the direction of propagation, the quartz transducer (which had metallic electrodes) was isolated from the rochelle salt specimen by a two-inch length of an ammonium dihydrogen phosphate single crystal.

III. THE TEMPERATURE DEPENDENCE OF S_{44}^E

For the Z cut specimen with the Y cut transducer oriented as described above, the velocity v is

$$\rho v^2 = C_{44}^* = 1/S_{44}^E,$$

where ρ is the density. The plotted points on Fig. 1 give the results of the measurements of this quantity through temperature ranges on either side of the upper Curie point. Velocity measurements were not possible between 22.7°C and 26.8°C because of the high attenuation.

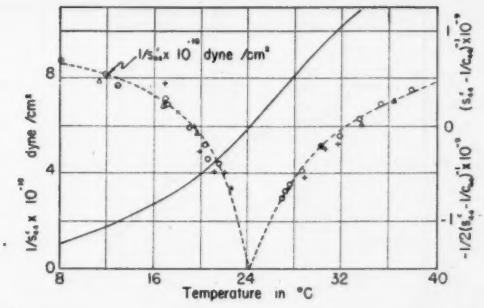

FIG. 1. Temperature dependence of $1/S_{44}^E$, the elastic compliance for a foiled crystal, for rochelle salt. Dotted curve is computed from data in Fig. 2. Plotted points are from velocity measurements of a transverse mode in the Z direction. Solid curve shows the Curie-Weiss law for S_{44}^E.

For propagation along a 45° direction of a 45° X cut specimen, a quasi-compressional mode with velocity v_b and a quasi-transverse mode with velocity v_d are coupled together. These velocities are related by the equation[3]

$$C_b + C_d = (C_{22} + C_{33})/2 + C_{44}^*, \qquad (1)$$

where $C_b = \rho v_b^2$ and $C_d = \rho v_d^2$. The temperature variation of the quantity C_b is given by Fig. 2. The quantity $C_d - (C_{22} + C_{33})/2$ varies slowly with temperature having a temperature coefficient of -0.001/°C.[3] The minimum value of C_{44}^* occurs with minimum value of C_b at the temperature of 24.2°C.

These measurements result in a value of 24.2°C ±0.1 for the upper Curie temperature. Values have been reported in the literature from 22.25°C to 24.5°C, the most widely accepted value being 23.7°C.[4] This wide spread in the results seems more likely to be due to the method in which the quantity is measured than to a difference in specimens.

If one assumes that C_{44}^* vanishes at the Curie temperature, one has

$$C_d - (C_{22} + C_{33})/2 = -C_{b(\text{min.})} = -2.64 \times 10^{11}.[5]$$

If one computes C_{44}^* from C_b making use of the above values for the magnitude and temperature coefficient of $C_d - (C_{22} + C_{33})/2$, one obtains the dotted curve in Fig. 1. Also, the quantities $(1/C_{44}^* - 1/C_{44})^{-1}$ and $-1/2(1/C_{44}^* - 1/C_{44})^{-1}$ are plotted for temperatures above and below 24.2°C,

[3] This temperature coefficient was computed from temperature coefficients of the elastic compliances given by Mason (see reference 1, p. 132).

[4] H. Mueller, Phys. Rev. **57**, 829 (1940).

[5] Huntington's values (see reference 2) give -2.58×10^{11} for $C_d - (C_{22} + C_{33})/2$; this value equals 2.64×10^{11} within the combined errors.

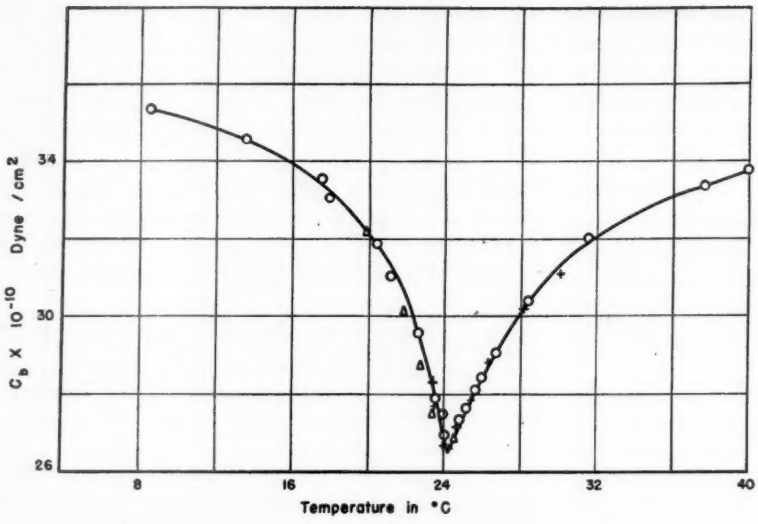

FIG. 2. Temperature dependence of the velocity v of a compression mode in 45° X cut crystals of rochelle salt. $C_b=\rho v^2$.

respectively. Through a limited temperature range around 24.2°C, a straight line results as predicted by the interaction theory.[4] The slope of the line leads to a value of 67.3×10^{-12} for σ, the Curie constant. Mason's data for $S_{44}{}^E$ gives a value for σ of 66.7×10^{-12}.[4]

IV. THE TEMPERATURE DEPENDENCE OF ATTENUATION

The temperature dependence of the attenuation of 10 Mc/sec. ultrasonic pulses in rochelle salt is given in Fig. 3. Curves *a*, *b*, and *c* give the attenuation in db/cm for the quasi-compression mode which travels in the 45° direction of the 45° X cut specimens, for the transverse mode in the 90° Z cut specimens, and for the compression mode propagated along the crystallographic axes, respectively.

Both of the modes which have a maximum in the attenuation at the Curie temperature contain a component of shear strain in the X plane and the expressions for their velocities contain $C_{44}{}^*$. Therefore, this anomalous temperature dependence of the attenuation apparently has the same origin as the

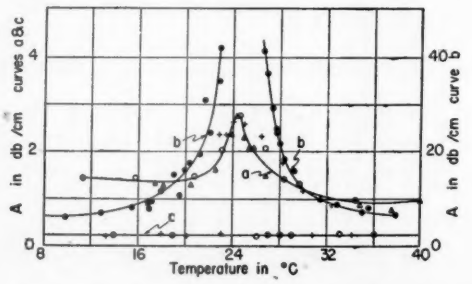

FIG. 3. Temperature dependence of A, the attenuation in decibels per cm of travel, for 10 Mc/sec. ultrasonics in rochelle salt single crystals. Curve *a*—compression mode in 45° X cut crystals. Curve *b*—transverse mode travelling in Z direction. Curve *c*—compression mode propagated along crystallographic axes. ○ Z direction + Y direction. Correction for curve *c*, one-half A is plotted.

other well-known anomalies in the properties of rochelle salt and can be formulated in terms of the interaction theory.

Mason has shown[6] that the low values of "Q" which were observed by him in the foiled 45° X cut bars of rochelle salt vibrating at their resonant frequencies were principally a result of dielectric loss rather than mechanical loss. Mason introduced this loss into his analysis by use of a complex inverse dielectric susceptibility χ_{c1} for the X crystallographic direction. The wave equation for the 90° Z cut specimens becomes

$$\rho(\partial^2u_2/\partial t^2)=C_{44}{}^{**}(\partial^2u_2/\partial x_3{}^2), \tag{2}$$

where

$$C_{44}{}^{**}=C_{44}-f_{14}{}^2/\chi_{c1}. \tag{3}$$

u_2 is the displacement along the Y crystallographic axis, and x_3 is the position coordinate along the Z direction.

The solution of this equation is

$$u_2=u_{20}\exp(-i\omega t)\exp[-(\alpha_2-i\beta)x_3],$$

where

$$\alpha_2-i\beta=-i\omega(C_{44}{}^{**}/\rho)^{-\frac{1}{2}}. \tag{4}$$

Combining Eqs. (3) and (4), one obtains

$$\alpha_2-i\beta=-i\omega\rho^{\frac{1}{2}}\left\{\frac{\chi_1D_{14}+\chi_1{}'{}^2C_{44}-i\chi_1'f_{14}{}^2}{D_{14}{}^2+(C_{44}\chi_1')^2}\right\}^{\frac{1}{2}}, \tag{5}$$

where χ_{c1} has been written as

$$\chi_{c1}=\chi_1-i\chi_1', \quad \text{and} \quad D_{14}=\chi_1C_{44}-f_{14}{}^2. \tag{5}$$

Mueller has pointed out[4] that f_{14} and C_{44} are nearly independent of temperature, but that χ_1 varies with temperature in such a manner as to cause D_{14} to vanish at two temperatures. This

[6] W. P. Mason, Phys. Rev. **58**, 744 (1940).

vanishing of D_{14} in the interaction theory is the origin of the Curie points.

Except very near the Curie temperatures, where D_{14} vanishes, the second degree terms in χ_1' can be neglected, and

$$\beta=\omega/v=\omega(c_{44}^*/\rho)^{-\frac{1}{2}}, \tag{6}$$

while

$$\alpha_2=-\rho v(\chi_1' f_{14}^2\omega)/2D_{14}^2. \tag{7}$$

Since D_{14} tends toward zero, α_2 tends to very large values. For small values of D_{14} the exact expression, Eq. (5), must be used; it predicts finite values of attenuation and non-vanishing values of velocity. However, in the temperature range, where the attenuation is sufficiently small to allow measurements to be made (see Fig. 3), Eqs. (6) and (7), the approximate expressions hold.

The attenuation due to the electrical loss also can be formulated for the 45° X cut specimens. The attenuation coefficient α_2' is

$$\alpha_2'=\frac{-\rho V'\chi_1' f_{14}^2\omega}{2[D_{14}+(C_{22}+C_{33}+2C_{23})/4]^2}, \tag{8}$$

where v' is the velocity. This attenuation is also seen to pass through a maximum at the temperature for which D_{14} vanishes.

The compression modes along the crystallographic axes involve no electromechanical coupling. Therefore, the losses shown by Fig. 3, curve c, include no dielectric loss; instead these losses are made up of apparent attenuation inherent in the pulsed method and of true mechanical absorption. The apparent absorption arises from beam spreading, pulse distortion, and scattering of the ultrasonic energy. If one assumes that both the modes with and without electromechanical coupling experience the same attenuation due to causes other than dielectric losses, one can obtain values of α_2' and α_2 by subtracting Fig. 3, curve c from Fig. 3, curve a and curve b, respectively. The results are shown in Fig. 4, curves b and c.

By combining Eqs. (7) and (8), one obtains a relationship between α_2 and α_2'. If one computes α_2 by using α_2' from Fig. 4, curve c and Mueller's data[7] on the temperature variation for χ_1, one obtains Fig. 4, curve a. The temperature scale on the data for χ_1, was shifted so that the minimum of χ_1 occurred at 24.2°C, our Curie temperature. The constant f_{14} was taken as 7.8×10^4 c.g.s. units.[8] A value of $C_{44}=11.97\times10^{10}$ dyne/cm^2 then was chosen so that D_{14} vanished at 24.2°C.

Values of χ_1', the complex part of the dielectric susceptibility, have been computed from Eq. (8). The temperature variation of this quantity is given by the 10 Mc/sec. curve on Fig. 5. The quantity

[7] See reference 1, p. 620.
[8] W. P. Mason, Phys. Rev. 55, 775 (1939).

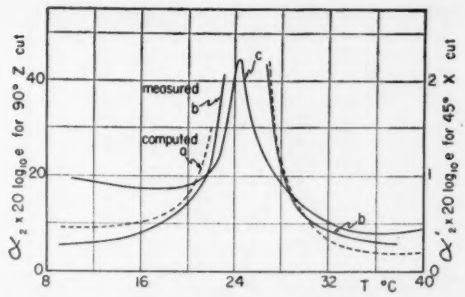

FIG. 4. Temperature dependence of the part of the attenuation as a result of dielectric loss for 10 Mc/sec. ultrasonics in single crystals of rochelle salt. Curve a is α_2 for transverse mode travelling in Z direction computed by Eqs. (7) and (8). Curve b is measured values of α_2 for the same mode. Curve c is the measured value of α_2' for the compression mode in 45° X cut crystals.

$-\chi_1'$ can be shown to be equal to ωR, where ω is the angular frequency and R is the series resistivity of the dielectric. In Fig. 5, values of ωR given by Mason[6] at three frequencies are compared with χ_1'.

The quantity $-\chi_1'$ is proportional to the energy loss per cycle. If the dielectric loss is a hysteresis type, one would expect the loss per cycle and therefore χ_1' to be independent of frequency. On the other hand, if the dissipation is a conduction type, χ_1' will be proportional to frequency. The results shown in Fig. 5 indicate that below the Curie temperature χ_1' is essentially constant for the three dielectric measurements indicating a hysteresis type loss; however, $-\chi_1'$, measured by the pulsed method at 10 Mc/sec., is considerably lower. This result is believed to arise from the much lower amplitude of polarization in the pulsed measurements than in the dielectric measurements. Above the Curie temperature χ_1' is seen to increase with frequency although less rapidly than ω. Therefore, for that temperature range the dissipation of the conduction type is the predominant term.

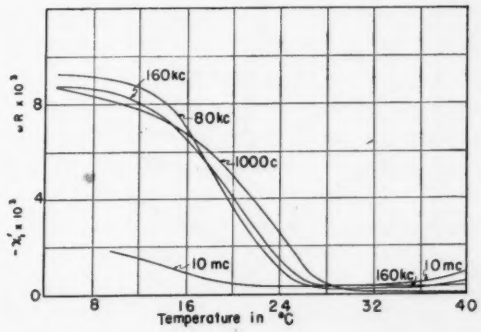

FIG. 5. Comparison of the temperature dependence of the dielectric resistivity R with χ_1', the imaginary part of the complex inverse susceptibility of rochelle salt crystals. The resistivity R was taken from dielectric measurements by Mason (6) at 1000 c/sec., 80 kc/sec. and 160 kc/sec. The quantity χ_1' was measured by the pulsed ultrasonic method at 10 Mc/sec.

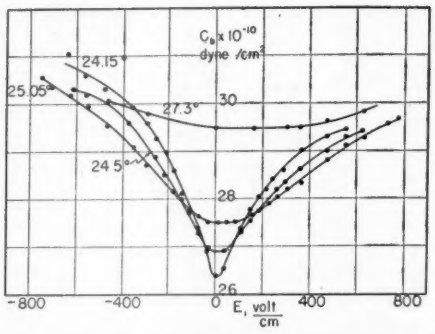

FIG. 6. Dependence of the velocity v of a compression mode in 45° X cut rochelle salt crystals on E_1, the electric field strength in the X direction for temperatures above the Curie temperature. The quantity C_b is equal to ρv^2.

V. THE ELECTRIC FIELD EFFECT

When a d.c. bias field is applied along the X crystallographic axis of a rochelle salt crystal at a temperature near the Curie temperature, a marked increase in the velocity occurs in all modes which contain the elastic compliance $S_{44}{}^E$ (or the elastic moduli C_{44}*) as a major term in the velocity equation. The dependence of $S_{44}{}^E$ on field strength E_1, is adequately predicted by the following formula from the interaction theory.[9]

$$1/S_{44}{}^E = C_{44} - f_{14}{}^2/(\chi_1 + 3BP_1{}^2), \qquad (9)$$

where the polarization P_1 is a function of E_1. B is the coefficient of the fourth degree term in P_1 introduced in the stress-strain energy functions to account for saturation effects. Mueller[10] and Matthias[11] used the self-resonance method to study the dependence of the velocity in 45° X cut bars on field strength and their results were consistent with Eq. (9).

When the pulse technique was applied to study the dependence of velocity in rochelle salt on E_1, the polarity of the bias field was observed to have a large effect. This unipolarity was not observed by the self-resonance method and is not predicted by Eq. (9). The dependence of the velocity on the electric field strength in 45° X cut specimens is given for several different temperatures in Figs. 6, 7, and 8. For each of these curves the direction of propagation was along one of the two 45° directions and the electric field was applied along the X axis, perpendicular to the direction of travel. The temperature was held constant by thermostating the specimen and the electric field strength was varied.

Figures 6 and 7 show the variation of C_b with field strength for a series of temperatures above and below the Curie temperature, respectively. These curves contain data on several specimens. However, in all cases the 45° direction along which an expansion occurred upon the application of a positive voltage was chosen as the direction of propagation. In a 45° X cut rochelle salt crystal an electric field applied in the X crystallographic direction causes an expansion along one 45° direction and a contraction along the other. It is apparent that there is a large asymmetry in the field effect with respect to the polarity of the bias field. Below the Curie temperature even the sign of the initial change in C_b is reversed upon the reversal of the polarity.

Figure 8 gives the results of two sets of measurements which were made on the same specimen. Curve a was taken for propagation along the 45° direction which expanded upon the application of the positive voltage while curve b was taken along the other 45° direction.

In all cases the asymmetry was such that the velocity was larger for the polarity of the field that caused a contraction of the crystal along the direction of propagation.

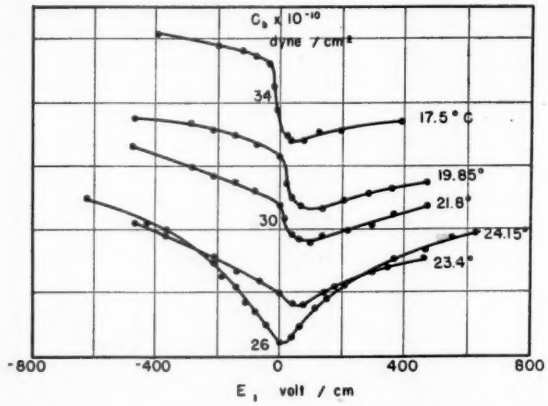

FIG. 7. The quantity $C_b = \rho v^2$ as a function of electric field strength E_1. Same as Fig. 6, except temperatures are below the Curie temperature.

VI. DISCUSSION OF THE MEASUREMENTS OF THE ELECTRIC FIELD EFFECT

Rochelle salt is normally assigned to the rhombic hemihedral class, No. 6. However, it has been pointed

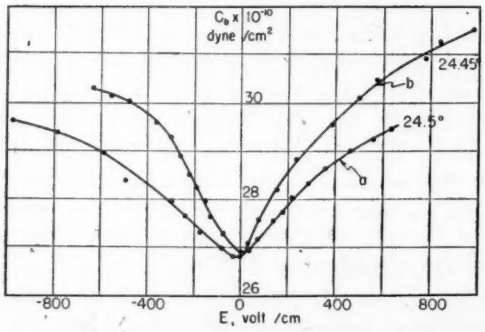

FIG. 8. The quantity $C_b = \rho v^2$ as a function of electric field strength E_1 for the two perpendicular 45° directions in a 45° X cut rochelle salt crystal. Curve a—propagation along 45° direction which elongates with positive field strength; curve b—propagation along other 45° direction.

[9] H. Mueller, Phys. Rev. **58**, 565 (1940).
[10] H. Mueller, Phys. Rev. **57**, 842 (1940).
[11] B. Matthias, Helv. Phys. Acta **16**, 99 (1940).

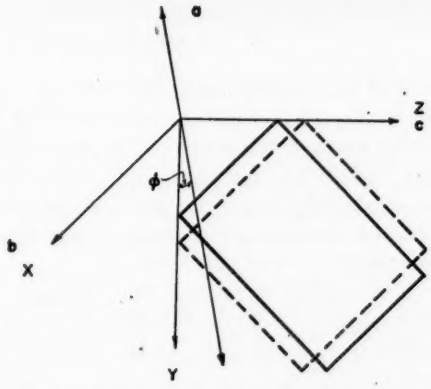

FIG. 9. Convention for assigning crystallographic axes to rochelle salt with monoclinic structure.

out by Jaffe[12] that when the crystal lattice is sheared the symmetry of the crystal is reduced. The reduction in symmetry occurs spontaneously in the ferroelectric temperature range even in the absence of an electric field and artificially in any temperature range when a d.c. bias field is applied in the X crystallographic direction. Jaffe has shown that in the sheared condition the crystal should be assigned to the monoclinic hemimorphic class, No. 3. As a result of the deformation, new physical constants come into being in the crystal. Mueller has given the name "morphic effects" to the effects that arise with the new constants.

The author believes that the asymmetry observed in these measurements is a morphic effect arising from the new elastic constants introduced when the crystal is sheared by the electric field. To test this theory one must see how the new constants enter into the velocity equation.

When the crystal lattice is sheared in the X plane through the angle ϕ as shown in Fig. 9, the monoclinic crystallographic axes a, b, and c are assigned as indicated. By the convention chosen for the case of rochelle salt the X axis coincides with the polar axis b, the Z axis coincides with the c axis, and the Y axis is chosen to complete a right-handed system.

The change from the rhombic crystal structure to the monoclinic structure adds the elastic constants C_{14}, C_{24}, C_{34}, C_{56}, and the piezoelectric constant f_{26} to the constants necessary to describe the system. If one computes the transformed elastic constant C_{22}' in the monoclinic crystal for a system of axes rotated 45° around the X axis, one obtains

$$C_{22}'=\frac{C_{22}+C_{33}+2C_{23}+4C_{44}}{4}\pm(C_{24}+C_{34}), \quad (10)$$

the minus and plus signs holding for a rotation from the positive Y direction toward the positive and negative Z axes, respectively. Therefore, by

[12] H. Jaffe, Phys. Rev. 51, 43 (1937).

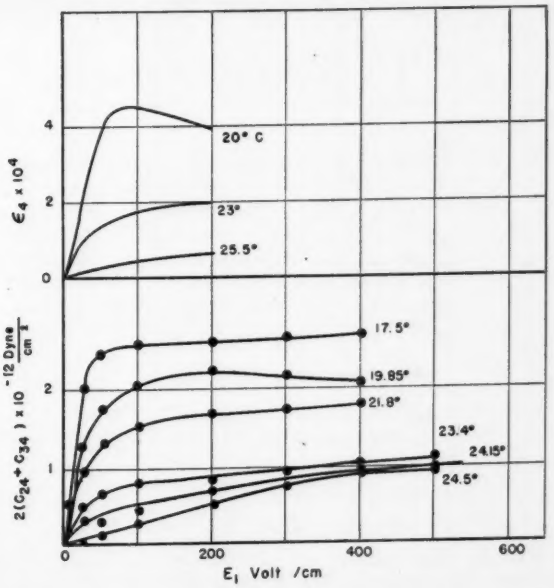

FIG. 10. Lower curves—the dependence of the sum of the induced monoclinic elastic constants C_{24} and C_{34} on the electric field strength E_1 for rochelle salt crystals. Upper curves—dependence of strain on static fields, from Vigness (see reference 13).

use of Fig. 9 showing the expansion and contraction of the 45° X cut crystal when the crystal lattice is sheared, it is seen that the positive and negative signs hold for the contracted and expanded dimensions, respectively.

The velocity in the 45° direction is given by

$$\rho v^2=C_b\cong C_{22}'-f_{14}^2/\chi_1. \quad (11)$$

The induced piezoelectric constant f_{26} can be neglected in the piezoelectric term.

From Eq. (11) it follows that the difference in the quantity C_b for positive and negative fields of the same magnitude is $2(C_{24}+C_{34})$. The dependence of this difference on field strength is given in Fig. 10 for several different temperatures. On the same figure static measurements made by Vigness[13] of the piezoelectric strain as a function of field strength are shown. The striking similarity between the two sets of curves indicates a very definite correlation between the observed asymmetry and the distortion of the crystal lattice and helps to verify the hypothesis that this is a morphic effect.

Neither the elastic nor the piezoelectric data are sufficiently complete to allow one to determine an exact relationship between $(C_{24}+C_{34})$ and the strain ϵ_4. However, if one assumes that the two quantities are proportional, one has

$$C_{24}+C_{26}=k\epsilon_4,$$

where

$$k\sim 3\times 10^{13} \text{ dyne/cm}^2\text{/radian}.$$

[13] I. Vigness, Phys. Rev. 46, 255 (1934).

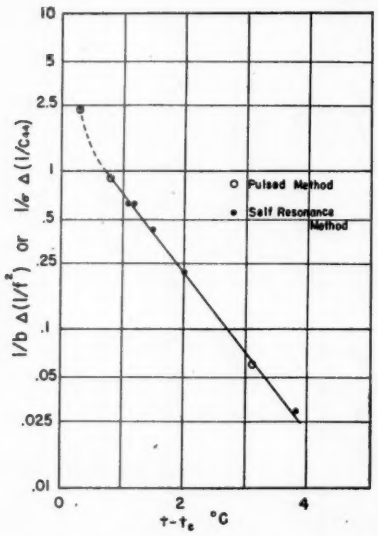

FIG. 11. The temperature dependence of $1/\sigma\,\Delta(1/C_{44})$ on rochelle salt crystals. The applied field strength was 300 volt/cm. The quantity t_c is the upper Curie temperature. Self-resonance data is from Mueller (see reference 9).

The question arises as to why this unipolarity was not observed by the investigators who studied the field effect by the self-resonance method. The resonant frequency is proportional to the reciprocal of Young's modulus Y which for the 45° X cut bar in the monoclinic state is given by

$$1/Y=1/4[S_{22}+S_{33}+2S_{23}+S_{44}{}^{E}\pm(S_{24}+S_{34})],$$

where the sign to be taken again depends on the polarity of the bias field.

By computing $(S_{24}+S_{34})$ from the value of the elastic moduli of rochelle salt one obtains

$$S_{24}+S_{34}=[-1.86\times(C_{24}+C_{34}),\\ +1.89\times C_{14}]\times10^{-23}. \quad (12)$$

The value of C_{14} is unknown, but one can say that the effect of $S_{24}+S_{34}$ could be at the most 5 percent of the total change with field. Therefore, it is not surprising that the morphic effect has not been reported previously, since the self-resonance method is considerably less sensitive to the effect than is the pulsed method.

The relationship between the change in the resonant frequency f of the 45° X cut bar and in the elastic moduli $S_{44}{}^{E}$ (or $1/C_{44}{}^{*}$) is[9]

$$1/\sigma\,\Delta(1/C_{44}{}^{*})=1/\sigma\,\Delta S_{44}{}^{E}=1/b\,\Delta(1/f^2),$$

where b is a constant depending on the mode of the bar. The changes which were produced in these two quantities by the application of a field of 300 volt/cm are shown in Fig. 11 for several values of $(t-t_c)$, where t is the temperature of the crystal and t_c is the Curie temperature. The values of $1/b\,\Delta(1/f^2)$ were taken from Mueller's data;[9] for those experiments t_c was 23°C. The data for $1/\sigma\,\Delta(1/C_{44}{}^{*})$ were obtained from Fig. 6 by computing the average value of the change in C_b for values of E_1 of +300 and −300 volt/cm; the temperature t_c of course was 24.2°C. Since all these points lie on a single curve, it follows that the same dependence of $S_{44}{}^{E}$ (or $1/C_{44}{}^{*}$) on field strength E_1 has been found by the self resonance and pulsed methods.

VII. ACKNOWLEDGMENT

The author expresses his gratitude to Dr. H. B. Huntington for his encouragement and advice throughout the course of this work.

Temperature Dependence of the Work Function of Semiconductors*

A. H. SMITH**
Randal Morgan Laboratory of Physics, University of Pennsylvania, Philadelphia, Pennsylvania
(Received September 13, 1948)

Samples of *P*-type and *N*-type silicon and of *N*-type germanium have been examined to determine the temperature dependence of the work function of these semiconductors as they are heated to near intrinsic temperatures. High temperatures of the semiconductors were obtained by passing current directly through the sample, and observations were made as the sample cooled. The method of determining change in work function was to observe the current *versus* voltage curves of photoelectrons emitted from a tantalum surface and arriving at the semiconductor surface. This experiment indicated negligible change in work function of semiconductors at high temperatures from that at 200 degrees C. These results are consistent with the hypothesis of surface energy states.

LIST OF SYMBOLS

The symbols used through this paper are defined as follows:

χ—difference in energy between the electrochemical potential and the surface energy level, the subscript s referring to semiconductors and m to metals.
θ_s—difference in energy between the top of the filled band and the surface energy level.
ϕ_s—energy separation of the bottom of the conduction band and the surface energy level.
ΔE_1—width of the forbidden band in semiconductors.
ϵ_n—separation of the electrochemical potential from the bottom of the conduction band in *N*-type semiconductors.
ϵ_p—separation of the electrochemical potential level from the top of the filled band in *P*-type semiconductors.
V_c—negative bias (stopping potential) necessary to just stop electrons from reaching the semiconductor at room temperature.
V_h—stopping potential in the intrinsic range.
ΔV_s—energy rise at the surface due to occupied surface energy levels.
ϵ—activation energy from temperature variation of conductivity. In the intrinsic case it is equal to $\Delta E_1/2$.

I. INTRODUCTION

THE work of a semiconductor[1] in the experiments to be described is defined as the energy necessary to remove an electron possessing the electrochemical potential of the interior to the field free region outside the semiconductor. The value of the work function is important for a quantitative consideration of the action of the rectifying barrier established when metal semiconductor contacts are formed. Meyerhof[2] has measured the difference of work function of metals and semiconductors by a modified Kelvin method and the contact potential difference of intimate metal semiconductor contacts by the temperature variation of resistance[3] and finds little connection between these two types of observations. The rectification properties of *N*- and *P*-types are supposedly dependent upon the work function of the metal in contact with the surface, *N*-type giving rectification only with metals of higher work function than the semiconductor, and *P*-type only with lower work function metals. This hypothesis is found to be contrary to experience. The above difficulties have been resolved by Bardeen[4] who assumes there exist surface states which result in the formation of a dipole layer 10^{-5} to 10^{-6} cm deep.

The work function of a semiconductor has been thought to be temperature dependent for *N*-type and *P*-type semiconductors; for example, a change of about a half volt is expected for silicon of either type as the temperature is raised to the intrinsic range.[2] With increasing temperature, this change would be an increase for *N*-type and a decrease for *P*-type. The change should arise from a shift of the electrochemical potential in the semiconductor toward a point halfway between the top of the filled band and bottom of the conduction band. The number of useful acceptor or donator energy levels becomes negligible in comparison with the number of occupied levels in the conduction band at higher temperatures (greater than 750°C with silicon having 10^{17} donators per cm^3). The energy level schemes for semiconductors are illustrated in Fig. 1.

The measurements of the work function are made by allowing a monochromatic beam of light to

* This work constituted a thesis in partial requirement for the Ph.D. degree at the University of Pennsylvania.
** Now at Wheaton College, Wheaton, Illinois.
[1] The type of semiconductor can be determined by measurements of the Hall effect, thermoelectric characteristics, or rectification properties. *P*-type is identified by a positive Hall coefficient, a negative hot electrode in the Seebeck effect, or easy flow of current when the semiconductor is positive in a metal-semiconductor rectifying junction. The identification in this experiment was made by the last method.
Intrinsic semiconductors combine the conductivity by holes of *P*-type with electron conductivity of *N*-type, the number of holes being equal to the number of conduction electrons and the source of electrons in the filled band. The sign of the Hall and Seebeck constants depends in the intrinsic case, on the relative mobilities and masses of the carriers. The conductivity varies with temperature as $\exp\epsilon/kT$ where the activation energy ϵ is large compared with that for *N*- or *P*-type, and is approximately half the energy gap between the top of the filled band and the bottom of the conduction band.
[2] W. E. Meyerhof, Phys. Rev. **71**, 727 (1947).
[3] W. E. Stephens, B. Serin, and W. E. Meyerhof, Phys. Rev. **69**, 42 (1946).
[4] J. Bardeen, Phys. Rev. **71**, 720 (1947).

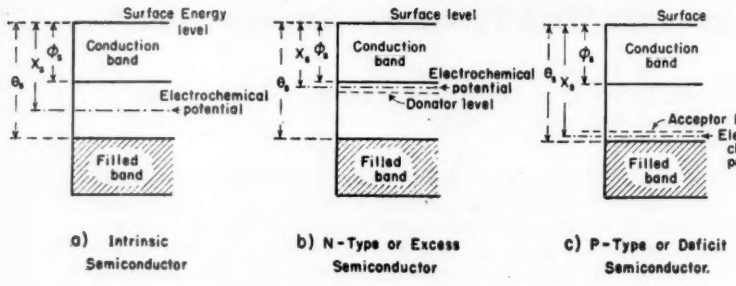

FIG. 1. Energy level schemes for various types of semiconductors.

strike a metal emitter. The electron current which arrives at the semiconductor collector when plotted as a function of the potential of the semiconductor relative to the metal yields stopping potential curves from which the work function of the semiconductor is determined. It can be shown that this work function is measured independently of the work function of the metal. Figure 2 illustrates for low and high temperatures of the semiconductors the energy relationships in the experiment. A more detailed account of the theory is found in the companion paper.

The following equation[5] applies at room temperature to N-type semiconductors:

$$h\nu=\chi_s+V_c=\phi_s+\epsilon_n+V_c; \qquad (1)$$

while the material is heated to the intrinsic range, the following relationship holds approximately

$$h\nu=\chi_s+V_h=\phi_s+(\Delta E_1/2)+V_h. \qquad (2)$$

Here ϕ_s is the energy interval between the bottom of the conduction band and the surface. It is to be distinguished from χ_s which is the work function of the sample. Thus $V_h-V_c=-[(\Delta E_1/2)-\epsilon_n]$ where $\Delta E_1\simeq 1.0$ volts and $\epsilon_n\simeq 0.01$ volt. If a P-type semiconductor is used

$$V_h-V_c=(\Delta E_1/2)-\epsilon_p \text{ where } \epsilon_p\simeq 0.01 \text{ volt.}$$

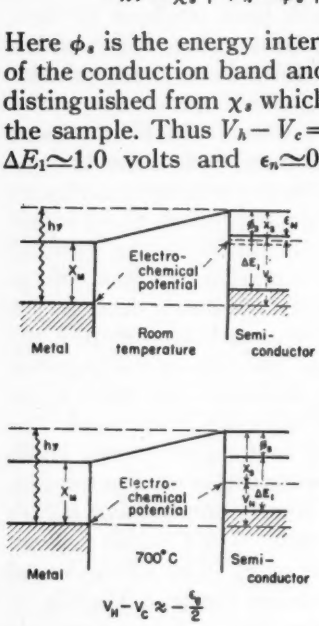

FIG. 2. Energy diagram for photoelectric measurement of work function of a semiconductor having no surface states.

II. MEASUREMENT OF WORK FUNCTION

The arrangement of the apparatus is shown schematically in Fig. 3. A beam of monochromatic light falls on the tantalum surface from which photoelectrons travel to the semiconductor surface. Silicon and germanium were selected for these experiments because samples can be prepared whose bulk conductivity at a given temperature is influenced very little by prolonged heating in a vacuum.

The source of light is a Hanovia Utility High Pressure Mercury Vapor lamp, from which 120-cycle light is obtained. The radiation is filtered by a Corning No. 791 ultraviolet filter which cuts out all principle wave-lengths shorter than 2536A and passes those above. The threshold of all metal used in the apparatus except the tantalum is less than 3000A, thus the longer wave-lengths are of negligible importance. All computation is done using the 2536 resonance line. The light is focused by a quartz lens and passes through a quartz window to illuminate the tantalum surface from which the electrons are emitted.

Figure 4 shows a detailed drawing of the apparatus which houses the sample. The assembly is machined out of brass and silver-soldered together. All leads to the sample and tantalum are of No. 8 copper wire. These serve as leads through which current for heating and out-gassing pass, as well as for mechanical support. The vacuum is maintained at about 10^{-6} mm of Hg by a two-stage oil diffusion pump using Octoil, and a liquid air trap directly below the cavity in which the sample and tantalum are mounted. The arrangement of the tantalum relative to the sample is such as to cause a small amount of direct reflection of the mercury resonance line on the latter surface. Since the sidewalls of the housing receive the reflected light and are a possible source of spurious photoelectrons, the whole apparatus is nickel-electroplated. Experiment shows that there is no background of photoelectrons from this nickel plating.

[5] All symbols are defined in Appendix. The subscript s refers to semiconductors and m to metals.

The preamplification of the photoelectron current arriving at the semiconductor surface is accomplished by an RCA No. 38 tube used with low plate and filament voltages to permit the use of a high grid resistance (10^8 ohms) as shown in Fig. 5. A Decade Amplifier Model 102A, made by Kay Laboratories, San Diego, California is used as the next stage of amplification. A "Twin T" 60-cycle band elimination filter is used to reduce pick-up before feeding the signal to the oscilloscope amplifier. The total amplification is such that 1 millivolt (10^{-11} ampere) fed into the preamplifier gives an inch deflection on the oscilloscope. Figure 3 is the block diagram showing the assembly of these components.

The temperature of the sample is estimated to plus or minus 50°C by means of a platinum wire bolometer consisting of a strand of 0.0012-inch wire mounted about 1 mm in back of the sample. The error arises from thermal lag in the bolometer element.

The instantaneous values of the stopping potential of the semiconductor for photoelectrons from the tantalum are observed, as the sample cools from 750°C to room temperature, by plotting on an oscilloscope the electron current to the semiconductor *versus* the potential of the tantalum relative to the semiconductor and photographing the resultant pattern on the system.

It would be expected that a retardation curve of the type in Fig. 6 would be obtained if an alternating voltage were placed between the sample and the tantalum, the light source being of constant intensity. However, the capacity between the sample and the tantalum is sufficiently large that the displacement current is of the same order of magnitude as the conduction current of photoelectric origin, so a one-second sweep must be used. The horizontal sweep of the oscilloscope is accomplished by a relaxation circuit, shown in Fig. 5. A fractional part of this voltage is applied to the tantalum surface, so that a certain position on the screen always corresponds to a definite voltage of the sample relative to the tantalum regardless of the condition of the batteries. Three ranges of voltages of sample with respect to the tantalum are obtainable: plus or minus 4 volts, plus or minus 1 volt, and plus or minus 0.5 volt. When the tantalum is negative relative to the sample, the pulsating photoelectron beam produced by the modulated light source arrives at the semiconductor and is a sufficiently large signal to be amplified and cause a vertical deflection on the oscilloscope screen; no signal is apparent when the tantalum is positive. A typical photograph of the oscilloscope screen is shown in Fig. 7.

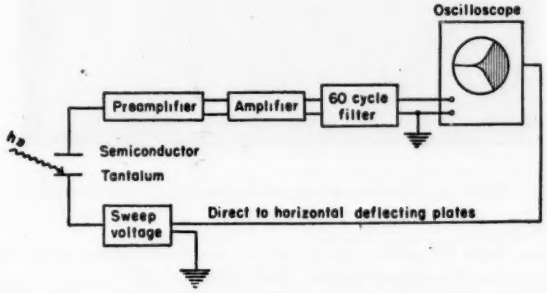

FIG. 3. Schematic diagram of apparatus.

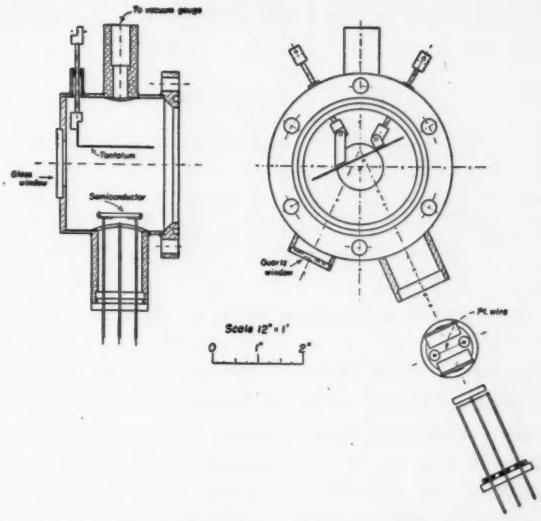

FIG. 4. Diagram of apparatus for housing semiconductor sample and tantalum.

The series of photographs by which a run is recorded is made by triggering the sweep simultaneously with the shutter of a Sept 35-mm robot camera. As the sample cools, the pattern on the oscilloscope screen is photographed at 100° intervals from 750°C to 450°C and at 50° intervals from 450° to 200°C.

The out-gassing operating is one in which the tantalum and sample are both heated to incandescence and so maintained until the vacuum re-

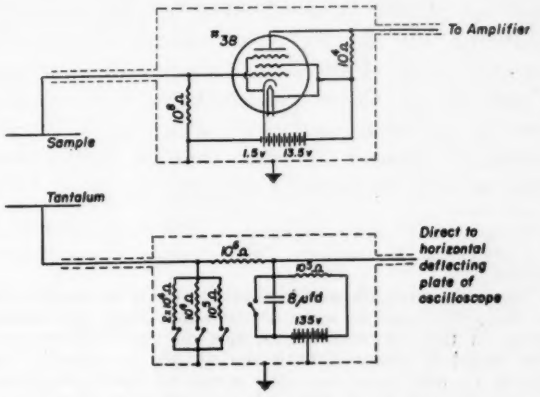

FIG. 5. Pre-amplification circuit and relaxation sweep circuit.

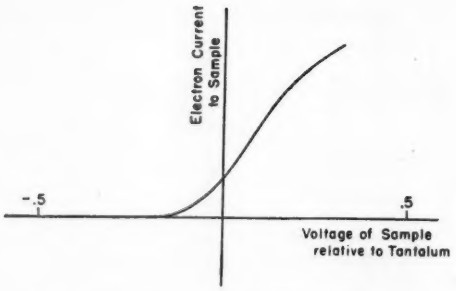

FIG. 6. Simple stopping potential curve.

mains better than 10^{-5} mm of mercury. By the time the surfaces have cooled to room temperature, the vacuum remains below 2×10^{-6} mm of mercury although the sample receives short heating to approximately 1000°C. It is necessary to heat the sample this high in order to begin observations at 750°C because the sample cools very rapidly Melting of the supports and sample at this high temperature is not uncommon. Therefore, higher temperatures in the intrinsic range cannot be explored in the apparatus.

A sample of silicon or germanium is prepared in the following way for use in the apparatus. The *P*-type silicon was supplied by the M.I.T. Radiation Laboratory. The doping of these samples is known and in most cases is beryllium and boron. Tin-doped germanium was furnished by Sylvania,[6] in slices about 1-mm thick and one and seven-eighths inches in diameter. Bell Laboratories[7] supplied *N*-type phosphorus-doped silicon, 1-inch square and about 1-mm thick. Those samples not already in thin slabs are cut thus on a diamond wheel, after which they are trimmed to shape roughly one inch square. Both sides of the slabs are ground flat with No. 600 carborundum, floated in water, and ground on plate glass. One side is then nickel-electroplated, the nickel-plating adhering to the freshly ground surface very satisfactorily; 20 milliamperes per square inch for 5 minutes gives adequate backing. Cracking of the semiconductor because of local heating results when no plating is used. After mounting in the apparatus, the sample is out-gassed by repeated flashing to 800°–1000°C until there is little change in pressure at these temperatures. This requires about a half hour of flashing after which the apparatus is allowed to reach thermal equilibrium. After an hour or more, a run may be made.[8] The conductivity of the *N* and *P* silicon samples was about 10 ohm^{-1} cm^{-1}. In order to approach the intrinsic range, a temperature of 700°C is required for silicon of this conductivity. For the germanium samples the intrinsic range is obtained at the temperature reached in this experiment.

Projections of the photographed patterns are made on graph paper as shown in Fig. 8. The method of determining the stopping potential for any one pattern is to observe as nearly as possible the point at which the curve leaves the horizontal axis. A current increase of 1 percent of the saturation value is easily discerned. Fortunately, the curves as a function of temperature are of quite similar shape. Because of the geometry of apparatus and the limited range of currents observed, a detailed examination of the shapes of the photocurrent *vs.* bias curves is not meaningful. DuBridge plots[9] (current *vs.* bias voltage/kT) were of reasonable shape and indicated that our stopping potential agreed within ±0.1 volt of the stopping potential for a uniform emitter at absolute zero of temperature.

Within the limits of experimental error, all values of the stopping potential for a given semiconductor remain constant between 750°C and 200°C as shown in Fig. 9, which summarizes all the experimental data for *N*- and *P*-type silicon and *N*-type germanium. Each point represents the average of three or more runs. The precision in an

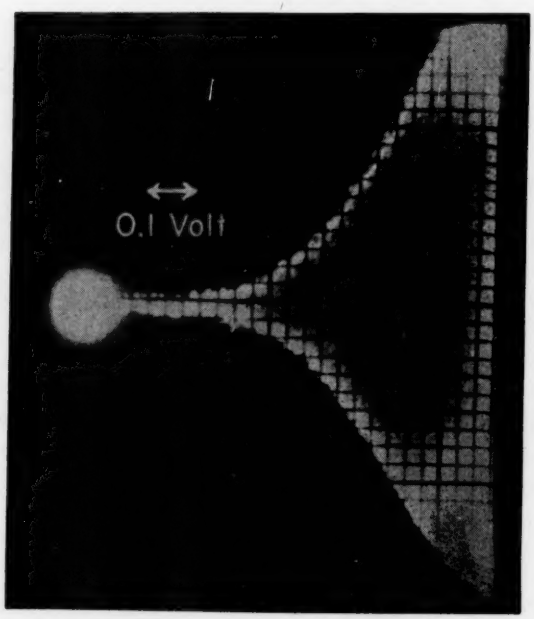

FIG. 7. Photograph of stopping potential curve with modulated light source.

[6] Courtesy of H. Heins, Sylvania Special Products Division.
[7] Courtesy of W. Shockley, Bell Telephone Research Laboratories.
[8] When the tantalum alone is heated to glowing temperature and allowed to cool to room temperature, there is a marked change in the pattern's appearance on the oscilloscope. A large signal is observed with the sample at negative bias relative to the tantalum. This seems to imply that some impurity is driven off from the tantalum to the sample, making the sample more photosensitive than the metal. This results in a photocurrent from the semiconductor to the metal rather than from the metal to the semiconductor. Once the sample has been heated, the effect disappears.
[9] L. A. DuBridge, *New Theories of the Photoelectric Effect* (Hermann and Cie, Paris, 1935).

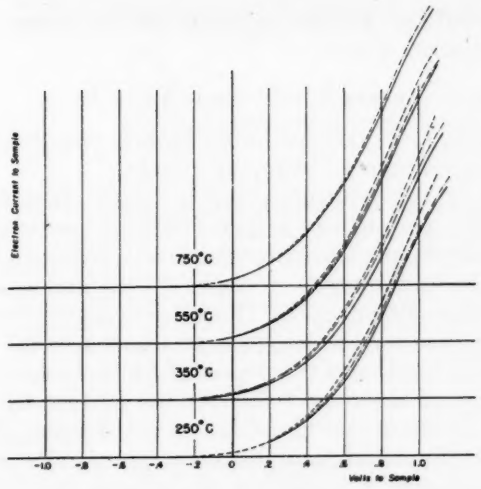

FIG. 8. Stopping potential curves (envelope) for *P*-type silicon for various temperatures. Several runs are represented by the various shadings of the lines.

individual point is believed to be plus or minus 0.05 volt.[10]

The values of the work function of semiconductors found from estimates of the cut-off point are as follows:

	T	
N-type silicon	250°C	4.5 volts
	750°C	4.6 volts
P-type silicon	250°C	4.5 volts
	750°C	4.6 volts
N-type germanium	250°C	4.5 volts
	750°C	4.5 volts

It should be emphasized that these values do not represent the work function of a clean silicon or germanium surface but merely are typical of the out-gassing procedure peculiar to this experiment.

III. DISCUSSION OF RESULTS

The changes in cut-off voltage predicted by Eqs. (1) and (2) have not been observed. The results are in agreement with Bardeen's assumptions as to the nature of surface states. Meyerhof[2] made extensive measurements of the contact potential difference between metals and silicon and germanium. Reasoning from the above energy schemes, it can be shown that metals with low work function should give high rectification with acceptor semiconductors and conversely, high work function metals rectify with the donator semiconductors. But his experiments show that there is little dependence on the work function of the metal in respect to rectification properties, the same metal giving rectification with both deficit and excess semiconductors. Their behavior was as if the semiconductors carried with them a potential barrier of almost constant height, thus causing rectification properties to be practically independent of the metal.

The concept that there may be surface states on a semiconductor has been discussed but has lacked experimental proof. Bardeen[4] has summarized the theory of surface states indicating that results of the type reported by Meyerhof and by the author are to be expected. For discussion, it is convenient to consider the donator (*N*-type) semiconductor. On the clean surface of this substance there is thought to appear a dipole layer consisting of ionized impurity atoms, positively charged and an equalizing negative charge just inside the surface

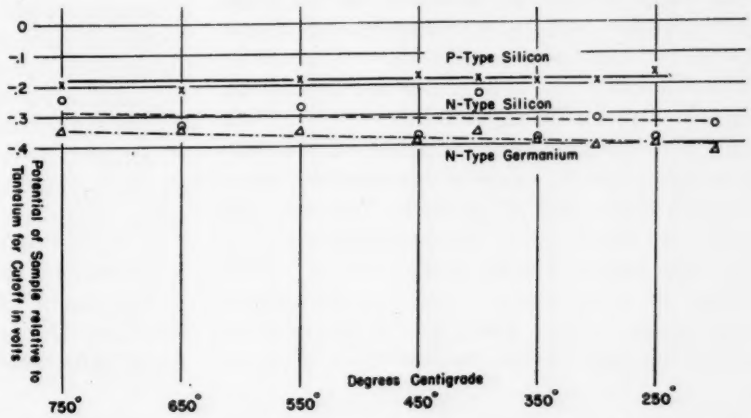

FIG. 9. Summary of cut-off potential values as a function of temperature for various semiconductors.

[10] In the first sets of observations, the sample was permitted to return nearly to room temperature. It was observed that the stopping potential varied in the temperature regions below 200°C. The vacuum was held between 10^{-6} and 2×10^{6} mm of mercury. At this pressure and room temperature, calculation shows that if each molecule that hits the silicon surface sticks, a mono-molecular layer of gas can form on the surface of the semiconductor in about one second. The contamination of the surface is apparently avoided if the temperature of the sample is maintained above 200°C. The evidence for this is the reproducibility of the retarding potential curves during the three successive trials that constitute a run. If surface layers are formed, their characteristics should be the same for both *N*- and *P*-type silicon, provided once the molecules are on the surface there is no tendency to group around the surface impurity atoms. Such deposited atoms may effect the number of surface states but as long as the original number of surface states is large their contribution can be neglected.

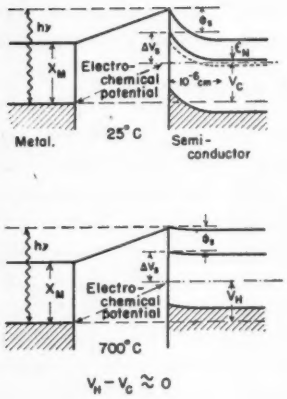

FIG. 10. Energy diagrams for photoelectric measurement of work function of a semiconductor having surface states of very high density.

due to electrons in the surface states. (At high temperature the spacial distribution of electrons and holes must also be considered.) Thus the blocking layer is electrically neutral yet possesses a potential barrier of the correct type to explain this phenomena. This is the barrier pictured in Fig. 10 for N-type semiconductor at low and high temperature.

When two substances at the same temperature are electrically connected together, but not in contact, the electrochemical potential of one becomes equal to that of the other. There is an electrical field in the empty space between the two surfaces. If there exist surface states, there is a curving up of the potential levels near the surface for N-type silicon, penetrating 10^{-5} to 10^{-6} cm. While the electrochemical potential is still the same as the surface and the interior, the electronic levels are raised near the surface. The potential gradient between these surfaces will be different from the expected $\chi_m - \chi_s$, where χ_s is the work function without surface states (Fig. 2). When surface states are present, the work function of N-type semiconductors is changed because of the curving up or down of the potential levels at the surface. Figure 10 illustrates the application of this energy scheme to the present experiment, where the metal is the source of photoelectrons and the semiconductor the receptor. The stopping potential to which the semi-conductor must be raised is not determined by the position of the electrochemical potential of the interior alone, but is influenced by the energy scheme of the surface itself. From a study of Fig. 10, the equation for the lower temperature is

$$h\nu = \chi_m + \text{K.E.} = \varphi_s + \Delta V_s + V_c,$$

where K.E. is the maximum kinetic energy of the electrons liberated from the metal.

When the semiconductor is raised toward the intrinsic region, say above 500°C in germanium, the electrochemical potential in the interior of the semiconductor begins to approach the mid-position in the forbidden region. This is because all electrons in the donator level have been excited to the conduction band, and the source of further electrons is the top of the filled band. At the surface there is still the energy distance, ϕ_s, to the bottom of the conduction band, and then a drop of ΔV_s to the electrochemical potential to which the cut-off potential is referred. In Fig. 10, we see that $V_h - V_c$ may be very small.

In brief, all that is inherent in this result is the assumption that the electrochemical potential at the surface be independent of temperature. From Fig. 9, it is evident that the V's for N- and P-type silicon differs by only 0.1 volt. This means that the electrochemical potential for N-type surface states and P-type surface states must be about the same distance below the conduction band. In the figures shown it is assumed for reasons of simplicity only, that the electrochemical potential of the surface lies approximately halfway between the top of the filled band and the bottom of the conduction band, i.e., $\Delta V_s \simeq \Delta E_1/2$. Comparable results are obtained for P-type semiconductors.

In the preceding discussion the change in the electrochemical potential, resulting from the thermal gradient within the metal connecting the hot semiconductor with the cold photo surface, has been neglected since the change in energy of the electrochemical potential level expected is the order of thermoelectric voltages, namely millivolts.

The author takes great pleasure in thanking Dr. P. H. Miller, Jr. for the suggestion of this experiment and for his constant advice and encouragement. Thanks are also due to Mr. Edwin Hahn for his help in organizing this material. This work was sponsored by the Office of Scientific Research and Development under Contract OEMsr-388 and by the Navy Department Bureau of Ships, under Contract NObs-34144.

The Effect of Surface States on the Temperature Variation of the Work Function of Semiconductors*

JORDAN J. MARKHAM** AND P. H. MILLER, JR.
Randal Morgan Laboratory of Physics, University of Pennsylvania, Philadelphia, Pennsylvania
(Received September 13, 1948)

The effect of surface states on the temperature variation of the work function of semiconductors is considered in this paper. In the first part the variation of the electrochemical potential is given on the basis of an equation due to Fowler. An attempt is made to show at what temperature a semiconductor becomes intrinsic. In the last part the temperature variation of the work function is considered for various densities of surface states and numbers of donator (or acceptor) levels. To carry this calculation through a new expression, which is temperature dependent, is suggested for the number of electrons in the surface states. By using appropriate values obtained from experiment one is able to explain A. H. Smith's results.

I. INTRODUCTION

RECENT results[1–5] indicate that the conventional statistical thermodynamic approach to surface phenomena[6–8] of semiconductors is at variance with experiment. Bardeen[9] has suggested that the discrepancy in the theory can be rectified by the introduction of surface states of high density. His development of the theory is not complete enough so that one can describe in detail the expected temperature variation of the work function. We have therefore attempted to develop the theory sufficiently to predict these variations under conditions which might occur in practice.

An energy diagram of the N-type of semiconductor is illustrated in Fig. 1. The cross hatching represents the topmost filled band at 0°K. ΔE_1 above the top of this level is the next allowed band which is empty at 0°K while ΔE_2 above the filled band are the donator levels. Except at absolute zero there are electrons in the upper (conduction) band which arise from the ionization of the donator levels and excitation of the electrons in the highest filled band. φ_s represents the work necessary to take an electron from the lowest level in the conduction band to a position at rest outside of the solid. For our purposes we may think of φ_s as being a dipole layer which confines the electron to the solid. This is essentially the Drude-Sommerfeld model which, though not strictly correct, can be reconciled with the modern theory of solids by using an effective mass for the free electron mass; also φ_s is more than simply a dipole layer.[10] μ is the height of the electrochemical potential[11] (e.c.p.) above the filled band.

It follows from thermodynamical arguments that if there is a battery between a metal and a semiconductor the difference in the e.c.p.'s is equal to the e.m.f. of the battery. As illustrated in Fig. 2, Smith measured such a difference by adjusting the e.m.f. so that an electron ejected photoelectrically from the metal will just be stopped before reaching the semiconductor. We are interested in the potential difference between an electron at rest outside the semiconductor and the potential of this battery —i.e., the level of the e.c.p. relative to an electron at rest outside. Since Smith did his work at various temperatures, we are particularly interested in how this quantity will vary. The work function[8] (which to a good approximation is equal to the depth of the e.c.p. relative to the outside) for the model illustrated in Fig. 1 is $\Delta E_1 - \mu + \varphi_s$. Measurements of the work function of metals indicate a small variation with temperature. In metals this is a result of a change in φ_s arising from changes in the surface structure since changes in the e.c.p. are very small. For semiconductors the e.c.p. may vary with temperature, but the experimental value of the work

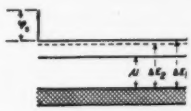

FIG. 1. Conventional model of levels in N-type semiconductor.

* This work was supported by Contract NObs-34144 with the Bureau of Ships.
** Now at Brown University, Providence, Rhode Island.
[1] W. E. Meyerhof, Phys. Rev. **71**, 727 (1947).
[2] W. H. Brattain and W. Shockley, Phys. Rev. **72**, 345 (1947).
[3] W. H. Brattain and J. Bardeen, Phys. Rev. **74**, 231 (1948).
[4] W. Shockley and G. L. Pearson, Phys. Rev. **74**, 232 (1948).
[5] A. H. Smith, preceding paper.
[6] N. F. Mott and R. W. Gurney, *Electronic Processes in Ionic Crystals* (Oxford University Press, New York, 1940), Chapter V.
[7] R. H. Fowler, *Statistical Mechanics* (Cambridge University Press, London, 1936), Chapter XI.
[8] An excellent treatment of the general background needed for this subject is found in R. H. Fowler and E. A. Guggenheim, *Statistical Thermodynamics* (Cambridge University Press, London, 1939), Chapters II and XI.
[9] J. Bardeen, Phys. Rev. **71**, 717 (1947).
[10] F. Seitz, *The Modern Theory of Solids* (McGraw-Hill Book Company, Inc., New York, 1940), particularly Chapter XI.
[11] Following Bardeen, we shall use the expression "electrochemical potential" in agreement with E. A. Guggenheim, *Modern Thermodynamics by the Method of Willard Gibbs* (Methuen and Company, Ltd., London, 1933). References 7 and 8 use the term "partial potential."

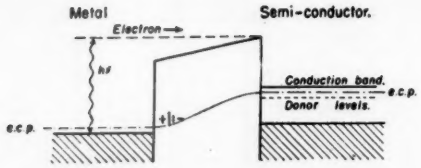

FIG. 2. Illustration of Smith's experiments.

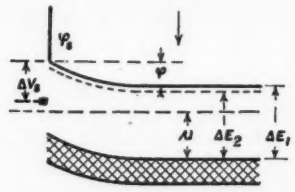

FIG. 3. Effect of surface charge on levels of N-type semiconductor.

function remains essentially constant. Bardeen's explanation is to postulate electron states on the very surface (surface states). As illustrated in Fig. 3, these states will cause an additional dipole layer of moment, $\varphi/4\pi$, which lowers (or raises) the levels inside the solid by φ. If one postulates an appropriate number of surface states, the observed phenomena can be explained.

In this paper an attempt has been made to examine the temperature variation of the work function on a model similar to Bardeen's. The study has been limited to a free neutral surface though the equations could be adapted to the case where there are induced charges. We hope that these calculations will give suggestions for future experimental work as well as an interpretation of Smith's results.

The conclusions reached in the paper are summarized in the final section, and the reader who does not want the details may omit the intermediate parts.

II. TEMPERATURE VARIATIONS OF THE ELECTROCHEMICAL POTENTIAL

Fowler (reference 7, Eq. (1137)) has obtained an expression for the e.c.p. of the N-type model we are using. He obtains

$$[\lambda\omega_1(2\pi m_1 kT)^{\frac{3}{2}}/h^3]\epsilon^{-\Delta E_1/kT}=[n/(\lambda\epsilon^{-\Delta E_2/kT}+1)]+[\omega_2/\lambda][(2\pi m_2 kT)^{\frac{3}{2}}/h^3], \quad (1)$$

where the subscript 1 refers to the conduction (upper) band and the subscript 2 refers to the filled (lower) band. The following notation is used:

the m's are the effective masses of the electrons and the positive holes,
the ω's are the statistical weights of the bands,
n is the number of donor levels per unit volume,
$\lambda=e^{\mu/kT}$,
h is the Planck constant,
k is the Boltzmann constant, and
T is the temperature in degrees Kelvin.

In deriving this equation, Fowler assumes that Boltzmann statistics apply to the electrons in the conduction band and to the holes in the filled band. Fermi statistics, however, govern the behavior of the electrons in the donor levels. It is further assumed that the levels of the electron states are independent of temperature. This is justified for the non-polar crystals of interest here where the temperature shift is too small to measure.[12]

Equation (1) gives a cubic equation which can readily be solved by Newton's method.[13] Over most of the temperature range the cubic term is negligible. In Fig. 4 are plots of the variation of the e.c.p. for a semiconductor similar to silicon. In making the calculations, the following assumptions were made: $\Delta E_1=1.2$ electron volts; $\Delta E_2=1.0$ ev; the effective mass of the electrons in the conduction band and the effective mass of the holes in the filled band equal the free electron mass, and the ω's equal two. The value of 1.0 ev was selected for ΔE_2, so that the gap between the donor levels and the conduction band would appear on the graph; actually the gap is a good deal smaller. The value of 1.2 ev for ΔE_1 is approximately the value found in the literature. By more carefully selecting the values of various parameters in the equation, the e.c.p. could be made to correspond more closely to an actual sample of silicon. This would cause only a small quantitative difference and was not deemed worth while at present. In general,

$$\omega_1 m_1^{\frac{3}{2}}=\omega_2 m_2^{\frac{3}{2}} \quad (2)$$

does not hold, and the e.c.p. is not halfway between the filled and the conduction band even at elevated temperatures. At high temperatures, where the number of electrons from the filled band overwhelm the donor electrons, the first term on the right of Eq. (1) drops out, and one may show that, if (2) holds, μ is half of ΔE_1. Since (2) does not hold in general, μ varies with temperature by the order of kT, and a variation of 0.1 ev from the halfway value can be expected at high temperature. Our graphs have not been plotted carefully around absolute zero where there is an increase in μ.

One may say that the semiconductor becomes intrinsic when the donor term (first term on the right in Eq. (1)) does not affect the value of μ. In this region, for our sample, $\mu=0.6$ ev. One may show, by direct substitution into standard equations,[7] that in this region the number of conducting electrons caused by jumps from the filled band overwhelms (ratio of 3 to 1 or larger) the number from the donors. Figure 4 shows that a reasonably

[12] A. Radkowsky, Phys. Rev. **73**, 749 (1948).
[13] H. Margenau and G. M. Murphy, *The Mathematics of Physics and Chemistry* (D. Van Nostrand Company, Inc., New York, 1943), p. 477.

pure sample (10^{17} donors per cm^3) becomes intrinsic at about 1200°K, while for a sample of low purity the transition point between N-type and intrinsic occurs at a temperature well beyond the melting point. This latter situation corresponds more closely to the samples Smith used, so that one would not expect a change of about $\Delta E_1/2$ with temperature for the work function of silicon but about half that amount. This variation is several tenths of an ev, an amount larger than the experimental error.

Once the variation of e.c.p. is known, one may readily calculate the number of electrons in the conduction band. Such a calculation leads to curves similar to conductivity *vs.* temperature graphs and will not be reproduced here.

In Fig. 5, e.c.p. is plotted against temperature for a semiconductor similar to germanium. In this case $\Delta E_1=\Delta E_2=0.75$ ev, while the other parameters have the same values as in the previous case. The number of electrons in the conduction band at 1000°K is smaller by about a factor of ten than the value obtained for germanium by Johnson[14] from experimental data. The discrepancy is not surprising in view of the arbitrary values for ΔE_1, the m's, and the ω's.

If there are no surface effects, then, we should expect a variation of work function with temperature large enough to have been observable in the experiments of Smith. Since no variation occurred, one must consider the effect of surface states.

III. MECHANISM OF FORMING A DIPOLE LAYER

If negative charges are accumulated on the surface of the semiconductor, there will be a rise in potential energy per electron at the surface, as illustrated in Fig. 3. This rise causes a redistribution

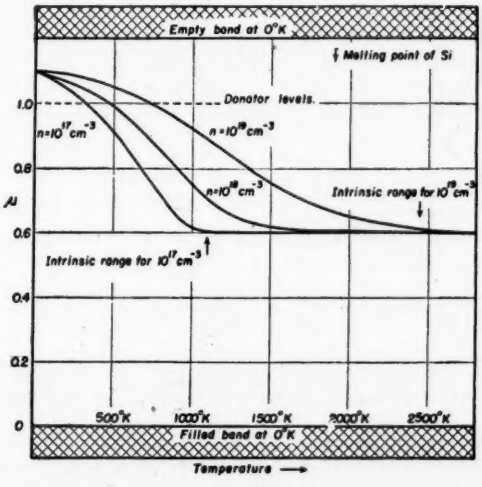

FIG. 4. Electrochemical potential *versus* temperature for semiconductor similar to silicon.

[14] V. A. Johnson, Phys. Rev. **74**, 1255 (1948).

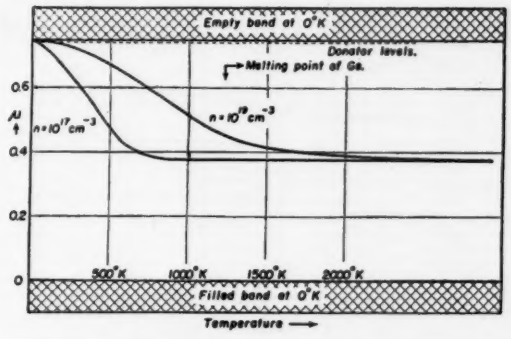

FIG. 5. Electrochemical potential *versus* temperature for semiconductor similar to germanium.

of the negative electrons and the positive holes so that there may be a net charge in the potential layer. This does not include the trapped electrons in the surface states. If there is no induction, the net charge on the body will be zero, so that the charge accumulated in the surface states is balanced by the charge in the potential layer. We shall not consider the effect of the induced charges although our method could readily be extended to include those cases. We shall talk about electrons being accumulated on the surface, but there is no reason (at the present condition of our knowledge of surface states) why positive charges could not accumulate on the surface. Our equations can easily be adapted to this situation.

The surface states cause an additional dipole layer which the electrons must overcome to get out (or get in) to the semiconductor. Referring to Fig. 3, the work function is given by $\varphi_s+\varphi+\Delta E_1-\mu$.

To calculate φ, we shall consider the case of a semi-infinite crystal, which for convenience will be divided into two parts by a plane parallel to the crystal's surface. The plane may be thought of as passing through the arrow in Fig. 3 at right angles to the plane of the paper. We have, therefore, two thermodynamic systems in equilibrium, which means that their e.c.p.'s are equal. μ for the body of the crystal—right in the figure—is given by Fowler's equation. The e.c.p. for the surface—left part—must be calculated from the condition that there is no net accumulation of charge. If N_- is the number of electrons or filled acceptor levels, in the potential layer, N_+ the number of holes or vacant donor levels, and N_s the number of electrons in the surface states, then

$$N_+-N_-=N_s. \tag{3}$$

The N's depend on φ and the e.c.p. Thus Eq. (3) gives a relation between μ and φ, but since μ is known from Eq. (1) the above relation gives us a means of determining φ.

To use (3) one must have a model of the semiconductor so as to relate the N's to the e.c.p. of

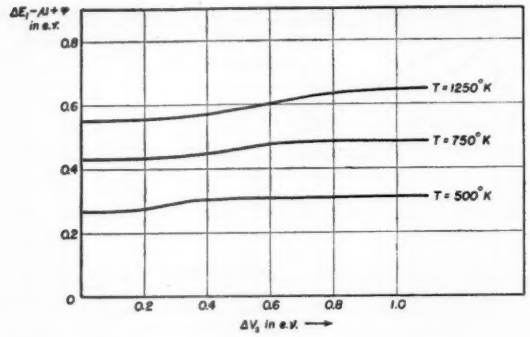

FIG. 6a. "Work function" against ΔV_0 for semiconductor similar to silicon (N type); $n=10^{17}$ cm^{-3}, $N=10^{11}$ cm^{-2}.

the surface and φ. Fortunately, models can be obtained which give fairly simple equations. While these models are not free from some objections, the authors believe that they are satisfactory for this study. We shall now consider the case when there is a negligible number of holes in the filled band and the fraction of time which the electrons spend in the donar levels is small—i.e., the donors are ionized. This is a Schottky exhaustion layer and represents the condition in N-type silicon and germanium at intermediate temperatures. The next section will consider the case where the number of electrons from the filled band completely overwhelms the number from the donor levels, so that the effect of the donor electrons on the potential can be disregarded. This corresponds to high temperatures, i.e., 1250°K, in silicon for $n=10^{17}$ per cm^3 and 1000°K in germanium (same n).

IV. INTERMEDIATE TEMPERATURE—SCHOTTKY LAYER

At room temperature and somewhat above, the conductivity of N-type silicon and germanium is due to the fact that the donor levels lose their electrons to the conduction band. What actually happens statistically is that the conduction band has a much higher statistical weight than the donor levels, and the factor $\exp-(\Delta E_1-\Delta E_2)/kT$ is not too small, so that the electrons spend most of their time in the conduction band. As stated, for simplicity we shall assume that the donor levels are completely ionized and neglect the very small contribution from the filled band. We make the further assumption that the donor levels are uniformly distributed throughout the volume. This last point has been investigated by Schottky for selenium and by Becker for copper oxide.[15] The evidence is that the uniformity can be justified for selenium but not for copper oxide.

On these assumptions the net number of charged particles per cm^3 (number of positive minus the number of negative) is

$$n-ne^{-V/kT},$$

where V is the potential energy of the electron relative to the conduction band. ($V=0$ at large distances from the surface.) The first term represents the number of donor centers which are assumed fixed in the lattice and uninfluenced by the potential hill. We assume that the donor levels diffuse at a negligibly slow rate even though they are not in thermal equilibrium.[16] The second term in the equation above assumes that the electrons which obey Boltzmann statistics are in thermal equilibrium with the potential. When $V=0$ there will be no net charge density. For the equilibrium condition one would expect Poisson's equation to hold, or

$$d^2V/dx^2=[4\pi e^2n/\kappa][1-e^{-V/kT}], \qquad (4)$$

where κ is the static dielectric constant. The net number of charged particles per cm^2 in the layer is

$$\int_0^{V=0}\nu(x)dx=(\kappa/4\pi e^2)\int_0^{V=0}(d^2V/dx^2)dx$$

$$=-(\kappa/4\pi e^2)(dV/dx)_{x=0}, \qquad (5)$$

where $\nu(x)dx$ is the net number per cm^2 of positive

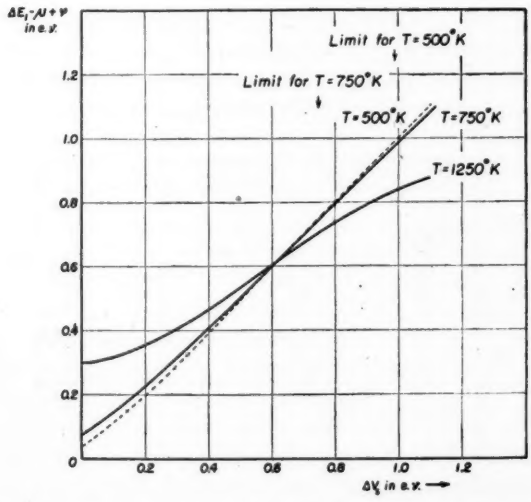

FIG. 6b. "Work function" against ΔV_0 for semiconductor similar to silicon (N type); $n=10^{17}$ cm^{-3}, $N=10^{13}$ cm^{-2}.

[15] S. J. Angello, *The Theory of Semiconductor Rectifiers* (Westinghouse Research Laboratories, Scientific Paper No. 1251, East Pittsburgh, Pa., 1946). This is an excellent summary of the theory and experiments to 1946. Subsequently it was found necessary to introduce the assumption of surface states. The original paper of W. Schottky is found in Zeits. f, Physik 118, 539 (1942), while Becker's work was communicated privately to Dr. Angello.

[16] The assumption bears further consideration. If a surface of a semiconductor stays at the same temperature for a long time, it is quite possible that the donors will diffuse. A. V. Joffe, J. Phys. U.S.S.R. 10, 49 (1946), has noticed changes of the work function with time in some semiconductors. One could develop a theory on the assumption that donors diffuse as well as the electrons.

charges in the element dx at x ($x=0$ at surface) and the gradient of V is evaluated at the semiconductor boundary. Equation (5) was obtained by the use of Poisson's equation and the assumption that $dV/dx=0$ where $\nu(x)=0$, i.e., $V=0$. Returning to (4), we can solve for the gradient and obtain an expression for the net number of charges per cm² in the potential layer, namely:

$$N_+-N_-=\pm(\kappa n/2\pi e^2)^{\frac{1}{2}}[\varphi-kT(1-\epsilon^{-\varphi/kT})]^{\frac{1}{2}}. \quad (6)$$

The positive sign goes with positive values of φ. This derivation is in no way restricted to positive φ's. For negative φ's one gets an excess number of electrons in the potential layer, and from physical reasoning one can see that one should use the negative sign. The double sign appears because one has to take a square root after integrating Eq. (4).

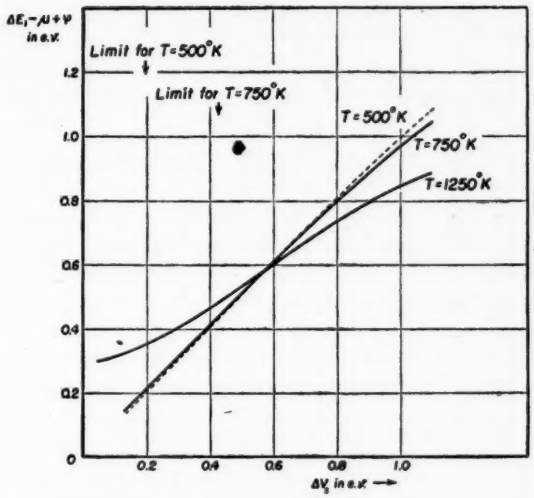

FIG. 6c. "Work function" against ΔV_s for semiconductor similar to silicon (P type); $n=10^{17}$ cm^{-3}, $N=10^{13}$ cm^{-2}.

An equation similar to (6) appears in the literature,[17] but the drift of the electron (second term on the right in Eq. (4)) is not considered there. This omission is clearly justified when kT is small compared to a positive φ.

Before solving (3) we must obtain an expression N_s. The reason for not using Bardeen's expression is that it has no temperature dependence. Here, as far as the authors know, there is little to be used as a guide. Attempts have been made to calculate wave functions of surface states by Shockley[18] and others, but Shockley[19] doubts that there is much direct connection between the states he calculated and the ones which play an important role in the surface effects of semiconductors. Intuitively one would be led to believe that the trapped electrons could be represented by two-

[17] Reference 6, p. 174.
[18] W. Shockley, Phys. Rev. 56, 317 (1939).
[19] Private communication to the authors.

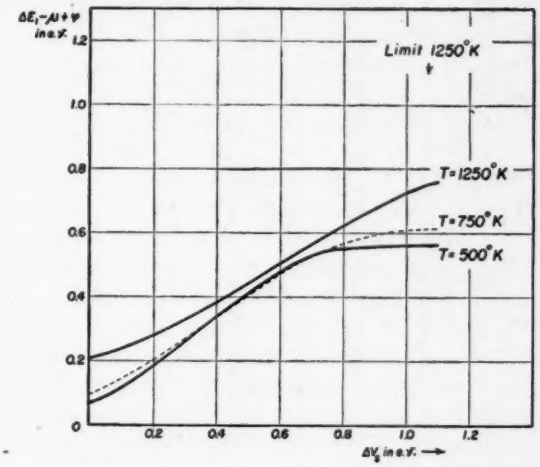

FIG. 6d. "Work function" against ΔV_s for semiconductor similar to silicon (N type); $n=10^{19}$ cm^{-3}, $N=10^{13}$ cm^{-2}.

dimensional Bloch functions on the surface. In the third direction, at right angles to the surface, it can be imagined that the wave function is damped as one proceeds in both directions from the surface. Also, most probably there are surface states associated with imperfections in the surface of foreign atoms. We have simplified this picture by assuming that an electron trapped in one of these states is on the very surface. This is clearly only approximately true. Further, we assume that all the levels are of nearly the same energy. There seems to be no reason why positive charges cannot accumulate on the surface. We therefore assume that if the levels are half full there is no charge; if less than half, there is a positive charge; if more, a negative charge. Mathematically, this can be put in the form

$$N_s=\left[\frac{2}{1+\exp(\Delta E_1+\varphi-\Delta V_s-\mu)/kT}-1\right]N, \quad (7)$$

where N is the number of electrons that have to be captured in order to have no charge and ΔV_s is the position of the surface states relative to the conduction band. The first term on the right is just the number of electrons in the surface states on our model, while the second term appears since we require that the state be half-filled to have no net surface charge. The surface states are roughly symmetric with respect to the accumulation of positive and negative charges. When the levels are near the e.c.p. Equation (7) gives states similar to the ones assumed by Bardeen, since when $\Delta E_1+\varphi-\Delta V_s-\mu \ll kT$,

$$N_s=(-N/2kT)(\Delta E_1+\varphi-\Delta V_s-\mu). \quad (7a)$$

These states are more dense about the e.c.p. but are soon saturated. The expression was concocted so that the surface states have some reasonable temperature dependence.

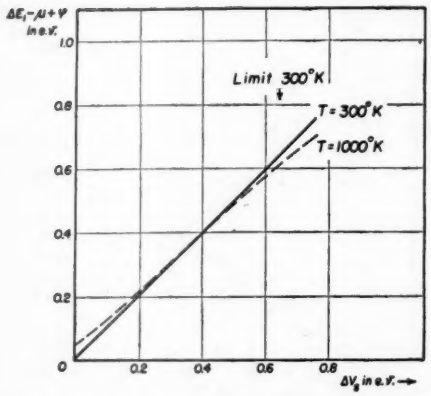

FIG. 7. "Work function" against ΔV_s for semiconductor similar to germanium (N type); $n=10^{17}$ cm^{-3}, $N=10^{13}$ cm^{-2}.

Combining Eqs. (3), (6), and (7) we obtain a relation between μ and φ once the other parameters are fixed. μ, however, is given by (1) and we have the desired solution for φ.

Unfortunately, two parameters in (7) are unknown, N and ΔV_s. One may estimate N within limits from various experiments on silicon[2] and germanium[4] to be of the order of 10^{13} per cm^2 or several orders of magnitude higher, depending on the treatment of the surface. If one assumes two surface states per atom, N should be about 10^{15} cm^{-2} for silicon. Using fixed values for N we have plotted the work function, to an additive constant φ_s, against ΔV_s for several temperatures. Some of these graphs are shown in Fig. 6 for silicon and in Fig. 7 for germanium. The curves for the P-type semiconductor are obtained from equations very similar to the ones for N-type will not be explicitly given. The values of the κ's were 25 for silicon and 15 for germanium.[20]

The use of Eq. (4) must be justified, of course. We must be sure that the donors are almost all ionized and that there is a negligible number of holes. For silicon with $n=10^{17}$ cm^{-3} at 500°K and 750°K there are, respectively, 6.5×10^{16} and 8.2×10^{16} conduction electrons per cm^3 for our model but only 10^{10} and 10^{15} holes per cm^3 in the filled band. Had we used a value of ΔE_2 closer to ΔE_1, the first set of figures would have been closer to 10^{17}. This means that the donor levels are almost completely ionized. Because of the rise in potential, as we shall see in the next section, there will be a slight accumulation of holes in the potential layer. To use Eq. (4) we must require that $n_+\epsilon^{\varphi/kT}\ll n$, where n_+ is the number of holes per cm^3. For $T=750$°K and $\varphi=0.3$ ev, $n_+\epsilon^{\varphi/kT}=10^{17}$ per cm^3. This means that for this case we must require that $\varphi<0.3$ ev. At 1250°K, on the other hand, there are 8.3×10^{17} electrons per cm^3 in the conduction band under the same condition, so that about 7×10^{17} per cm^3 come from the filled band. The method developed here will not hold for this temperature.

[20] These constants are not too well known. The value used for silicon may be somewhat too large. The interpretation of our calculations does not depend on the values used for the dielectric constants.

V. HIGH TEMPERATURE POTENTIAL LAYER

If there is a potential hill, there will be a tendency for the electrons to diffuse away from it while the holes will diffuse towards it. The final results will be a Boltzmann distribution of the electrons and the holes. Since we shall ignore the donors in this case, we have with the use of Poisson's equation

$$d^2V/dx^2=(4\pi e^2n_1/\kappa)(\epsilon^{V/kT}-\epsilon^{-V/kT}), \quad (8)$$

where n_1 is the number of electrons per cm^3 in the conduction band for $V=0$. This gives for dV/dx at $x=0$, $V=\varphi$,

$$dV/dx=\pm(8\pi e^2n_1kT/\kappa)^{\frac{1}{2}}[\epsilon^{\varphi/2kT}-\epsilon^{-\varphi/2kT}], \quad (8a)$$

where the additional condition $V=0$, $dV/dx=0$ has been used. Combining the expression with Eq. (5) we obtain

$$N_+-N_-=\pm(\kappa n_1kT/2\pi e^2)^{\frac{1}{2}}[\epsilon^{\varphi/2kT}-\epsilon^{-\varphi/2kT}]. \quad (9)$$

The number of electrons and holes is given by the standard expression (Fowler's reference 7, Eq. (1133)), where we replace the effective electron mass by the free mass,

$$n_1=[\omega(2\pi mkT)^{\frac{3}{2}}/h^3]\epsilon^{-(\Delta E_1-\mu)/kT},$$

or finally

$$N_+-N_-=(\omega\kappa kT/2\pi e^2)^{\frac{1}{2}}[(2\pi mkT)^{\frac{3}{2}}/h^{\frac{3}{2}}]\times[\epsilon^{\varphi/2kT}-\epsilon^{-\varphi/2kT}]\epsilon^{-(\Delta E_1-\mu)/2kT}. \quad (9a)$$

Combining Eqs. (3), (7), and (9) we obtain a relation between φ, N, and ΔV_s. In this case μ is just $\frac{1}{2}\Delta E_1$, corresponding to the graphs for the highest temperature in Figs. 6 and 7. The only exception is the case for silicon, with $n=10^{19}$ per cm^3. Here the equations developed in the previous section hold.

Equation (8) assumes that the charge per unit volume caused by the diffusion of the electrons and the holes is much larger than the charge caused by the ionization of the donor levels. If $V=0.05$ ev, the diffusion charge density obtained from Eq. (8) is 8×10^{17} per cm^3 at $T=1250$°K for $\mu=0.6$ ev, which is considerably larger than 10^{17} per cm^3. For much smaller values of V, one is not justified to use Eq. (8) for it neglects the ionized donors and their electrons. If φ is bigger than 0.05 ev, there can be little doubt that the equations derived in this section are good approximations.

One may readily integrate Eq. (8a) once more and obtain an expression for V itself. This is done in the appendix to this paper where this type of potential is more fully discussed.

VI. SUMMARY OF THE CALCULATIONS AND CONCLUSION

Figures 6 and 7 show plots of the work functions (to an additive constant φ_s) *vs.* ΔV_s, the assumed depth of the discrete surface states level below the conduction band. In Fig. 6a it is assumed that the density of the donors is 10^{17} per cm^3, while the number of surface states ($2N$) is 2×10^{11} per cm^2 of surface. For the two lower temperatures, 500°K and 750°K, the potential hill was a Schottky exhaustion layer, while at the higher temperature, 1250°K, a diffusion potential layer was assumed. The graphs show that the work function is roughly independent of the position of the surface states. Physically this means that the charge that can accumulate on the surface will not cause an appreciable effect. Had Smith performed his experiments on such a sample, he would have observed a change of about 0.15 ev when cooling from 1250°K to 750°K and about 0.2 ev if he continued to cool down to 500°K. This would have been detected.

In Fig. 6b we considered the case where $n=10^{17}$ per cm^3 but $N=10^{13}$ per cm^2. The method of obtaining these curves was the same as for Fig. 6a. The graphs obtained in this way are considerably different from the previous one since we have a different physical situation. If the surface states were 1.2 ev below the conduction band, the work function would decrease by about 0.2 ev when the temperature dropped from about 1250°K to 750°K. Further cooling, however, will cause little effect on the work function. By arbitrarily selecting ΔV_s to lie in the range between 0.4 ev and 0.8 ev, the net change in the work function can be made less than 0.05 ev. The arrows indicate the limit of the validity of the calculations because of the diffusion of holes.

Figure 6c is similar to Fig. 6b in that the same values of n and N were used, but this graph is for a P-type conductor. The acceptor levels are 0.2 ev above the full band. Since the equations have to be modified very slightly, we shall not develop the specific equations used. The same general conclusions hold here as in the previous case, Fig. 6b. A comparison of the two last sets of graphs shows that, if φ_s does not change from N-type to P-type conductor, the work function will be almost the same. Of course, we are assuming the specific values of n and N in making this statement. It would not hold for case 6a. This is in agreement with Bardeen's theory and the experiments of Brattain and Shockley. The final graph of silicon is shown in Fig. 6d. Here $n=10^{19}$ per cm^3, and N is 10^{13} per cm^2. Since n is higher than previously at all three temperatures, Schottky exhaustion layers must be used. At $T=1250$°K, the number of holes in the conduction band is only 10^{17} per cm^3 compared to 10^{19} per cm^3. This means that the effect of the holes is negligible unless φ becomes larger than about 0.4 ev. There is a small change in the work function from $T=750$°K to 1250°K, but this is much smaller than one would expect from Fig. 4.

Figure 7 gives a similar set of graphs for germanium. At lower temperature the Schottky exhaustion layer method was used, while at the higher temperature the diffusion potential layer was employed. For 300°K the number of holes in the filled band was 10^9 per cm^3 while at 1000°K the number of conducting electrons was 2×10^{18} per cm^3. Conductivity experiments on germanium[4] suggest that N is of the order of 10^{13} per cm^2 while ΔV_s is about the size of ΔE_1.

If calculations were made for higher densities of surface states, the difference between the curves for various temperatures would disappear. At $n=10^{17}$ per cm^3 the temperature difference would practically vanish for $N=10^{14}$ per cm^2. From an examination of the equations, one sees that the value of N, where the curves converge, is affected by the value of n. Thus, for $n=10^{19}$ per cm^3, N should be 10^{15} per cm^3, though the variation for $N=10^{14}$ per cm^3 would be small, and the maximum variation to be expected (any value of ΔV_s) for $N=10^{13}$ per cm^3 should be less than 0.2 ev. Since Brattain and Shockley conclude that the surface density is 10^{13} per cm^2 or higher for silicon and since there is no reason to believe that ΔV_s should take extreme values, one would expect from these calculations that the variation in the work function of these semiconductors is very small. This is in complete agreement with the work of Smith. For the case of germanium if n were larger than 10^{17} per cm^3, it is possible that there would be a measurable temperature change in the work function, since, from the experiments of Brattain and Bardeen, one must conclude that ΔV_s has an extreme value. This point has not been fully explored because the exact value of n for the samples used by Smith is unknown. It is quite possible that one

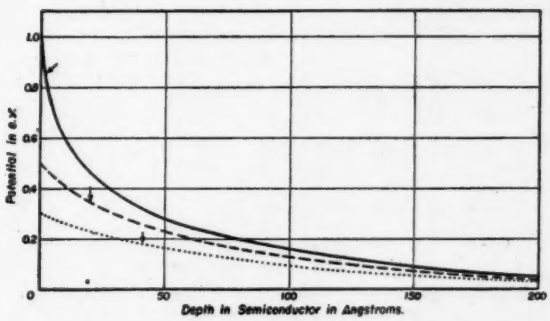

FIG. 8. Diffusion layer of a semiconductor similar to silicon at 1250°K (for meaning of arrows see Appendix).

should consider here the diffusion of electrons and holes, plus the effect of donors.

The question remains as to whether or not the samples used by Smith in his work really come to an equilibrium, if the average time for an electron to jump from a surface state to the conduction band is assumed to be given by[21]

$$10^{-13}\exp(+\Delta V_s/kT).$$

Thus the time required at 500°K for the electron to jump is 10^{-1} sec. for an extreme value of ΔV_s—i.e., $\Delta V_s=1.2$ ev while it takes only 10^{-7} sec. for $\Delta V_s=0.6$ ev. This implies that the time to attain equilibrium is very short at a temperature of 500°K and above.

While our calculations are not based on a model free from objection, we would be surprised if the analysis of a more refined model led to radically different conclusions.

The authors would like to thank the U. S. Navy (Bureau of Ships) for support during this work. Thanks are also due Professor F. Seitz and Dr. W. Shockley for discussing various phases of this problem with us and to Mr. A. Lemonick for assistance in the calculations.

APPENDIX

We should like to examine the diffusion layer in more detail in this appendix. The differential equation for the potential energy of an electron in the layer is given by Eq. (8a) of the text, namely:

$$dV/dx=akT[\epsilon^{V/2kT}-\epsilon^{-V/2kT}], \tag{A1}$$

where we have set

$$a=(1/kT)[8\pi e^2 n_1 kT/\kappa]^{\frac{1}{2}}.$$

With the substitution $y=\epsilon^{V/2kT}$ and some algebra we obtain

$$ax=2\int[dy/(y^2-1)]+C. \tag{A2}$$

This gives, with the use of a standard integration formula,

$$\epsilon^{ax}=(1/F)[(\epsilon^{V/2kT}+1)/(\epsilon^{V/2kT}-1)], \tag{A3}$$

where

$$F=(\epsilon^{\varphi/2kT}+1)/(\epsilon^{\varphi/2kT}-1). \tag{A4}$$

To obtain Eq. (A3) we have used the boundary condition that at $x=0$, $V=\varphi$. The equation says that V approaches zero asymptotically; actually, however, V differs from zero only by a very small amount within a few hundred angstroms of the surface. Using the above expressions, we may find an alternate way to calculate the number of electrons and holes in the diffusion layer. From (A3) we have

$$\epsilon^{-V/2kT}=F\epsilon^{ax}-1/F\epsilon^{ax}+1, \tag{A5}$$

or the total number of electrons between $X=L$ and $x=0$ is given by

$$N(L)=n_1\int_0^L\{(F\epsilon^{ax}-1)/(F\epsilon^{ax}+1)\}^2dx. \tag{A6}$$

This leads to a simple integration if one uses the substitution $z=\epsilon^{ax}$ and gives for N_-

$$N_-=-[4n_1/a(F+1)]+nL+\delta_-(L), \tag{A7a}$$

where $\delta_-(L)$ equals approximately $4n_1\epsilon^{-aL}/a$ and can be made as small as we please by increasing L. For instance, for silicon $\delta_-(10^{-6}$ cm) equals 10^{12} while $\delta_-(10^{-4}$ cm) equals 10^{-33} for $\varphi=1$ ev. In exactly the same manner, N_+ can be calculated and gives

$$N_+=[4n_1/a(F-1)]+nL+\delta_+(L). \tag{A7b}$$

The difference between the two is

$$N_+-N_-=8nF/a(F^2-1), \tag{A8}$$

where we have neglected the δ's. This is the same equation as the one found in the text Eq. (9), obtained by a simpler and more direct method. This can be shown by substitution back for F.

In Fig. 8 we have plotted V against x for silicon (using the same parameters as in the text). The most striking feature of this type of potential layer is its shallow depth. For 1 ev the layer depth is approximately 50 angstroms; however, the most important part is much smaller. N_+-N_- increases exponentially, as can be seen from Eq. (9), so that half of N_+-N_- occurs within 2A from the surface for $\varphi=1.0$ ev (shown by the arrow); within 20A for $\varphi=0.5$ ev; and within 40A for $\varphi=0.3$ ev. This should be contrasted with the depth of the Schottky exhaustion layer, about 2000A for $n=10^{17}$ cm^{-3} and 1 ev.

In view of the shallowness of the diffusion layer, one may question the method used to derive the various relations. The two most important effects neglected are:

1. The atomic structure.—At the surface of the crystal there are undoubtedly distortions which would modify the electron wave function very near the surface. Since the region where these distortions occur is very important for the diffusion layer, it should be taken into account in detail.

2. The image force.—Near the surface an electron in the semiconductor will see its image in

[21] This is the expression for the jump time of a lattice defect—see reference 6, p. 33 or p. 130. A similar argument can be used in this case. Admittedly this expression is not on too firm a foundation in this case. For one thing, it is based entirely on Boltzmann statistics, and it does not consider the statistical weights of the levels. The expression probably gives a rough order of magnitude. Certainly it would be very desirable to know from experiment that the samples are in thermal equilibrium.

the adjoining medium. When the electron is near the surface one is not allowed to smooth out the charge and consider that we have a uniform layer of charge. The reason for this is that the electron or the hole sees its image in the adjoining medium and the image follows the detailed motion of the particle. This effect will cause a raising or a lowering of the potential of 0.1 ev at a distance of 1A° from the surface. If the adjoining medium is a dielectric of lower κ, as in the case of silicon and air, the image charge will have the same sign as the charged particle.[22]

For these two reasons one cannot rely completely on the derivation just given when φ is larger than 0.5 ev. Most probably the equations are correct to within an order of magnitude but should not be trusted further. For $\varphi=0.3$ ev or less, the surface effects are not so important and the theory should be fairly reliable. Most fortunately, the maximum value of φ we used for the diffusion layer in the case of silicon is less than 0.3 ev, and only one point is greater than this value for germanium.

Since the potential layer is very thin, tunneling effects can be very important. This would be true of a semiconductor metal junction. For the experiments of Smith this does not play a major role, since there is a large gap between the two surfaces which creates a large potential barrier between the conduction band of the metal and the semiconductor.

[22] M. Abraham and R. Becker, *The Classical Theory of Electricity and Magnetism* (Blackie and Son, Limited, London, 1937), p. 76.

PHYSICAL REVIEW VOLUME 75, NUMBER 6 MARCH 15, 1949

Relativistic Field Theories

T. S. CHANG
Carnegie Institute of Technology, Pittsburgh, Pennsylvania
(Received August 9, 1948)

The study of the change of the Schroedinger wave functionals on space-like surfaces as the surface changes is formulated simply. In this formulation, we let S be any space-like surface with the curvilinear coordinates u, introduce $\langle q(u)S|\rangle$ as the Schroedinger functional on it, with the nature of the functions $q(u)$ not specified for the moment, and write the Schroedinger equation as

$$\hbar i\{\langle q(u),\ S'|\rangle-\langle q(u),\ S|\rangle\}=J\langle q(u),\ S|\rangle, \qquad (1)$$

where S' is a surface slightly different from S, and J is an operator operating on $q(u)$ and depending on S, S', and the choice of their coordinates u. Obviously, the only necessary conditions for J is that J is Hermitian and that (1) is integrable. To get a theory resembling the existing ones, we require further that if we construct the expectation value of a certain field quantity at a point P from $\langle q(u),\ S|\rangle$, S being a surface passing through P, the expectation value is independent of choice of S and its coordinates u, and satisfies certain differential equations.

When these differential equations follow from a Langrangian principle, an expression for J was effectively given by Weiss. His work is given here in a complete form and the proof of the satisfaction of all requirements completed.

Finally, by a simple transformation on the wave functions and the observables, we deduce from the Weiss's formalism the Tomonaga's formalism. As a consequence, it is pointed out that the Tomonaga's formalism will encounter essentially the same difficulties as the orthodox Heisenberg-Pauli formalism.

1. INTRODUCTION

A QUANTUM theory of fields was given by Heisenberg and Pauli[1] as early as 1929. The theory given by them was completely apart from one aspect, i.e., there was no investigation of the transformation between the wave functionals for two different Lorentz observers. It is obvious, though never pointed out explicitly in the literature, that the operator transforming the Schroedinger functional for one Lorentz-frame to that for another must be related to the integral over space of the $\mu\nu 4$ component of the angular momentum tensor $M_{\mu\nu\rho}$. It is also obvious that as the Schroedinger functionals form a representation basis of a representation of the homogeneous and the inhomogeneous Lorentz group, these operators together with the space integral of the $\mu 4$ component of the energy momentum tensor $T_{\mu\nu}$ must satisfy certain well-known commutation laws.

Recently, Dirac introduced the study of the Schroedinger wave functionals on any arbitrary space-like surface.[2] He introduced certain deformation operators to describe the deformation of the surfaces and studied their commutation laws. Though the theory is the most general quantum mechanics of localizable dynamical systems and can be employed to check whether any given theory is relativistic, the explicit construction of the operators

[1] W. Pauli and W. Heisenberg, Zeits. f. Physik **56**, 1 (1929).

[2] P. A. M. Dirac, Phys. Rev. **73**, 1092 (1948).

II corresponding to a given parametrization of the surface, and the operators P corresponding to a given dynamical system is not simple work. A simpler and equivalent formulation of Dirac's work is as follows.

Let S be any space-like surface, (u_1, u_2, u_3) any arbitrary set of curvilinear coordinates on the surface, so that on the surface, we have

$$x_\mu = b_\mu(u_1, u_2, u_3). \tag{1}$$

Now let us introduce the Schroedinger wave functional Ψ, which depends on S and its coordinate system u (i.e., is a functional of the functions $b_\mu(u_1, u_2, u_3)$), and is further a functional of certain functions $q(u)$ whose nature we shall not specify at the moment. Such a functional may be considered as a vector depending on $b_\mu(u)$ with components (or coordinates) labelled by functions $q(u)$, and will be denoted by

$$\langle q(u)\,;\, b_\mu(u)\,|\,\rangle. \tag{2}$$

In a deformation of S to S' given by

$$x_\mu = b_\mu'(u) = b_\mu(u) + \Delta x_\mu(u), \tag{3}$$

the corresponding change in Ψ is defined by

$$\Delta\Psi = \langle q(u)\,;\, b_\mu'(u)\,|\,\rangle - \langle q(u)\,;\, b_\mu(u)\,|\,\rangle. \tag{4}$$

Obviously, we must introduce an equation

$$\hbar i \Delta\Psi = J\Psi, \tag{5}$$

where J is an operator operating on the coordinates $q(u)$ of Ψ and may be looked upon as a matrix with both rows and columns labelled by functions $q(u)$. Obviously, (i) Eq. (5) considered as a total differential equation for Ψ must be integrable. This condition replaces the study of the Poisson brackets between the operators Π's and P's in Dirac's paper. (ii) J must be Hermitian, so that the length of Ψ does not change. As Ψ is a functional, its length can be best pictured by first letting (u_1, u_2, u_3) take discrete values $(m_1 a, m_2 a, m_3 a)$ only, $(m_1, m_2, m_3 = 0, \pm 1, \pm 2, \cdots)$ so that the square of the length is

$$\int dq(u') \int dq(u'') \cdots |\langle q(u'), q(u''), \cdots; b_\mu(u'), b_\mu(u''), \cdots |\rangle|^2, \tag{6}$$

where $u', u'', \cdots$ denote the different discrete values of (u_1, u_2, u_3), and then passing to the limit $a \to 0$.

The above gives us rules for the determination of Ψ, but to get a physically sensible theory, we must construct expressions for the different "expectation values" in the state Ψ. For this purpose, let us consider any given point P with coordinates x_μ, draw a space-like surface S passing through P, introduce a coordinate system u on the surface so that $x_\mu = b_\mu(u)$ on it, and assume

$$\int dq(u') \int dq(u'') \cdots |\langle q(u'), q(u''), \cdots; b_\mu(u'), b_\mu(u''), \cdots |\rangle|^2 q(u_P) \tag{7}$$

divided by the length (6) be the expectation value of a certain field quantity $q(x)$ at P, u_P in (7) being the u-coordinates of P on this surface S. Under this assumption, we naturally expect (iii) the expectation value given by (7) divided by (6) is independent of the choice of S and that of the coordinate system u on S, and (iv) the expectation value will satisfy certain differential equations, known as the field equations for $q(x)$. The last two conditions are not absolutely necessary, they may be discarded or replaced by similar ones, but their satisfaction will bring the present theory very close to the usual field theory of Heisenberg and Pauli.

For fields $q(x)$ whose field equations are deduced from the variation of a Lagrangian, an equation of the same nature as Eq. (5) was given some time ago by Weiss.[3] Unfortunately he has effectively only considered a one-parameter family of surfaces and thus we do not have the requirements (i) and (iii). In §2 we shall extend his work to general deformations of surfaces and point out that all conditions mentioned above are satisfied. We shall only indicate how the proof of the integrability is carried out and leave out all mathematical details.

The restriction to fields satisfying the Lagrangian principle is a serious one, though this does not exclude us from considering any of the existing fields in quantum mechanics. At the same time, it is difficult to see how one can get rid of the Lagrangian principle. As soon as one has the Schroedinger equation,

$$\hbar i(\partial\Psi/\partial t) = H\Psi,$$

one has the Heisenberg equation of motion,

$$df/dt = -(\hbar i)^{-1}[H, f]. \tag{8}$$

If H contains only operators q and $\partial/\partial q$, (8) are the classical Hamiltonian equations of motion, and these are derivable from a Lagrangian.

In the last section (§3), we show that it is possible to get from our Eq. (5) Tomonaga's formalism[4] by a simple transformation. The result obtained here is slightly more general than the original Tomonaga's formalism which does not allow points on the surface S to interact. The possibility of obtaining Tomonaga's formalism from the Weiss's formalism implies that the Tomonaga's formalism will encounter essentially the same difficulties as the orthodox Heisenberg-Pauli formalism and will not give us anything essentially now.

[3] P. Weiss, Proc. Roy. Soc. **A156**, 192 (1936).
[4] S. Tomonaga, Prog. Theoretical Phys. **1**, 27 (1946).

2. THE THEORY OF WEISS IN COMPLETE FORM

Let x_μ be (x, y, z, ict) as usual, and let q^α be the field quantities. Let $q_\mu{}^\alpha$ denote $\partial q^\alpha/\partial x_\mu$ and let q^α satisfy equations obtained from the variation of a Lagrangian L. We have thus

$$\partial L/\partial q^\alpha - \partial/\partial x_\mu(\partial L/\partial q_\mu{}^\alpha) = 0. \tag{9}$$

Let us introduce

$$N_\mu = \epsilon_{\nu\rho\theta\mu}\frac{\partial x_\nu}{\partial u_1}\frac{\partial x_\rho}{\partial u_2}\frac{\partial x_\theta}{\partial u_3}, \tag{10}$$

where $\epsilon_{\nu\rho\theta\mu}$ is plus or minus one according to whether $\nu\rho\theta\mu$ is an even or odd permutation of 1 2 3 4 and is zero otherwise. Let us introduce

$$p_\alpha = N_\mu(\partial L/\partial q_\mu{}^\alpha), \tag{11}$$

$$G_\mu = LN_\mu - \sum_\alpha p_\alpha q_\mu{}^\alpha, \tag{12}$$

$$q_\tau{}^\alpha = q_\mu{}^\alpha(\partial x_\mu/\partial u_\tau). \tag{13}$$

Then, following the spirit of Weiss's method, we let J in (5) be

$$i\int du_1 du_2 du_3 (G_\mu \Delta x_\mu), \tag{14}$$

where G_μ are functions $G_\mu(q, q_\tau, p, \partial x_\mu/\partial u_\tau)$ [5] of q, q_τ, p, $\partial x_\mu/\partial u_\tau$ as given by (10), (11), (12), (13) and q, q_τ, p are operators satisfying

$$\left.\begin{aligned} q(u^a)\langle q'(u);\ |\rangle &= q'(u^a)\langle q'(u);\ |\rangle, \\ q_\gamma(u^a)\langle q'(u);\ |\rangle &= (\partial q'(u^a)\partial u_\gamma{}^a)\langle q'(u);\ |\rangle, \\ p(u^a)\langle q'(u);\ |\rangle &= \hbar\delta\langle q'(u);\ |\rangle/\delta q'(u^a), \end{aligned}\right\}^6 \tag{15}$$

u^a being a given value of u. The form (14) for J is slightly more general than the corresponding one in Weiss's original formulation, since we do not restrict ourselves to a one-parameter family of surfaces.

To prove the integrability of (5) with J given by (14), we calculate by means of (5), (14), the change $\Delta\Psi$ of Ψ as the functions b_μ change from initial values $b_\mu{}^{(0)}(u)$ to the final values

$$b_\mu{}^{(J)}(u) = b_\mu{}^{(0)}(u) + \Delta_1 x_\mu(u) + \Delta_2 x_\mu(u) \tag{16}$$

in two ways, one by letting $b_\mu(u)$ pass through the intermediate functions

$$b_\mu{}^{(1)}(u) = b_\mu{}^{(0)}(u) + \Delta_1 x_\mu(u), \tag{17}$$

and the other by letting $b_\mu(u)$ pass through the intermediate functions

$$b_\mu{}^{(2)}(u) = b_\mu{}^{(0)}(u) + \Delta_2 x_\mu(u), \tag{18}$$

and compare the two results for $\Delta\Psi$ to the second order in $\Delta_1 x_\mu$, $\Delta_2 x_\mu$. Let us say that their difference is $B\Psi^{(0)}$ where $\Psi^{(0)}$ is the initial wave function. Equation (5) is integrable if $B\Psi^{(0)} = 0$.

Let us consider the Hamilton-Jacobi equation from the Lagrangian L, which is

$$\Delta I = \int G_\mu\left(q, \frac{\partial q}{\partial u_\tau}, \frac{\delta I}{\delta q(u)}, \frac{\partial x_\mu}{\partial u_\tau}\right) du. \qquad (du = du_1 du_2 du_3) \tag{19}$$

This is always integrable provided that the field equations are consistent and admit solutions, and the solution $I(q(u), b_\mu(u))$ of (19) is

$$\int L(q, q_\mu) dx_1 dx_2 dx_3 dx_4, \tag{20}$$

where the integral extends over a volume bounded by two space like parametrized surfaces, $b_\mu{}^{(00)}$ and b_μ, and the surfaces at infinity, q and q_μ, in L satisfy the field equations, and the whole integral is considered as a functional of $b_\mu{}^{(00)}$ and b_μ and the functions $q^{(00)}(u)$ and $q(u)$, which are the values q, take on the surfaces. From (19), we calculate the change ΔI of I as b_μ changes from $b_\mu{}^{(0)}$ to $b_\mu{}^{(J)}$ in the above two ways, and the difference of these two ΔI's must be zero, since (19) is integrable. It can be easily verified that this difference is precisely B if we replace p contained in B by $\delta I^{(0)}/\delta q(u)$, $I^{(0)}$ being the value of I on the surface $b^{(0)}$. Thus $B\Psi^{(0)} = 0$ and the integrability of (5) is proved.[7]

It is possible to verify directly that the operator B is zero, but the direct verification will be left out. The above proof indicates incidentally what changes in the formalisms are necessary for Fermi-Dirac fields.

The other requirements are easily seen to be satisfied. For (ii) we note that the Hermitian character of J can be ensured with a proper choice of the Lagrangian. For (iii), let us first consider two surfaces passing through the same point P with u_P taking the same value on them. Thus

$$\Delta x_\mu = 0 \text{ at } u = u_P. \tag{21}$$

The Heisenberg equations of motion,

$$(\Delta q)(u) = -(\hbar i)^{-1}[J, q(u)], \tag{22}$$

gives us immediately $\Delta q = 0$. Next we consider a change of parameters from u to some new parameters, say v. If a change of parametrization is considered as a change of $b_\mu(u)$, we may employ (22) again and we prove readily that there is no change of q at the point P as this b_μ changes. Finally, (iv) must be satisfied, as it must be in a Weiss theory.

[5] We drop the suffix α.

[6] Equation (15) restricts us to Einstein-Bose fields, but this restriction is really not essential.

[7] That the integrability of (5) may follow from that of (19) is learned by the author from Professor Dirac.

3. TOMONAGA'S FORMALISM

Another study of the change of Schroedinger wave functionals on space-like surfaces was given by Tomonaga and has been found useful in formulating a relativistic quantum electrodynamics.[8] Let us see if this formalism can be obtained from our formulation (5).

Let us consider for definiteness only electrons and the Maxwell field. Then

$$G_\mu = G_\mu^0 + eG_\mu^1, \tag{23}$$

where both G_μ^0 and G_μ^1 do not contain the charge constant e. Let $\bar{G}^0$, $\bar{G}^1$ denote $\int G_\mu^0 \Delta x_\mu du$ and $\int G_\mu^1 \Delta x_\mu du$, and let us write the wave functions $\langle q; b|\rangle$ as $\langle q|b\rangle$. Obviously, the equation

$$\hbar\Delta\Psi = \bar{G}^0\Psi \tag{24}$$

is integrable and the solution may be written in the form

$$\langle q(u)|b\rangle = \langle q(u)|R(bb_0)|b_0\rangle, \tag{25}$$

where b_0 is any given b and R is an unitary operator. With respect to variations Δx_μ of b, we have

$$\hbar\Delta R = \left(\int G_\mu^0 \Delta x_\mu du\right) R, \tag{26.1}$$

and with respect to variations Δx_μ of b_0, we have

$$\hbar\Delta(R^{-1}) = \left(\int G_\mu^0 \Delta x_\mu du\right) R^{-1},$$

or

$$\hbar\Delta R = -R\left(\int G_\mu^0 \Delta x_\mu du\right). \tag{26.2}$$

Let us introduce a wave function $\langle q(u)|b_1 b\rangle$ connected to the general wave function $\langle q|b\rangle$ in (5) by

$$\langle q(u)|b_1 b\rangle = \langle q(u)|R(b_1 b)|b\rangle. \tag{27}$$

Looked upon as a $\langle q(u)|b_1\rangle$, it satisfies the wave equation (5) without the interaction terms. Its variation with respect to b for a constant b_1 is given by

$$\begin{aligned}&\hbar\Delta\langle q(u)|b_1 b\rangle\\ &=\langle q(u)|R(b_1 b)[\bar{G}^0+e\bar{G}^1]|b\rangle+\langle q(u)|\hbar\Delta R|b\rangle\\ &=\langle q(u)|R(b_1 b)e\bar{G}^1|b\rangle\\ &=\langle q(u)|e\bar{G}^{1*}(bb_1)|b_1 b\rangle,\end{aligned} \tag{28}$$

where operators with *'s are defined in $q(u)$ representation by

$$l^*(b_2 b_1) = R(b_1 b_2) l R^{-1}(b_1 b_2) = R^{-1}(b_2 b_1) l R(b_2 b_1). \tag{29}$$

Considered as a function of u and b_2, $q^*(u)(b_2 b_1)$ satisfies the Heisenberg's equation of motion without the interaction terms. It reduces further at $b_2 = b_1$ to $q(u)$.

For the interaction between the electrons and the electromagnetic field, G_μ^1 is equal to $N_\mu L^1$, where eL^1 is the interaction term in the Lagrangian. Hence if Δx_μ are nearly zero everywhere except at a certain value of u, the operator in (28) is

$$eL^{1*}(bb_1)$$

evaluated at this value of u times the volume ΔV between the original surface S and the displaced surface S'. This fact has been employed by Schwinger to introduce a differentiation of Ψ with respect to the surface at a point on the surface.

(28) can be put in a nicer form by introducing a representation $\langle q^{*\prime}(b_1 b_2)|\rangle$. As q^* and q have the same eigenvalues, we may let $q^{*\prime}$, q' (and similarly $q^{*\prime\prime}$, q'') denote the same eigenvalues. Defining $\langle q^{*\prime}(b_1 b_2)|\rangle$ by

$$\langle q^{*\prime}(b_1 b_2)|\rangle = \langle q'|R(b_1 b_2)|\rangle, \tag{30}$$

we have

$$\begin{aligned}&\langle q^{*\prime}(b_1 b_2)|q^*(b_1 b_2)|\rangle\\ &\quad=\langle q'|R(b_1 b_2)\{R^{-1}(b_1 b_2) q R(b_1 b_2)\}|\rangle\\ &\quad=q'\langle q'|R(b_1 b_2)|\rangle = q'\langle q^{*\prime}(b_1 b_2)|\rangle\end{aligned} \tag{31}$$

and thus $q^*(b_1 b_2)$ is diagonal in this representation. From (28) and (30)

$$\begin{aligned}\hbar\Delta\langle q^{*\prime}(b_1 b)|b\rangle &= \hbar\Delta\langle q'|R(b_1 b)|b\rangle\\ &=\langle q'|R(b_1 b)e\bar{G}^{(1)}|b\rangle = \langle q^{*\prime}(b_1 b)|e\bar{G}^1|b\rangle.\end{aligned} \tag{32}$$

A further simplification is obtained by introducing $\langle q'(b_1)|b\rangle$ defined by

$$\langle q'(b_1)|b\rangle = \langle q'|R(b_1 b)|b\rangle = \langle q'|b_1 b\rangle, \tag{33}$$

so that

$$\langle q'(b_2)|b\rangle = \textstyle\sum_{q''}\langle q'|R(b_2 b_1)|q''\rangle\langle q''(b_1)|b\rangle,$$

etc., and an operator $l(b)$ by

$$\langle q'(b_1)|l(b_2)|q''(b_1)\rangle = \langle q'|l^*(b_2 b_1)|q''\rangle. \tag{34}$$

Then (28) becomes

$$\begin{aligned}\hbar\Delta\langle q'(b_1)|b\rangle &= \textstyle\sum_{q''}\langle q'|e\bar{G}^{1*}(bb_1)|q''\rangle\langle q''|b_1 b\rangle\\ &=\textstyle\sum_{q''}\langle q'(b_1)|e\bar{G}^1(b)|q''(b_1)\rangle\langle q''(b_1)|b\rangle\\ &=\langle q'(b_1)|e\bar{G}^1(b)|b\rangle.\end{aligned} \tag{35}$$

When $G_\mu^1 = N_\mu L^1$, we obtain precisely Tomonaga's formalism. As it stands, (35) is slightly more general than Tomonaga's formalism, since the operator in (35) may be an integral over u of non-commuting quantities. Though the formulas giving the change of the wave functional with respect to the surface S still depend on the parametrization of S, the coordinates of the wave function do not, as pointed out by Dirac.

The expectation value of an operator $l(u)$ on the surface b is, in terms of the wave functions in (5),

[8] J. Schwinger, Conference of physics, Pocono Manor, National Academy of Science, April 1948.

$\langle b|l|b\rangle$ or

$$\sum_{q'}\langle b|q'\rangle\langle q'|l|b\rangle. \tag{36}$$

Transforming to wave functions of the type $\langle q'|b_1b\rangle$, it becomes

$$\langle b_1b|l^*(bb_1)|b_1b\rangle. \tag{37}$$

Transforming to wave functions of the type $\langle q'(b_1)|b\rangle$, it becomes

$$\sum_{q'q''}\langle b|q'(b_1)\rangle\langle q'(b_1)|l(b)|q''(b_2)\rangle\langle q''(b_2)|b\rangle \tag{38}$$

or simply $\langle b|l(b)|b\rangle$.

The passage to Tomonaga's formalism consists essentially of introducing $\langle q'(b_1)|b\rangle$ by (33) and operator $q(b)$ by (34). Thus all features in the orthodox Heisenberg-Pauli formalism are more or less retained in the new formalism. For example, we have in electrodynamics supplementary conditions on the wave functions in (5), and by introducing the transformation (33), (34), we deduce the corresponding supplementary conditions on the new wave functions. If the supplementary conditions on the wave functions in (5) are consistent and are satisfied always if satisfied for one surface b, so are the new supplementary conditions. Further, Schwinger has shown for electrons interacting with the Maxwell field that from (35), a certain transformation of the wave function produces a wave equation with the same left-hand side but with the operator on the right-hand side as a power series of e with the leading power e^2. Thus similarly, a certain transformation on the wave function in (5) will also produce the same result. In fact, if we let the wave function in (5) be subjected to the transformation

$$\langle q|b\rangle_{\text{new}}=e^{iS(b)}\langle q|b\rangle_{\text{old}}, \tag{39}$$

where $S(b)$ is an operator depending on b and satisfies

$$\hbar i\Delta S=-e\bar{G}^1-i[S,\bar{G}^0], \tag{40}$$

we find that the above is integrable, and admits the solution

$$S(b)=-(e/\hbar i)\int R^{-1}(b_1b)\bar{G}^1R(b_1b), \tag{41}$$

where Δx_μ in G^1 is the change of b_1 and the integration is carried out with respect to such increments from any initial surface to the final surface b. The wave equation for the new wave function is

$$\hbar\Delta\Psi=\left\{\bar{G}^0+\frac{ie}{2}[S(b),\bar{G}^1]+0(e^3)\right\}\Psi. \tag{42}$$

A further transformation enables us to get rid of $\bar{G}^0$.

The question of the self-energy of an electron or a photon will not be discussed here, as it has been discussed already by a number of physicists. The purpose of the present section is to show that the Tomonaga's formalism is essentially the same as the Heisenberg-Pauli formalism and it seems likely that it will encounter the same difficulties.

In conclusion, the writer wishes to thank Professor P. A. M. Dirac and Professor H. C. Corben for many stimulating discussions.

Interpretation of the Thermal Conductivity of Glasses

CHARLES KITTEL
Bell Telephone Laboratories, Murray Hill, New Jersey
(Received November 30, 1948)

The thermal conductivity of glasses decreases with decreasing temperature, while the conductivity of crystalline substances increases with decreasing temperature. The behavior of glasses is interpreted in terms of an approximately constant free path for the lattice phonons, so that the conductivity decreases roughly with the specific heat. The value of the phonon mean free path at room temperature is of the order of magnitude of the scale of the disorder in the structure of glasses as determined from x-ray evidence—that is, of the order of 7A. This is about the size of the unit cell of the crystalline forms of silica.

IT was pointed out first by Eucken[1] that the temperature dependence of the thermal conductivity of glassy materials is quite different from that of crystalline materials. The thermal conductivity of glasses *decreases* fairly sharply with decreasing temperature, whereas the thermal conductivity of crystalline substances—whether single crystals or polycrystalline—*increases* fairly sharply with decreasing temperature[2] (Fig. 1). A second distinguishing characteristic of the thermal conductivity of glasses is that the spread of values of the conductivity from one glass to another, at a given temperature, is usually smaller than the spread in the care of crystalline substances. A third difference is that the thermal conductivity of glass is considerably lower than for crystalline substances. The point plotted for Thuringian glass at 1.3°K should be particularly noted.

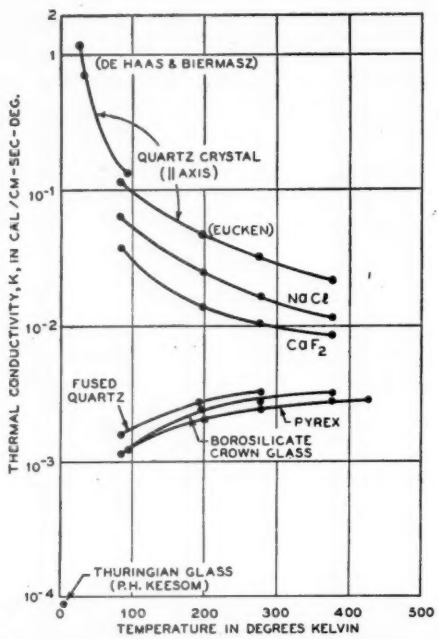

FIG. 1. Comparison of thermal conductivity of glasses and crystalline substances. (The data are principally from the Landolt-Börnstein tables. The measurement on Thuringian glass at liquid He temperature is by P. H. Keesom, Physica **11**, 339 (1944–46). Other measurements, not shown above, on four glasses at liquid He temperatures have been made by Dr. D. Bijl, and are to be published in Physica. The trend of the conductivity is quite similar in the four glasses measured by Bijl; for example, he finds $K=1.0\times10^{-4}$ cal./cm-sec.-deg. for Monax glass at 1.45°K, while Keesom found for Thuringian glass 0.8×10^{-4} at 1.3°K.)

While the mechanism of thermal conduction in crystalline substances is quite well understood in qualitative terms, the corresponding processes in glasses have not previously been considered. It is this subject with which the present paper is concerned, and we shall see that the thermal conductivity data find a natural explanation which is based on the x-ray evidence as to the nature of the glassy state; in fact, the thermal conductivity data may be regarded as a significant additional confirmation of the random lattice theory of glasses, as developed by Zachariasen[3] and Warren.[4]

The present concept of the nature of the glassy state pictures a glass such as fused quartz (SiO_2) as a random, but continuous, network of Si−O bonds. There is a definite structure in vitreous silica, but it is a structure with regard to immediate neighbors rather than a regularly repeating crystalline structure (Fig. 2). The local order which exists in the immediate environment of any atom is the same in vitreous silica as in the crystalline modifications of silica, but fused quartz does not possess the regularly repeating long range order of the crystal. Warren has shown that if we try to interpret the x-ray diffraction pattern of vitreous silica in

[1] A. Eucken, Ann. d. Physik (4) **34**, 185 (1911).

[2] The thermal conductivity of several single crystals has been found by de Haas and Biermasz to pass through a maximum near the liquid helium range; the fall-off on the low temperature side of the maximum has been explained very satisfactorily by Casimir, who showed that the maximum occurs when the phonon mean free path becomes of the same order as the diameter of the test specimen, while at lower temperature the thermal conductivity is approximately proportional to the specific heat. See W. J. de Haas and T. Biermasz, Physica **2**, 673 (1935); **4**, 752 (1937); **5**, 47, 320, 619 (1938); H. B. G. Casimir, Physica **5**, 495 (1938); R. E. B. Makinson, Proc. Camb. Phil. Soc. **34**, 474 (1938); see also R. Peierls, reference 6.

[3] W. H. Zachariasen, J. Am. Chem. Soc. **54**, 3841 (1932).

[4] B. E. Warren, J. App. Phys. **8**, 645 (1937); **13**, 602 (1942).

terms of the older concept of a glass as composed of small crystallites, rather than as a continuous bonded network, then we must conclude from the width of the diffraction lines that the crystallites are 7A in size. This is, however, just the size of the unit cell of a typical crystalline form of silica, and it is rather meaningless to speak of material as polycrystalline when the crystallites are reduced to single unit cells. The idea of glass as a continuous random network is based on this and a number of other considerations.

The mechanism of heat conduction in *crystalline substances* has been explained by Debye,[5] Peierls,[6] and others, as sketched below. By analogy with the corresponding expression in the kinetic theory of gases the thermal conductivity K is written

$$K=\tfrac{1}{4}cv\Lambda, \qquad (1)$$

where c is the heat capacity per unit volume, v is average velocity of a sound wave (phonon) in the material, and Λ is the mean free path of phonons; the factor $\frac{1}{4}$ is somewhat arbitrary. In an ideal infinite crystal lattice the mean free path will be infinite if the lattice interactions are strictly harmonic; finite values of Λ in an ideal crystal lattice are the result of anharmonic terms in the lattice interactions. The anharmonic terms have two effects: they limit the mean free path by coupling together the various lattice vibrations, and by the same mechanism they are able to produce a distribution of phonon frequencies corresponding to thermal equilibrium.

The numerical value of Λ in a perfect crystal will depend on the magnitude of the anharmonic interactions, and also on the total density of phonons, since the greater the density of phonons, the greater are the number of possibilities for a given phonon to interact with other phonons. The phonon density decreases with decreasing temperature, so that we should expect the mean free path and thus the thermal conductivity to increase as we lower the temperature. This feature of the theory is in agreement with the experimental data which suggest that the conductivity of crystalline materials usually varies approximately as $1/T$ over the range of ordinary temperatures.

HEAT PROPAGATION IN GLASSES

In the case of glasses the anharmonic lattice interactions are still responsible for establishing thermal equilibrium among the phonons, but the mean free path which enters into the equation for the conductivity will usually be limited by geometrical effects associated with the disordered nature of the structure.

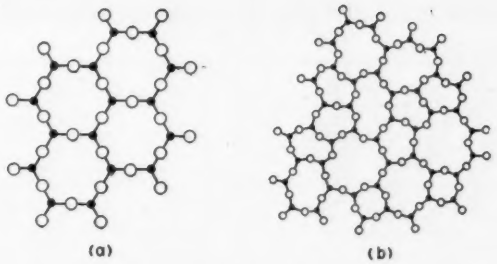

FIG. 2. Schematic two-dimensional figures, after Zachariasen, illustrating the difference between: (a) the regularly repeating structure of a crystal; and (b) the random network of a glass.

If, to take an extreme case, the disorder determines a mean free path Λ_0 which is a constant, independent of phonon wave-length and phonon density, then the thermal conductivity may be written as

$$K=\tfrac{1}{4}cv\Lambda_0 \qquad (2)$$

so that the ratio K/c is approximately constant. Since the heat capacity decreases with decreasing temperature, the thermal conductivity would also be expected to decrease, on the assumption of constant mean free path.

Values of Λ for glasses are given in Table I, as calculated from the experimental values of the conductivity, heat capacity, density and sound velocity. It is seen that the values of Λ are all of the order of magnitude of the dimensions of a "unit cell"—that is, of the order of 7A.

The phonon free path in quartz glass at room temperature is seen from Table I to be longer than in the other two glasses for which data are given. This result may be accounted for by the presence of foreign atoms introduced in the commercial glasses as "modifiers"; these give additional scattering.

The increase in the phonon free path at low temperatures can be understood as a consequence of

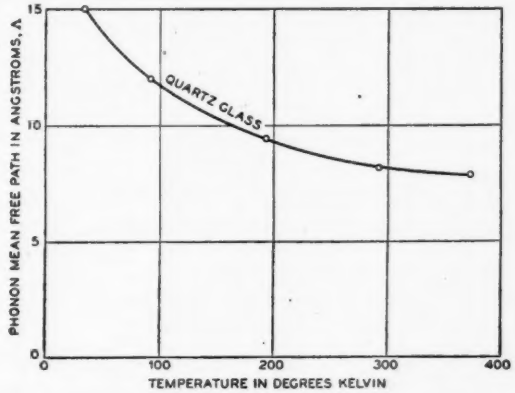

FIG. 3. Phonon mean free path Λ as a function of absolute temperature for quartz glass.

[5] P. Debye, in *Vorträge über die kinetische Theorie der Materie und Elektrizität*, by M. Planck *et al.* (B. G. Teubner, Leipzig, 1914).

[6] R. Peierls, Ann. d. Physik (5) **3**, 1055 (1929); M. Blackman, Phil. Mag. **19**, 989 (1935).

TABLE I. Calculation of the phonon mean free path Λ for glasses.*

Material	Temp.	K	c'	$\rho v l$	$\langle \rho v \rangle$	Λ
Quartz glass	100°C	(0.0037)	0.194	——	(0.97×10^{6})	7.8A
	room	0.0034	0.172	1.45×10^{6}	(0.97×10^{6})	8.1
	−80°C	0.00275	0.12	——	(0.97×10^{6})	9.5
	−180°C	0.0017	0.059	——	(0.97×10^{6})	12.0
	−238°C	(0.0009)	0.014	——	(0.97×10^{6})	15.0
Crown glass	room	0.00163	0.161	1.41×10^{6}	0.94×10^{6}	4.2
Flint glass	room	0.00143	0.117	1.54×10^{6}	1.02×10^{6}	4.8

* For purposes of comparison we may mention that Λ for a quartz crystal ($\|$ axis) is of the order of 700A at −190°C. The data used above are taken from the *Landolt-Börnstein Tabellen* and from Bergmann *Der Ultraschall*. K is in cal./cm-sec.-deg.; c' is in cal./g-deg.; ρv is in g/cm²-sec.; the mean value $\langle \rho v \rangle$ is arbitrarily taken as $\frac{2}{3}$ of the value ρv for longitudinal waves.

the more uniform propagation conditions which obtain when the wave-length of the dominant phonons becomes substantially larger than the dimensions of a unit cell of the glass. The mean free path may be expected to begin to increase when the temperature drops significantly below the value given by

$$kT_0 = hv/D$$

where D is the unit cell length. For glasses

$$T_0 \approx \frac{(6.6\times10^{-27})(4\times10^{5})}{(1.4\times10^{-16})(7\times10^{-8})} \approx 270°\text{K},$$

and this value is more or less in agreement with experiment (see Fig. 3, where Λ *vs.* T is plotted for quartz glass).

There are several ways in which we can understand qualitatively the mechanism by which a disordered structure limits the free path of a phonon of wave-length λ appreciably smaller than the scale D of the disorder.

1. One method is based on the distinction between plane elastic waves and normal modes of vibration. In a regular periodic lattice the normal modes of vibration are essentially identical with plane waves, so that in an infinite medium a plane wave will, if we neglect anharmonic interactions, propagate indefinitely without loss of energy to other modes of vibration. But in a disordered lattice the normal modes are no longer plane waves: if we set up a plane wave it will soon become highly distorted, as the original wave may be viewed as the sum of a number of normal modes with various eigenfrequencies. The resulting distortion may be described approximately in terms of a mean free path.

2. Another method is based on a consideration of Fig. 1b which shows the random network of a glass. A plane elastic deformation started along one side of the network will not propagate in plane form, since different portions of the original plane deformation will travel down bond linkages of different overall length, leading to phase destruction and to distortion of the character of the deformation.

3. Another approach to the problem utilizes the concepts which have been developed by the present author,[7] and by Mason and McSkimin,[8] in analyzing the results of measurements of the attenuation of ultrasonic waves (~20 mc/sec.) in polycrystalline solids. It is found experimentally that when the wave-length is much smaller than the grain size the "free path" is a constant, independent of frequency. We have the following physical picture of the mechanism responsible for a constant Λ_0 in this limit: the sound wave loses a certain proportion of its energy by reflection at each interface between adjacent crystal grains. The intensity penetrating a distance x will be reduced with respect to the incident intensity by a factor of the order of $e^{-Rx/D}$, where D is the grain size, and R is the reflection coefficient. The phonon free path here is then $\Lambda_0 = D/R$.

It should be mentioned that the viewpoint developed in the present paper is applicable to heat conduction in liquids, as it is well known that in liquids the phonon free paths are of molecular dimensions, and that the lattice structure is in some respects similar to that of a disordered solid.

I wish to thank Dr. W. P. Mason, Dr. W. Shockley, and Professor P. Debye for stimulating discussions which led up to the analysis given in this paper. The 1948 Shelter Island Low Temperature Conference sponsored by the National Academy of Sciences provided further opportunity for discussion. I am indebted to Dr. D. Bijl of Leiden for his kind permission to refer to his measurements in advance of publication, and to Professor C. J. Gorter for informing me of the existence of these measurements.

[7] C. Kittel, "Ultrasonics research and the properties of matter," Reports on Progress in Physics 11, 205–247 (1946–1947).

[8] W. P. Mason and H. J. McSkimin, J. Acous. Soc. Am. 19, 464–474 (1947); also J. App. Phys. 19, 940–946 (1948).

Total Neutron Cross Sections of Compounds with Different Crystalline Structures*

LESTER WINSBERG, DAVID MENEGHETTI, AND S. S. SIDHU**
Argonne National Laboratory, Chicago, Illinois

(Received November 22, 1948)

The total neutron cross sections of polycrystalline compounds, such as close-packed hexagonal ZnO, body-centered cubic TlBr, and face-centered cubic CaO and TiC were determined with the Argonne neutron velocity selector and neutron crystal spectrometer in the energy region of 0.001 to 1.0 electron volt. From the size of the cross-section peaks which are due to coherent scattering of neutrons the following scattering amplitudes were determined: Ca, $+0.46\times10^{-12}$ cm; Ti, -0.25×10^{-12} cm; Tl, $+0.75\times10^{-12}$ cm. The previously reported value of $+0.58\times10^{-12}$ cm for Zn was confirmed. The free atom scattering cross section of Ca is 2.5 barns.

INTERFERENCE effects are observed when photons or particles of appropriate wave-length impinge on crystalline matter. For diffraction to occur the wave-length of the impinging radiation must be less than twice the largest interplanar distance in the crystal but not smaller by too large an order of magnitude. The intensity of the scattered beam is usually measured as a function of the scattering angle and the wave-length of the impinging radiation. Since the intensity of the transmitted beam is decreased by the amount of scattered and absorbed radiation, diffraction effects may also be observed if transmission measurements are made as a function of the wave-length of the incident beam.

Halpern, Hamermesh, and Johnson,[1] and Weinstock[2] have theoretically determined the nature of the transmission curve as a function of wave-length for neutrons passing through a monoatomic microcrystalline substance. Fermi, Sturm, and Sachs[3] extended this treatment to diatomic substances and determined the theoretical and experimental curves for Be and BeO. In the present investigation the method was applied to the study of crystalline and nuclear properties of some simple diatomic substances with body-centered and face-centered cubic, and hexagonal close-packed structures.

EXPERIMENTAL PROCEDURE AND RESULTS

The two devices used for velocity selection of neutrons from the Argonne heavy water pile were the rotating shutter mechanism designed by Brill and Lichtenberger[4] and the crystal spectrometer described by Zinn[5] and Sturm.[6] The rotating shutter mechanism employs the time of flight method for determining the energy of neutrons. Its operating range was 0.001 to 0.2 electron volt. The energy range of neutrons obtained by means of the crystal spectrometer was 0.1 to 1.0 electron volt.

The samples were in the form of powders ground to finer than 200 mesh and were contained in aluminum containers with inner end dimensions of $1\frac{1}{2}''\times4\frac{1}{2}''$ and lengths varying from $2''$ to $10''$, depending on the desired transmissions in the region of 0.25 to 0.5. In the case of samples with high absorption and low scattering of neutrons it was necessary to use a sample having low transmission in order to determine with sufficient accuracy the contribution of coherent scattering to the total cross section of the material.

The transmission T of the sample for neutrons of given velocity was determined from the ratio of the counting rates obtained with and without the sample in the path of the beam corrected for the fast neutron background. From the weight of the sample and the inner end area of the container the number N of formula molecules per unit end area was calculated. The cross section was then determined from

$$\sigma=(1/N)\ln(1/T). \tag{1}$$

The theoretical cross-section curves due to coherent scattering alone were calculated from the relation:[3]

$$\sigma=\sum_{n/d\leq2/\lambda}\frac{FM\lambda^2d}{gV8\pi n}\exp(-\omega(n/d)^2) \tag{2}$$

* This document is based on work performed under the auspices of the Atomic Energy Commission at the Argonne National Laboratory.

** On leave from the University of Pittsburgh.

[1] O. Halpern, M. Hamermesh, and M. H. Johnson, Phys. Rev. 59, 981 (1941).

[2] R. Weinstock, Phys. Rev. 65, 1 (1944).

[3] E. Fermi, W. J. Sturm, and R. G. Sachs, Phys. Rev. 71, 589 (1947).

[4] T. Brill and H. V. Lichtenberger, Phys. Rev. 72, 585 (1947).

[5] W. H. Zinn, Phys. Rev. 71, 752 (1947).

[6] W. J. Sturm, Phys. Rev. 71, 757 (1947).

TABLE I. Structure factors and multiplicity factors of CaO, TiC, TlBr, and ZnO.

Element	Miller indices	M	$F/4\pi$	$FM/4\pi$ $\times 10^{-24}$ cm^2
CaO	111	8		3
	311	24	$16(Ca-O)^2$	9
	331	24		9
	—			
	200	6		110
	220	12	$16(Ca+O)^2$	220
	222	8		146
	—			
TiC	111	8		109
	311	24	$16(Ti-C)^2$	326
	331	24		326
	—			
	200	6		17
	220	12	$16(Ti+C)^2$	34
	222	8		23
	—			
TlBr	100	6		0.2
	111	8	$(Tl-Br)^2$	0.3
	210	24		0.9
	—			
	110	12		20.6
	200	6	$(Tl+Br)^2$	10.3
	211	24		41.3
	—			
ZnO	100	6	$(Zn+O)^2$	8.5
	002	2	$4(Zn^2+O^2-0.070\ Zn\cdot O)$	5.5
	101	12	$3(Zn^2+O^2-1.39\ Zn\cdot O)$	7.8
	102	12	$(Zn^2+O^2-0.070\ Zn\cdot O)$	8.2
	110	6	$4(Zn+O)^2$	34.0
	103	12	$3(Zn^2+O^2+1.49\ Zn\cdot O)$	44.4
	200	6	$(Zn+O)^2$	8.5
	112	12	$4(Zn^2+O^2-0.070\ Zn\cdot O)$	32.8
	201	12	$3(Zn^2+O^2-1.39\ Zn\cdot O)$	7.8
	004	2	$4(Zn^2+O^2-1.995\ Zn\cdot O)$	0.02

in which the structure factor F of the lattice made up of diatomic substance was calculated as follows:

$$F=4\pi\left|A_1\sum_{u_1v_1w_1}\exp[2\pi i(hu_1+kv_1+lw_1)\right.$$
$$\left.+A_2\sum_{u_2v_2w_2}\exp[2\pi i(hu_2+kv_2+lw_2)]\right|^2, \quad (3)$$

where A_1 and A_2 are the scattering amplitudes of atoms of species 1 and 2, u, v, and w are the coordinates of the atoms in the unit cell, and h, k, and l are the Miller indices. In expression (2) M is the multiplicity factor (the number of different orientations of the unit cell such that the Bragg condition for a given set of crystal planes is satisfied), λ the wave-length of the neutrons, V the volume of the unit cell, d the interplanar spacing for a given set of crystal planes, n the order of reflection, and g the number of molecules per unit cell. The exponential term is a Debye-Waller type correction factor for thermal agitation, in which ω is a function of the Debye temperature.[2]

Where the scattering amplitudes were known, the coherent scattering cross section as a function of energy was calculated from Eqs. (2) and (3). The contribution due to absorption was calculated from the value of the absorption cross section at 0.025 electron volt[7] on the assumption that the absorption cross section varied inversely proportional to the neutron velocity. The sum of the two calculated cross sections was compared with the experimentally obtained values. Where the scattering amplitude was not known, its value was taken to be that which gave the best fit of the resultant curve above and below the position of the first appearance of diffraction effects.

It should be noted that for nth order diffraction from a given set of parallel planes the maximum cross section occurs at the wave-length $\lambda=2d/n$. The energy values corresponding to these wave-lengths are marked on all the figures given below. The coherent scattering cross section for neutrons of wave-length longer than $2d/n$ is zero for the given value of n and d.

A. CaO

An 8-inch long container was filled with 476.8 grams of chemically pure CaO which had been dried for several days at 950°C. The sample was kept in a desiccator at all times except during an

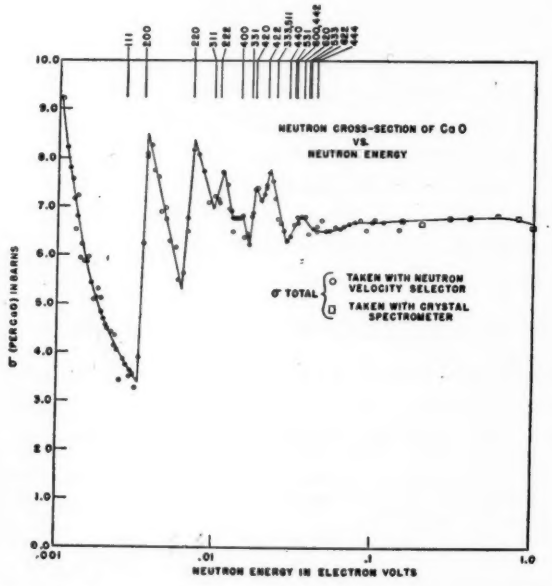

FIG. 1. Neutron cross section of CaO *vs.* neutron energy.

[7] Project Handbook—CL—697, Chapter IVA, 3.1, p. 21.

actual cross-section measurement. These precautions were necessary to avoid absorption of water.

The structure of calcium oxide is face-centered cubic. Fermi and Marshall[7] give the scattering amplitudes of Ca and O as 0.79 and 0.61, respectively, in units of 10^{-12} cm. The signs of the scattering amplitudes are both positive, i.e., the change in the phase of the neutron wave on scattering by Ca is the same as for O. As given in Table I, the structure factors for diffractions involving all odd indices are proportional to the factor (Ca−O) where the chemical symbols represent the scattering amplitudes. For all even indices the factors are proportional to (Ca+O). This is confirmed by Fig. 1. The first two peaks can be unambiguously assigned to diffraction involving even indices (200) and (220). Furthermore, the (111) peak is either very weak or completely absent. The positions of the other peaks are in accord with the assigned signs of the scattering amplitudes, although the agreement in these cases is not as definite. Because of the limited resolution of the instrument, the cross-section peaks obtained experimentally occur at slightly higher energies than the calculated values.

The calculated cross-section curve, based on the data of Fermi and Marshall[8] and a value of 570°K for the Debye temperature determined from the heat capacity data, is larger than the experimental curve obtained here by a factor of almost 2. The best fit of the experimental and calculated curves was for a value of 0.46±0.05 for the scattering amplitude of Ca based on the value of 0.61 for O. The free atom scattering cross section of Ca can be calculated by the formula $\sigma=4\pi A^2\mu^2$, where A is the value of the scattering amplitude and μ is the reduced mass of a neutron and a free Ca atom. This formula is strictly valid only for mono-isotopic elements but is assumed accurate enough here within the uncertainty in the scattering amplitude, since the isotopic abundance of Ca^{40} is 97 percent, the remainder being divided among 5 isotopes. The free atom scattering cross section based on the value of 4.1 barns for O was also determined from the experimental curve at one electron volt. The value obtained by both the rotating shutter method and the crystal spectrometer was 2.5±0.3 barns. It is much less than any value previously reported.

[8] E. Fermi and L. Marshall, Phys. Rev. **71**, 666 (1947).

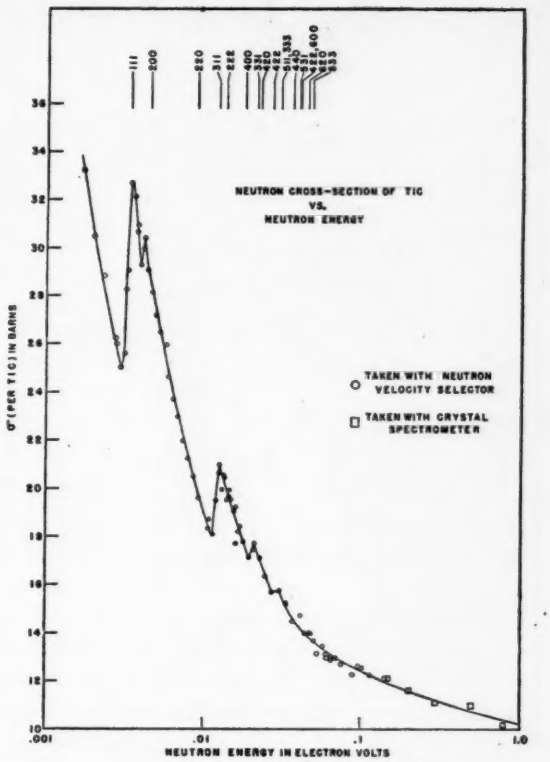

FIG. 2. Neutron cross section of TiC *vs.* neutron energy.

B. TiC

A 2-inch long container was filled with 378.2 grams of TiC. Since the compound has a low avidity for water, further drying was unnecessary.

Like CaO, TiC crystallizes in a face-centered cubic structure. While the scattering amplitude of C is given as +0.67,[8] neither the sign nor the magnitude of the scattering amplitude of Ti has been known.

Whereas in the case of CaO the cross-section values for diffractions involving even indices was large and those involving odd indices very small, the situation is reversed in the case of TiC. As seen in Fig. 2, the intense peaks can be unambiguously assigned to diffractions from the (111) and (311) planes. Possible peaks corresponding to the (200) and (220) planes are relatively weak. The change in the phase of the neutron on scattering by Ti is, therefore, different by the angle π from that for C, i.e., the sign of its scattering amplitude is negative. The large continuous rise of the curve with decreasing energy is due primarily to the high 1/v absorption cross section of titanium. The scattering amplitude was calculated from the curve to be −0.25±0.03. The Debye temperature was not known. Calculations

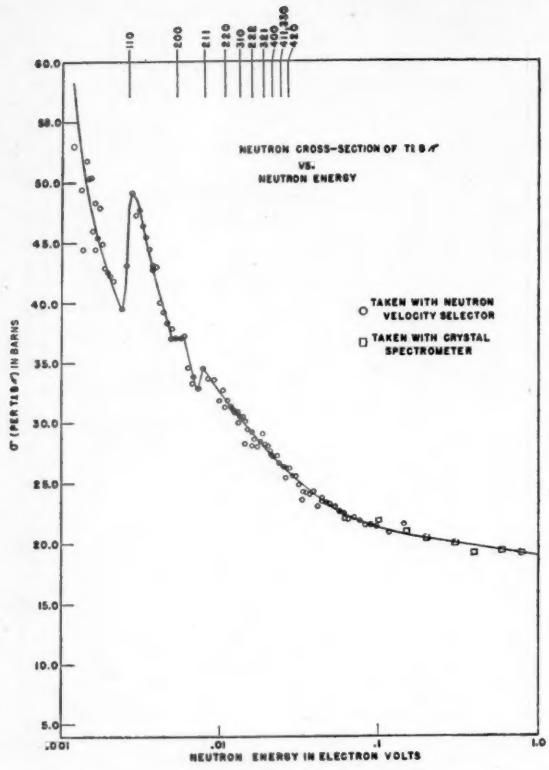

FIG. 3. Neutron cross section of TlBr *vs.* neutron energy.

were, therefore, made by assuming it to be 500°K, 1000°K, and 1500°K. The lowest value of the exponential term in Eq. (2) for the (111) planes was 0.96 for a Debye temperature of 500°K. Because the term decreases in magnitude for larger indices, the value of the scattering amplitude was calculated primarily from the (111) peak and is, therefore, relatively reliable. The structure factors for various crystalline planes of TiC, based on the above value of the scattering amplitude of Ti, and the multiplicity factors are given in Table I.

C. TlBr

A container similar to that used for TiC was filled with 887.5 g of TlBr which had been dried for 3 days at 400°C. The scattering amplitude of Br is given as $+0.56$,[8] and that of Tl is determined here.

The structure of TlBr is of the CsCl type, in which the cross-section values depend strongly on whether the sum of the Miller indices is even or odd. For scattering amplitudes with like sign, large cross-section peaks will occur at positions corresponding to indices of even sum. On the other hand, if the Tl and Br atoms scatter neutrons out of phase the peaks corresponding to indices of odd sum would be prominent.

As shown in Fig. 3, the peaks in the cross-section curve occur at positions corresponding to an even sum of Miller indices. Thus, Tl and Br scatter in phase, i.e., the sign of the scattering amplitude of Tl is positive. From analysis of the curve the magnitude of the scattering amplitude was found to be 0.75 ± 0.08, based on the value of $+0.56$ for Br[8]. A Debye temperature $\sim$500°K, determined from heat capacity data, was used in the calculations. The structure and the multiplicity factors for this compound are also given in Table I.

D. ZnO

A 6-inch long container was filled with 873.7 grams of ZnO, which had been dried for several days at 900°C, and a total cross-section curve as a function of energy was obtained as shown in Fig. 4. Since this compound crystallized in a close-packed hexagonal structure with the following coordinates of the atoms in the unit cell, Zn: $0,0,0;\ \frac{1}{3},\frac{2}{3},\frac{1}{2}$, and O: $0,0,\mu;\ \frac{1}{3},\frac{2}{3},(\frac{1}{2}+\mu)$, where $\mu=0.3725$, its structure factor is given by the expression:

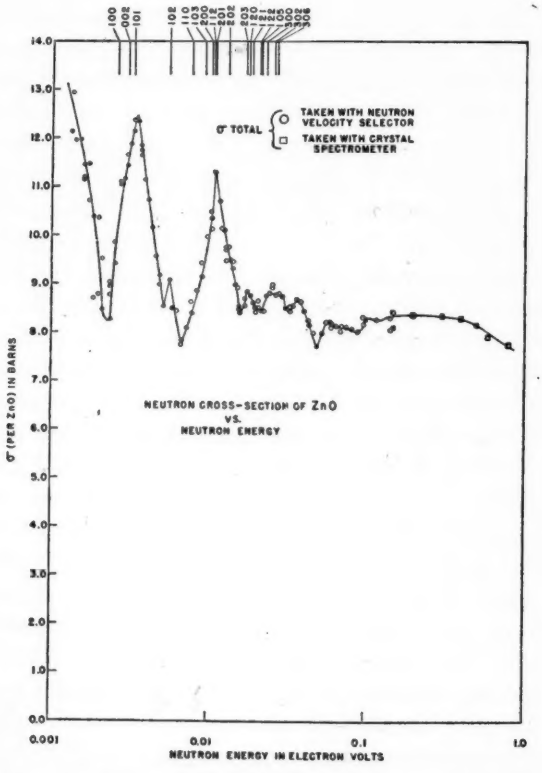

FIG. 4. Neutron cross section of ZnO *vs.* neutron energy.

$$F=8\pi[1+\cos 2\pi(h/3+2k/3+l/2)]\times[Zn^2+O^2+2\,ZnO\cos 2\pi\mu l], \quad (4)$$

in which Zn and O represent scattering amplitudes of the corresponding nuclei. When the previously determined values[8] of the scattering amplitudes, +0.58 for Zn and +0.61 for O, are substituted in (4) the expression reduces to:

$$F=17.8+10^{-24}[1+\cos 2\pi(h/3+2k/3+l/2)]\times[1+\cos 0.745\pi l]. \quad (5)$$

A cross-section curve calculated from the structure factors obtained by means of (5) and the multiplicity factors given in Table I gave a good fit with the experimentally determined curve. This confirmed both the magnitudes and the signs of the previously determined scattering amplitudes. Were the sign of Zn opposite from that of O, the last factor in (5) would be $(1-\cos 0.745\pi l)$.

In an x-ray diffraction pattern of ZnO, lines of relatively strong intensities are observed from planes such as (100), (002), (101), (102), (110), (103), (200), (112), (201), etc., whose Miller indices satisfy the following conditions—when l is odd, $h+2K=3n\pm 1$; when l is even, $h+2K=3n$, $3n\pm 1$ (i.e., any integer)—where $n=0, 1, 2, 3\cdots$.

Because of poor resolution of the rotating shutter device the peaks in the total neutron cross-section curve are actually caused by several planes which give strong reflections.

DISCUSSION OF RESULTS

As seen from the curves presented here, most of the diffraction effects are observed in the energy region 0.001 to 0.2 electron volt, which is covered by the rotating shutter device. While the resolution of the device is not comparable to that of the neutron or x-ray crystal spectrometer, enough diffraction peaks characteristic of the crystal system studied are observed that they permit unambiguous determinations of the magnitude and the sign of the scattering amplitudes as summarized in Table II.

TABLE II. Scattering amplitudes of Ca, Ti, Tl, and Zn.

Element	Scattering amplitude (units of 10^{-12} cm)	Remarks Based on scattering amplitude of:
Ca	$+0.46\pm0.05$	O, as $+0.61\times10^{-12}$ cm
Ti	-0.25 ± 0.03	C, as $+0.67\times10^{-12}$ cm
Tl	$+0.75\pm0.08$	Br, as $+0.56\times10^{-12}$ cm
Zn	+0.58	Same as reported previously (see reference 8)

The experimentally determined values of the total cross sections were somewhat higher than the corresponding calculated values for coherent scattering and absorption. The difference is significant and is a proper problem for future investigation.

This method of studying crystalline effects seems to be relatively feasible for those substances that have sufficiently low neutron absorption cross sections. An important application of this method can be made in the determination of the structures of compounds containing hydrogen and deuterium. By means of the usual x-ray diffraction methods the positions of all but the hydrogen and deuterium atoms can usually be determined. This limitation does not exist for neutrons, however, since hydrogen and deuterium have substantial scattering cross sections. If only a limited number of possible arrangements remain for the hydrogen and deuterium atoms after x-ray analysis, the method reported here might supply just the information required for a complete establishment of the structure.

ACKNOWLEDGMENT

We wish to acknowledge the interest and helpfulness of Professor A. H. Weber in this work.

Letters to the Editor

PUBLICATION of brief reports of important discoveries in physics may be secured by addressing them to this department. The closing date for this department is five weeks prior to the date of issue. No proof will be sent to the authors. The Board of Editors does not hold itself responsible for the opinions expressed by the correspondents. Communications should not exceed 600 words in length.

Coincident Bursts in Small Ionization Chambers*

C. G. MONTGOMERY AND D. D. MONTGOMERY
*Sloane Physics Laboratory, Yale University, New Haven, Connecticut***
February 7, 1949

EVIDENCE has already been reported[1] to show that many bursts of ionization occurring in a large unshielded ionization chamber result from nuclear disintegrations in the chamber walls rather than from showers of electrons from the atmosphere. Similar conclusions have also been drawn by other experimenters.[2] These observations have been extended to smaller chambers by measuring bursts occurring simultaneously in two spherical chambers 3 inches in diameter and coincidences between bursts and the discharges of a counter set that detected electrons in air showers. The chambers were similar to those of R. T. Young[3] who made observations of bursts under lead shielding. A pressure of 200 lbs./in.^{2} of argon was used and the bursts were recorded photographically by means of an electrometer tube, a galvanometer, and a motor-driven camera. The counter discharges flashed a lamp which also made a record on the sensitive paper. The two chambers were separated 9 cm center to center and three counter trays were placed at various distances in the same horizontal plane. The ionization produced in the chamber corresponded to that from about 10 or more electrons traversing the chamber, or to an energy loss in the chamber of about 1.5 Mev. The counter trays each had an area of 350 cm^2 and hence their efficiency for the detection of an air shower in the range of densities involved was very nearly 100 percent.

Observations were made both at sea level and at an elevation of 3500 meters at Climax, Colorado. The size-frequency distribution of bursts is approximately a power-law distribution with an exponent which increases slightly with increasing size of burst. For the integral distribution the exponent is about 3. It was found that no coincidences between the chambers or between chambers and counters occurred that could not be explained by the finite resolving time of the apparatus. This resolving time was determined by the galvanometer period and by the speed of the photographic recorder and was found to be 1.5 sec. The fraction f of the bursts which were coincident fortuitously is equal to $2NT$, where N is the rate of occurrence of the bursts and T the resolving time. The observed values of N were between 100 per hour and 10 per hour and hence f was between 8.6 percent and less than 1 percent, depending on the sizes of bursts considered. Similarly the observed triple coincidences could also be accidental. We must conclude therefore that air showers do not contribute appreciably as a cause of the bursts in these chambers.

Since the chamber walls were thin ($\frac{1}{32}$-inch steel) and care was taken to remove all heavy material from the neighborhood of the chambers, cascade showers produced locally also cannot be the cause of the bursts observed. Heavily ionizing particles must therefore be invoked. By a lucky accident, one of the spheres was contaminated with a source of alpha-particles and observations made at low pressure showed about 10 times as many bursts in one chamber as in the other. At the high pressure[3] used, however, the numbers of bursts in the two chambers were the same. The alpha-particle ionization was suppressed by recombination in the weak field near the chamber walls and did not contribute. The bursts must therefore be explained by heavily ionizing particles of long enough range to bring them within the high field region of the chamber. Protons, fast alpha-particles, and slow mesons produced by nuclear disintegrations in the chamber walls remain as possible sources of the ionization bursts. From the known range-energy relation, a single slow meson would have to have an energy between 4.1 and 1.5 Mev to produce a burst. It seems unlikely that many such particles are present.

* A preliminary account of these observations was presented at the Cambridge meeting of the New England Section of the American Physical Society, May, 1948.
** Assisted by the joint program of the Office of Naval Research and the Atomic Energy Commission.
[1] C. G. Montgomery and D. D. Montgomery, Phys. Rev. **72**, 131 (1947).
[2] Bridge, Hazen, Rossi, and Williams, Phys. Rev. **74**, 1083 (1948); H. Carmichael, Phys. Rev. **74**, 1667 (1948).
[3] R. T. Young, Phys. Rev. **52**, 559 (1937).

Microwave Absorption Spectra of Paramagnetic Salts*

YU TING, ROY C. WEIDLER, AND DUDLEY WILLIAMS
Ohio State University, Columbus, Ohio
January 27, 1949

WE have recently observed magnetic resonance absorption in the following paramagnetic salts: chromium fluoride, CrF_3, chromium bromide, $CrBr_3$, chromium sulfite, $Cr_2(SO_3)_3$, manganese tartrate, $MnC_4H_4O_6$, manganese carbonate, $MnCO_3$, manganese acetate, $Mn(C_2H_3O_2)_2$, and ferric ammonium sulfate $FeNH_4(SO_4)_2\cdot 12H_2O$. With incident radiation of wave-length 3.3 cm, intense absorption was noted when the external magnetic field was in the range 3000–4000 gauss; the observed absorption peaks were in the vicinity of 3500 gauss. In the measurements completed thus far, powdered samples of the salts were mounted in a resonant cavity. Further work on single crystals of the above salts is in progress.

* This study is associated with work done under Contract No. W28-099 ac-179 between Watson Laboratories of the Air Materiel Command and the Ohio State University Research Foundation.

The Variational Method for the Continuous Wave Function of an Electron in the Field of a Neutral Atom

SU-SFU HUANG
Yerkes Observatory, University of Chicago, Williams Bay, Wisconsin
January 27, 1949

SINCE L. Hulthén first formulated the variational method for the treatment of the continuous spectrum[1] in the quantum theory, several papers have appeared[2] in which his method has been applied to problems of nuclear scattering. In this note we shall generalize Hulthén's principle for the case of electron scattering by a neutral atom.

Considering first the simplest case of a free electron in the field of a neutral hydrogen atom, we have the following asymptotic form for the wave function

$$\psi_\infty = (2l+1/4\pi)^{\frac{1}{2}}\{(l/\gamma_2)^{-\gamma_1}P_l(\cos\theta_2)\sin(k\gamma_2 - l\pi/2+\eta) \pm (e/\gamma_1)^{-\gamma_2}P_l(\cos\theta_1)\sin(k\gamma_1 - l\pi/2+\eta)\}. \quad (1)$$

(We have adopted the Bohr radius and Rh as the unit of length and of energy, respectively. The other symbols have their standard meanings.)

Considering

$$\mathfrak{L}=\int\int_{\infty}\psi(L-E)\psi d\tau_1 d\tau_2, \tag{2}$$

where

$$L=-\nabla_1^2-\nabla_2^2-(2/\gamma_1)-(2/\gamma_2)+(2/\gamma_{12}), \tag{3}$$

we have by Green's theorem

$$\int\psi\nabla_1^2\delta\psi d\tau_1=\int\delta\psi\nabla_1^2\psi d\tau_1 + \oint_{\infty}[\psi(\partial\delta\psi/\partial\gamma_1)-\delta\psi(\partial\psi/\partial\gamma_1)]dS_1. \tag{4}$$

Now substituting the asymptotic expansion of the wave function (1) in the surface integral of (4) (evaluated at $\gamma_1\to\infty$), we can show that

$$\int\int_{\infty}\psi\nabla_1^2\delta\psi d\tau_1 d\tau_2=\int\int_{\infty}\delta\psi\nabla_1^2\psi d\tau_1 d\tau_2-\pi k\delta\eta. \tag{5}$$

The corresponding integral with the subscript 2 can be similarly transformed. Hence

$$\delta\mathfrak{L}=2\int\int\delta\psi(L-E)\psi d\tau_1 d\tau_2+2\pi k\delta\eta. \tag{6}$$

If ψ satisfies the wave equation, then we have

$$\delta\mathfrak{L}=2\pi k\delta\eta, \tag{7}$$

which provides the generalization of Hulthén's principle for the present case.

From this derivation it is evident that the same result would follow, also, for the case of a free electron in the field of a *neutral* atom with more than one electron. In case the atom is not neutral the asymptotic form of ψ will be different from (1); but the necessary modifications can be easily made.

In practical applications, some form for ψ, involving certain constants, can be assumed and the constants be then determined by the condition $\mathfrak{L}=0$ and $\delta\mathfrak{L}=0$. This procedure will be analogous to what Hulthén has adopted in his paper.

In spite of the general nature of the above method, the mathematical formula for actually working out the variational integral are very complicated. It would therefore seem that a somewhat less general but a mathematically simpler formulation of the principle is more suitable. This is the generalization of Tamm's formulation for the case considered by Hulthén.

For the case of S scattering by a neutral hydrogen atom we can choose the three coordinates γ_1, γ_2, and γ_{12} (which is the distance between the two electrons) to describe the wave function, since for this case, we have spherical symmetry. The wave equation can be written in terms of these coordinates and with the substitution

$$\psi=(e^{-\gamma_1}/\gamma_2)[\sin k\gamma_2+u(\gamma_1,\gamma_2,\gamma_{12})\cos k\gamma_2], \tag{8}$$

it can be shown that the resulting differential equation for $u(\gamma_1,\gamma_2,\gamma_{12})$ is the Euler equation of the following variational integral:

$$\delta\mathfrak{F}=\delta\int_0^{\infty}d\gamma_2\int_0^{\infty}d\gamma_1\int_{|\gamma_1-\gamma_2|}^{\gamma_1+\gamma_2}d\gamma_{12} \times F(u_1,u_2,u_{12},u;\gamma_1,\gamma_2,\gamma_{12})=0, \tag{9}$$

where

$$F=e^{-2\gamma_1}\cos^2 k\gamma_2\left[\frac{\gamma_1\gamma_{12}}{\gamma_2}(u_1^2+u_2^2+2u_{12}^2) +\frac{\gamma_1^2-\gamma_2^2+\gamma_{12}^2}{\gamma_2}u_1u_{12}+\frac{\gamma_1(\gamma_2^2-\gamma_1^2+\gamma_{12}^2)}{\gamma_2^2}u_2u_{12} -\frac{2\gamma_1\gamma_{12}}{\gamma_2}\left(\frac{1}{\gamma_2}-\frac{1}{\gamma_{12}}\right)(2u\tan k\gamma_2+u^2)\right] \tag{10}$$

and

$$u_1=\partial u/\partial\gamma_1,\qquad u_2=\partial u/\partial\gamma_2,\qquad u_{12}=\partial u/\partial\gamma_{12}. \tag{11}$$

The foregoing two formulations of the variational principle can be shown to be equivalent: For, with the form of the wave function expressed in (8) $\delta\mathfrak{L}$ becomes $(\frac{1}{2})\delta\mathfrak{F}$ provided $u(\gamma_1,\gamma_2,\gamma_{12})$ satisfies the equation governing it.

It is of interest to note that the integral reduces to that given by Tamm in the special case $u=u(\gamma_2)$ only, and $-2(1/\gamma_2-1/\gamma_{12})$ can be approximated by an expression which involves γ_2 only (as for example by a potential $V(\gamma_2)$ of the Hartree field of the hydrogen atom). For, in this special case, the integration with respect to γ_{12} and γ_1 can be effected directly and the final integral

$$\mathfrak{F}=\tfrac{1}{2}\int_0^{\infty}d\gamma_2[u_2^2\cos^2 k\gamma_2+Vu^2\cos^2 k\gamma_2 +2Vu\cos k\gamma_2\sin k\gamma_2] \tag{12}$$

is identical with what Tamm gives.

Further work on this problem is in progress.

My sincere thanks are due Professor S. Chandrasekhar who suggested this problem to me and also made invaluable discussions.

[1] L. Hulthén, K. Fysiogr. Sällsk. Lund Förhandl. **14**, No. 21 (1944).
[2] N. E. Tamm, J. Exper. Theor. Phys. (Russian) **18**, No. 4 (1948); L. Hulthén, Arkiv. f. Mat. Astr. o. Fys. **35A**, No. 25 (1948); W. Kohn, Phys. Rev. **74**, 1763 (1948); B. Holmberg, K. Fysiogr. Sällsk. Lund Förhandl. **18**, No. 7 (1948).

Čerenkov Radiation Effect in Meson Theory

W. W. WADA
Randall Laboratory of Physics, University of Michigan, Ann Arbor, Michigan
February 4, 1949

IN the present note the idea of Čerenkov radiation is applied to the equations of a scalar meson in the hope of accounting for some instances of multiple meson production in a phenomenological way. The mesonic Čerenkov radiation is expected to occur if the source of the mesonic field, *viz.*, the nucleon, moves with velocity greater than the phase velocity of the propagation of the meson field itself.

The relativistic energy-momentum relationship gives $\omega/\kappa=c(1+\kappa_0^2/\kappa^2)^{\frac{1}{2}}$ as the phase velocity of the meson wave in vacuum, where ω and κ are the frequency and the wave number of the phase wave respectively, κ_0 is the reciprocal Compton wave-length of the meson, and c the velocity of light. This phase velocity is always greater than c. Therefore, in order to have conditions necessary for the mesonic Čerenkov radiation, phenomenological field equations endowed with constants analogous to the ϵ and μ of Maxwellian theory will have to be used.

In the simplest case, that of a scalar meson field, at most three such nuclear material constants may occur; but when the Gordon-Klein equation is formed by elimination, only two constants n_1 and n_2 can appear:

$$\Delta\phi-(n_1^2/c^2)(\partial^2\phi/\partial t^2)-(\kappa_0^2/n_2^2)\phi=0.$$

The fact that the Gordon-Klein equation has three terms indicates that, no matter what kind of meson field is considered, there would occur at most two "indices of refraction," one corresponding to the electromagnetic case, *viz.*, n_1, and the other to be associated with the Compton wave-length, *viz.*, n_2.

Assuming a plane wave solution to this equation one obtains

$$\omega/\kappa=(c/n_1)(1+\kappa_0^2/(n_2^2\kappa^2))^{\frac{1}{2}}$$

as the phase velocity of meson wave in nuclear matter. It is clear from this expression that for $n_1>1$ and for large values of κ, the phase velocity of the meson wave may become less than c and hence less than the velocity of the incident nucleon.

Considerations similar to those of Cox,[1] who obtained the expression for the electromagnetic Čerenkov radiation in which

a quantum-mechanical correction term occurs, give in our case

$$\cos\theta = c/(n_1\beta)\cdot(1+\kappa_0^2/(n_2^2\kappa^2))^{\frac{1}{2}} + \tfrac{1}{2}\Lambda\{\kappa(1-1/n_1^2)-\kappa_0^2/(n_1^2n_2^2\kappa)\},$$

where θ is the angle between the direction of the emitted meson and that of the incident nucleon before the emission of the meson and β is the v/c ratio of the nucleon before the emission. Λ is the de Broglie wave-length of the nucleon before the emission given by $\Lambda=\hbar(1-\beta^2)^{\frac{1}{2}}/Mv$.

The second term in the expression for $\cos\theta$ is obviously the quantum-mechanical correction term since it contains $\hbar$. If one lets the rest mass of the meson go to zero, one obtains Cox's formula in the electromagnetic Čerenkov radiation.

The first term in the present formula for $\cos\theta$ may be regarded as a classical term, for when replacing the square root by the phase velocity of the meson the classical formula for the sine of the Mach angle results. However, θ still depends upon κ, the momentum of the meson.

I wish to thank Dr. O. Laporte for advice and encouragement.

[1] R. T. Cox, Phys. Rev. 66, 106 (1944).

Nuclear Capture of L_I Electrons

B. Pontecorvo, D. H. W. Kirkwood, and G. C. Hanna
Chalk River Laboratory, National Research Council of Canada, Chalk River, Ontario, Canada
January 28, 1949

THE phenomenon of L-capture, the observation of which we reported a few months ago,[1] has been investigated in detail. Proportional counters filled with various gases and traces of A^{37} were used. The technique in measuring carefully the ratio of energies was described previously.[2] Two counter types and four fillings were used, as indicated in Table I. The highest gas multiplication factor used was about 2×10^5. The A^{37} K-capture disintegration provides[1] a peak at an energy equal to the K ionization potential of Cl, 2.8 kev. Nuclear capture of L electrons should result in the liberation in the counter of an energy equal to the L ionization potential, about 1/10 of the K ionization potential. We have in fact observed such a low energy peak at about 1/10 of the energy of the main peak, using counters I and II with "argon" fillings. However, quite apart from the nuclear capture of L electrons, there must be a low energy peak in addition to the 2.8-kev peak for the following reasons. K-capture in A^{37} results in the formation of a Cl atom with an ionized K shell. In most cases (about 90 percent)[3] the whole of the 2.8-kev K binding energy is dissipated in the counter as Auger electrons. However, in about 10 percent of the cases a $K\alpha$-x-ray photon is emitted with consequent ionization of the L_{II} or L_{III} shell. This $K\alpha$-quantum may escape from the counter, i.e., there is a small probability, dependent on the absorptive power of the counter gas, that only the L_{II} or L_{III} ionization potential of Cl (200 ev)[4] is released in the counter. Consequently, in experiments with "argon" fillings where the escape probability* ϵ for the $K\alpha$-quantum is high (see Table I), the presence of a low energy peak should not in itself be considered as a proof of L orbital electron capture. The proof arises, rather, from the fact that the intensity of the low energy peak is definitely greater than would be expected only on the basis of the escape of K-radiation. Moreover, there is a difference between the low energy peak due to K-escape and that due to L-capture. The escape peak involves the L_{II} or L_{III} shell (200 ev), but in the nuclear L-capture L_I electrons are expected to be involved (i.e., S electrons) with release of about 280 ev.[5] We cannot resolve two peaks at 200 and 280 ev because the statistical spread[2] is too great. We can, however, reduce the K quantum escape probability to a small value by adding xenon, and thus be left substantially with the effects of L-capture alone (see Table I). This was done with the "xenon" fillings.

TABLE I. Counter types used.

	Counter I	Counter II
Active length (cm)	30	20
Internal diameter (cm)	2.35	4.65
"Argon" filling (cm Hg)	40 cm A, 12 cm CH_4 } $\epsilon=0.75$	41 cm A, 11 cm CH_4 } $\epsilon=0.66$
"Xenon" filling (cm Hg)	50 cm Xe, 10 cm CH_4 } $\epsilon=0.13$	26 cm Xe, 14 cm A, 10 cm CH_4 } $\epsilon=0.15$

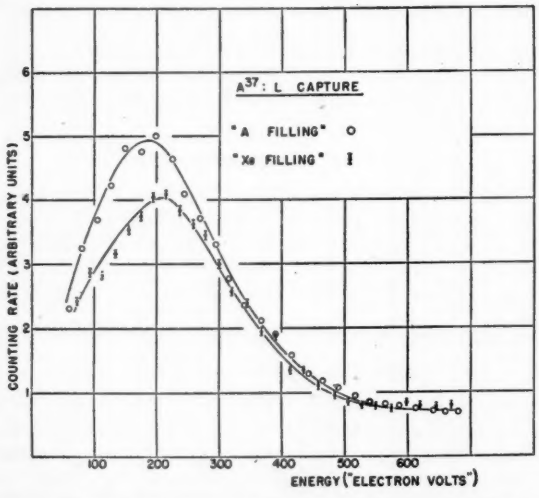

FIG. 1. L-capture in A^{37}. The energy scale is derived for convenience from a comparison of pulse amplitudes with the 2.8-kev K-capture line.

The curves in Fig. 1 have been normalized to refer to the same total disintegration rate of A^{37}. They show essentially L-capture with "xenon" filling, and L-capture+K-escape with "argon" filling. The two effects produced by Xe—decrease in intensity of the peak and the shifting of the peaks to higher energy—are apparent, and quantitatively they are in agreement with expectations within the experimental errors. Similar results were obtained with counter I.

The energy scale of Fig. 1 is obtained from the position of the 2.8-kev peak. It is noticed that the values for the L_I peak, as well as the value for the (L_I, L_{II}, L_{III}) peak, correspond to an energy smaller than the theoretical value. This is due in part to an increase in the mean energy necessary to produce an ion pair at low energy, and in part to a distortion of the shape due to an "end-effect tail."** The second difficulty enters also in estimating the ratio of the probabilities of L- and K-capture. A value of 8 to 9 percent is obtained for the L/K ratio with both Xe and A fillings when corrections for K-escape are made. The theoretical value is only 6 percent, according to Marshak,[6] but in view of the difficulties connected with the subtraction of background, we are not sure that the discrepancy is significant.

[1] D. H. W. Kirkwood, B. Pontecorvo, and G. C. Hanna, Phys. Rev. **74**, 497 (1948).
[2] G. C. Hanna, D. H. W. Kirkwood, and B. Pontecorvo, Phys. Rev. **75**, 985 (1949).
[3] M. Haas, Ann. d. Physik **16**, 473 (1933); P. K. Weimer, J. D. Kurbatov, and M. L. Pool, Phys. Rev. **66**, 209 (1944).
[4] F. Holweck, *De la Lumière aux Rayons-X* (Paris, 1927).
* In evaluating ϵ, we have used as absorption coefficients of the Cl $K\alpha$-line: in A 260 cm²/g, in Xe 800 cm²/g, and in C 130 cm²/g.
[5] M. Siegbahn, *Spectroskopie der Rönigenstrahlen*, (Berlin, 1931).
** Counter I, having small end effect due to its high length to diameter ratio, gives energy values close to the expected one. Curves referring to Counter I are not shown here for lack of space, a pertinent curve having been shown in another letter (see reference 2).
[6] Robert E. Marshak, Phys. Rev. **61**, 431 (1942).

Note on the Rochester Cyclotron

S. W. Barnes, A. F. Clark, G. B. Collins, C. L. Oxley, R. L. McCreary, J. B. Platt, and S. N. VanVoorhees
Department of Physics, University of Rochester, Rochester, New York
February 7, 1949

THE 130-inch cyclotron has accelerated protons out to a radius of 58½" (approximately the $n=0.2$ point) or to an estimated energy of 240 Mev since the first of the year. Measurement of the C'' activity of a carbon-tipped probe indicates average currents of about 0.1μa at this radius and radio-autographs of the target show the beam to be about 1" in height and well centered vertically on the probe. Eastman Kodak NTB plates placed along the probe show, among many proton recoil tracks, π^- and π^+ tracks.

About 15 kw of r-f power for the Dee is furnished by a grounded grid oscillator with feedback through the Dee. The natural frequency of the Dee is varied from 26 to 18 megacycles by a rotating condenser. The condenser which is in the Dee tank consists principally of a rotor of copper-plated, thin-toothed zircon disks mounted on a shaft parallel to the back edge of the Dee and a Dee stator which is on the back edge of the Dee. The magnetic drag of this rotor up to 2000 r.p.m. is small compared to the power taken by the rotor shaft seals. The copper-plated ceramic disks already give promise of satisfactory life.

Ion loading of the Dee is obviated by a negatively biased grid structure covering the linear above and below the Dee. Globar resistors break the grid into lengths too short to resonate to the Dee frequencies.

This work was assisted by the joint program of the Office of Naval Research and the Atomic Energy Commission.

Fluorescence of Anthracene Excited by High Energy Radiation*

Louise Roth
Purdue University, Lafayette, Indiana
February 7, 1949

SINGLE crystals of anthracene were prepared by a method similar to that of P. R. Bell[1] and used for scintillation counters. At the suggestion of K. Lark-Horovitz, the spectra of the scintillations produced by high energy bombardment have been studied and compared with the fluorescence bands produced by ultraviolet excitation.

Spectrograms of the fluorescence excited by copper $K\alpha$-radiation, 10-Mev deuterons, and a 10-millicurie radium-beryllium source were made with a small Hilger quartz spectrographs using Eastman 103–0 plates. For the spectrum with x-ray excitation a crystal was mounted at the tube slit at an angle of about 45 degrees to the beam, and the visible fluorescence was focused by means of an aluminum mirror on the collimator lens of the spectrograph. A similar mounting was used for bombardment with the cyclotron beam. For the radium-beryllium exposure the crystal was fastened over the spectrograph slit with the radiation source in contact with it. No attempt was made to distinguish between the effects of neutrons and gamma-rays. A five-minute exposure to x-rays with a 0.1-millimeter slit was sufficient to bring out the bands found. A ten-minute exposure was used with the deuteron beam and twenty-four hours with radium-beryllium.

In each case three bands were observed between 4120 and 4720A with the most intense band at 4440A. No other bands were found between 2500 and 5000A. The wave-lengths of band intensity maxima were determined. The values found agree with those observed using ultraviolet excitation to the same extent as the ultraviolet values agree among themselves. Wave-length values in Table I, with the exception of the writer's, are for ultraviolet excitation.

To correlate the known bands with the counting properties, counts were taken with a series of Wratten filters placed between the scintillating crystal and the 931-A photo-multiplier tube using a Co^{60} gamma-source at a constant distance from the crystal. Counts were taken at different pulse heights with and without each filter, and a graph of counts against discriminator setting was made. Since the discriminator setting fixes the minimum pulse voltage to be registered, it is proportional to the intensity of the weakest scintillations which are recorded. Thus it is possible to determine the transmittance for a given filter by determining the discriminator setting for a fixed number of counts with and without the filter.

TABLE I. Wave-lengths of intensity maxima for anthracene.

Data of	Intensity maxima in angstrom units							
Dowell[a]	—	—	4250	—	4490	—	4740	4980
Ganguly[b]	4030	—	4220	4380	4450	—	—	—
Ganguly[c]	4000	4140	—	4400	—	—	4680	—
Kortüm and Finkh[d]	4000	—	4200	4400	—	—	4700	4950
Obreimov[a]	—	4090	—	4340	—	4610	4750	4950
Pringsheim[e]	4025	—	4220	—	4450	—	4735	5090
Writer	—	—	4240	—	4440	—	4700	—

[a] Shishlovskii, Comptes Rendus **15**, 29 (1937).
[b] S. C. Ganguly, Nature **153**, 652 (1944).
[c] S. C. Ganguly, J. Chem. Phys. **13**, 128 (1945).
[d] Kortüm and Finkh, Zeits. f. physik. Chemie **B52**, 263 (1942).
[e] P. Pringsheim, Trans. Faraday Soc. **35**, 28 (1939).

No counts above background occurred when the fluorescence range was blocked by filters. For Wratten filter 2-A the transmittance found experimentally was 0.74. According to the manufacturer, the average transmittance of this filter between 4200 and 4700A is 0.78. The agreement is satisfactory; the slight difference may be due to the fact that the transparency of the filter drops rather sharply just below 4200A, whereas the fluorescence bands extend to about 4120A.

The above investigations again point to the fact that the fluorescence of anthracene is particularly suited to scintillation counting with a 931-A or 1P-21 photo-multiplier tube, which are most sensitive in the spectral range 3500–4500A.

* Research carried out during the summer of 1948, supported in part by the Office of Naval Research and Signal Corps.
[1] P. R. Bell, Phys. Rev. **73**, 1405 (1948).

The β-Spectrum of H^3

G. C. Hanna and B. Pontecorvo
Chalk River Laboratory, National Research Council of Canada, Chalk River, Ontario, Canada
January 28, 1949

THE proportional counter technique previously described[1,2] has been used to study the β-spectrum of H^3, an investigation of which has recently been reported by Curran *et al.*[3]

The two counters *I* and *II* described in reference 2 were used. The fillings are given in Table I.

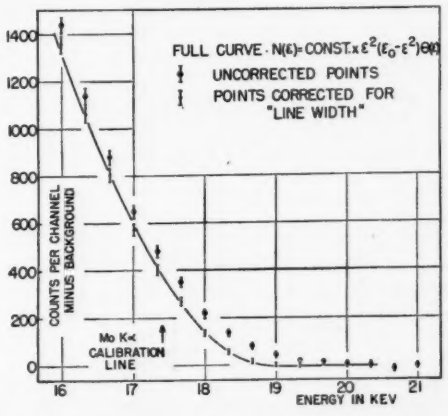

FIG. 1. The spectrum of H^3 in the region of the end

TABLE I. Counter fillings used.

	Counter *I*	Counter *II*
Xenon	50 cm Hg	26 cm Hg
Argon	—	14 cm Hg
Methane	10 cm Hg	10 cm Hg
Hydrogen	~1 cm Hg	~0.2 cm Hg
H^3	~7000 counts/min.	~30,000 counts/min.
A^{37}	—	~6000 counts/min.

Both counters were operated at gas multiplication factors of several thousand. The absolute energy scale was obtained by firing into the counter a beam of Mo $K\alpha$-x-rays (17.4 kev) from a crystal spectrometer. In counter *I* this beam was parallel to the counter wire, in *II* perpendicular to it. The assumption that these energy calibrations were representative of the properties of the counter as a whole was checked directly for counter *II* by measuring the Mo $K\alpha/A^{37}$ pulse size ratio,* and is inferred for counter *I* from the agreement between the end point energy determinations in the two counters.

The complete spectrum was investigated in counter *I*. Since counter linearity had to be maintained up to 20 kev, we were not able to use multiplication factors as high as those used in the investigation[4] of the Cl L_I peak (280 ev). Consequently the amplifier noise was apparent at energies as high as about 600 ev.

At the ends of the counter the multiplication falls off due to reduced field strength. Disintegrations occurring in this region will produce pulses of spuriously low amplitude. Clearly the shape of the spectrum is most affected at low energy. Due to lack of data the correction to be applied is uncertain, a fact which precludes a quantitative comparison of our results with Fermi's theory in the region near the most probable energy (~2.5 kev). However the results agree with the theory within the limits of the correction uncertainty (~10 percent at 1 kev).

Above 5 kev the correction is very small, and close agreement with the theory is obtained (wall effects are negligible). We have concentrated on this energy region, in particular we have used both counters for a careful investigation of the end point. Using a biased amplifier, the spectrum above 15 kev was expanded over the pulse analyzer. The results were compared with Fermi's theory, assuming a zero neutrino rest-mass. The theoretical distribution $N(\epsilon)$ can be written as constant $\times \epsilon^2(\epsilon_0-\epsilon)^2\theta(Z,\epsilon)$, where θ gives the Coulomb field effect.[5] In counter *I* the 17.4-kev calibration line was found to have a Gaussian shape of standard deviation $\sigma=700$ ev, over a range of at least $\pm 3\sigma$. In counter *II* σ was 1100 ev. The corrections to be applied for this line width were obtained by calculating the effect of a Gaussian spread on the theoretical distribution. A provisional value for the end point energy is adopted:** the corrected data are then used to redetermine the end point.

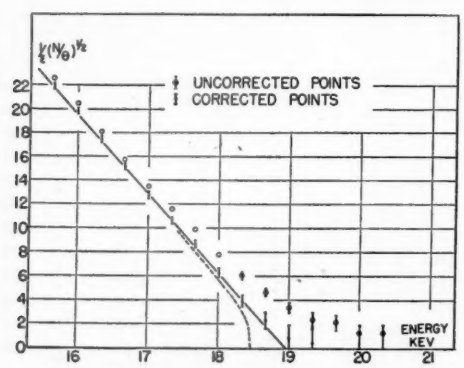

FIG. 2. "Kurie" plot of the end of the H^3 spectrum. The theoretical curve (shown dotted) corresponding to a finite neutrino mass of 500 ev (or 1 kev —see text) has been included for comparison.

A theoretical curve based on this new value is then used as before. The progress of successive approximations is extremely rapid.

Figures 1 and 2 show the experimental and corrected points obtained using counter *I*. The fact that the corrected points lie on the assumed theoretical curve from which the corrections were computed means that our initial assumption of a zero neutrino mass is correct, within our limits of error.

The dotted curve in Fig. 2 has been drawn to show the effect of a neutrino mass of 500 ev[6] (or 1 kev if a later modification[7] of the theory is accepted). If this distribution were used to correct for line width, a smaller correction would result and the discrepancy between the corrected data and the dotted curve would be even more marked than shown in Fig. 2. Nevertheless, in view of the width correction magnitude and the finite (300 ev) pulse analyzer channel width, we do not feel justified in definitely excluding a finite value of 500 ev (or 1 kev) for the neutrino mass.

Very similar results were obtained from the data of counter *II*: there is again no evidence for a neutrino mass greater than zero. The corrections for line width, however, are greater than for counter *I*.

The extrapolated end-point energy from the corrected data, is for counter *I*, 18.95, and for counter *II*, 18.9 kev. We believe that the true end point is at 18.9(5) kev within ±0.5 kev.

The first publication[3] of Curran *et al.* gave a value of 16.9 ±0.3 kev. This has recently[8] been increased to 17.9±0.3 kev. Calibration lines (Cu and Ni *K* x-rays) of energy about one-half of the end-point energy were used.

[1] D. H. W. Kirkwood, B. Pontecorvo, and G. C. Hanna, Phys. Rev. **74**, 497 (1948).
[2] G. C. Hanna, D. H. W. Kirkwood, and B. Pontecorvo, Phys. Rev. **75**, 985 (1949).
[3] S. C. Curran, J. Angus, and A. L. Cockcroft, Nature **162**, 302 (1948).
* A^{37} gives a 2.8-kev calibration line which is truly representative, since, as for H^3, the disintegrations occur uniformly throughout the counter volume.
[4] B. Pontecorvo, D. H. W. Kirkwood, and G. C. Hanna, Phys. Rev. **75**, 982 (1949).
[5] E. Bleuler and W. Zünti, Helv. Phys. Acta **19**, 375 (1946).
** Fortunately the correction is small for points lying more than 1.5σ away from the end point so that a fairly good value of the end point is available immediately from the extrapolation of a "Kurie" plot (Fig. 2) of uncorrected data. For example in counter *I* this value is greater by only 300 ev than the one finally derived.
[6] O. Kofoed-Hansen, Phys. Rev. **71**, 451 (1947).
[7] J. R. Pruett, Phys. Rev. **73**, 1219 (1948); C. S. Cook, M. L. Langer, and H. C. Price, Phys. Rev. **73**, 1395 (1948).
[8] S. C. Curran, J. Angus, and A. L. Cockroft, Phil. Mag. **40**, 53 (1949).

Ferromagnetic Alloys in the System Copper-Manganese-Indium

ROBERT R. GRINSTEAD AND DON M. YOST
Gates and Crellin Laboratories of Chemistry, California Institute of Technology, Pasadena, California
January 28, 1949

IN a recent publication by Hames and Eppelsheimer on ferromagnetic manganese alloys,[1] reference was made to an article by S. Valentiner,[2] who has reported the existence of ferromagnetic alloys in the system Cu-Mn-In, with a maximum intensity of magnetization at the point Cu_2MnIn. We have been working on this same system, and since the journal containing Valentiner's report is not available as yet, we wish to report some of the results of our work.

About fifteen alloys have been prepared, most of them containing a constant atomic ratio of 2Cu:1Mn and with the indium content increasing from zero in steps of 5 atom percent to 60 atom percent, the latter being the most recent preparation. Except for the Cu-Mn binary alloys all of the specimens prepared were definitely ferromagnetic. No quantitative measurements of intensity of magnetization have yet been made; the Curie point of an alloy composed of copper, manganese, and indium in the approximate atomic ratio of 45:20:35 is about 250°C.

Our work has consisted mainly of thermal analyses, since the system had been previously unreported, and thorough knowledge of the phase relations was deemed necessary before proceeding to the measurement of magnetic and other properties. In most cases, two or three breaks were observed in the cooling curves during solidification; however, in one, namely, for the alloy of composition corresponding to Cu_2MnIn, only one break could be found. The plateau that followed was at about 617°C and probably indicates a compound or an eutetic mixture at this composition.

Further thermal measurements are in progress, and it is intended to supplement them with microscopic examinations of the properly heat-treated alloys. By means of these data, it should be possible to determine whether a single phase is responsible for the magnetism, and if so, to determine its composition and temperature limits. However, in view of the large range of composition which exhibits ferromagnetism, it would not be surprising to find more than one magnetic phase in this system.

[1] Hames and Eppelsheimer, Nature 162, 968 (1948).
[2] S. Valentiner, Naturwiss. 4, 123 (1947).

Discharge of a Geiger Counter at Voltages above the Plateau

H. R. Crane
Randall Laboratory of Physics, University of Michigan, Ann Arbor, Michigan
January 17, 1949

WHEN a voltage higher than that corresponding to the upper end of the plateau is applied to a Geiger counter, a discharge occurs which is spoken of as continuous, but which, in fact, is a very rapid succession of pulses. I have been interested in trying to learn something about the mechanism by which a counter first breaks into such a discharge and the mechanism by which succeeding pulses are produced. It is difficult to see how the existence of the electric field can, of itself, produce the first electron or ion in order to initiate the breakdown. The onset of field emission from the cathode surface surely would not be expected to occur at the potential gradients dealt with in Geiger counters, and other mechanisms, for instance the pulling apart of atoms in the gas, also seem to be out of the question because of the magnitude of the field which would be required.

Experiments I made some time ago seemed to substantiate the idea that high voltage alone cannot initiate the discharge. After allowing a counter to remain at its plateau or below for a few minutes, the voltage was suddenly raised to several hundred volts above the plateau. The first count after raising the voltage occurred substantially no sooner than it would have occurred under normal operation on the plateau. After the first count, further discharges came in rapid succession, as is normally observed above the plateau.

Lately I have carried the experiment somewhat further. By means of a system of relays, timers, etc., a counter was put through the following cycle: voltage raised to some high value (above plateau); time measured to first discharge; voltage dropped back to one-half the high value immediately after first discharge; resting period allowed at half-voltage; voltage again raised to high value. Precautions were taken to prevent any surges produced by the relay contacts from reaching the counter. The apparatus ran automatically, and at least 300 cycles were recorded at each setting of the time and voltage. The average time between the raising of the voltage and the first discharge is plotted in the two graphs (see Fig. 1); the first showing the time as a function of voltage with constant resting period and the second showing the time as a function of resting period with constant voltage. Data on the counter tube used are; wire, 10-mil tungsten; cathode, brass ¾-inch diameter; gas, 9-cm argon, 1-cm alcohol vapor. A

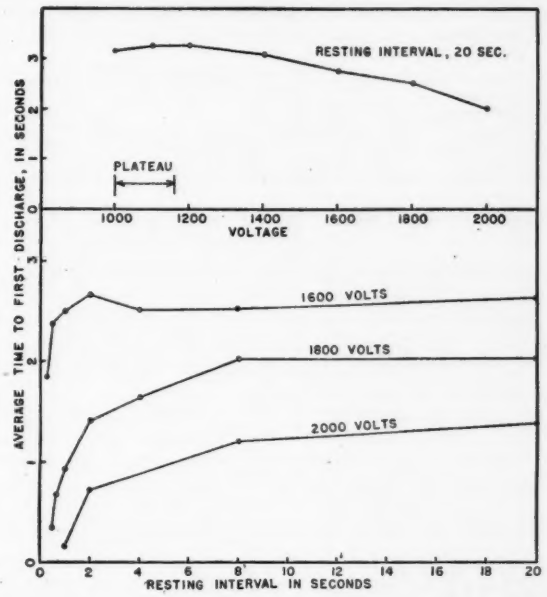

FIG. 1. Average time between raising of the voltage and the first discharge of a Geiger counter. Upper curve for constant resting period; lower curve for different resting periods and various constant voltages. Correction: The three curves in the lower part of the figure should have been labeled 1600, 2000, and 2300 volts, respectively.

Neher-Harper quench circuit was used. The plateau extended from 1000 to 1160 volts. The counter was housed in 2 inches of lead and was subject only to natural radiation background, which gave 20 counts per minute. This agreed with the average time for firing found with the relay scheme, when the voltage applied was within the plateau range.

The results make it reasonable to suppose that in the region above the plateau, spurious discharges may be initiated by an after-emission of electrons or photons, due to activation of the surfaces or gas produced by the *previous* discharge, rather than by ionization produced directly by the application of the high voltage. Since the curves show that in some cases it requires seconds for the after-emission to die away, it does not seem possible to account for the effect on the basis simply of gas ions which fail to be collected during the resting period. Activation of the metal or gas would be expected to depend strongly upon the kinds of materials present and to increase with increasing intensity of discharge. It appears to decay in a way similar to radioactive decay, as is indicated by the second set of curves. It would not be sensible, however, to try to derive the decay law of the after-emission from the curves because of the complexity of materials in the counter.

It should not be assumed that meager results presented here are representative of all counters, since only one example was used, but the measurements do indicate a line of investigation which well might lead to methods of increasing the width of the Geiger counter plateau.

I am grateful to Professors W. C. Parkinson, M. L. Wiedenbeck, R. W. Pidd, and L. Madansky for helpful discussions.

High Multiplication Proportional Counters for Energy Measurements

G. C. Hanna, D. H. W. Kirkwood, and B. Pontecorvo
Chalk River Laboratory, National Research Council of Canada, Chalk River, Ontario, Canada
January 24, 1949

DEVELOPMENTS have been reported recently in the application of proportional counters to the detection[1] of electrons and to the measurement[2] of electron or β-ray

TABLE I. Typical counters used.

	Counter *I*	Counter *II*
Effective length	30 cm	20 cm
Cathode diameter	2.5 cm	5 cm
Wire diameter	0.01 cm	0.01 cm
"Xenon" filling (cm Hg)	50 cm Xe, 10 cm CH_4	26 cm Xe, 14 cm A, 10 cm CH_4
"Argon" filling (cm Hg)	40 cm A, 12 cm CH_4	40 cm A, 12 cm CH_4

energies particularly in the low energy range (200 to about 50,000 ev). We describe here the essentials of the technique used in the investigation of L-capture[2] in A^{37} and the H^3 spectrum,[4] and discuss the problems of linearity and "line-width." It is concluded that the energy resolution is better than predicted by current theories.

Counters are connected to a fast, stable, linear amplifier feeding a 30-channel pulse analyzer.[5] A signal generator feeds pulses of known size into the counter through a small capacity, enabling the multiplication factor to be measured. All energy measurements are made in terms of signal generator output: this avoids the effects of any amplifier non-linearity, and, further, facilitates the use of a biased amplifier to obtain an expanded view of any part of a spectrum.

Two typical counters used are described in Table I.

Two calibrating radiations were used: Mo$K\alpha$-x-rays (17.4 kev) from a crystal spectrometer, and, from the decay of A^{37} by K-capture, radiation of energy 2.8 kev (the Cl K ionization potential). Another line at about 250 ev (the Cl L ionization potential) was also available[3] from the A^{37} decay. (See Fig. 1.)

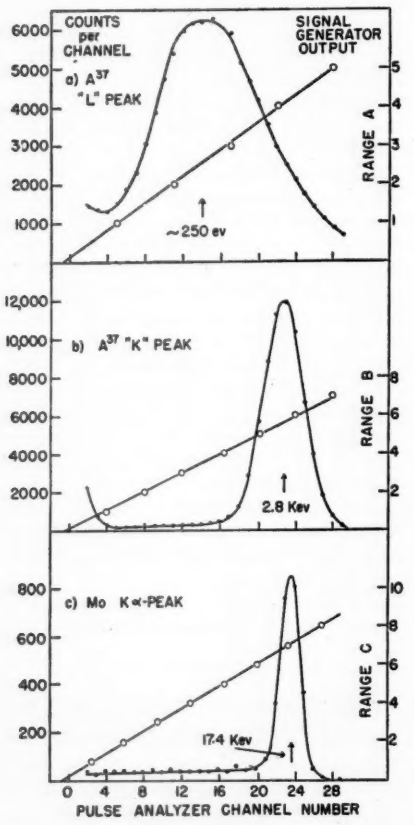

FIG. 1. Peaks produced by ~250-ev, 2.8-kev, and 17.4-kev radiations showing the decrease in percent width with increasing energy. The straight lines refer to the signal generator calibration. Precise measurements of widths, however, were made using a biased amplifier to spread the 2.8-kev and 17.4-kev peaks over many channels of the pulse analyzer.

TABLE II. Experimental results from counter *I*.

Radiation energy (ev) E	Estimated mean number of ion pairs released by radiation, n	Observed standard deviation (% of pulse size)
17,400	700	$(4.0\pm0.2)\%$
2800	110	$(8.8^{+0.3}_{-0.1})\%$
~250	~10	$(36\pm4)\%$

The linearity of gas amplification was established within the experimental accuracy of 2 percent, by measuring (in counter *II*) the ratio of the mean pulse sizes produced by the 17.4- and 2.8-kev radiations. Further, the widths of the peaks were found to be independent of the gas multiplication M up to a critical value M_c, which is a function of the radiation energy E, where the widths suddenly increased. For $M>M_c$ lack of linearity was apparent. These facts strongly suggest that proportionality is maintained up to that multiplication factor which produces a certain total output pulse, that is $E\times M_c=$constant, which in this counter was about 10^8 ev.* It follows, and may be specially noted, that for low energy measurements correspondingly large multiplication factors may be used.

Correcting for the low energy tail, the shape of the peaks produced by the 17.4- and 2.8-kev radiations was found to be Gaussian, at least over an energy range (±3 standard deviations) where background fluctuations do not disturb the measurements.

Since this spread is due not only to statistical fluctuations, but also to instrumental causes (such as irregularities in wire diameter), we cannot conclude that the "ideal" peaks (i.e., peaks with a spread due to statistical causes only) would be Gaussian. However, it seems almost certain** that the observed value of the standard deviation obtained by fitting the experimental data to a Gaussian distribution will give an upper limit to the standard deviation of the corresponding "ideal" peak.

The theories of Snyder and Frisch[6] give a mean square deviation at the output, referred back to the initial number of ions, n, equal to $(n/K)+n$. K is a constant discussed by Fano[7] and may be about 3. The first and second terms represent, respectively, the fluctuation in the initial number of ions and the contribution added by the statistics of the multiplication process.

The experimental results from counter *I*, which is one of our counters giving the least spread, are presented in Table II.

The results are most consistent with a mean square deviation of n. Since K is unlikely to be very great,*** and in any case the observed values represent lower limits for the mean square deviation, our results show definitely that the gas amplification introduces less spread than predicted. An attempt to formulate a more accurate theory of the process is being made in this Laboratory.

[1] Bruce B. Benson, Rev. Sci. Inst. 17, 533 (1946); C. J. Borkowski and E. Fairstein, Phys. Rev. 74, 1243 (1948); these authors also mention the possibility of measuring β-particle energies.
[2] D. H. W. Kirkwood, B. Pontecorvo, and G. C. Hanna, Phys. Rev. 74, 497 (1948); S. C. Curran, J. Angus, and A. L. Cockcroft, Nature 162, 302 (1948).
[3] B. Pontecorvo, D. H. W. Kirkwood, and G. C. Hanna, Phys. Rev. 75, 982 (1949).
[4] G. C. Hanna and B. Pontecorvo, Phys. Rev. 75, 983 (1949).
[5] C. H. Westcott and G. C. Hanna, Rev. Sci. Inst. 20, 181 (1949).
* The condition is certainly less stringent than this when the original ionization is spread over a large distance.
** In principle this conclusion is not certain because the "ideal" distribution might be a pointed curve with extremely long tails which would evade detection.
[6] Hartland S. Snyder, Phys. Rev. 72, 181 (1947); O. R. Frisch, *The Statistics of Multiplicative Processes*, as yet unpublished.
[7] Ugo Fano, Phys. Rev. 72, 26 (1947).
*** Previously (see reference 2) we obtained a value for K of at least 2.4, assuming the validity of the Snyder formula. This might have been in good agreement with Fano's estimate. Our better accuracy would now yield impossibly high values for K.

Scattering of High Energy Neutrons by Protons with Non-Central Interaction

K. N. Hsu and T. M. Hu
University College, London, England
February 4, 1949

CALCULATIONS have been made by several authors[1-6] for the scattering of high energy neutrons by protons, using various forms of interactions. Bethe and Camac[1] have shown that with a purely central interaction of the spherical-well type, both the angular distribution and the total cross section for 80 Mev neutrons can be correctly predicted if the range is assumed to be 2.0×10^{-13} cm. Similar results have been reported by Barker[2] for an exponential-well type of potential with range 1.0×10^{-13} cm. If a non-central interaction of the spherical-well type is assumed, it is found that while the observed angular distribution can be approximately reproduced if a purely exchange interaction is used, the total cross section is much larger than the empirical value.[3,4] In these calculations, the range is assumed to be 2.8×10^{-13} cm. If the same range is used for both the tensor and the central part of the interaction, it is not possible to reduce the range much.[7] Furthermore, a detailed investigation with the Born's approximation by Burhop and Yadav[6] shows that due to the rapid increasing of the tensor interaction, reduction of the range may even cause the total cross section to increase. It seems desirable to try other types of radial variation of the interaction. In this work, we wish to report the results of similar calculations for 83 Mev neutrons with Yukawa and exponential-well type of interaction.

The potential for even states is assumed,

$$V_{\text{even}}(r)=-\{A+\tfrac{1}{2}B(\sigma_1-\sigma_2-1)+CS_{12}\}V(r/r_0)$$

where, for Yukawa well,

$$V(r/r_0)=(r_0/r)e^{-r/r_0}$$
$$r_0=1.18\cdot10^{-13}\text{ cm}$$
$$A=10.4\text{ Mev},\quad B=-18.25\text{ Mev},\quad C=79.6\text{ Mev},$$

and for exponential well

$$V(r/r_0)=e^{-2r/r_0}$$
$$r_0=1.74\cdot10^{-13}\text{ cm}$$
$$A=85\text{ Mev},\quad B=6.26\text{ Mev},\quad C=70\text{ Mev}.$$

The ranges in both cases are consistent with the results of proton-proton scattering experiments. The constants for exponential well are those calculated by Massey and Hu[7] and those for Yukawa well are determined by one of us (K. N. Hsu).

For odd states, the potentials are fixed by the assumed exchange property of the interaction. We have studied the usual alternatives, namely, the exchange property is either similar to that predicted by the charged or the symmetrical meson theory. It is interesting to note that in the case of the Yukawa well of the assumed range, the charged theory will predict a stable $^3P_0$ state lower than the $^3S_1+{}^3D_1$ state, in direct contradiction to the experimental fact that the deuteron has spin unity. This case is still included in the calculation for the interest of comparison with other cases.

The results are given in Fig. 1 and Table I, together with the results for the spherical-well case obtained by Massey, Burhop, and Hu.[5] It is clear from the figure that angular distribution varies considerably with the shape of the potential well. From the preliminary reports of the measured angular distribution,[8] the Yukawa well with the symmetrical interaction fits the empirical results better than the other two shapes of interaction. The total cross section is not sensitive to the shape of the interaction provided a reasonable range is chosen for a given shape. The values given in the table are much larger than the empirical value for all shapes of well with exchange or symmetrical interaction.

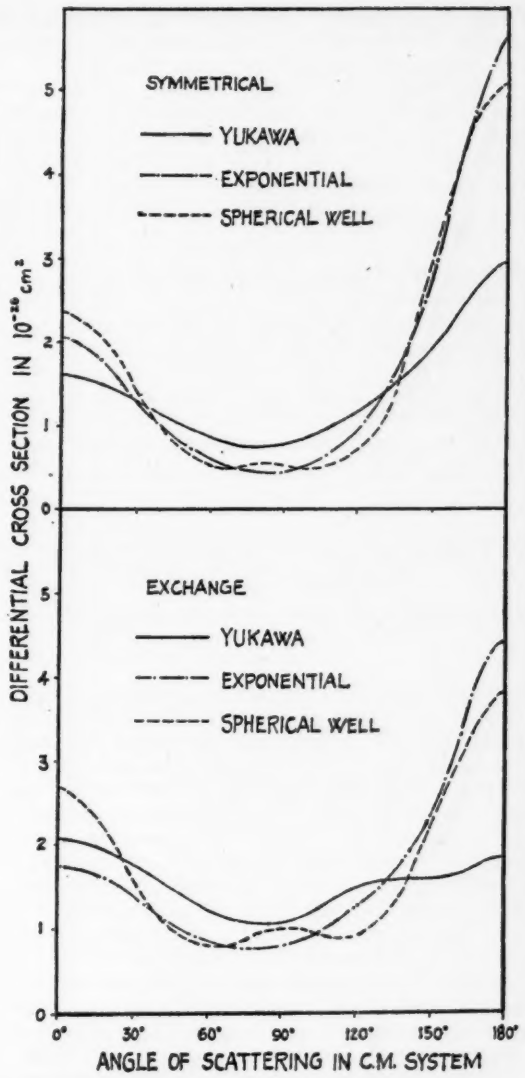

FIG. 1. Angular distribution of scattered neutrons.

One of the obvious ways to reduce the total cross section is to assume that the nucleons do not interact in odd states.* Total cross sections calculated under this assumption are given in the last column Table I. This assumption, however, will predict an angular distribution perfectly symmetrical with respect to the plane $\theta=\pi/2$, which does not seem to agree very well with the measured distribution.[8] Analysis of the proton-proton scattering experiments also indicates a repulsive interaction for ^3P states.[9]

Another possible modification is to assume different ranges for the central, tensor, and singlet interactions. This view is supported by the scattering experiments of thermal neutrons by para- and orthohydrogen molecules[10] and the coherent

TABLE I. Total cross section for 83 Mev neutrons in 10^{-26} cm².

	Symmetrical	Exchange	No interaction in odd states	Experiment (90 Mev)*
Yukawa	14	17	11	
Exponential	13	15	9.4	8.3±0.4
Spherical well	14	16	—	

* Cook, McMillan, Paterson and Sewell, Phys. Rev. 72, 1264 (1947).

scattering of neutrons by NaH crystals.[11] Investigations along this line are in progress in this department. A more detailed account of the present work may appear elsewhere.

It is our pleasure to thank Professor Massey and Dr. Burhop for their interest in this work. We are much indebted to Miss K. Blunt for solving the simultaneous differential equations necessary for the calculation of the phases of the coupled states. Thanks are due to Mr. Yadav for his assistance in the calculation of the angular distribution for the exponential-well case.

* This type of interaction was first suggested by Serber.

[1] M. Camac and H. A. Bethe, Phys. Rev. **73**, 191 (1948).
[2] Barker, Nature **161**, 726 (1948).
[3] J. Ashkin and T. Wu, Phys. Rev. **73**, 973 (1948).
[4] G. F. Chew and M. L. Goldberger, Phys. Rev. **73**, 1409 (1948).
[5] Massey, Burhop and Hu, Phys. Rev. **73**, 1403 (1948).
[6] Burhop and Yadav, Proc. Roy. Soc. (in press).
[7] Massey and Hu, Proc. Roy. Soc. (in press).
[8] Reported in the Birmingham Conference by R. L. Thornton, (1948).
[9] Wilson, Lofgren, Richardson, Wright, and Shankland, Phys. Rev. **72**, 1131, (1947).
[10] Sutton, Hall, Anderson, Bridge, DeWire, Labatelli, Long, Snyder, and Williams, Phys. Rev. **72**, 1147 (1947).
[11] Shull, Wollan, Morton, and Davidson, Phys. Rev. **73**, 842 (1948).

Comparison of the Flow of Isotopically Pure Liquid He^3 and He^4

DARRELL W. OSBORNE, BERNARD WEINSTOCK, AND BERNARD M. ABRAHAM
Argonne National Laboratory, Chicago, Illinois
January 14, 1949

IN order to determine whether liquid He^3 has a transition to a superfluid state such as that exhibited by liquid He^4, the isothermal flow of isotopically pure liquid He^3 through a narrow channel or superleak has been studied from 3.02°K (0.18° below the normal boiling point[1,2]) to 1.05°K. The rate of flow of liquid He^3 was observed to decrease monotonically as the temperature was lowered. In contrast, the rate of flow of liquid He^4 through the same channel was observed to decrease as the temperature was lowered, until the lambda-point (2.19°K) was reached, and below this point the rate rose very sharply. The mass rate of flow of the two isotopes as a function of temperature is shown in Fig. 1. From these results it is clear that no superfluid transition occurs in He^3 down to 1.05°K.

The He^3 used in this experiment was obtained from the decay of tritium gas which had been initially freed from helium by passage through a palladium valve. After sufficient He^3 had grown in by decay, the bulk of the tritium was removed from it by means of a palladium valve, and the residual tritium was then removed by circulating the He^3 through a U-tube immersed in liquid helium. No He^4 was detected in a spectrographic analysis of the sample (kindly performed by Mr. J. K. Brody). The limit of detection was estimated to be 0.1 percent.

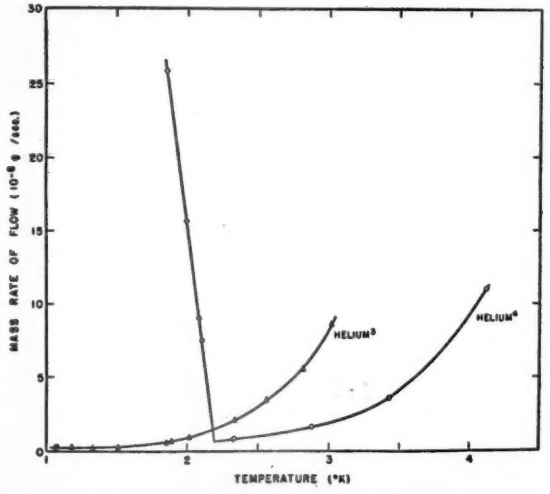

FIG. 1. Mass rate of flow of liquid He^3 and of liquid He^4 through a 7×10^{-5} cm annulus, as a function of temperature.

The experiment was similar to that which Giauque, Stout, and Barieau[3] performed to measure the viscosity of liquid He^4. The superleak was constructed by shrinking 0.05-cm i.d. Pyrex glass capillary around a platinum wire 0.013 cm in diameter and 5.5 cm long. On cooling, a narrow channel was formed due to the difference in the coefficients of expansion of the two materials. By measuring the rate of flow of He^4 gas through the leak at 4.22°K and at various pressures and by using the known viscosity[4] and virial coefficients[5] of He^4 gas, the width of the annulus was estimated to be 7×10^{-5} cm. The whole assembly was in the shape of long U-tube, which was supported vertically in the liquid helium cryostat, with the superleak near the bottom of one leg. The upper part of the superleak was connected to the filling system with 0.05-cm i.d. capillary. The other leg of the U-tube was expanded from 0.05-cm to 0.20-cm i.d. above the helium bath level and went to the measuring system. To make a measurement, liquid He^3 or He^4 was condensed on top of the leak until a liquid height of a few mm was observed. The material that flowed through the superleak expanded into an 1100-cc volume, and the rate at which the pressure developed was observed with a Pirani gauge. A mercury diffusion pump was used to exhaust the measuring system prior to each rate measurement. The exhaust gas from the diffusion pump was fed back to the filling system by means of a Toepler pump.

Other experimenters[6-10] have looked for superfluidity of He^3 by studying transport properties of dilute solutions of He^3 in He^4 at temperatures down to 1.5°K. However, as has been pointed out elsewhere,[6,11] the absence of a superfluid state of He^3 can be demonstrated only by studies of the pure liquid. The present experiment with the pure liquid has demonstrated that there is no superfluid transition in He^3 down to 1.05°K, but the question remains as to whether this temperature is sufficiently low. In this connection, it should be noted that the lambda-transition of He^4 occurs at 0.52 times the normal boiling point, and that the vapor pressure at the lambda-point is 38.3 mm; whereas in this experiment no lambda-transition was observed in He^3 down to a temperature which is 0.33 times the normal boiling point, where the vapor pressure is 11 mm.[2] In any case, the experimental results lend support to the hypothesis that the lambda-transition of He^4 is due to Boise-Einstein statistics.

The authors are indebted to Professor J. W. Stout of the Institute for the Study of Metals, University of Chicago, for many helpful discussions.

[1] S. G. Sydoriak, E. R. Grilly, and E. F. Hammel, Phys. Rev. **75**, 303 (1949).
[2] Abraham, Osborne, and Weinstock, unpublished results.
[3] W. F. Giauque, J. W. Stout, and R. E. Barieau, J. Am. Chem. Soc. **61**, 654 (1939).
[4] A. Van Itterbeek, and W. H. Keesom, Commun. Leiden No. 252a; Physica's Grav. **5**, 257 (1938).
[5] W. H. Keesom, *Helium* (Elsevier Publishing Company, Amsterdam, Inc., 1942), p. 49.
[6] Daunt, Probst, Johnston, Aldrich, and Nier, Phys. Rev. **72**, 502 (1947).
[7] J. G. Daunt, R. E. Probst, and H. L. Johnston, J. Chem. Phys. **15**, 759 (1947).
[8] Lane, Fairbanks, Aldrich, and Nier, Phys. Rev. **73**, 256 (1948).
[9] J. G. Daunt, R. E. Probst, and H. L. Johnston, Phys. Rev. **73**, 638 (1948).
[10] J. G. Daunt, R. E. Probst, and S. R. Smith, Phys. Rev. **74**, 495 (1948).
[11] L. Landau and I. Pomeranchuk, Comptes Rendus, U. S. S. R. **59** (No. 4) 669 (1948).

Yields of Some Photo-Nuclear Reactions

M. L. PERLMAN*
Research Laboratory, General Electric Company, Schenectady, New York
February 7, 1949

IT has been shown that in the neighborhood of mass number 60 a transition occurs in the relative yield values for the

TABLE I. Yields relative to $N^{14}(\gamma, n)N^{13}$ yield as unity.

Reaction	Product half-life	Product betas and energies (Mev)	Relative yield 100 Mev	Relative yield 50 Mev
$_{24}Cr^{50}(\gamma, n)_{24}Cr^{49}$	42 min.	$\beta^+1.45$	13	12
$_{26}Fe^{54}(\gamma, n)_{26}Fe^{53}$	8.9 min.	β^+[a]	15	15
$_{28}Ni^{58}(\gamma, n)_{28}Ni^{57}$	36 hr.	$\beta^+0.67$ K[b]	>6.3	>6.0
$_{29}Cu^{65}(\gamma, n)_{29}Cu^{64}$	12.8 hr.	$\beta^+0.66(15\%)$ $\beta^-0.58(32\%)$ K[c,d] (53%)	41	32
$_{30}Zn^{64}(\gamma, n)_{30}Zn^{63}$	38 min.	$\beta^+0.5(1\%)$ 1.4(7%) 2.4(85%) K[e] (7%)	26	26
$_{32}Ge^{76}(\gamma, n)_{32}Ge^{75}$	89 min.	$\beta^-1.1$	54	
$_{53}I^{127}(\gamma, n)_{53}I^{126}$	13 days	$\beta^-1.1$ K	>29	>30
$_{59}Pr^{141}(\gamma, n)_{59}Pr^{140}$	3.5 min.	$\beta^+2.40$	73	76
$_{32}Ge^{74}(\gamma, p)_{31}Ga^{73}$	5 hr.	$\beta^-1.4$	2.5	
$_{32}Ge^{70}(\gamma, pn)_{31}Ga^{69}$	68 min.	$\beta^+1.9$	3.4	

[a] Energy not known but self-absorption of betas found to be small in this case.
[b] The writer is indebted to Dr. G. Friedlander for the information that Ni^{57} decays by K-capture as well as by positron emission.
[c] H. Bradt *et al.*, Helv. Phys. Acta **19**, 219 (1946).
[d] C. S. Cook and L. M. Langer, Phys. Rev. **74**, 1241A (1948).
[e] Huber, Medicus, Preiswerk, and Steffen, Helv. Phys. Acta **20**, 495 (1947).

(γ, n) reaction induced by 100-Mev and by 50-Mev x-rays.[1] For reactions studied on nuclides of mass number less than 60, the (γ, n) yield values relative to the yield of the reaction $N^{14}(\gamma, n)N^{13}$ vary from 1 to 6; in the range of mass numbers between 60 and 120 yield values vary from 33 to 46. The one (γ, n) reaction investigated above mass number 121, $Re^{187}(\gamma, n)Re^{186}$, has a yield of 85.

Further work has now been done with (γ, n) reactions in the vicinity of mass number 60. Measurements have been made also on two additional (γ, n) reactions in heavy elements. Incidental to this work, data on two other reactions have been obtained. The experimental method, which has been described in detail,[1] depends upon the measurement of the radioactivity of product nuclei. New results are summarized in Table I. The yield of the reaction $N^{14}(\gamma, n)N^{13}$ has been taken as unity at each x-ray energy.

To avoid the possibility that yield values for the first two reactions listed might be in error because of the production of Cr^{49} and Fe^{53} by $(\gamma, 3n)$ processes from Cr^{52} and Fe^{56}, whose abundances are roughly 15 times those of Cr^{50} and Fe^{54}, materials enriched[2] in Cr^{50} and in Fe^{54} were used for targets. It has been assumed that the measurement of the Cr^{49} and Fe^{53} activities was not complicated by the decay of daughters V^{49} and Mn^{53} in the two cases, respectively. This assumption is in agreement with what is known about V and Mn activities; if, however, the half-lives of V^{49} and Mn^{53} are short compared with those of Cr^{49} and Fe^{53}, the yield values in these two instances are too large by a factor 2. The yield values in the Ni and I cases are lower limits because of uncertainties in the decay schemes of Ni^{57} and I^{126}. The data for the three reactions in which isotopes of Ge are parents were obtained by measurement of chemically separated Ga and Ge fractions from a bombarded sample of pure GeO_2. The time elapsed between end of bombardment and measurement of activity was too great to permit observation of 20-minute Ga^{70}. The yield value for the reaction $Ge^{76}(\gamma, n)Ge^{75}$ may be perhaps 10 percent large if Ga^{75}, the product of a (γ, p) reaction, is short-lived compared with Ge^{75}.

The data for the Cr, Fe, and Ni(γ, n) reactions would make it seem that the increase in the (γ, n) yields in the vicinity of mass number 60 occurs over a range of mass numbers perhaps as great as 15. The yield for the reaction $Pr^{141}(\gamma, n)Pr^{140}$ is high compared with yields for lighter nuclides. This is true also for the Re reaction previously studied; it may be that (γ, n) yields values will show another general increase in the vicinity of mass number 130. The correlation between (γ, n) yields with 50-Mev and with 100-Mev x-rays is not unexpected; it has been found that quanta having energies greater than 50 Mev do not contribute very much to the (γ, n) yields in the two cases thus far investigated.[3,4]

The yield for the only (γ, pn) reaction investigated is of the same order as (γ, p) yields. It may be pointed out in comparison that in the three $(\gamma, 2n)$ cases for which data are available yields are at least a factor 10 smaller than (γ, n) yields at corresponding mass numbers and, moreover, that the known $(\gamma, 2p)$ yields are smaller by a factor approximately 20 than (γ, p) yields.[1]

The writer is indebted to Dr. G. Friedlander for stimulating discussions. He wishes to express his appreciation to Dr. E. E. Charlton for his cooperation and to Mr. G. Jaffe for his valuable assistance.

* Present address: Department of Chemistry, University of Wyoming, Laramie, Wyoming.

[1] M. L. Perlman and G. Friedlander, Phys. Rev. **74**, 442 (1948).
[2] The isotopically enriched materials were produced by the Carbide and Carbon Chemicals Corporation, Y-12 Plant, Oak Ridge, Tennessee, and were obtained on allocation from the Isotopes Division, U. S. Atomic Energy Commission.
[3] G. C. Baldwin and G. S. Klaiber, Phys. Rev. **73**, 1156 (1948).
[4] J. L. Lawson and M. L. Perlman, Phys. Rev. **74**, 1190 (1948).

Dielectric Constant of Barium Titanate at High Temperatures

SHEPARD ROBERTS
Research Laboratory, General Electric Company, Schnectady, New York
January 31, 1949

FOR some time it has been thought that the dielectric constant of barium titanate at temperatures above the Curie point (120°C) could be accurately represented by the Curie-Weiss law.[1-4]

$$K = C/(T - T_c), \tag{1}$$

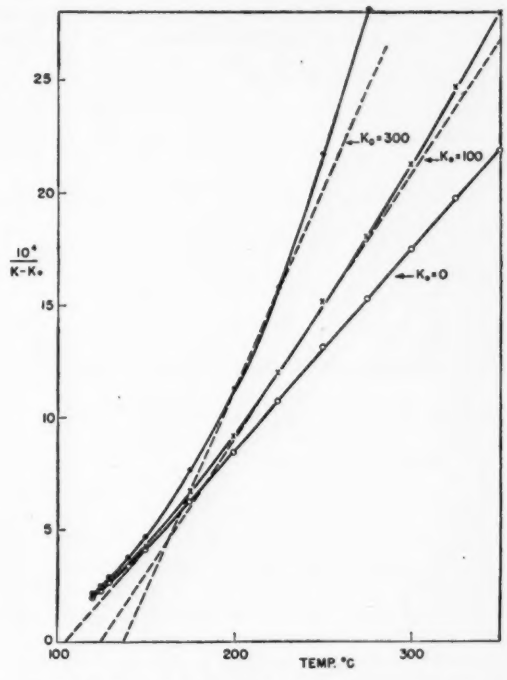

FIG. 1. Reciprocal of $(K - K_0)$ *versus* temperature for different values of K_0

TABLE I. Dielectric constant (K) and loss (tanδ) of barium titanate at one megacycle.

Temp. °C	K	tanδ	Temp. °C	K	tanδ
25	1525	0.009	150	2450	0.002
50	1413	0.011	175	1610	0.001
75	1440	0.010	200	1190	0.001
100	1750	0.014	225	933	0.002
110	2450	0.016	250	761	0.002
115	5070	0.013	275	656	0.007
120	5070	0.009	300	572	0.016
125	4430	0.006	325	506	0.040
130	3820	0.004	350	457	0.087
140	2970	0.003			

where C and T_c are parameters suitably chosen to fit the experimental data and T is the temperature.

However, a new parameter has been introduced in this equation in a more recent article.[5]

$$K=K_0+C/(T-T_c), \tag{2}$$

where K_0 is thought to be the dielectric constant of barium titanate at extremely high or extremely low temperatures. A value of 350 was quoted for K_0, since the dielectric constant reached this value at temperatures near absolute zero. Previously published data, extending only to about 200°C, may be interpreted by either equation since the choice of K_0 is not critical in this range of temperature. The object of the present note is to report measurements of dielectric constant of barium titanate up to much higher temperatures and from these data to determine the value of K_0 directly.

Table I shows results of measurements of dielectric constant and loss of barium titanate ceramic at temperatures up to 350°C. The frequency was one megacycle and the sample was of commercial purity.

In order to find the value of K_0, which most closely fits the experimental data, the reciprocal of $(K-K_0)$ is shown plotted *versus* temperature for different values of K_0 (see Fig. 1). According to Eq. (2), the points corresponding to the correct choice of K_0 should lie on a straight line. This occurs when $K_0=0$ and clearly fails when $K_0=100$ or 300. The line determined by the experimental data, assuming $K_0=0$, is so accurately straight that one can estimate the value of K_0 to be less than 10, if it exists at all, a value quite negligible compared to the dielectric constant measured at ordinary temperatures.

These results at a frequency of one megacycle indicate that Eq. (1) gives a perfectly satisfactory interpretation of the experimental data for temperatures above 150°C. For temperatures nearer the Curie point, there are slight deviations which are not consistent with either equation.

[1] D. F. Rushman and M. A. Strivens, Trans. Faraday Soc. **42A**, 231 (1946).
[2] B. Wul, J. Phys. U.S.S.R. **10**, 95 (1946).
[3] S. Roberts, Phys. Rev. **71**, 890 (1947).
[4] G. H. Jonker and J. H. Van Santen, Chem. Weekblad **43**, 672 (1947); Nature **159**, 334 (1947).
[5] W. P. Mason and B. T. Matthias, Phys. Rev. **74**, 1622 (1948).

Fission Fragment Energies in U^{235} and U^{233}

D. C. BRUNTON AND G. C. HANNA
Chalk River Laboratory, National Research Council of Canada, Chalk River, Ontario, Canada
January 18, 1949

MANY measurements have been made of the energy distribution of fission fragments.[1–7] Among these, several experiments[3–5] have used a coincident pulse technique. In particular, Deutsch and Ramsey[5] have compared the energy distributions from U^{235} and Pu^{239}. The present experiments were undertaken to extend this comparison to U^{233} and to improve the statistical accuracy of the results.

A double "back-to-back" ionization chamber was used with a thin source mounted on the common cathode. Electron collection was employed with Frisch grids shielding the collecting electrodes.[8] Fragments in a small energy interval were selected from one side of the chamber by an electronic "gate" and the energy distributions of the coincident fragments from the other side were recorded on a thirty-channel pulse analyzer.[9] Energy measurements were made at the collecting electrode (to eliminate the effects of any amplifier non-linearity) by comparison with artificial pulses fed in at this point from a pulse signal generator. The absolute energy calibration of the signal generator was obtained by using the natural α-particles from the sources and assuming that the mean energy spent per ion pair in argon is the same for fission fragments and α-particles.

TABLE I. Slow neutron fission in U^{235}.

	Jentschke and Prankl	Flammersfeld, Jensen, and Gentner	Jentschke	Deutsch and Ramsey	Fowler and Rosen	Present experiment
Most probable energy of light group (Mev)	91	92	92.5	94	92.5	92.7
Most probable energy of heavy group (Mev)	57	59	65	60	61.2	59
Ratio of most probable energies	1.60	1.56	1.47	1.57	1.51	1.57
Most probable mass ratio of coincident pairs (on an equal ratio-interval curve)	—	—	—	1.49	—	1.485
Width at half-maximum of high energy peak (Mev)	17	15	13	12	15	12
Width at half-maximum of low energy peak (Mev)	22	19	20	19	24.5	20
Ratio of peak heights	1.3	1.22	1.49	1.57	1.46	1.37
Foil thickness (mg/cm²)	~0.03	~0.01	0.04	0.012	0.029	0.014

The fission source was a collodion film of ~14 μg/cm² containing 3–5 μg/cm² of U dissolved in it and mounted on a 0.01" collimator plate with 0.01" collimator holes. Thus the fragments were collimated in only one chamber but the counting of only coincidence pulses effectively produced an equal collimation in the other chamber. The neutron source was the thermal column of the Chalk River pile.

The energy distribution was measured, first with the energy gate wide open so that the whole range of fission energies was recorded. The result was the usual double-humped curve. Then the energy gate, 5 Mev wide, was set on the low energy end of the distribution and the coincident pulses recorded. The position of the gate was increased in 5-Mev steps to cover the whole spectrum and in each case the corresponding distribution recorded.

The results of these gated runs are interesting. When the gate is set on the heavy fragment group, the energy distribution of the corresponding light group is almost independent of the

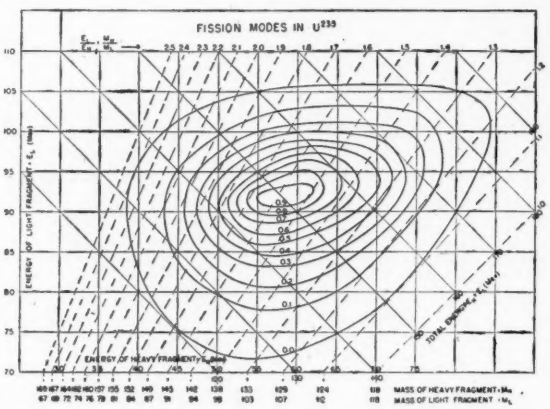

FIG. 1. Contour diagram for the fission modes in U^{235}.

TABLE II Comparison of slow neutron fission in U^{233}, U^{235}, and Pu^{239}.

	Present experiment U^{233}	Present experiment U^{235}	Deutsch and Ramsey Pu^{239}
Most probable energy of the light fragment (Mev)	91.2	92.7	93
Most probable energy of the heavy fragment (Mev)	55.5	59	65
Ratio of most probable energies	1.64	1.57	1.43
Most probable mass ratio (from an equal ratio interval curve)	1.60	1.485	1.32
Width at half-maximum of high energy peak (Mev)	14	12	12
Width at half-maximum of low energy peak (Mev)	22	20	20
Most probable fission mode (total energy	147.5	151.5	156
Most probable fission mode (mass ratio	1.64	1.57	1.43

position of the gate and conversely. For example, a shift of 25 Mev in the gate position produces a total shift in the mean energy of about 4 Mev and a change of width of the distribution of about 1.5 Mev. Moreover, this shift is such that as the gating energy is increased, the energy of the corresponding distribution maximum also increases. Hence, the usual double-peaked fragment energy curve is not, even approximately, a simple inversion of the double-peaked mass curve.

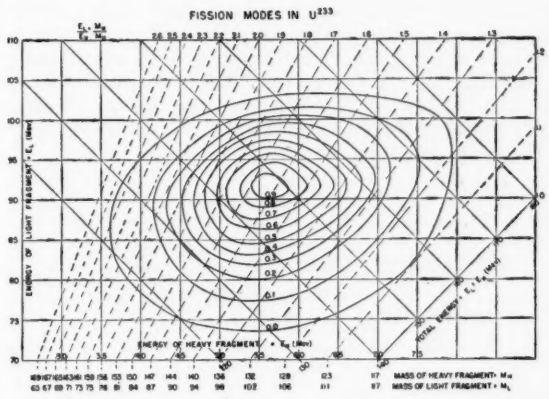

FIG. 2. Contour diagram for the fission modes in U^{233}.

Comparison of the present results on U^{235} with that of previous experiments is given in Table I.

A comparison of slow neutron fission in U^{235}, U^{233}, and Pu^{239} is given in Table II.

The experimental results for U^{235} and U^{233} are presented in the contour diagrams, Figs. 1 and 2. The contour lines represent relative frequency of occurrence of the fission modes. Figure 3 shows the variation of total kinetic energy with mass ratio. Energy calculations from nuclear masses predict a maximum in the total energy (kinetic+excitation energy) for unity mass ratio. Since the kinetic energy decreases as the mass ratio decreases below 1.25, the fraction of excitation energy must be increasing rapidly in this region. In this regard,

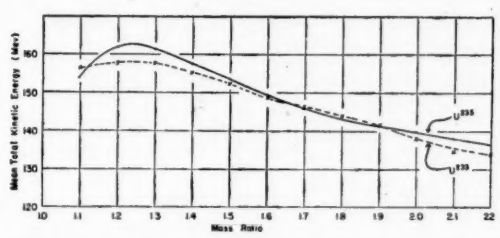

FIG. 3. Variation of total kinetic energy with mass ratio for U^{235} and U^{233}.

Katcoff, Miskel, and Stanley[10] working on the range distributions of plutonium fission fragments have interpreted their results to indicate a decrease in kinetic energy in the vicinity of a ratio of 1.2.

This work will be submitted in greater detail for publication in the Canadian Journal of Research.

[1] M. H. Kammer and H. H. Barschal, Phys. Rev. **70**, 372 (1940).
[2] W. Jentschke and F. Prankl, Zeits. f. Physik **119**, 696 (1942).
[3] W. Jentschke, Zeits. f. Physik **120**, 165 (1943).
[4] A. Flammersfeld, P. Jensen, and W. Gentner, Zeits. f. Physik **120**, 450 (1943).
[5] M. Deutsch and M. Ramsey, MDDC-945 (1945).
[6] J. L. Fowler and L. Rosen, Phys. Rev. **72**, 926 (1947).
[7] D. H. Frisch, LADC-146.
[8] T. E. Cranshaw and J. Harvey, Can. J. Research, July 1948.
[9] C. H. Westcott and G. C. Hanna, Rev. Sci. Inst. **20**, 181 (1949).
[10] S. Katcoff, J. A. Miskel, and C. W. Stanley, Phys. Rev. **74**, 631 (1948

Energies of Heavy Nuclei in Cosmic Rays

PHYLLIS FREIER, EDWARD P. NEY, AND FRANK OPPENHEIMER
Department of Physics, University of Minnesota, Minneapolis, Minnesota

January 27, 1949

IN Table I we have summarized for fifteen heavy nuclei[1] the velocity on entering plates, nuclear charge, and calculated energy per nucleon at the top of the atmosphere. This latter quantity has been obtained by taking into account the observed angle in the photographic emulsions and the altitude at which the balloon spent the majority of the time. Inasmuch as it usually takes the balloon only about 25 minutes to rise from 70,000 to 90,000 feet and the balloon then remains aloft for three to five hours, we presume that the majority of the measured flux is recorded at the higher altitudes.

Inspection of Table I shows that a fairly large number of the measured nuclei had the rather low energies of 0.5 to 0.7 Bev upon entering the atmosphere. If we take into account the charge-to-mass ratio of the incoming particles, we find (using Vallarta's[2] curves distributed June, 1948) that no nuclei with energies less than 0.5 Bev/nucleon can enter the earth's magnetic field from the vertical at a latitude less than 51°N magnetic latitude. Shadow effects will presumably have completely disappeared for this energy at about 55°N magnetic latitude. The flights were made from Camp Ripley, Minnesota, i.e., at 55°N magnetic latitude.

Our results, therefore, suggest that the sun's magnetic field does not produce an energy cut-off noticeable at latitudes less than 51° and probably is not cutting off any particles even at the flight latitude of 55°.

Some indirect evidence substantiates this conclusion. The measured total flux of heavy nuclei for Z greater than 10 is $2.1\pm3\times10^{-4}$/cm²·sec.·ster. assuming 100 percent detection efficiency of the emulsions for these nuclei. If we compare this flux with the flux given by V-2 rocket data[3] at 41° magnetic

TABLE I. Summary of data on electric charge, entrance velocity, and energy per nucleon at top of atmosphere, for 15 heavy cosmic-ray particles.

Z	$\beta=v/c$ on entering plates	Energy/nucleon at top of atmosphere	Angle with vertical
11	0.63	0.5 Bev/nucleon	15°
14	0.86	1.1	23°
20	0.8	1.1	42°
26	0.85	1.3	27°
17	0.61	0.6	38°
12	0.53	0.8	71°
12	0.69	0.6	24°
41	0.8	1.2	30°
15	0.7	0.71	45°
13	0.7	0.61	35°
19	0.7	0.83	48°
12	0.55	0.54	41°
22	0.6	1.2	68°
10	0.6	0.45	10°
20	0.6	1.0	64°

latitude, we find that there are 450 protons for each nucleus of Z greater than ten. If, on the other hand, we use Harrison Brown's data on natural abundances of the elements to estimate the relative flux of nuclei, we would expect about 2000 protons for each such heavy nucleus. This inconsistency can be removed if we assume that the flux of protons increases between 41° and 55° latitude, rather than remaining constant as would be indicated by the sea level latitude effect or the supposition of a 50-gauss sun's magnetic field.

We have used Millikan's[4] data on the increase of total ionization at high altitudes between 41° and 56°N magnetic latitude to estimate the increase in primary flux. Millikan's[4] data would indicate that the flux increased by a factor of very roughly five in this interval and is consistent with a differential power law with an exponent -2.3. If this interpretation of Millikan's data is correct, then our measured flux of heavies with atomic number greater than ten would be consistent with Harrison Brown's[5] estimates of the relative abundance of the elements.

In order to throw further light on the problem presented here and to definitely exclude the possibility that some of the observed nuclei penetrate the magnetic field only partially stripped of orbital electrons, we plan to make flights at more southerly latitudes.

This work has been supported by the Office of Naval Research.

[1] Bradt and Peters, Phys. Rev. **74**, 1828 (1948); Freier, Lofgren, Oppenheimer, and Ney, Phys. Rev. **74**, 1818 (1948).
[2] M. S. Vallarta, Phys. Rev. **73**, 245 (1948).
[3] J. A. Tatel and H. E. Van Allen, Phys. Rev. **73**, 245 (1948).
[4] Millikan, Neher, and Pickering, Phys. Rev. **66**, 295 (1944).
[5] Harrison Brown, private communication.

Determination of e/m from Recent Experiments in Nuclear Resonance

H. A. Thomas, R. L. Driscoll, and J. A. Hipple
National Bureau of Standards, Washington, D. C.
January 31, 1949

In a recent experiment reported by H. Taub and P. Kusch,[1] the g value for the proton was measured relative to the atomic g factors of some of the alkali atoms with improved accuracy by the molecular beam method. Their result is $g_H = 30.4211 \times 10^{-4} \pm .005$ percent. Combining this value with our recent measurement[2] of the absolute value of the gyromagnetic ratio of the proton, which gave a value $\gamma_p = (2.6752 \pm .0002) \times 10^4$, a more precise value of $e/m = 2\gamma_p/g_H = (1.75878 \pm .00016) \times 10^7$ is obtained.

A comparison of this value with other experimental values summarized by DuMond and Cohen[3] is shown in Fig. 1. Work is proceeding to improve the accuracy of the proton gyromagnetic ratio which will, in turn, lead to a more precise value of e/m.

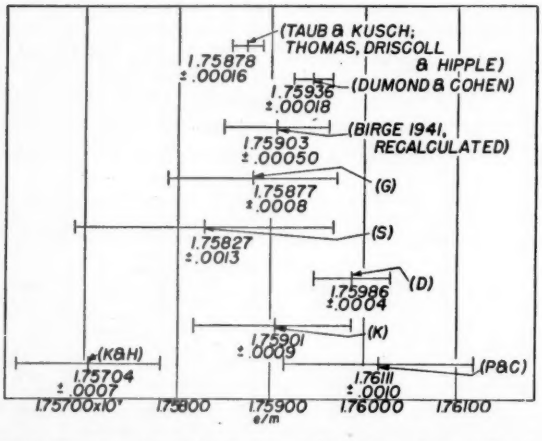

FIG. 1. Experimental determination of e/m. The values reading from top to bottom are: 1. The value reported here. 2. Least square fitted value (DuMond and Cohen). 3. Recalculated Birge value (1941). 4. Goedicke (1939). 5. Shaw (1938). 6. Dunnington (1933, 1937). 7. Kirchner (1931, 1932). 8. On left. Kinsler and Houston (1934). Correcting for the new value of the electron moment (P. Kusch and H. M. Foley, Phys. Rev. **73**, 412 (1947); J. Schwinger, Phys. Rev. **73**, 415 (1948)), this value is revised to $1.75908 \pm .0007$ which is in agreement with the other values. 9. On right. Perry and Chaffee (1930).

[1] H. Taub and P. Kusch, Bull. Am. Phys. Soc. **24**, No. 1, W8A (1949).
[2] Thomas, Driscoll, and Hipple, Phys. Rev. **75**, 902 (1949).
[3] J. W. M. DuMond and E. R. Cohen, Rev. Mod. Phys. **20**, 82 (1948).

Erratum: Acoustical Birefringence

[Phys. Rev. **74**, 1889A (1948)]

W. J. Price
Rensselaer Polytechnic Institute, Troy, New York

FURTHER consideration has shown that in ammonium dihydrogen phosphate a transverse mode with wave normal in the 011 direction and polarization in the 100 directional will travel in a direction lying in the X plane and making an angle of 7° with the wave normal. In the above abstract it was stated erroneously that this mode should travel along the wave normal. With this present consideration it follows that all three modes with wave normals in the 011 direction of ADP travel in directions making angles different from zero with the wave normal.

"Cross-Over Transitions" in Cl^{38}, Co^{60}, Br^{82}, and Sb^{124}

V. Myers and A. Wattenberg
Argonne National Laboratory, Chicago, Illinois
January 17, 1949

THE threshold reactions of photo-disintegration of Be^9 and D^2 provide a convenient method for detecting weak high energy gamma-rays in the presence of intense gamma-radiation of lower energy. It is possible to detect gamma-rays that occur with a frequency of as low as 10^{-6} photon per disintegration. Such weak gamma-rays may arise either from a weak beta-ray branch or from high energy radiation from known excited levels.

TABLE I. Cross-over energy and transition probabilities for Cl^{38}, Co^{60}, Br^{82}, and Sb^{124}.

Source	Cl^{38}	Co^{60}	Br^{82}	Sb^{124}
Target material	D_2O	D_2O	Be	D_2O
Half-life	37 min.	5.3 yr.	34 hr.	60 days
Ratio to Na^{24} of photo-neutrons/curie	4×10^{-4}	$<2\times10^{-6}$	9×10^{-4}	2×10^{-4}
Photons/disintegration*	$<3\times10^{-4}$	$<2\times10^{-6}$	1.4×10^{-3}	5×10^{-4}
Measured energy	—	—	1.7–2.0	2.2–2.5
Cross-over energy E_c(Mev)	3.75	2.4	2.90	2.3
Cascade energies E_1(Mev) / E_2(Mev)	1.60 / 2.15	1.1 / 1.3	1.35 / 0.55	1.7 / 0.6
Transition probabilities $\frac{E_c(l+1 \text{ pole})}{E_1(l \text{ pole})}$	1×10^{-1}	4×10^{-2}	3×10^{-2}	5×10^{-2}
Transition probabilities $\frac{E_c(l+2 \text{ pole})}{E_1(l \text{ pole})}$	6×10^{-5}	1×10^{-5}	1×10^{-4}	2×10^{-4}

* Corrected for change of photo-disintegration cross section with energy

In Cl^{38},[1] Co^{60},[2] Br^{82},[3] and Sb^{124},[4] gamma-rays are known to be emitted in cascade. An attempt has been made to investigate the frequency of occurrence of "cross-over transitions," namely, the single step process from the initial to the final state. The techniques employed for determining the frequency of occurrence and energy of these gamma-rays are essentially the same as those previously described.[5]

Because of the poor yield of photo-neutrons, it was necessary to use comparatively large quantities of D_2O and Be (10-cm diameter spheres) and sources of approximately 10 curies in strength. All measurements were made relative to Na^{24} where one energetic gamma-ray of 2.76 Mev is believed to be emitted per disintegration.[6]

The detector for the energy measurements was embedded in a 10-cm diameter cylinder of paraffin. Only rough limits can be set for the energy of the gamma-rays because of the low statistics obtainable, and it is only in the cases of Br^{82} and Sb^{124} that the results are definitely indicative of the cross-over transition. For the yield measurements, a 20-cm cylinder of paraffin surrounded the detector to make a "long counter." The results are shown in Table I.

No photo-neutrons were observed from $Co^{60}+D_2O$ or from $Br+D_2O$ indicating that these cross-over transitions occur with a frequency less than 2×10^{-6} photon/disintegration. In Cl^{38} there is a 4.9-Mev beta-ray branch. The bremsstrahlung from this beta-ray gave rise to some photo-neutrons so we can only set an upper limit for the cross-over transition.

The transition probabilities for electric radiation have been calculated using a liquid drop model[7] and are listed in the bottom rows of Table I. A comparison of these transition rates with the experimentally determined values of the number of photons per disintegration seems to indicate that the high energy gamma-rays in Br^{82} and Sb^{124} are consistent with $(l+1)$ pole radiations if the cascade is l pole and that the direct transition in Co^{60} must be forbidden or of $(l+3)$ pole or higher. The result for Co^{60} is not what would be expected from the results of Brady and Deutsch.[8] No conclusions can be drawn at present from the Cl^{38} data.

[1] Hole and Siegbahn, Arkiv f. Mat. Astr. o. Fys. 33A, 9 (1946).
[2] Deutsch, Elliott, and Roberts, Phys. Rev. 68, 193 (1945).
[3] Roberts, Downing, and Deutsch, Phys. Rev. 60, 544 (1941).
[4] W. E. Meyerhof and M. Goldhaber, Phys. Rev. 72, 273 (1944).
[5] A. Wattenberg, Phys. Rev. 71, 497 (1947).
[6] K. Siegbahn, Phys. Rev. 70, 127 (1946).
[7] H. Bethe, Rev. Mod. Phys. 9, 69 (1937).
[8] E. Brady and M. Deutsch, Phys. Rev. 72, 870 (1947).

THE AMERICAN INSTITUTE OF PHYSICS

INCORPORATED

57 East [illegible] New York 22, N.Y.

MEMBER SOCIETIES:

American Physical Society
KARL K. [illegible], *Secretary*, Columbia University, New York 27, New York

Optical Society of America
ARTHUR C. [illegible], *Secretary*, Massachusetts Institute of Technology, Cambridge 39, Massachusetts

Acoustical Society of America
WALLACE [illegible], *Secretary*, [illegible] Street, New York 22, New York

Society of Rheology
EARL K. [illegible], *Secretary*, Institute of Textile Technology, Charlottesville, Virginia

American Association of Physics Teachers
R. F. [illegible], *Secretary*, University of Illinois, Urbana, Illinois

AFFILIATED SOCIETIES:

American Society for X-Ray and Electron Diffraction
Electron Microscopy Society of America
Physical Society of Pittsburgh
Physics Club of [illegible] College
Physics Club of Washington
Cleveland Physical Society
Physics Club of the Lehigh Valley

ASSOCIATES:

Over seventy leading industrial corporations and other institutions which contribute to the support of the [illegible]

JOURNALS:

The Physical Review
JOHN T. [illegible], *Editor*, University of Minnesota, Minneapolis, Minnesota

Reviews of Modern Physics
J. W. [illegible], *Editor*, University of Minnesota, Minneapolis, Minnesota

Journal of the Optical Society of America
GEORGE R. [illegible], *Editor*, Massachusetts Institute of Technology, Cambridge 39, Massachusetts

The Journal of the Acoustical Society of America
FLOYD A. [illegible], *Editor*, 3318 [illegible] Street, N.W., Washington, D.C.

American Journal of Physics
THOMAS [illegible], *Editor*, Michigan State College, East Lansing, Michigan

The Review of Scientific Instruments
GAYLORD [illegible], *Editor*, [illegible]an Laboratory of Physics, [illegible] of Pennsylvania, [illegible]delphia, Pennsylvania.

The Journal of Chemical Physics
JOSEPH E. [illegible], Kent Chemical Laboratory, University of Chicago, Chicago 37, Illinois.

Journal of Applied Physics
ELMER [illegible], *Editor*, Case Institute of Technology, Cleveland 6, Ohio

Physics Today
DAVID A. [illegible], *Editor*, American Institute of Physics, 57 East 55 Street, New York 22, New York

OFFICERS

[illegible] R. HARRISON, *Chairman*
Massachusetts Institute of Technology
[illegible] WATERFALL, *Secretary*
The Colonial Corporation
GEORGE B. PEGRAM, *Treasurer*
Columbia University
JOHN T. TATE
Director, on Publications
University of Minnesota

GOVERNING BOARD

LUIS W. ALVAREZ
ROBERT B. BRODE
E. U. CONDON
A. J. DEMPSTER
W. F. FAIR, JR.
HARVEY FLETCHER
R. C. GIBBS
GEORGE R. HARRISON
W. V. HOUSTON
PAUL E. KLOPSTEG
F. W. LOOMIS
PHILIP M. MORSE
GEORGE B. PEGRAM
A. H. PFUND (*deceased*)
JOHN T. TATE
WALLACE WATERFALL
W. W. WHITE
A. G. WORTHING
Consultant on Printing
MELVIN LOOS

ADMINISTRATIVE STAFF

HAROLD A. BARTON, *Director*
CLEVELAND NORCROSS, *General Manager*
THEODORE VORBURGER, *Business Manager*
RUTH F. BRYANT, *Publication Manager*
EMMA HORSTADTER, *Office Manager*
EUGEN B. NEUBERGER, *Circulation Manager*

The American Institute of Physics was founded in 1931 as a federation of leading societies in the field of Physics. It combines into one operating agency those functions on behalf of physics which can best be done by the Societies jointly. Its purpose is the advancement and diffusion of physical knowledge and its applications to human welfare. To this end it publishes for each of the Societies the nine journals listed on this page; promotes efficiency and effectiveness of [illegible] among all who are interested in physics; renders numerous [illegible] services to physicists and to the [illegible]; and cooperates with governmental agencies, national associations, educational institutions, [illegible] industries, and numerous individuals in such manner as to realize the opportunities and fulfill the responsibilities of physics as an important and constructive human activity.

CONTENTS

THE PHYSICAL REVIEW — SECOND SERIES, VOL. 75, NO. 6 — MARCH

Scattering of Fast ... in Gas . . . . . H. W. ...

Energy Spectrum of ... Protons from Cl³⁷ . . . . . EVANS HAYWARD

Upper Limits of the ... of Bismuth, Lead, Mercury, Gold, Iridium, and Tungsten for 14-Mev ... ANNE M. PHILLIPS, LOUIS ROSEN, AND R. F. ...

Intensity of Heavily ... Particles at 4300-Meter Altitude . . . . . FRANK L. ...

Reflection and Refraction ... Waves in Viscoelastic Media . . . . H. T. O'...

Measurement of Shear ... Viscosity of Liquids at Ultrasonic Frequencies . . . . . E. ... MASON, W. O. BAKER, H. J. MCSKIMIN, AND J. H. ...

Ultrasonic Measurement ... Salt Crystals . . . . . W. J. ...

Temperature Dependence ... Work Function of Semiconductors . . . . . A. H. ...

Effect of Surface States ... Temperature Variation of the Work Function of Semiconductors . . . . . NORMAN J. MARKHAM AND P. H. MILLER, JR.

Relativistic Field Theories . . . . . T. S. CHANG

Interpretation of the ... Ferromagnetism of Gadolinium . . . . . CHARLES KITTEL

Total Neutron Cross ... of Compounds with Different Crystalline Structures . . . . . LEONARD WIENBERG, DAVID MENEGHETTI, AND S. S. ...

Letters to the Editors:

Coincident Beams ... Chambers . . C. G. MONTGOMERY AND D. D. MONTGOMERY

Microwave Absorption ... Bulk . . . . . E. ... TSU, ROY C. WHEELER, AND DUDLEY WILLIAMS

Variational Method ... Wave Equation of an Electron in the Field of a Nuclear Atom . . . . . SU-GOU HUANG

Čerenkov Radiation ... Theory . . . . . W. W. WADA

Nuclear Capture ... B. FERRETTI, D. H. W. KIRKWOOD, AND G. C. HANNA

Note on the Radiation ... . S. W. BARNES, A. F. CLARK, G. B. ...

... J. L. MCCRARY, J. B. PLATT, AND S. N. VAN VOORHIS

Fluorescence of ... to High Energy Radiation . . . . . LOUISE ...

β-Spectrum of ... . G. C. HANNA AND B. PONTECORVO

Ferromagnetic Alloys ... Copper-Manganese-Indium . . . . . ROBERT R. GRINSTEAD AND DON M. YOST

Discharge of a ... Gases about the Filament . . . . . H. R. CRANE

High Multiplication ... Measurements . . . . . G. C. ..., D. H. W. KIRKWOOD, AND B. PONTECORVO

Scattering of High ... by Protons with Hard Central Interaction . . . . . K. N. HSU AND T. M. ...

Comparison of the ... Beam Lengths for and . . . ., RICHARD WOLDOCK, AND BERNARD M. ...

Yields of Some ... . M. L. ...

Dielectric Constant ... at High Temperatures . . . . . SIEGFRIED ...

Fission Fragment ... . D. C. ... AND G. C. ...

Energies of Heavy ... ., CHARLES ..., REGINALD P. NEY, AND FRANK ...

Determination of ... Resonance Neutron Resonance . . . . . A. ..., R. L. ..., AND J. A. ...

Erratum: Acoustic ... . W. J. ...

"Cross-Over Trans... ... and ... . V. MYERS AND A. ...

LANCASTER PRESS, INC., LANCASTER, ...